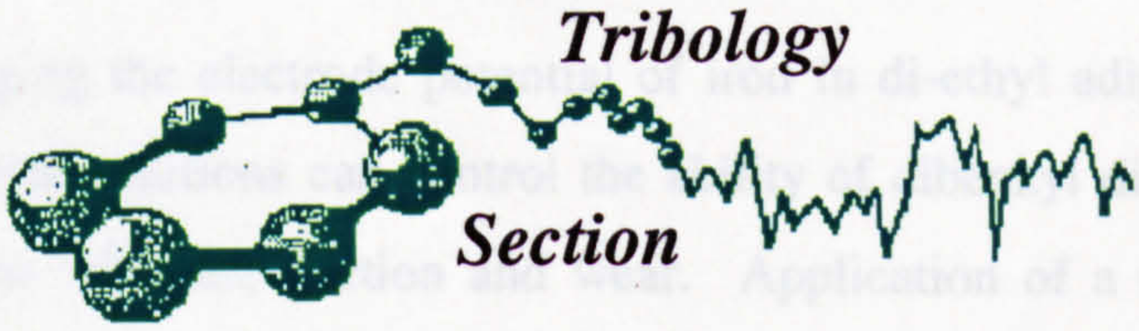
Electrochemical Control of Friction and Wear

- Satoshi Ogano -

A thesis submitted to the University of London in partial fulfilment
of the requirements of the degree of Doctor of Philosophy
and Diploma of Imperial College

November, 1998



Department of Mechanical Engineering
Imperial College of Science, Technology and Medicine
Exhibition Road, London, SW7 2BX

BIBL
LONDON
UNIV.

Abstract

This thesis describes an investigation into metal-lubricant additive interactions under controlled electrode potential, and also the effect of these interactions on friction and wear performance. It is well known that there is a strong relationship between the electrode potentials of metal / lubricant interfaces and friction and wear. However, it is difficult to investigate this relationship using chemical and electrochemical techniques, because of the low conductivity of most non-aqueous lubricants.

This study has attempted to address this problem by: (1) judicious selection of electrolytes and non-aqueous liquids to give adequate conductivity, (2) determination of the tribological characteristics of steel surfaces at both macro- and nano-metre scales under controlled electrode potential.

Di-ethyl adipate and propylene carbonate electrolyte solutions were selected as non-aqueous systems, and used to investigate the redox systems of disulphides and organic acids. The electrochemical kinetics of metal oxidation, together with the film forming ability of organic acids, was related to the effect of applied electrode potential on friction and wear. Atomic force microscopy was also employed to measure topography of an iron electrode in PC electrolyte solution, and used to correlate the spatial distribution of the effects of electrode potentials on local friction behaviour at the nano-metre scale.

This study shows that changing the electrode potential of iron in di-ethyl adipate and propylene carbonate electrolyte solutions can control the ability of dibenzyl disulphide and alkyl carboxylic acids to influence friction and wear. Application of a reducing electrode potential promotes the wear reducing properties of the disulphide and enhances the friction reducing capabilities of alkyl carboxylic acids in pure siding systems. An oxidising electrode potential appears to result in the formation of a soluble carboxylate soap which is unable to reduce friction in sliding conditions although it promotes film formation in rolling contacts.

Good overall agreement is found between macroscopic and nanometre-scale friction behaviour under controlled potential.

"A first class will and a second class brain will defeat a first class brain and a second class will." *Anonymous*

Acknowledgement

I wish to express my sincere gratitude to Prof. H. A. Spikes and Prof. G. H. Kelsall for their supervision and encouragement throughout this work. This thesis would not be completed without their guidance and support.

I am also indebted to Dr. Y-Y. Zhu and Dr. R. Wayte for their friendship and support to operate newly build-up instruments and to solve technical problems, especially for AFM works.

During my life at Imperial College in London, all the members at Tribology section and Electrochemical engineering laboratory created friendly atmosphere and helped me a lot how to survive. I deeply appreciate their hospitality, experimental support and invitation to Southside bar on Friday.

I am much obliged to Tonen Corporation for giving me a chance to carry out this work at Imperial College, and also for their financial support and encouragement, especially for Dr. J. Mitsui and Mr. T. Kuribayashi at lube development division.

I am grateful to my parents and parents in law, Mr. and Mrs. Ogano and Mr. and Mrs. Ito, for their support during our stay in London.

Finally, my special thanks are extended to my wife, Miho, for her love, support and encouragement throughout this work.

Table of Contents

Abstract 1

Acknowledgement 4

Table of Contents 5

List of Figures 17

List of Tables 27

Nomenclature 29

CHAPTER 1:General introduction 33

1.1 Introduction 33

1.2 Project objectives 35

1.3 Thesis structure 35

CHAPTER 2:Literature review 37

2.1 Introduction 37

2.2 Historical overview of triboelectrochemistry 37

2.2.1 Early work 37

2.2.2 Rehbinder effect 38

2.2.3 Charge effect of the metal surface on friction 38

2.2.4 Non-aqueous work 39

2.2.5 Exoelectron emission 39

2.2.6 Typical apparatus used to measure triboelectochemical effect 40

2.3. Boundary lubrication and origin of triboelectrochemistry 43

2.3.1 Friction and wear in boundary regime 43

2.3.1.1 Introduction 44

2.3.1.2 Principle factors involved in the mechanism of boundary lubrication 44

2.3.2 Possible origin of triboelectrochemistry 45

2.3.3 Model of exoelectron effect 46

2.3.3.1 Electron transfer and radical formation 46

2.3.3.2 Model of exoelectron effect on lubricant anion formation 47

2.3.4 Theory of potential repulsion effect 48

2.3.4.1 Van der Waals interaction pressure 48

2.3.4.2 Electrostatic interaction pressure 48

2.3.4.3 Total surface interaction pressure 49

2.3.4.4 Effect of inter-surface pressure on friction coefficient 49

2.3.5 Potential effect on redox process for boundary lubrication 52

2.3.5.1 Correspondence between boundary lubrication and electrochemistry 52

2.3.5.2 Mechanism of redox process effects on friction and wear 53

2.4 Tribology and electrochemistry of organic compounds in this study 55

2.4.1 Esters 55

2.4.1.1 Introduction 55

2.4.1.2 Electrochemistry of esters 57

2.4.2 Carbonate esters 58

2.4.2.1 Introduction 58

2.4.2.2 Electrochemistry of propylene carbonate 58

2.4.3 Disulphides 59

2.4.3.1 Introduction 59

2.4.3.2 Mechanism of action of disulphides with exoelectrons 59

2.4.3.3 Effect of chemical structure on lubricity performance with the above model 61

2.4.3.4 Cathodic reactions of disulphide 62

2.4.3.5 Anodic reactions of disulphide 62

2.4.4 Carboxylic acids 65

2.4.4.1 Introduction 65

2.4.4.2 Effect of chain length of carboxylic acids on lubrication 66

2.4.4.3 Effect of carboxylic acids on forming mono-, or multi-molecular layers 67

2.4.4.4 Cathodic reactions of carboxylic acids 68

2.4.4.5 Anodic oxidation reactions of carboxylic acid 69

2.4.5 Metal carboxylate 70

2.4.5.1 Solubility of metal carboxylates in aqueous solution 70

2.4.5.2 Solubility of metal carboxylates in non-aqueous solution 71

2.5 Recent electrochemical studies using aqueous lubricated systems 73

2.5.1 Effect of types of metals on friction and wear 73

2.5.1.1 Behaviour of nickel 73

2.5.1.2 Behaviour of steel and stainless steel 74

2.5.2 Effect of pH value on friction and wear 75

2.6 Recent studies using non-aqueous lubricated systems 77

2.6.1 Problem of two-electrode systems with previous works 77

2.6.1.1 Hydrodynamic or elastohydrodynamic (EHD) lubrication 77

2.6.1.2 Boundary lubrication 78

2.6.1.3 Experiments with three electrode systems 78

2.6.2 Using mineral oil as a lubricant 81

2.6.2.1 Effect of application of voltage on friction and wear 81

2.6.2.2 Effect of application of voltage on additive performance for friction and wear 82

2.6.2.3 Effect of application of voltage on lubricating film properties 83

2.6.2.4 Effect of application of constant electrical current on wear 84

2.6.3 Using other non-aqueous lubricants 85

2.6.3.1 With phosphate ester 85

2.6.3.2 With DMF or acetnitrile 86

2.7 Conclusion 86

CHAPTER 3:Experimental techniques 87

3.1 Introduction 87

3.2 Electrochemical techniques 87

3.2.1 Voltammetry 87

3.2.1.1 Transport processes in electrochemical system 87

3.2.1.2 Cyclic voltammetry 89

3.2.1.3 Reversible and irreversible electron transfer reaction 90

3.2.1.4 Electrochemical cell used 92

3.2.2 Conductivity determination 93

3.2.3 Infrared analysis of surfaces under controlled electrode potential 93

3.2.3.1 In-situ IR measurements 93

3.2.3.2 Electrochemical cell for in-situ FT-IR spectroscopy 94

3.2.3.3 Test procedure 95

3.2.4 Electrochemical impedance spectroscopy 96

3.2.4.1 Introduction 96

3.2.4.2 Equivalent circuits for the interpretation of electrochemistry 97

3.2.4.3 Frequency response analyser 99

3.3 Friction and wear test methods 100

3.3.1 High Frequency Reciprocating (HFR) rig 100

3.3.1.1 Introduction 100

3.3.1.2 Test condition and method 101

3.3.1.3 Estimation of lubricating condition in HFR tests 101

3.3.2 Nano-probe spectroscopy 104

3.3.2.1 Introduction 104

3.3.2.2 STM / AFM system 104

3.3.2.3 Electrochemical cell for nano-scale work 107

3.3.3 Film thickness measurement 108

3.3.3.1 Basic principles of optical interferometry 108

3.3.3.2 Ultra-thin film technique 111

3.3.3.3 EHD rig modifications and test conditions 114

CHAPTER 4:Chemicals and materials used 117

4.1 Chemicals 117

4.1.1 Chemicals as supporting electrolytes and solvents (base oils) 117

4.1.2 Other chemicals and additives for friction or wear reducer 118

4.2 Materials 119

CHAPTER 5:Selection of non-aqueous systems for electrochemical work 122

5.1 Introduction 122

5.2 Solubility test of electrolytes with non-aqueous solvents 122

5.2.1 Estimation of polarities for non-aqueous lubricants 122

5.2.2 Solubility tests results 123

5.3 Prediction of the suitability of non-aqueous systems 124

5.3.1 Electrochemical behaviour of DEA electrolyte systems 125

5.3.1.1 Electrochemical behaviour of electrolytes in DEA 125

5.3.1.2 Voltammetric behaviour of ferrocene in DEA 126

5.3.1.3 Analysis of the voltammetry with ferrocene in DEA electrolyte solutions 129

5.3.2 Electrochemical behaviour of PC and THF electrolyte solutions 133

5.3.2.1 Pre-selection of electrolytes for triboelectrochemistry with PC and THF 133

5.3.2.2 Conductivity measurements of non-aqueous electrolyte solutions 134

5.3.2.3 Voltammetric behaviour of ferrocene in PC and THF 135

5.3.2.4 Analysis of the voltammetry with ferrocene in PC electrolyte solutions 138

5.3.3 Effect of electrolyte concentration on friction and wear 141

5.3.3.1 Effect of electrolyte concentration on dynamic friction 141

5.3.3.2 Effect of electrolyte concentration on wear 143

5.4 Conclusion 143

CHAPTER 6:Electrochemical study of metal-additive interactions 144

6.1 Introduction 144

6.2 Metal-additive interactions in DEA 144

6.2.1 Interactions without lubricant additives in DEA 144

6.2.1.1 Determination of range of electrode potentials to be studied 144

6.2.1.2 Voltammetric behaviour of iron in ester 146

6.2.1.3 Chronoamperometry with 0.8 M $LiClO_4$ DEA 148

6.2.2 Effect of aryl disulphide on redox processes on the metal surface 150

6.2.2.1 With Fe as a working electrode 150

6.2.2.2 With Pt as a working electrode 151

6.2.2.3 Comparison of chronoamperometry with and without 2.0 wt.% DBDS 152

6.2.3 Effect of organic acids on redox processes on the metal surface 154

6.2.3.1 Voltammetric behaviour 154

6.2.3.2 In-situ FT-IR measurement 156

6.2.3.3 Chronoamperometry with 0.8 M $LiClO_4$ DEA + 0.5 wt.% dodecanoic acid 157

6.3 Metal-additive interactions in PC 159

6.3.1 Interactions without additives in PC 159

6.3.1.1 Voltammetry of Pt in PC electrolyte solution 159

6.3.1.2 Effect of water on voltammetric behaviour 161

6.3.1.3 Voltammetry of iron in ferrocene-containing PC electrolyte solution 162

6.3.1.4 Chronoamperometry with 0.01 M $(Et)_4NBF_4$ PC solution 165

6.3.2 Effect of organic acids on redox processes on a metal surface 166

6.3.2.1 Voltammetric behaviour of iron 166

6.3.2.2 Chronoamperometry with 0.05 wt.% hexadecanoic acid + PC electrolyte 168

6.3.3 Impedance spectra analysis of iron in PC electrolyte solutions 170

6.3.3.1 Impedance spectra 170

6.3.3.2 Determination of equivalent circuit 172

6.3.3.3 Analysis of parameters for the equivalent model 174

6.4 Conclusion 175

CHAPTER 7:Effect of electrode potential on friction and wear 177

7.1 Introduction 177

7.2 Tribological behaviour of steel under controlled potential in DEA 177

7.2.1 Effect of electrode potential on dynamic friction 177

7.2.1.1 Average friction values 177

7.2.1.2 Friction coefficient over reciprocating cycle 179

7.2.2 Effect of electrode potential on wear of ball 181

7.2.2.1 Wear of ball without friction and wear reducing additives 182

7.2.2.2 Wear of ball with DBDS 182

7.2.2.3 Wear of ball with dodecanoic acid 184

7.2.3 Effect of electrode potential on wear of disc 185

7.2.3.1 Wear of disc with HFR rig 185

7.2.3.2 Wear scar appearance at cathodic potential 186

7.3 Tribological behaviour of steel under controlled potential in PC 188

7.3.1 Effect of electrode potential on dynamic friction 188

7.3.1.1 Average friction values 188

7.3.1.2 Friction coefficient over reciprocating cycle 189

7.3.1.3 Analysis of the charge passed during friction testing 191

7.3.2 Effect of electrode potential on wear of ball 193

7.3.2.1 Wear of ball without carboxylic acids 193

7.3.2.2 Wear of ball with carboxylic acid 194

7.3.3 Effect of electrode potential on wear of disc 195

7.3.3.1 Wear of disc at cathodic potential 195

7.3.3.2 Wear of disc at anodic potential 196

7.4 Conclusion 197

CHAPTER 8:Effect of electrode potential on lubricant film thickness 198

8.1 Introduction 198

8.2 Film thickness abilities in PC without carboxylic acid 198

8.2.1 Lubricating film thickness at rest potential 198

8.2.1.1 Result of film thickness against rolling speed 198

8.2.1.2 Origins of non-linearity 200

8.2.2 Effect of negative potential on lubricating film thickness 200

8.2.2.1 Result of film thickness against rolling speed 200

8.2.2.2 Deviation from EHD theory 201

8.2.3 Effect of positive potential on lubricating film thickness 202

8.2.3.1 Result of film thickness against rolling speed 202

8.2.3.2 Origin of boundary film 202

8.3 Film forming abilities in PC with carboxylic acid 204

8.3.1 Effect of rest potential on lubricant film thickness 204

8.3.1.1 Result of film thickness against rolling speed 204

8.3.1.2 Boundary film formed with hexadecanoic acid 204

8.3.2 Effect of negative potential on lubricant film thickness 205

8.3.2.1 Result of film thickness against rolling speed 205

8.3.2.2 Deviation from EHD theory 206

8.3.3 Effect of positive potential on lubricant film thickness 207

8.3.3.1 Result of film thickness against rolling speed 207

8.3.3.2 Origin of boundary film 207

8.4 Conclusion 209

CHAPTER 9:Triboelectrochemistry in nano-metre scale 210

9.1 Introduction 210

9.2 Nano-tribological behaviour in PC solution without carboxylic acid 201

9.2.1 Effect of electrode potential on friction and surface images 210

9.2.1.1 Measurements with constant electrode potential controlled at -0.8 V 210

9.2.1.2 Measurements with constant electrode potential at -0.1 V 212

9.2.1.3 Measurements with constant electrode potential controlled at 0.8 V for 1 min. 216

9.2.1.4 Measurements with electrode potential controlled at 0.8 V for 10 mins. 218

9.3 Nano-tribological behaviour in PC solution with carboxylic acid 220

9.3.1 Effect of electrode potential on friction and surface images 220

9.3.1.1 Measurements with constant electrode potential controlled at -0.8 V 220

9.3.1.2 Measurements with constant electrode potential controlled at -0.1 V 222

9.3.1.3 Measurements with constant electrode potential controlled at 0.8 V for 1 min. 222

9.3.1.4 Measurements with electrode potential controlled at 0.8 V for 10 mins. 227

9.4 Conclusion 229

CHAPTER 10: Conclusions and suggestions for future work 231

10.1 Conclusions 231

10.1.1 Selection of non-aqueous lubricated system 231

10.1.2 Electrochemical study of metal-additive interactions 231

10.1.3 Effect of electrode potential on friction and wear by HFRR 232

10.1.4 Effect of electrode potential on lubricant film thickness 232

10.1.5 Nano-tribological behaviour by AFM technique 233

10.1.6 General conclusion 233

10.2 Suggestions for future work 235

10.2.1 Film thickness in PC solutions at negative electrode potential 235

10.2.2 Electrochemical behaviour of DBDS on iron electrode 236

10.2.3 Triboelectrochemistry with other additives 236

10.2.4 Improved supporting electrolyte 237

References 238

List of Figures

Fig. 2.1 Schematic friction apparatus consisting of a pendulum-like structure, P, which is provided with a fulcrum, F, shaped in the form of a sphere. C:conical cavity of the test electrode, D:potential divider, M:constant-speed motor, MA:microammeter, S:external voltage source.Fig.2.1. Theoretical net internal pressure between flat surface of Fe_2O_3 separated by an electrolyte as a function of surface potential.

Fig. 2.2 Electrochemical cell for static friction measurement. 1: Counter electrode. 2: inlet, 3: outlet, 4: reference electrode connection, 5: right end piece, 6: left end piece, 7: metal supports, 8: Kel-F nuts to make seals, 9: Teflon nut, 10: threaded rod, 11: Kel-F sleeve with screw.

Fig. 2.3 Polaromicrotribometer. 1: Translation drive motor, 2: protractor for calibration, 3: cell, 4: displacement transducers, 5: spring blades, 6: friction measurement bead lift motor, 7: counterbalance, 8: manual height adjustment for the friction contact, 9: micrometer screw for lateral positioning (displacement of the friction contact between successive passes).

Fig. 2.4 A schematic model for boundary lubrication.

Fig. 2.5 Electron transfer model of lubrication in the presence of aromatics.

Fig. 2.6 Theoretical net internal pressure between two flat surfaces of Fe_2O_3 separated by an electrolyte as a function of surface potential **[45]**.

Fig. 2.7 Schematic rubbing contact region between two surfaces.

Fig. 2.8 Theoretical influence of surface potential dependence of friction coefficient for different values of β from Eq.(2-9), the effective area of contact **[45]**.

Fig. 2.9 Schematic illustration of two potential dependent surfaces, with pin-on disc type of friction and wear tester.

Fig. 2.10 Ester types and their chemical structures.

Fig. 2.11 Mechanism of extreme pressure additives' function involving exoelectron emission.

Fig. 2.12 Possible electrochemical oxidative reactions of disulphides.

Fig. 2.13 Electrochemical oxidation potentials of donor molecules.

Fig. 2.14 Schematic adsorption of carboxylic acids on iron-iron oxide substrate.

Fig. 2.15 Calculated Fe(II)-octanoic acid activity-pH diagram for aqueous solutions.

Fig. 2.16 Wear rate against electrode potential for 18Cr-10Ni stainless steel in aqueous solutions of different pH, at a load of 71.6 g cm^{-2}.

Fig. 2.17 Comparison of theoretical and measured friction coefficients for Al_2O_3 rubbing on Fe_2O_3 at different pH values (": 2.6 MPa, ': 7.8 MPa) **[130]**.

Fig. 2.18 Schematic potential drop between ball and plate as a two-electrode system.

Fig. 2.19 Schematic three-electrode system with independent reference electrode.

Fig. 2.20 Comparison of sliding friction between steel surfaces uncharged and *in-situ* charged at 20 V, with / without ZnDTP in mineral oil **[19]**.

Fig. 3.1 Time dependence of the applied potential in cyclic voltammetry.

Fig. 3.2 Typical cyclic voltammograms for reversible and irreversible electron transfer reactions.

Fig. 3.3 Schematic diagram of the electrochemical cell.

Fig. 3.4 Spectro-electrochemical cell to study the surface of an electrode using infrared spectroscopy.

Fig. 3.5 Typical impedance plots described in a complex plane.

Fig. 3.6 Electrochemical interface represented by an equivalent circuit (Randles circuit) and a corresponding complex plane diagram.

Fig. 3.7 HFR rig for friction and wear measurements under controlled electrode potential.

Fig. 3.8 Schematic diagram of the potentiostatic control of the ball-on-disc working electrode in an electrochemical cell.

Fig. 3.9 Operating principles of the atomic force microscope (AFM).

Fig. 3.10 Two modes for AFM cantilever tip.

Fig. 3.11 A free body diagram of the forces on the AFM tip.

Fig. 3.12 Schematic AFM / STM system and its electrochemical cell.

Fig. 3.13 Basic interferometric system for thin film measurements.

Fig. 3.14 Schematic of ultra-thin film thickness measurement technique.

Fig. 3.15 Schematic representation of spectrometric film thickness measurement system.

Fig. 3.16 EHD rig modified to enable control of the ball electrode potential.

Fig. 5.1 Effect of electrolyte type and concentration on the voltammetric behaviour of a Pt electrode in DEA, obtained at a scan rate of 100 mV s^{-1}.

Fig. 5.2 Cyclic voltammograms of Pt / 4 mM ferrocene at a scan rate of 100 mV s^{-1}, in DEA containing $LiClO_4$ and $LiBF_4$ supporting electrolytes, at concentrations of a) 0.1M and b) 0.8M.

Fig. 5.3 Comparison of the concentration dependence of the conductivities of DEA solutions obtained at 25 °C in the presence of $LiClO_4$ and $LiBF_4$ electrolytes.

Fig. 5.4 Cyclic voltammograms of 4 mM ferrocene in 0.8 M $LiClO_4$ DEA solution, at various potential scan rates.

Fig. 5.5 Cyclic voltammograms of 4 mM ferrocene in 0.8 M $LiBF_4$ DEA solution, at various potential scan rates.

Fig. 5.6 Relationship between cyclic voltammetric anodic peak current densities (i_{pa}) and potential scan rate (v) for ferrocene oxidation in DEA electrolyte solutions.

Fig. 5.7 Concentration dependencies of the conductivities obtained at 25 °C in various types of electrolyte solutions.

Fig. 5.8 Comparison of conductivity obtained at 50 °C in various types of electrolyte solutions, depending on electrolyte concentration.

Fig. 5.9 Comparison of cyclic voltammetry of ferrocene in various electrolyte PC solutions obtained at the scan rate of 100 mV s^{-1}.

Fig. 5.10 Comparison of voltammetry of ferrocene in 0.1 M $LiBF_4$ in THF, $(Bu)_4NBF_4$ in THF, and $(Et)_4NBF_4$ in PC, obtained at the potential scan rate of 100 mV s^{-1}.

Fig. 5.11 Relationship between potential scan rate (v) and a) cyclic voltammetric peak current densities (i_{pa}). b) potential scan rate and separation of potentials (E_{pa} - E_{pc}).

Fig. 5.12 Effect of electrolyte concentration on the rate-determining stage of anodic reaction of ferrocene at Pt electrode in the presence of various types of electrolyte.

Fig. 5.13 Effect of $(Et)_4NBF_4$ concentration on friction and wear characteristics in PC.

Fig. 6.1 Cyclic voltammograms of Pt in DEA containing 0.8 M $LiClO_4$ at the potential scan rate of 100 mV s^{-1}.

Fig. 6.2 Cyclic voltammograms of iron in DEA containing 0.8 M $LiClO_4$, to which 0.4 wt.% and 1.0 wt.% water were added subsequently.

Fig. 6.3 The electrolysis current of iron measured against a) time, b) time$^{(-0.5)}$ in 0.8 M $LiClO_4$ DEA, obtained at various electrode potentials.

Fig. 6.4 Cyclic voltammograms of iron in 0.8 M $LiClO_4$ DEA solution with and without 2.0 wt.% DBDS, at the scan rate of 100 mV s^{-1}.

Fig. 6.5 Cyclic voltammograms of Pt in 0.8 M $LiClO_4$ DBDS solution with / without 2.0 wt.% DBDS, obtained at the scan rate of 100 mV s^{-1}.

Fig. 6.6 Time dependence of the currents of Pt obtained at a) -1.8 V, b) -1.3 V, in 0.8 M $LiClO_4$ DEA with / without 2.0 wt.% DBDS; c) replots of currents against time$^{(-0.5)}$.

Fig. 6.7 Typical cyclic voltammograms of iron in DEA containing 0.8 M $LiClO_4$ with and without 0.5 wt.% dodecanoic acid, obtained at the scan rate of 100 mV s^{-1}.

Fig. 6.8 Dependence on cyclic number of voltammetric behaviour of iron in DEA containing 0.8 M $LiClO_4$ and 0.5 wt.% dodecanoic acid, at the scan rate of 100 mV s^{-1}.

Fig. 6.9 In-situ FT-IR spectra from an iron electrode in 0.8 M $LiClO_4$ DEA solution containing 0.5 wt.% dodecanoic acid at various electrode potentials.

Fig. 6.10 Time dependence of currents from Fe in 0.8 M $LiClO_4$ DEA containing 0.5 wt% dodecanoic acid, at various controlled potentials.

Fig. 6.11 Cyclic voltammograms of Pt in 0.01 M $(Et)_4NBF_4$ PC solution, depending on a) negative potential limit, b) positive potential limit.

Fig. 6.12 Effect of water on voltammetric behaviour of Pt in 0.01 M $(Et)_4NBF_4$ PC, at the scan rate of 100 mV s^{-1}.

Fig. 6.13 Comparison of cyclic voltammograms of iron in 0.01 M $(Et)_4NBF_4$ PC solution, with and without 2.0 mM ferrocene, obtained at the scan rate of 100 mV s^{-1}.

Fig. 6.14 Comparison of cyclic voltammograms of iron obtained at the potential scan rate of 100 mV s^{-1}, in 0.01 M $(Et)_4NBF_4$ PC, depending on the scanned potential range.

Fig. 6.15 Currents plotted against time$^{(-0.5)}$ at various electrode potentials in 0.01 M $(Et)_4NBF_4$ PC, with an iron electrode.

Fig. 6.16 Typical cyclic voltammograms of iron in 0.01 M $(Et)_4NBF_4$ PC solution, with and without 0.5 wt.% octanoic and hexadecanoic acids.

Fig. 6.17 Current behaviour for iron plotted against time$^{(-0.5)}$ at various electrode potentials in 0.01 M $(Et)_4NBF_4$ PC containing 0.05 wt.% hexadecanoic acid.

Fig. 6.18 Impedance spectra for iron electrode obtained at various controlled electrode potentials in 0.01 M $(Et)_4NBF_4$ PC solution.

Fig. 6.19 Impedance spectra for iron electrode obtained at various controlled potential in 0.05 wt.% hexadecanoic acid + 0.01 M $(Et)_4NBF_4$ PC solution.

Fig. 7.1 Effect of electrode potential on dynamic friction of iron-on-iron in 0.8 M $LiClO_4$ in DEA with and without 2.0 wt.% DBDS and 0.5 wt.% dodecanoic acid.

Fig. 7.2 Typical friction coefficient traces between reciprocating contact at electrode potentials corresponding to the minimum and maximum friction coefficients in a) 0.8 M $LiClO_4$ DEA solutions containing b) 0.5 wt.% dodecanoic acid :c) 2.0 wt.% DBDS.

Fig. 7.3 Effect of electrode potential on the ball's wear scar in 0.8 M $LiClO_4$ DEA solutions with and without 2.0 wt.% DBDS and 0.5 wt.% dodecanoic acid.

Fig. 7.4 Time dependence of the anodic and /or cathodic current controlled at -1.0 V and 0.3 V, under lubricated conditions, using three different types of lubricants.

Fig. 7.5 Effect of electrode potential on wear scar of disc in 0.8 M $LiClO_4$ solutions with and without 2.0 wt.% DBDS and 0.5 wt.% dodecanoate acid.

Fig. 7.6 Comparison of the appearances of wear scars of discs after wear tests conducted at the electrode potential of 0.3 V.

Fig. 7.7 Effect of electrode potential on dynamic friction of iron-on-iron in 0.01 M $(Et)_4NBF_4$ PC solutions with and without various types of 0.05 wt.% carboxylic acid as a function of alkyl-chain length.

Fig. 7.8 Typical friction coefficient traces in a reciprocating contact at two electrode potentials corresponding to the minimum and maximum friction coefficients in a) 0.01 M $(Et)_4NBF_4$ PC solutions containing b) 0.05 wt.% hexadecanoic acid.

Fig. 7.9 Effect of electrode potential on the wear scar of ball in 0.01 M (Et)4NBF_4 PC solutions with and without various types of 0.05 wt.% carboxylic acids as a function of alkyl-chain length.

Fig. 7.10 Effect of electrode potential on wear scar of disc in 0.01 M $(Et)_4NBF_4$ PC solutions with and without various types of 0.01 wt.% carboxylic acids.

Fig. 8.1 Effect of rolling speed on film thickness between a glass flat and a rolling steel ball at an electrode potential of -0.8 V vs. S.C.E. in 0.01 M $(Et)_4NBF_4$ PC solution.

Fig. 8.2 Effect of rolling speed on film thickness between a glass flat and rolling steel ball at an electrode potential of -0.8 V vs. S.C.E. in 0.01 M $(Et)_4NBF_4$ PC solution.

Fig. 8.3 Effect of rolling speed on film thickness between a glass flat and a rolling steel ball at an electrode potential of +0.8 V vs. S.C.E. in 0.01 M $(Et)_4NBF_4$ PC solution.

Fig. 8.4 Effect of rolling speed on film thickness between a glass flat and a rolling steel ball at an open-circuit potential of -0.1 V vs. S.C.E., in 0.01 M $(Et)_4NBF_4$ PC solution with and without 0.1 wt.% hexadecanoic acid.

Fig. 8.5 Effect of rolling speed on film thickness between a glass flat and a rolling steel ball at an electrode potential of -0.8 V vs. S.C.E. in 0.01 M $(Et)_4NBF_4$ PC solution with and without 0.1 wt.% hexadecanoic acid, together with a regression line for data at the rest potential of -0.1 V vs. S.C.E. in the presence of hexadecanoic acid.

Fig. 8.6 Effect of rolling speed on film thickness between a glass flat and a rolling steel ball at an electrode potential of +0.8 V vs. S.C.E. in 0.01 M $(Et)_4NBF_4$ PC solution with and without 0.1 wt.% hexadecanoic acid, together with a regression line for data at the open-circuit potential in the presence of hexadecanoic acid.

Fig. 9.1 Images from iron surface measured with the constant electrode potential controlled at -0.8 V vs. S.C.E. for 1 minute in 0.01 M $(Et)_4NBF_4$ PC solution: a) AFM topography image; b) AFM friction force image.

Fig. 9.2 Images from iron surface measured with the constant electrode potential controlled at -0.8 V vs. S.C.E. for 10 minutes in 0.01 M $(Et)_4NBF_4$ PC solution: a) AFM topography image; b) AFM friction force image.

Fig. 9.3 Images from iron surface measured with the constant electrode potential controlled at -0.1 V vs. S.C.E. for 1 minute in 0.01 M $(Et)_4NBF_4$ PC solution: a) AFM topography image; b) AFM friction force image.

Fig. 9.4 Images from iron surface measured after tip and surface have been subjected to constant electrode potential at -0.1 V vs. S.C.E. for 10

minutes in 0.01 M $(Et)_4NBF_4$ PC solution. a) AFM topography image; b) AFM friction force image.

Fig. 9.5 Images from iron surface measured with the constant electrode potential controlled at 0.8 V vs. S.C.E. for 1 minute in 0.01 M $(Et)_4NBF_4$ PC solution: a) AFM topography image; b) AFM friction force image.

Fig. 9.6 Images from iron surface measured after tip and surface have been subjected to constant electrode potential at 0.8 V vs. S.C.E. for 10 minutes in 0.01 M $(Et)_4NBF_4$ PC solution: a) AFM topography image; b) AFM friction image.

Fig. 9.7 Images from iron surface measured with the constant electrode potential controlled at -0.8 V vs. S.C.E. for 1 minute in 0.01 M $(Et)_4NBF_4$ PC containing 0.01 wt.% hexadecanoic acid: a) AFM topography image; b) AFM friction force image.

Fig. 9.8 Images from iron surface measured with the constant electrode potential controlled at -0.8 V vs. S.C.E. for 10 minutes in 0.01 M $(Et)_4NBF_4$ PC containing 0.01 wt.% hexadecanoic acid. a) AFM topography image; b) AFM friction image.

Fig. 9.9 Images from iron surface measured with the constant electrode potential controlled at -0.1 V vs. S.C.E. for 1 minute in 0.01 M $(Et)_4NBF_4$ PC containing 0.01 wt.% hexadecanoic acid: a) AFM topography image; b) AFM friction force image.

Fig. 9.10 Images from iron surface measured after tip and surface have been subjected to constant electrode potential at -0.1 V vs. S.C.E. for 10 minutes in 0.01 M $(Et)_4NBF_4$ PC with 0.01 wt.% hexadecanoic acid. a) AFM topography; b) AFM friction image.

Fig. 9.11 Images from iron surface measured after the electrode potential was controlled at +0.8 V vs. S.C.E. for 1 minute in 0.01 M $(Et)_4NBF_4$ PC solution containing 0.01 wt.% hexadecanoic acid: a) AFM topography image; b) AFM friction force image.

Fig. 9.12 Images from iron surface measured after tip and surface have been subjected to constant electrode potential at +0.8 V vs. S.C.E. for 10

minutes in 0.01 M $(Et)_4NBF_4$ PC containing 0.01 wt.% hexadecanoic acid. a) AFM topography; b) AFM friction image.

List of Tables

Table 2.1 Summary of the properties of several types of esters.

Table 2.2 Values of pK_{sp} of metal carboxylate.

Table 2.3 Contact potential and bias voltage at minimum wear rate.

Table 3.1 Test conditions for impedance spectroscopy.

Table 3.2 Test conditions for HFR rig.

Table 3.3 The minimum film thickness and λ value at the mid stroke.

Table 3.4 Test conditions for EHD film thickness measurement.

Table 4.1 Solvents used as a base oil.

Table 4.2 Salts used as supporting electrolytes.

Table 4.3 Chemicals and additives used in this study.

Table 4.4 Solid materials used.

Table 5.1 Solubility parameters for non-aqueous solvents.

Table 5.2 Test result of the solubility of electrolytes in non-aqueous solvents.

Table 5.3 Comparison of voltammetric data using $LiClO_4$ to the theoretical values.

Table 6.1 E_{onset} and E_{pa} as a function of water concentration.

Table 6.2 Metal dissolution at various potentials in DEA.

Table 6.3 Charge passed at various electrode potential for 60 minutes.

Table 6.4 Metal dissolution with hexadecanoic acid in PC at various potential.

Table 6.5 Parameters of equivalent model for PC without hexadecanoic acid.

Table 6.6 Parameters of equivalent model for PC with hexadecanoic acid.

Table 7.1 Electrochemical reactions at various electrode potentials in PC.

Table 7.2 Charge passed depending on electrode potential over 30 minutes.

Table 9.1 Summary of the data obtained by AFM in PC systems.

Nomenclature (1)

Symbol	Physical Meaning	Units
A	apparent rubbing contact area	m^2
A_{eff}	total inter-surface force effective area	m^2
A_H	Hamaker constant for a material in a solution	J
C_i	electrolyte concentration of species *i*	$mol\ m^{-3}$
C_L	double layer capacitance with polarisation resistance characterising surface layer	$\mu F\ cm^{-2}$
d	path distance	m
d_i	distance of a current pass through the ionically-conducting phase	m
D_i	diffusion coefficient of species *i*	$m^2\ s^{-1}$
e	electronic charge, 1.602×10^{-19}	C
E'	reduced Young's modules	$N\ m^{-2}$
F	Faraday constant, 9.64846×10^4	C/equiv.
f	frequency	Hz
h	physical gap thickness	m
h_{min}	minimum film thickness	m
H_i	rate of homogeneous chemical reaction involving species *i*	$mol\ m^{-3}\ s^{-1}$
I	ionic strength = $0.5\sum_i z_i^2 C_i$	$mol\ m^{-3}$
k	Boltzmann constant, 1.381×10^{-23}	$J\ K^{-1}$
M	molar concentration	$mol\ dm^{-3}$

Nomenclature (2)

Symbol	Physical Meaning	Units
L	Avagadro's constant, 6.02205×10^{23}	mol^{-1}
M	molecular weight	$g\ (mol)^{-1}$
n	number of electrons	-
P	pressure	$N\ m^{-2}$
r	refraction angle	-
R	gas constant, 8.314	$J\ mol^{-1}\ K^{-1}$
r_s	radii of the diffusing species	m
R_f	normal reaction force	N
R_L	Resistance of electrolyte within the pores	$\Omega\ cm^2$
R_p	Polarisation resistance at electrode surface in the pores	$\Omega\ cm^2$
R_{qi}	root mean square roughness of surface *i*	m
R_r	radii of contact	m
R_{sol}	solution resistance	$\Omega\ cm^2$
Q	charge	C
S	area of electrode	m^2
T	absolute temperature	K
u	velocity of substance	$m\ s^{-1}$
U	total cell voltage	V
V	volume of the solution used for ICP	m^3
v_s	electrophoretic velocity	$m\ s^{-1}$
ν_s	potential scan rate	$V\ s^{-1}$

Nomenclature (3)

Symbol	Physical Meaning	Units
w	total load for friction test	N
W	applied force	N
Z	impedance	$\Omega\ cm^2$
z_i	number of elementary charges on species *i*	-
Z_{app}	apparent electron number per mole of dissolved iron	$(mol)^{-1}$
α	deviation from ideal RC behaviour due to surface imhomogeneties	-
α	ratio of real contact area to the geometric contact area	-
α_P	pressure viscosity coefficient	Pa^{-1}
α_t	transfer coefficient	-
β	ratio of the effective area over which surface forces are significant to the total micro gap area.	-
ε_0	vacuum permittivity, 8.854×10^{-12}	$C\ V^{-1}\ m^{-1}$
ε_r	relative permittivity	-
ε	$\varepsilon_0\varepsilon_r$	$C\ V^{-1}\ m^{-1}$
ω	angular velocity	$rad\ s^{-1}$
λ	wave length	m
λ	specific film thickness or "lambda ratio"	-
η_0	viscosity of lubricant	$N\ m^{-2}\ s$
η_i	overpotential of electrode *i*	V

Nomenclature (4)

Symbol	Physical Meaning	Units
κ	Debye length = $\sqrt{\frac{2L\,e^2 I}{\varepsilon_0 \varepsilon_r k_B T}}$	m^{-1}
ϕ	phase angle	-
ϕ	electric field	V
δ	solubility parameter	$10^3 \times (J\ m^{-3})^{0.5}$
μ_f	friction coefficient	-
ψ_0	surface potential	V

CHAPTER 1

1. General introduction

1.1 Introduction

Environmental protection is now one of the world's key technological issues. In order to save natural resources, increased attention has been focused on providing low friction and low wear in the automobile industry, to save engine fuel consumption and to increase the service intervals of engines and other mechanical parts.

In this situation, a recent trend in lubrication has been the development of "smart fluids" to reduce friction and wear. These are lubricants whose response in lubricated contacts can be tailored by external control so as to optimise their performance in a given system. Examples include ferrofluids and liquid crystals, whose traction and film forming abilities may be controlled by applied magnetic and electric fields, respectively **[1,2]**. Thus far, this approach has been confined primarily to systems controlled in a physical, reversible manner and has had limited success.

An alternative approach, which has not yet been explored in any detail, is the possibility of controlling lubricant response at a chemical level, by applying electrochemical potential to promote specific chemical processes in contacts and thereby decrease friction and wear. In some respects, this seems a more practical approach than attempting to influence lubrication behaviour physically since a chemical effect is more permanent and does not require the continual supply of energy to maintain it.

It is well known that there is a strong relationship between the electrode potentials of metal / lubricant interfaces and their friction and wear characteristics **[3-5]**, since such potentials determine: (i) the oxidation state of metal surfaces, (ii) the chemical composition and thickness of oxide films; (iii) the surface charge at metal / lubricant interface; (iv) the adsorption of species from lubricants. All four of these are known to influence friction and wear. Thus, in principle, appropriate applied electrode potentials,

together with effective lubricants or additives, may be used to influence friction and wear.

Many workers have investigated the effects of applying electrode potentials of metals on their dynamic friction and wear under mixed or boundary lubrication in aqueous lubricants. In this case, there are both advantages and disadvantages. One advantage is that many of the available electrochemical techniques can be utilised to analyse the effects of electrode potential on the metal surface because of the high conductivity of aqueous solutions. However, the disadvantage is that aqueous lubricants have only a restricted range of applications and results from such systems may not be applicable to non-aqueous systems.

The very low conductivities of oils create experimental problems in the application of 'three-electrode' electrochemical techniques to study the behaviour of metals in such fluids, even with added electrolytes. Hence, almost all previous studies with non-aqueous lubricants have involved two-electrode systems, in which a voltage was applied directly between two rubbing surfaces, their electrode potentials with respect to a reference electrode in the electrolyte being unknown.

This project has attempted to address these problems by: (1) judicious selection of electrolytes and non-aqueous liquids, (2) determination of electrochemical kinetics of phenomena in those solutions with / without lubricating additives, (3) investigation of film forming properties of those additives, in dynamic lubricated conditions under metal-surface potential control, (4) determination of the tribological characteristics of steel surfaces at both macro- and nano-metre scales under controlled electrode potential in non-aqueous solutions.

1.2 Project Objectives

The main aims of this project were as follows:

a) To detect the electrochemical reactions of lubricant additives at the surface of electrodes under controlled potential in a non-aqueous system, and thence characterise the electrochemically deposited films formed by the reaction of additives.

b) To evaluate dynamic friction coefficient and wear characteristics in non-aqueous systems under electrode potential control, and to examine the effect of electrochemical potential on chemical and physical properties of electrode surface and lubricity performance.

c) To investigate the film forming ability of lubricant additives by applying electrode potentials under dynamic lubricated conditions, and thereby develop models to describe the tribological characteristics of these additives under controlled potential.

1.3 Thesis Structure

The rest of the thesis is divided up as follows.

Chapter 2 surveys the published literature relevant to triboelectrochemistry, and also covers the literature on the electrochemical behaviour of organic compounds which will be used in this study. This chapter sets the scene for a better understanding of previous work in triboelectrochemistry as well as the problems of previous work with non-aqueous lubricated systems, in terms of precise control of the electrode potential.

Chapter 3 presents a description of the principal techniques used in this study to measure electrochemical and tribological properties of non-aqueous systems. This chapter also explains the techniques and test rigs employed to measure film thickness under controlled potential by using an ultra-thin film technique, which was developed at Imperial College London.

Chapters 4 describes chemicals and materials used, and explains the function of the experimental instrumentation.

Chapters 5 deals with electrochemical behaviour of a model redox couple ferrocene in a range of organic solvents, to try to predict the suitability of the selected lubricant systems for subsequent electrochemical studies in typical three-electrode systems with appropriate supporting electrolytes which can dissolve in the solvents used.

Chapter 6 presents experimental studies of the electrochemical kinetics of iron and platinum in esters, *i.e.*, diethyl adipate and propylene carbonate solvents, mainly by determination of voltammograms (current-electrode potential curves) with and without aryl disulphides and organic acids as possible friction- and / or wear-reducing additives, to infer their interactions with the electrode surfaces.

Chapters 7 describes the tribological behaviour of iron as a function of electrode potential in diethyl adipate, and in propylene carbonate, with and without aryl disulphides or organic acids as friction / wear reducers. This chapter also discusses, together with the results of the previous chapters, the effect of electrode potential on friction and wear characteristics.

Chapter 8 is concerned with the film thickness properties measured under dynamic lubricated conditions, with propylene carbonate electrolyte solutions, and also discusses the film forming abilities of hexadecanoic acid as a lubricant additive, depending upon the electrode potential, to influence friction and wear.

Chapter 9 reports results of using atomic force microscopy on iron electrodes under potential control in propylene carbonate electrolyte solution with and without hexadecanoic acid. This enabled the topography (non-contact mode) to be measured in the solution, and correlated with the spatial distribution of the effect of electrode potentials on local friction behaviour (contact mode) at the nano-metre scale.

Finally, Chapter 10 draws conclusions from the whole project and offers suggestions for further work.

CHAPTER 2

2. Literature review

2.1 Introduction

This chapter is mainly concerned with surveys of the published literature relevant to triboelectrochemistry and the electrochemical behaviour of organic compounds used in this study. The chapter also explains how electrochemical techniques may be used to control the electrode potential of metal surfaces.

2.2 Historical overview of triboelectrochemistry

2.2.1 Early work

Over 100 years ago, in 1877, a significant effect of applied voltage on friction was discovered by Edison [1], the first person to study the frictional properties of rubbing metals in an aqueous electrolyte under controlled voltage. He studied lead, thallium, and platinum and explained the effect in terms of electrochemical reactions, and proposed that friction decreased when hydrogen was liberated, but increased when oxygen was liberated. Shortly after Edison's findings, Koch [2] reported an increase in the friction of platinum against glass with the application of an anodic potential. However, Edison's hypothesis was soon undermined by the work of Krouchkoll [3], who observed friction changes even when no gas evolution could take place.

These workers were at the frontiers of the interdisciplinary study of tribology and electrochemistry. Since then, there have been numerous studies in both aqueous and non-aqueous systems to demonstrate that friction and wear rate in rubbing contacts can be modified by applying an electrochemical potential to the surfaces of metal [4-7], and the technological term "triboelectrochemistry" has been coined to describe these phenomena [8,9].

2.2.2 *Rehbinder effect*

In the 1940s, Rehbinder found a large effect of the application of external voltage on tribological characteristics, by using a Herbert-type pendulum, involving a glass sphere in contact with a metal surface immersed in an electrolyte **[10]**. He attributed this effect to the variation of the hardness of the metal with the interfacial tension of the metal / electrolyte by implying that there was a formation of "reversible micro fissures" in the metal surface under deformation. He also explained that the electrode double layer penetrated the fissures formed, which decreased the cohesion and hardness of the metal. This hypothesis was controversial in this area of study.

However, subsequent work **[11]** by Bockris and Parry-Jones in the 1950s found that varying the electrode potential produced no measurable change in hardness and suggested instead that its effect on friction was due to its influence on surface adsorption of chemical species in the electrolyte.

2.2.3 *Charge effect of the metal surface on friction*

In the 1950s, Bowden and Young **[12]** measured the coefficient of static friction of platinum against platinum in 0.1 M sulphuric acid. Their technique involved placing a small cylinder on a wire in a cell, and tilting the apparatus at an angle such that the cylinder just slid down the wire. They showed that this platinum / platinum contact in electrolyte solutions gave low friction at high and low electrode potentials, but a maximum friction value at an intermediate potential.

Bockris and Sen **[13,14]** suggested that the curve of friction coefficient against potential exhibited a maximum at the potential of zero charge (pzc) of the metal surface, corresponding to the condition of minimum electrostatic repulsion between the like-charged surfaces. Thus, the friction decrease at potentials on either side of the pzc was attributed to increased double-layer repulsion.

Similar observations were reported by Clark **[15]**, who proposed that adsorbed hydroxyl or hydrogen ions were responsible for decreased friction at low and high electrode

potentials. This concept was also applied to explain the friction between rubber and glass lubricated with aqueous solutions **[16]**.

2.2.4 Non-aqueous work

Triboelectrochemistry with non-aqueous lubricated systems, which is the basis of this project, had never been investigated until the beginning of the 1970s **[5]**. This was mainly because the low conductivity of most non-aqueous lubricants precludes applying the voltage / potential effectively on the rubbing metal surfaces, and also usually precludes using electrochemical techniques, such as cyclic voltammetry from detecting chemical reactions under applied voltage / potential, in the absence of an appropriate supporting electrolyte.

Initial work with non-aqueous systems **[5,17,18]** simply studied the effect of applied voltage across a contact on the tribological characteristics in the lubricants without a supporting electrolyte. *In-situ* analytical techniques, under controlled potential, to correlate electrochemical behaviour with the friction and wear properties, were not examined until the late 1980s, when Tung **[19]** reported a voltammogram of iron in mineral oil. However, its poor definition possibly due to the absence of supporting electrolyte, precluded its use for explaining the electrochemical phenomena involved.

2.2.5 Exoelectron emission

Since Kramer's works **[20]** in the early 1950s, it has been known that some metals become electron emitters during mechanical or thermal treatment, as a consequence of plastic deformation. This concept may be important in the area of triboelectrochemistry because electron transfer processes in triboelectrochemistry are related to these electron emission processes.

As reported in literature **[21-25]**, exoelectron emission occurs when a material's surface is disturbed by plastic deformation, abrasion, fatigue cracking, or phase transformation, all of which can lead to increasing the mobility of surface and near surface electrons. The electron emission from a freshly formed surface reaches a maximum almost

immediately, then decays with time **[21,22]**. Electron emission has been observed from both metals and non-metals, and there is strong evidence that the existence of oxides or other non-metallic surface layers is necessary for electron emission. Exoelectron emission is generated from a clean, strain-free surface simply upon the adsorption of oxygen **[26]**.

The energy of exoelectrons is very low, usually of the order of 2-3 eV, but possibly up to 10 eV **[27,29]**, whereas high-energy electron emission (HEEE), observed during friction of dielectrics in vacuum, results in electrons with energies of tens of keV **[28]**.

2.2.6 Typical apparatus used to measure triboelectrochemical effect

In 1961, Staicopolus **[30]** designed an apparatus, shown in Fig.2.1, for measuring dynamic friction of metal surfaces under potential control. It consisted of a fulcrum F in the shape of a sphere, which fitted into a cavity C, the test electrode. During measurements, the electrode was rotated about its vertical axis by a constant speed motor M. Staicopolus showed that the friction, measured mainly in 0.5 M Na_2SO_4 aqueous solution, was a function of the potential and that application of a potential greater than the pzc (potential of zero charge), generally decreased friction by as much as half.

Bockris and Argade **[13,14]** examined a number of techniques to evaluate the pzc and used a sliding friction method to determine the coefficient of friction lubricated by 0.1 M $NaClO_4$ aqueous solution. In 1969, they developed an apparatus **[31]**, shown schematically in Fig.2.2 which consisted of a slider that was made to slide down the working electrode wire, by gradually changing the inclination of the electrode.

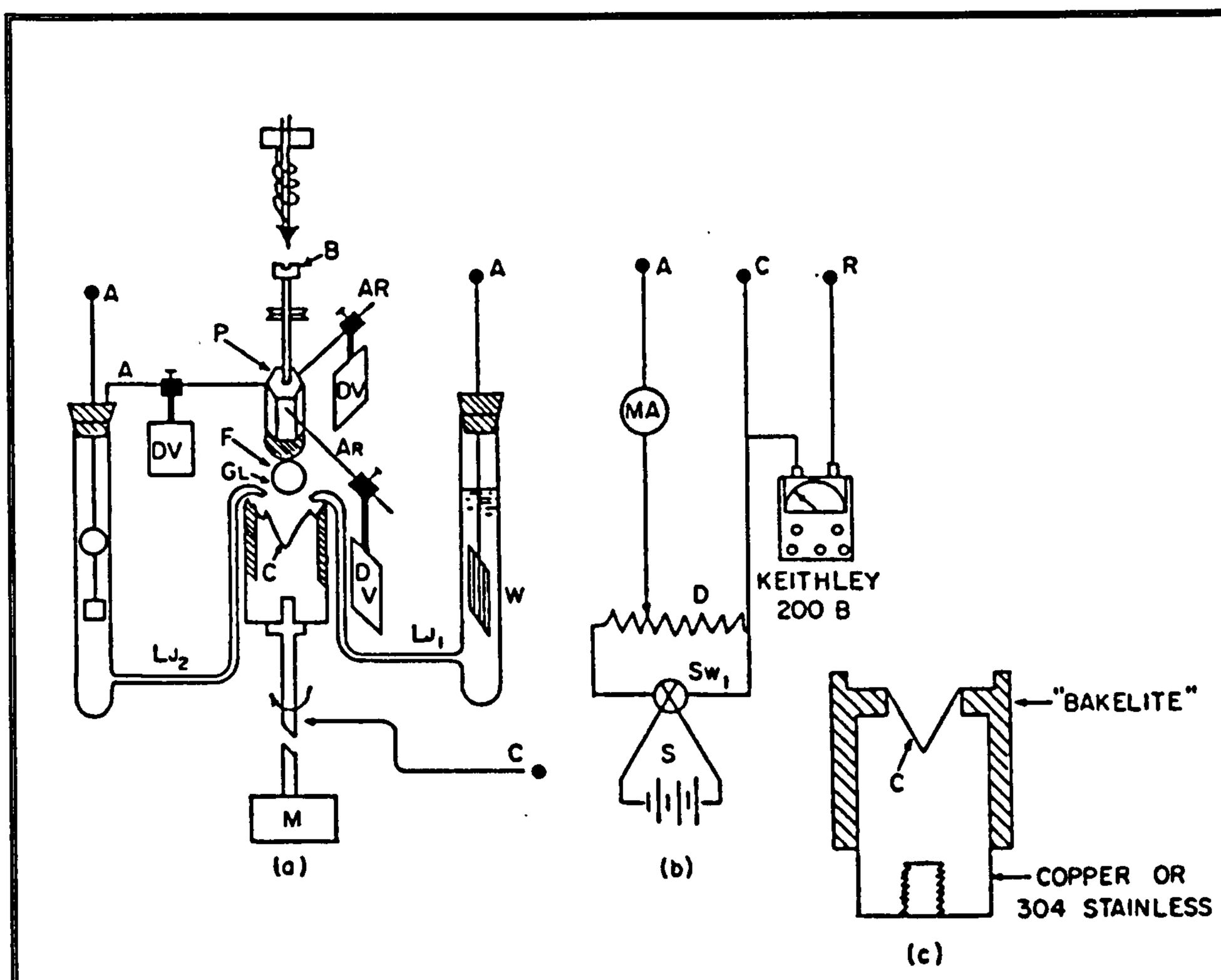


Fig.2.1 Schematic friction apparatus consisting of a pendulum-like structure, P, which is provided with a fulcrum, F, shaped in the form of a sphere. C:conical cavity of the test electrode, D:potential divider, M:constant-speed motor, MA:microammeter, S:external voltage source.

In 1975, Dubois and Lacaze *et al.* **[32]** coined the term *polaromicrotribometry* for the study of polarised metal surfaces. As shown schematically in Fig.2.3, the instrument they designed was a refinement of what Bockris and Argade **[13,14]** had developed previously, as this technique permitted the measurement of transient electrochemical phenomena as well as stationary ones. Dubois and Lacaze *et al.* **[32]** suggested that the dynamic friction of metal / metal contacts in 0.5 M H_2SO_4 aqueous solution depends on the redox processes on the metal surface caused by the change of electrode potential since the friction-potential curve is in agreement with the current-potential curve.

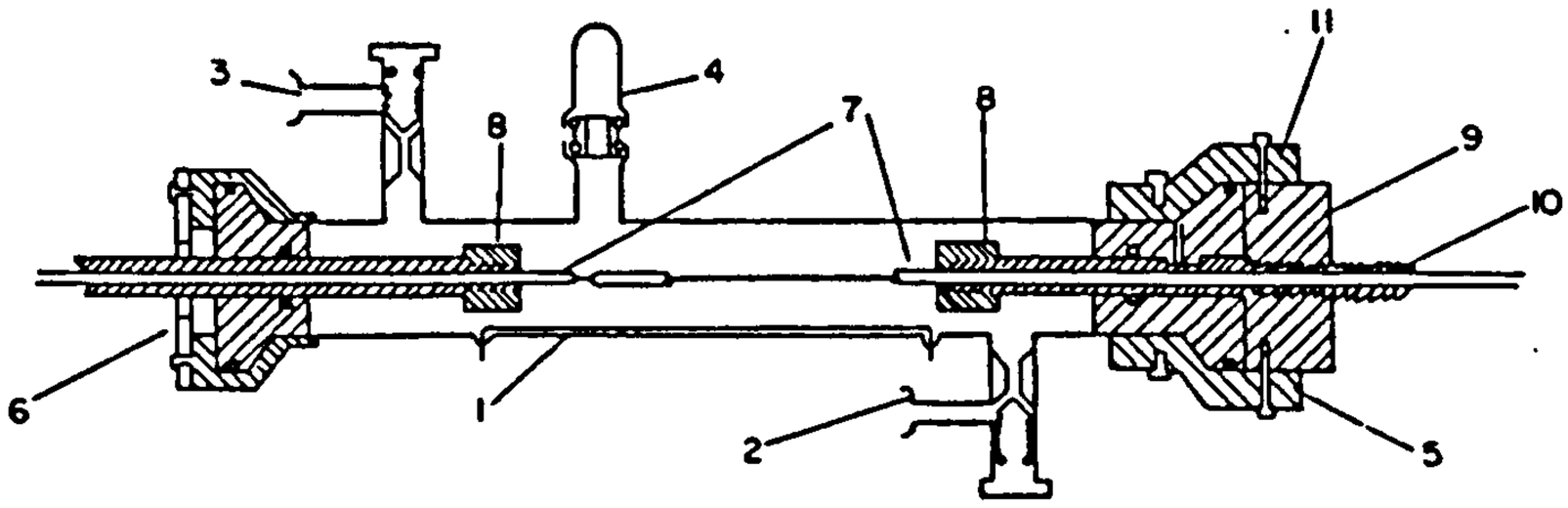


Fig.2.2 Electrochemical cell for static friction measurement. 1: Counter electrode. 2: inlet, 3: outlet, 4: reference electrode connection, 5: right end piece, 6: left end piece, 7: metal supports, 8: Kel-F nuts to make seals, 9: Teflon nut, 10: threaded rod, 11: Kel-F sleeve with screw.

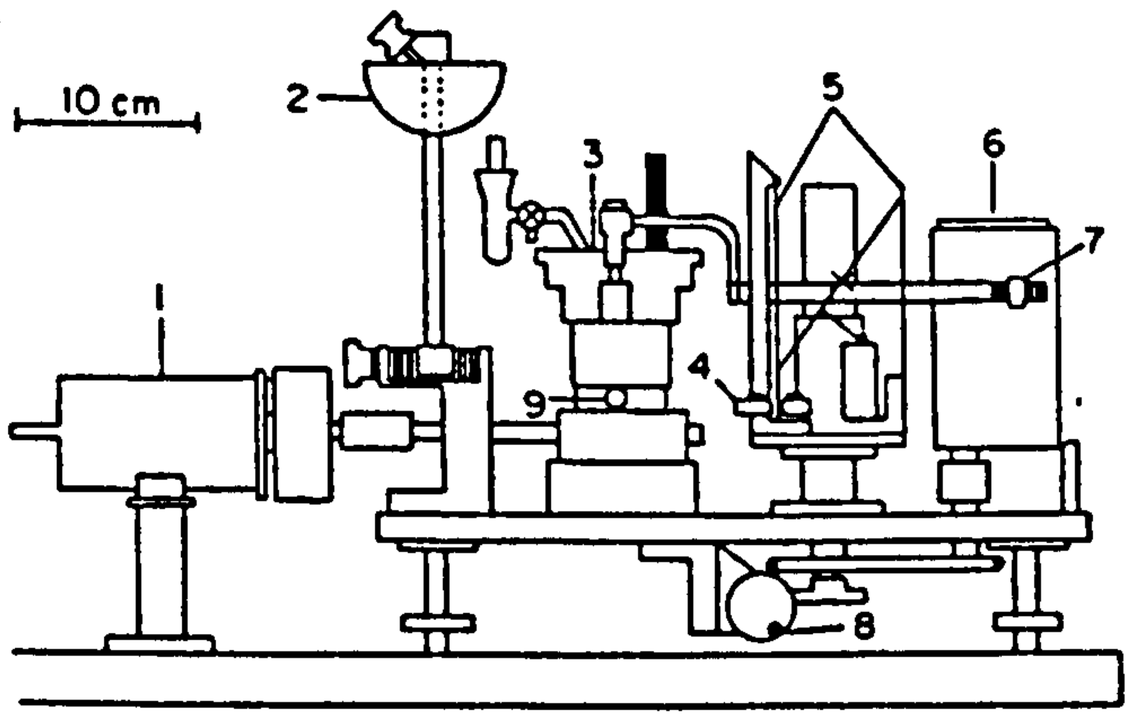


Fig.2.3 Polaromicrotribometer. 1: Translation drive motor, 2: protractor for calibration, 3: cell, 4: displacement transducers, 5: spring blades, 6: friction measurement bead lift motor, 7: counterbalance, 8: manual height adjustment for the friction contact, 9: micrometer screw for lateral positioning (displacement of the friction contact between successive passes).

2.3 Boundary lubrication and origin of triboelectrochemistry

The preceding brief historical overview is followed by descriptions to explain the relationship between tribology, especially boundary lubrication and electrochemistry, and also to present the possible origins of triboelectrochemistry in terms of the effect of applied potential on rubbing surfaces.

2.3.1 Friction and wear in boundary regime

2.3.1.1 Introduction

Boundary lubrication is encountered in liquid lubricated systems which operate at low speeds and viscosities under excessive loading and heating, continual stopping and starting or under starvation conditions **[33]**. In such conditions, insufficient fluid film is hydrodynamically entrained to separate the surfaces and most or all of the load is borne at asperity contacts. A schematic model for boundary lubrication is shown in Fig.2.4.

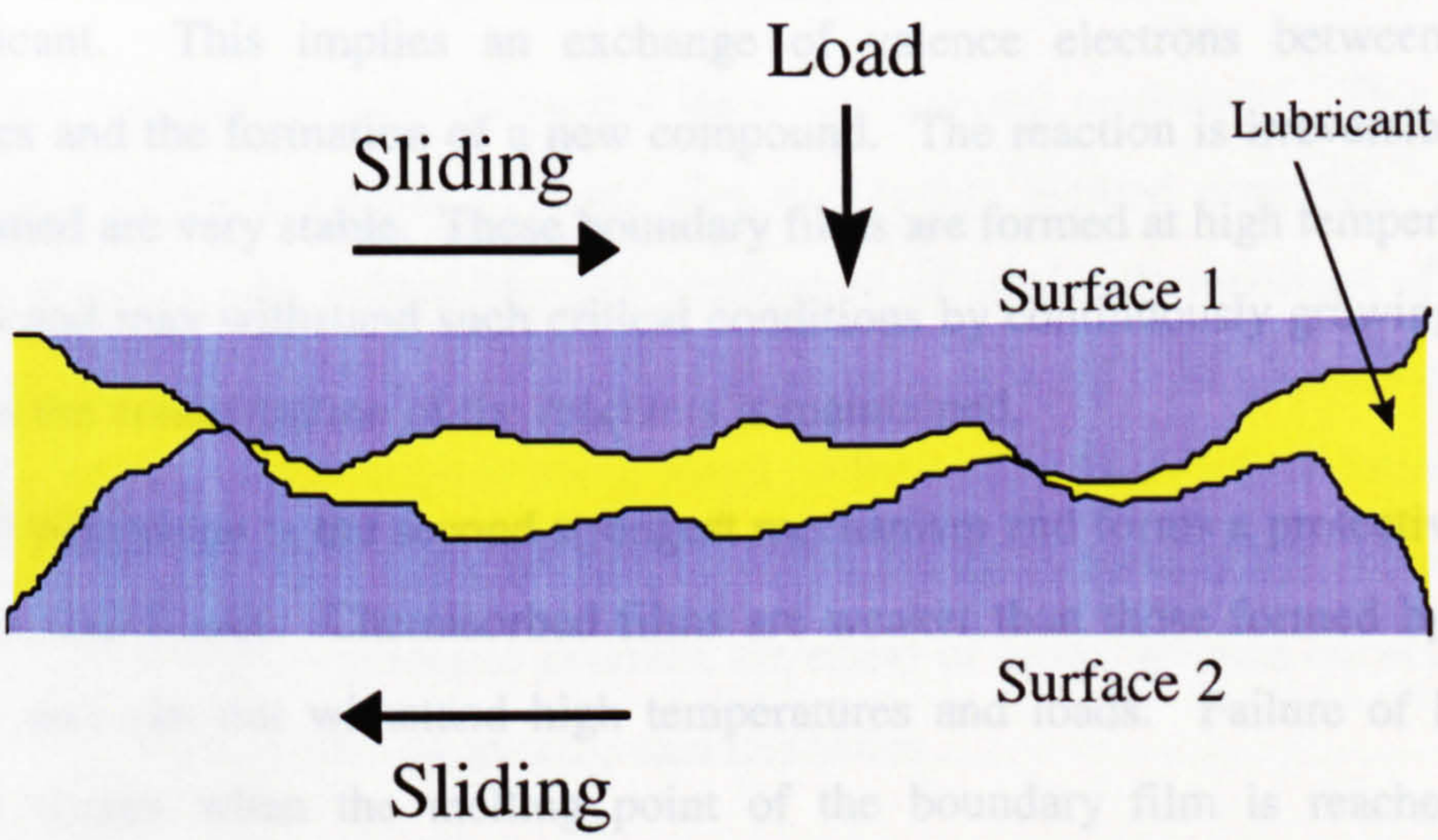


Fig.2.4 A schematic model for boundary lubrication.

In such conditions, friction and wear are essentially independent of the bulk fluid viscosity and are governed by the physical and chemical properties of the surface films (so-called *boundary films*). These films are formed as a result of the chemical and physical interactions between the metal and the fluid during use, and their structure and properties are different from the bulk fluid and the rubbing surfaces [33].

It is unlikely that many moving systems operate solely in the boundary regime, but for most of them, the time spent in this regime is quite considerable. For example, even in journal bearings, boundary friction and wear develop whenever the shaft passes through zero speed during starting or stopping.

2.3.1.2 Principle factors involved in the mechanism of boundary lubrication

As mentioned above, this type of friction and wear is basically independent of the bulk fluid viscosity and is governed by the physical and chemical properties of the surface films. The mechanisms which generate the surface films in boundary lubrication are considered to be three types of processes: (1) *chemical reaction*, (2) *chemical adsorption*, (3) *physical adsorption*. These may operate separately, sequentially (in a limited temperature range) or in conjunction.

The strongest process is a chemical reaction which takes place between the metal and the lubricant. This implies an exchange of valence electrons between the two substances and the formation of a new compound. The reaction is irreversible and the films formed are very stable. These boundary films are formed at high temperatures and pressures and may withstand such critical conditions by continuously growing the film, as long as the concentration of the reactants is maintained.

Chemical adsorption is the second strongest mechanism and forms a protective layer by ionic chemical bonds. Chemisorbed films are weaker than those formed by chemical reactions and can not withstand high temperatures and loads. Failure of lubrication normally occurs when the melting point of the boundary film is reached, usually between 120 and 180 °C.

The third interaction mechanism is physical adsorption. The protective films are held to the surface by weak physical van der Waals forces. No exchange of electrons takes

place between the fluid and the rubbing surfaces and the bond is thus reversible and weak. The film is unstable, temperature sensitive and is desorbed from the surfaces when the thermal energy approaches the bond strength (or when the film dissolves in the bulk lubricant when its solubilisation temperature is reached **[34]**). This type of bond is common with long chain polar surfactants which form dense layers of hydrophobic chains typically 2 to 3 nm long on polar surfaces. In addition, there may also be strong forces of lateral attraction between the chains which increase the strength of the film. These additives are often called "oiliness" additives.

2.3.2 Possible origin of triboelectrochemistry

Three main mechanisms have been proposed for the effect of applied potential or of electron emission process on friction properties in the boundary regime:

(1)*Exoelectron emission processes* (due to rubbing surfaces but possibly controlled by applied potential).

(2)*Electrostatic double layer repulsion forces* (between charged layers on opposing surfaces).

(3)*Electrochemical reactions* (redox processes on rubbing surfaces) to change the nature and shear strength of boundary films present.

These three mechanism have generally been investigated separately. This is in part because exoelectron emission does not directly involve applied potential. As for the other two mechanisms induced by the application of potential, repulsion effects have been investigated only in aqueous systems because most work with aqueous electrolytes has deliberately tended to employ noble metal rubbing pairs, to avoid oxidation of active metals such as iron, whereas the studies of electrochemical reaction have been primarily conducted in oil-based systems to examine the effect of redox systems between oils and steel surfaces, on the friction and wear characteristics .

The following sections will consider typical models for these mechanisms.

2.3.3 Model of exoelectron effect

2.3.3.1 Electron transfer and radical anion formation

Let us consider the formation of radical anions from aromatics with the concept of exoelectron emission. When aromatics are present in the lubricant, it has been suggested that a rapid electron transfer process replaces a relatively sluggish dehydrogenation-polymerisation process **[35]**. Initially, the aromatic adsorbs onto the abraded metallic surface, as indicated in Fig.2.5(1).

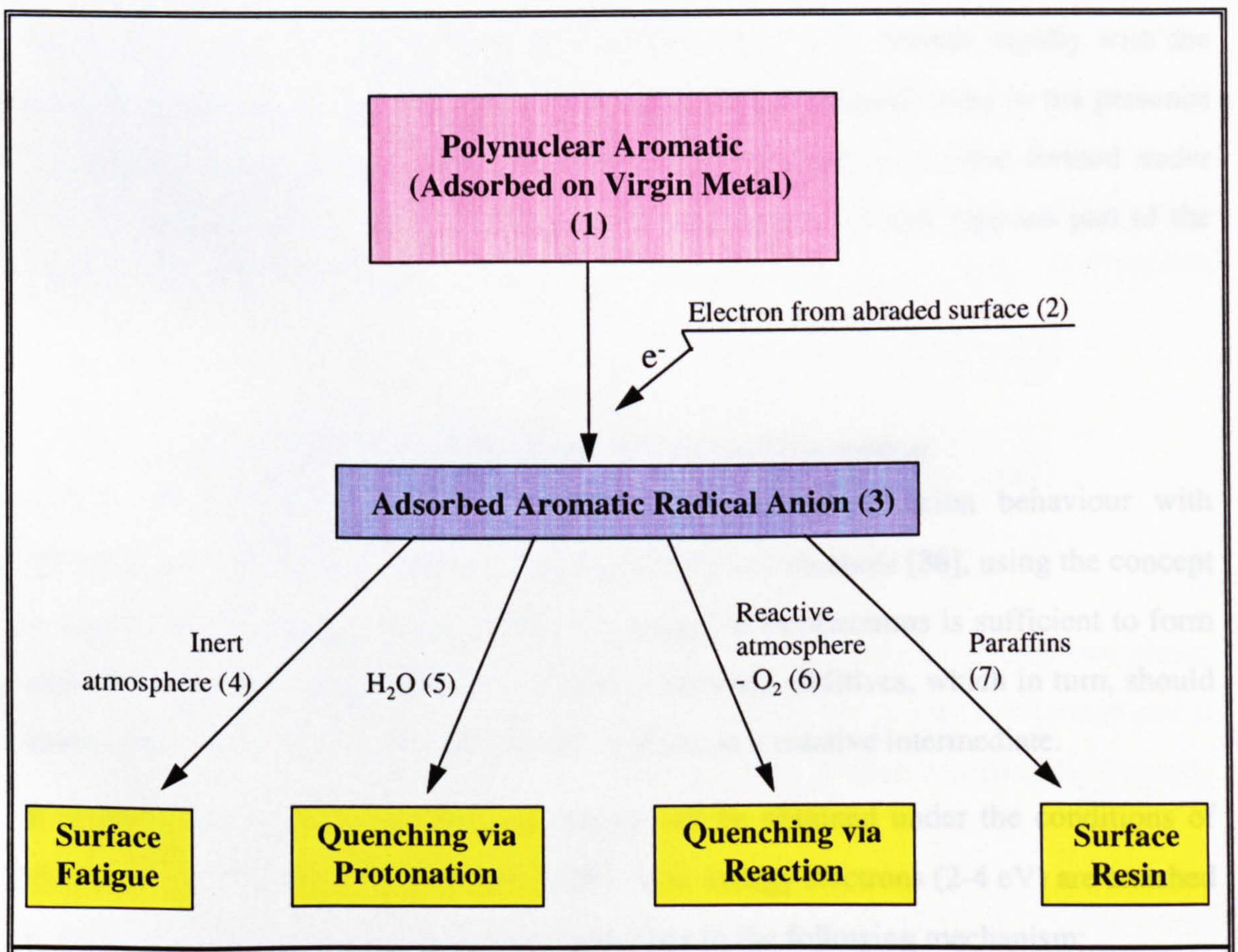


Fig.2.5 Electron transfer model of lubrication in the presence of aromatics.

In the presence of paraffinics, both the aromatic and paraffin co-adsorb, probably with the aromatic being preferentially adsorbed. The activated abraded metal is assumed to

transfer an electron to the aromatic (Fig.2.5(2)), leading to the formation of an adsorbed aromatic radical anion (Fig.2.5(3)).

This reaction intermediate may then undergo any of several processes depending upon the base-stock composition and environment. Under inert atmospheres in the absence of saturates, the aromatic radical anion, as will be described below, interacts with the surface and causes accelerated wear (Fig.2.5(4)). The aromatic radical anion may be quenched by interacting with either water (5) or oxygen (6) (Fig.2.5). Quenching of the aromatic radical anion reduces wear. The initial, rapid formation of the aromatic radical anion, probably reduces the rate of chemical attack by water and oxygen. Presumably this leads to the acceptable performance of aromatics in these aggressive environments.

In the presence of paraffins, the aromatic radical anion may interact rapidly with the paraffin to form surface resin (Fig.2.5(7)). This reaction proceeds even in the presence of oxygen, however, the products of reaction differ slightly from those formed under inert atmospheres. Since the surface resin which has been formed supports part of the applied load, wear is reduced.

2.3.3.2 Model of exoelectron effect on lubricant anion formation

Kajdas has recently proposed mechanisms for the radical anion behaviour with hydrocarbons **[36]**, organo-sulphur compounds **[37]** and alcohols **[38]**, using the concept of exoelectron emission. In his model, the energy of exoelectrons is sufficient to form anions of aromatics, hydrocarbons and typical lubricant additives, which in turn, should easily react with a positively charged steel surface, as a reactive intermediate.

It is well known that spectra of such anions can be obtained under the conditions of electron attachment mass spectrometry **[39]**. Low energy electrons (2-4 eV) are attached to the molecules and anions are formed according to the following mechanism:

(Resonance capture) $$AB + e^- \rightarrow AB^{\bullet -} \quad (2\text{-}1)$$

(Dissociative resonance capture) $$AB + e^- \rightarrow A^- + B^{\bullet} \quad (2\text{-}2)$$

(Ion attachment) $$AB + C^- \rightarrow ABC^- \quad (2\text{-}3)$$

where AB represents a molecule and C^- is an anion. Kadjas proposed that these radical anions would readily react with positively charged spots on the rubbing surface. A good example of the model will be presented later, with disulphide to form anions [37].

Exoelectron work up to publication of the paper has been largely speculative, although recent experimental studies by Nakayama [40,41] have described an *in-situ* technique to monitor electron transfer. If the exoelectron effect is significant in determining chemical boundary film formation, the applied potential is likely to induce similar effects to produce the chemical properties of boundary films.

2.3.4 Theory of potential repulsion effect

It has been suggested that electrochemical potential (*i.e.*, applied electrode potentials for electronic conductors and / or surface potentials dependent on solution composition, for dielectric or conducting materials) may influence friction via its effect on double layer electrostatic repulsion [31]. The theoretical background to this concept is described below.

2.3.4.1 Van der Waals interaction pressure

The van der Waals pressure (P_A) between two parallel plates is given by [42]:

$$P_A = -\frac{A_H}{6\pi H^3} \tag{2-4}$$

where A_H is the effective Hamaker constant, and H is the distance between two plates. This adhesive effect should always be present in contacts, but is very short range and is only significant for separations less than about 2 nm. It has been considered previously in contact mechanics models in tribology [43].

2.3.4.2 Electrostatic interaction pressure

The electrostatic interaction pressure (P_R) between two parallel plates for low surface potentials ($\Psi_0 < 25$ mV) relative to the bulk solution, is given by [42,44]:

$$P_R = -\frac{\varepsilon\kappa^2}{2}\cos ec(\kappa H)[(\Psi_{01}^2 + \Psi_{02}^2)\cos ec(\kappa H) - 2\Psi_{01}\Psi_{02}\coth(\kappa H)] \tag{2-5}$$

where ε is the permittivity of the solution media, ψ_{01} and ψ_{02} can be viewed as the effective surface potentials of plates 1 and 2, respectively, and κ is the reciprocal Debye length, given by:

$$\kappa = \sqrt{\frac{2Le^2I}{\varepsilon_0\varepsilon_r k_B T}} \tag{2-6}$$

where I is the ionic strength of the solution, L is an Avagadro's constant, k_B is the Boltzmann constant, ε_0 and ε_r are the vacuum permittivity and relative permittivity, respectively.

2.3.4.3 Total surface interaction pressure

The total inter-surface pressure is then:

$$P_{total} = P_A + P_R \tag{2-7}$$

Kelsall and Spikes **[45]** used the Deryaguin, Landau, Verwey and Overbeek (DLVO) theory **[42]** to calculate the surface potential and separation distance dependence of the total inner-surface pressure (shown in Fig.2.6) of two parallel Fe_2O_3 plates in 0.02 M aqueous Na_2SO_4.

At surface potentials > 40 mV, inter-surface repulsion was predicted at separations of 1 to 8 nm due to electrostatic interactions, whereas van der Waals attraction predominated at lower potentials.

2.3.4.4 Effect of inter-surface pressure on friction coefficient

The friction coefficient is generally defined as:

$$\mu_f = \frac{F_f}{R_f} \tag{2-8}$$

where F_f is the friction force and R_f is the normal reaction force. Classically, the normal force is taken as equal to the applied load, but if double-layer interactions are significant, then:

$$R_f = W + P_{surf} \times A_{eff} \tag{2-9}$$

BICL LONDON UNIV.

where W is the applied load and P_{surf} is the average interface pressure defined as:

$$P_{surf} = \frac{P_1 + P_2 + P_3 + \cdots + P_n}{n} \tag{2-10}$$

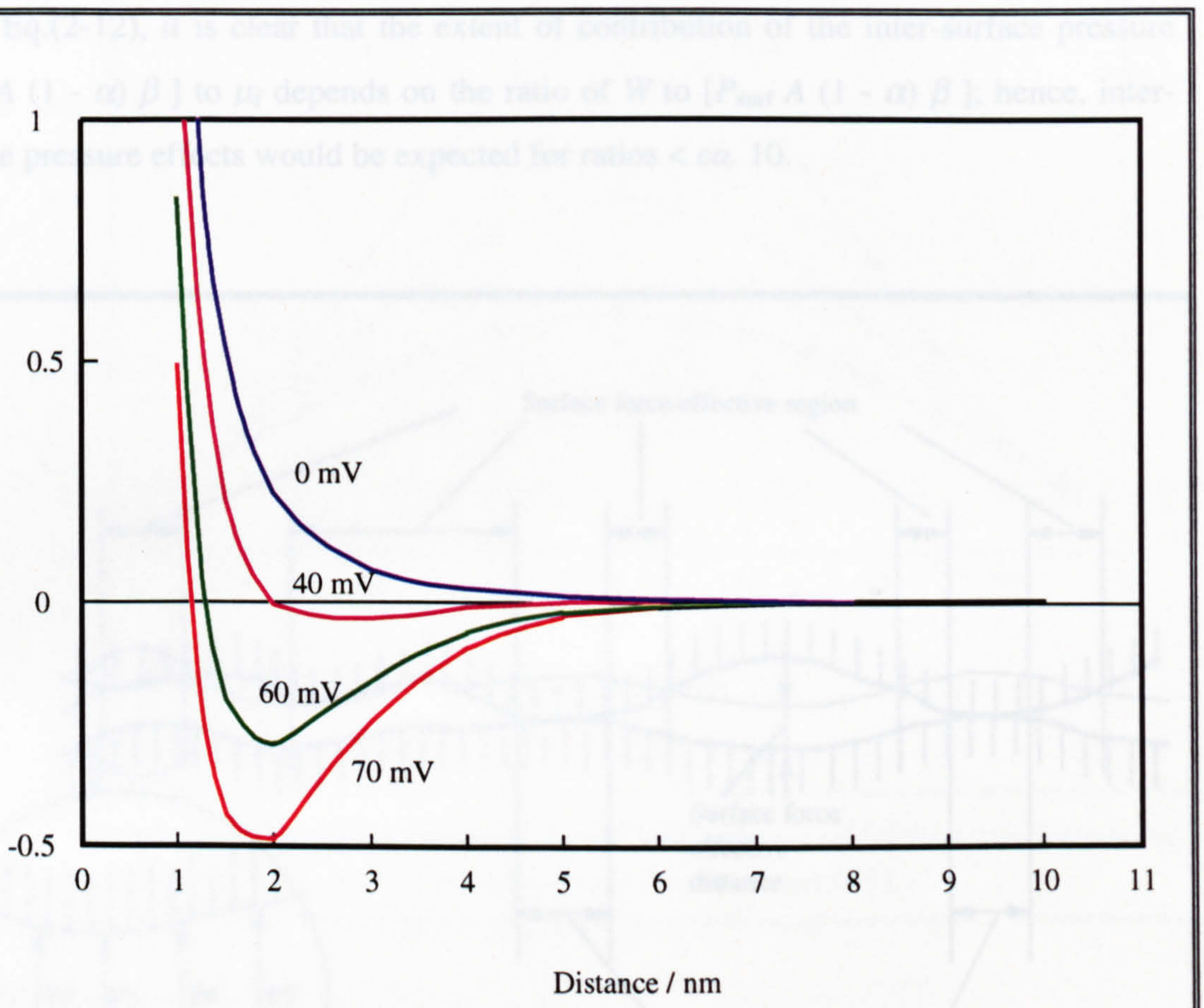


Fig.2.6 Theoretical net internal pressure between two flat surfaces of Fe_2O_3 separated by an electrolyte as a function of surface potential **[45]**.

A schematic diagram of the rubbing contact region is shown in Fig.2.7.

A_{eff} is the total effective surface area between the two plates defined as:

$$A_{eff} = A(1-\alpha)\beta \tag{2-11}$$

where A is the apparent rubbing contact area and α is the ratio of real contact area to the geometric contact area. β is the ratio of the effective area over which inter-surface forces are significant, to the total gap area. Therefore,

$$\mu_f = \frac{F_f}{W + P_{surf} \times A(1-\alpha)\beta} \tag{2-12}$$

α and β can be calculated using a model surface geometry of hemispherical asperities **[46]**.

From Eq.(2-12), it is clear that the extent of contribution of the inter-surface pressure [P_{surf} A (1 - α) β] to μ_f depends on the ratio of W to [P_{surf} A (1 - α) β]; hence, inter-surface pressure effects would be expected for ratios < *ca.* 10.

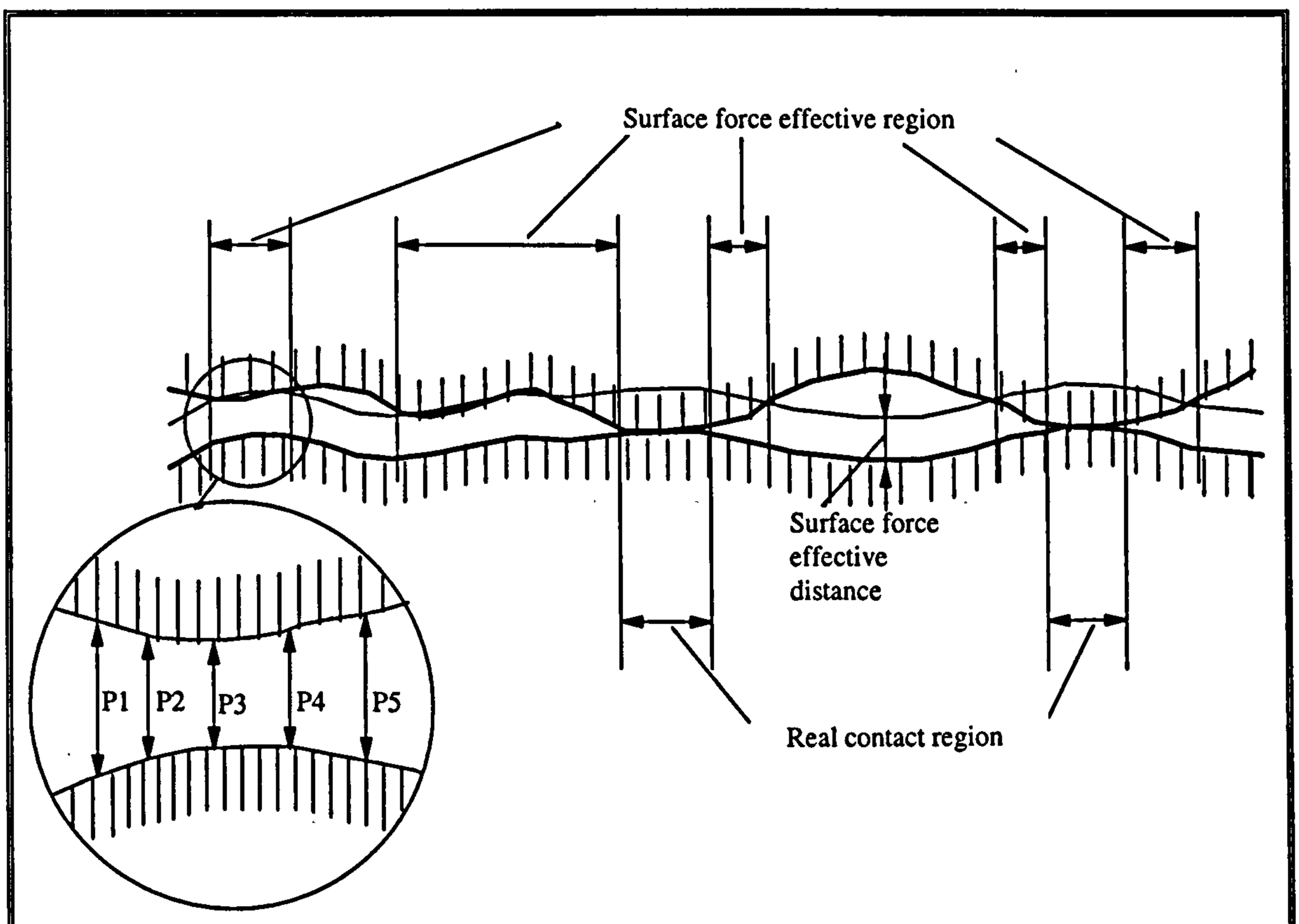


Fig.2.7 Schematic rubbing contact region between two surfaces.

The calculated relationship between friction coefficient and surface potential is shown in Fig.2.8, which indicates that inter-surface forces should influence the friction coefficient between Fe_2O_3 plates in aqueous solutions if the pressure due to applied load is less than ten times the pressure due to electrostatic repulsion.

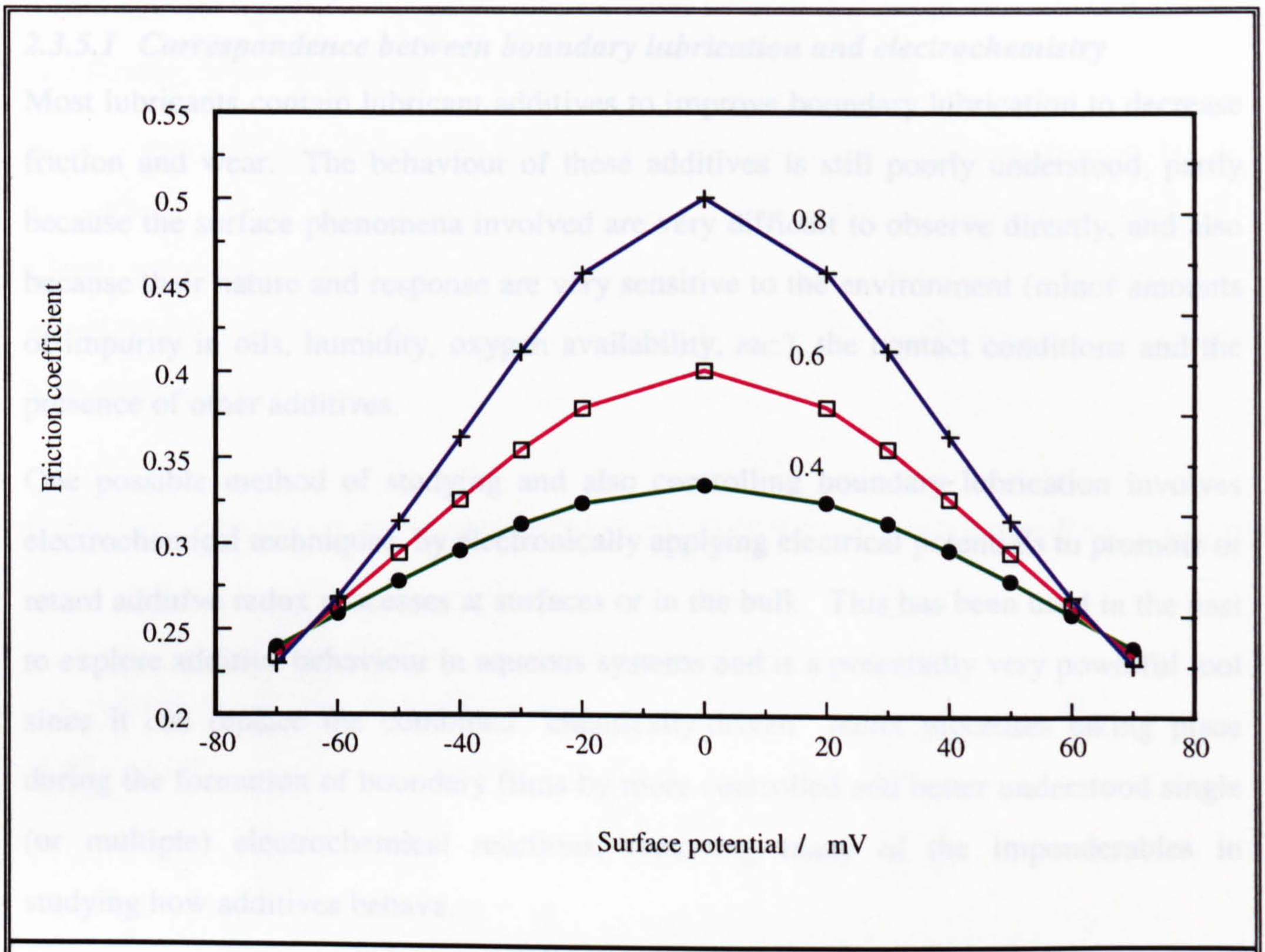


Fig.2.8 Theoretical influence of surface potential dependence of friction coefficient for different values of β from Eq.(2-9), the effective area of contact **[45]**.

2.3.5 Potential effect on redox process for boundary lubrication

Boundary lubrication, in which chemically-active species in the lubricant interact with the rubbing surfaces by redox processes, is arguably the most important and certainly the least well understood of the lubrication regimes. No mathematical model has yet been generally accepted for this regime.

2.3.5.1 Correspondence between boundary lubrication and electrochemistry

Most lubricants contain lubricant additives to improve boundary lubrication to decrease friction and wear. The behaviour of these additives is still poorly understood, partly because the surface phenomena involved are very difficult to observe directly, and also because their nature and response are very sensitive to the environment (minor amounts of impurity in oils, humidity, oxygen availability, *etc.*), the contact conditions and the presence of other additives.

One possible method of studying and also controlling boundary lubrication involves electrochemical techniques, by electronically applying electrical potentials to promote or retard additive redox processes at surfaces or in the bulk. This has been used in the past to explore additive behaviour in aqueous systems and is a potentially very powerful tool since it can replace the combined "chemically-driven" redox processes taking place during the formation of boundary films by more controlled and better understood single (or multiple) electrochemical reactions, removing many of the imponderables in studying how additives behave.

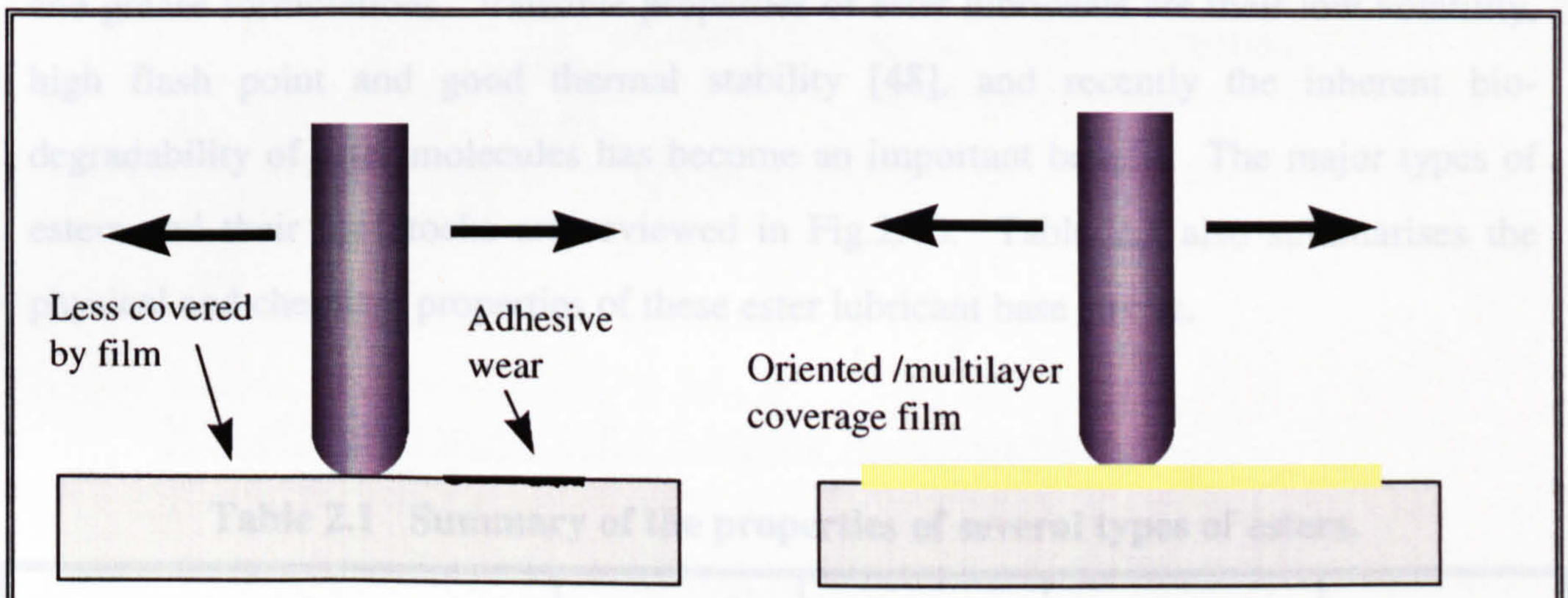
2.3.5.2 Mechanisms of redox process effects on friction and wear

A number of workers have developed mechanisms to explain the influence of applied potential on friction and wear in terms of electrochemically induced redox processes. In these, *e.g.* **[4,6]**, friction and wear response is explained by the formation of surface film of lubricant additives on metal surfaces. The film formed may be retained at the surface due simply to electrostatic interaction with the charged electrode, or may involve additive reaction with the metal surface to form a layer of metal-additive reaction product.

Figure 2.9 represents a schematic illustration of two potential-dependent surfaces, when carboxylic acid is employed as an additive in aqueous solution **[47]**. In Fig.2.9(a), the rubbing metal surface at reducing potentials is insufficiently covered by carboxylic acid, and hence adhesive wear would take place due to the metal-metal contact. Oxidising potentials result in higher carboxylate adsorption densities, which can reduce friction,

and may also cause the chemical reaction of carboxylic acid with the iron surface. This could take the form of a "carpet" of close packed, vertically oriented iron carboxylates, or a thicker, bi- or multi-layer adsorbed film, shown in Fig.2.9(b).

Wear is generally presumed to be dependent on the strength of boundary film formed on the surface. If the protective film is removed easily under rubbing conditions, this allows corrosion to occur within the wear scar. On the other hand, corrosive wear would be decreased if the film were stable enough to prevent metal-metal contact, under high shear strength.



(a) Less adsorption of carboxylic acid at cathodic potentials

(b) Oriented / multilayer coverage film on the rubbing surfaces at anodic potentials.

Fig.2.9 Schematic illustration of two potential dependent surfaces, with pin-on disc type of friction and wear tester.

In such a way, protective film formed on the rubbing surfaces may influence friction and wear. The properties of the film will however, depend strongly upon the electrode potential, type of carboxylic acid, base oil used, temperature and load *etc*.

2.4 Tribology and electrochemistry of organic compounds in this study

This section examines the properties and also electrochemical behaviour of the main lubricant components employed in this study.

2.4.1 Esters

2.4.1.1 Introduction

Esters are one of the most common synthetic lubricants in a wide range of applications, including automotive and marine engine oils, compressor oils, hydraulic fluids, gear oils and grease formulations. Valuable properties of ester lubricants are their low volatility, high flash point and good thermal stability [48], and recently the inherent bio-degradability of ester molecules has become an important benefit. The major types of esters and their feedstocks are reviewed in Fig.2.10. Table 2.1 also summarises the physical and chemical properties of these ester lubricant base stocks.

Table 2.1 Summary of the properties of several types of esters.

	Di-esters	Phthalates	Trimellitates	Polyols
Viscosity at 40 °C / $mm^2 s^{-1}$	6 to 46	29 to 94	47 to 366	14 to 35
Viscosity at 100 °C / $mm^2 s^{-1}$	2 to 8	4 to 9	7 to 22	3 to 6
Viscosity index	90 to 170	40 to 90	60 to 120	120 to 130
Pour point / °C	-70 to -40	-50 to -30	-55 to -25	-60 to -9
Flash points / °C	200 to 260	200 to 270	270 to 300	250 to 310
Thermal stability	Good	Very good	Very good	Excellent
Biodegradability / %	75 to 100	46 to 88	0 to 69	90 to100

Ester groups are polar and will therefore adsorb more strongly on polar metal surfaces than hydrocarbons. This means that they generally have superior lubricity properties compared to mineral oils. Esters can be classified in terms of their polarity or non-polarity by using the following formula suggested by Van der Waal [49]:

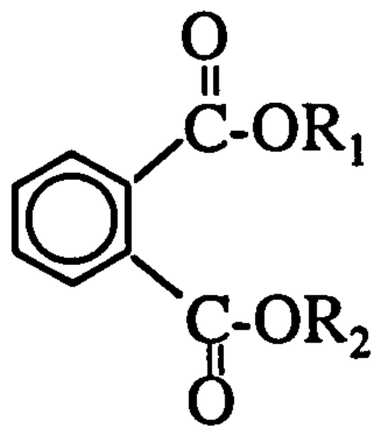
Diesters (dioate)

$R_1OOC\text{-}(CH_2)_n\text{-}COOR_2$

R_1, R_2 = Linear, branched or mixed alkyl chain

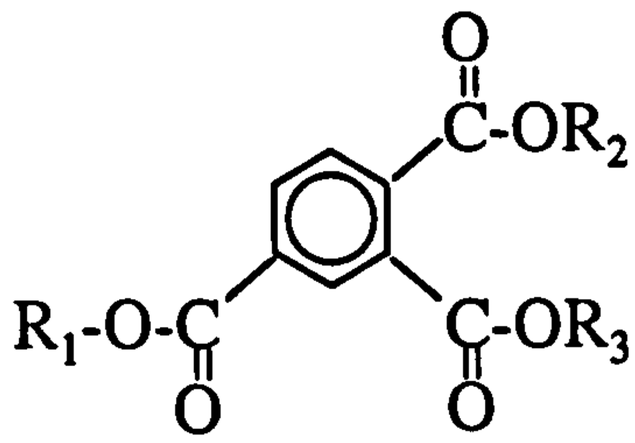
n = 4 : adipates n = 7 : azelates
n = 8 : sebacates n =10: dodecanedioates

Phthalate esters (1,2-benzene dicarboxylate)



R_1, R_2 = linear, branched or mixed alkyl chain

Trimellitate esters (1,2,4-benzene tricarboxylate)



R_1, R_2, R_3 = linear, branched or mixed alkyl chain

Polyols (hindered esters)

$C(CH_2OCOR)_4$	Pentaerythritol esters
$CH_3CH_2C(CH_2OCOR)_3$	Trimethylolpropane esters
$(CH_3)_2C(CH_2OCOR)_2$	Neopentylglycol esters

R = Linear, branched or mixed alkyl chain

Fig.2.10 Ester types and their chemical structures.

$$\text{Non - polarity index} = \frac{\text{Total number of C atoms} \times \text{molecular weight}}{\text{Number of carboxylic groups} \times 100} \quad (2\text{-}13)$$

Generally, the higher the non-polarity index the lower the affinity for the metal surface. Esters terminated by normal acids or alcohols have better lubricities than those made from branched acids / or alcohols, while esters made from mixed acids or alcohols have lubricities intermediately between those of esters of normal acids or alcohols and esters of branched acids or alcohols.

2.4.1.2 Electrochemistry of esters

To be suitable as an organic solvent for electrochemical studies, an ester must possess high polarity, for electrolyte dissolution, and have a wide range of electrochemical potential in which it is stable to oxidation and reduction **[50]**. In practice, esters are usually resistant to electrochemical reduction unless strongly acidic solutions are used, which causes their hydrolysis. When an ester is cathodically reduced in acidic media, the first step leads to an aldehyde, presumably via the hemiacetal:

$$RCOOR' + 2e^- + 2H^+ \rightarrow RCH(OH)OR' \rightarrow RCHO + HOR' \quad (2\text{-}14)$$

If not stabilised by an electro-inactive addition reaction, the aldehyde is then reduced in a second step to form the corresponding alcohol. However, a competing pathway for ester reduction in strongly acidic media is the formation of ethers, sometimes in good yield:

$$RCOOR' + 4e^- + 4H^+ \rightarrow RCH_2OR' + H_2O \quad (2\text{-}15)$$

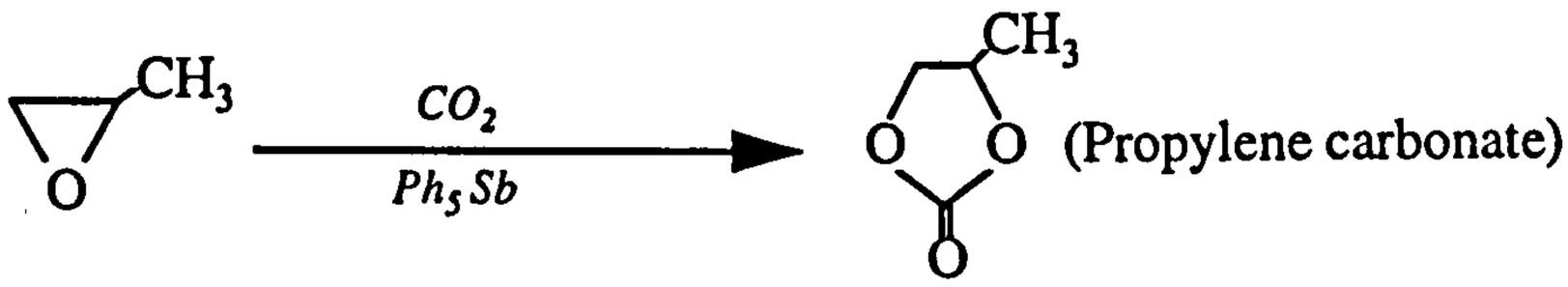
Unsaturated esters, such as α, β-unsaturated and aromatic esters, are reduced relatively easily because of the activating effect of the strongly electron-withdrawing ester group on reduction of the attached unsaturated function. In this case, voltammetric data for ester reductions are available in the literature for several aromatic esters **[51-56]**, and, in particular, cyclic voltammetry shows clearly that reversible formation of anion radicals occurs in the absence of proton donors **[57]**.

2.4.2 Carbonate esters

2.4.2.1 Introduction

Carbonate esters which have a basic chemical structure, R_1-O-CO-O-R_2, have recently received attention as possible new refrigerant lubricants compatible with HFC-134a. This is because of their miscibility with HFC-134a, low vapour pressure, relatively low toxicity and especially high chemical stability against production of carboxylic acids via hydrolysis, unlike normal esters. Carbonate esters are generally expected to show good lubricity because they have relatively high polarity, which is dependent on the type of R_1 and R_2, and therefore will adsorb more strongly on polar metal surfaces than mineral oils. However, like di-esters, carbonate esters are generally less efficient for lubricity than base oils containing friction modifiers or anti-wear additives.

On the other hand, carbonate esters are as one of the most popular group of aprotic solvent **[50]** for electrochemistry. A good example is propylene carbonate (PC), **[58]** which has a high dielectric constant ($\varepsilon = 69$), a wide liquid range (-49 to 242 °C), and readily dissolves many organic compounds, as well as some inorganic salts. PC is generally formed by the following organic reaction **[59]** to give high yields without the use of toxic gas:

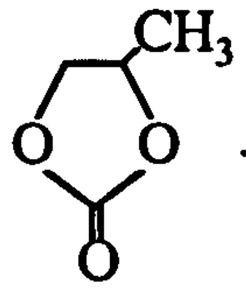


(2-16)

2.4.2.2 Electrochemistry of propylene carbonate

Hitherto PC has been used mostly for electrochemical generation of cation radicals **[60]**, because its potential limit for anodic reaction is relatively higher than those of other organic solvents. Above the anodic-limiting potential, PC can be decomposed to carbon dioxide (CO_2), which has been detected by mass spectrometry, and probably simultaneously forms polymers on the electrode surface **[61]**. The cathodic-limiting

reaction of PC containing $LiClO_4$ has been reported **[62,63]** as the formation of propene and carbonate ions, as follows:



$$+ 2\,e^- \longrightarrow CH_3\text{-}CH{=}CH_2 + CO_3^{2-} \qquad (2\text{-}17)$$

The coulombic efficiency of reaction (2-17) may be determined by measurement of the gas evolution rate **[62]**. If $LiClO_4$ is used as a supporting electrolyte, the carbonate ions formed by reaction (2-17) results in the stoichiometric formation of insoluble Li_2CO_3 **[61]**.

2.4.3 Disulphides

2.4.3.1 Introduction

If excessive mechanical stress either removes metal surface films, or wears away the metal, together with its adsorbed films, a surface is produced which contains areas of unoxidised or under-oxidised metal which is very prone to adhesion to the counterface and consequent scuffing. This adhesion can be prevented by the formation of low shear strength reaction films, and these films are provided by reactions of the metal surfaces with chemicals, which are so-called "extreme-pressure additives" **[64]**.

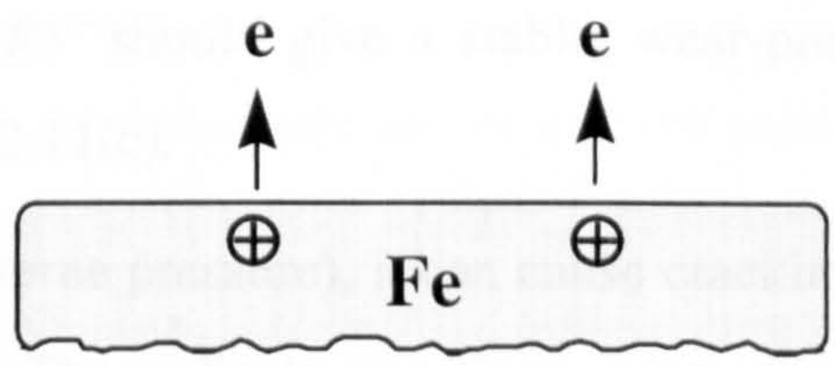
Organic disulphides are one of the commonest additives for this purpose because the S-S bond tends to break easily under severe mechanical stress or high temperature, and the resistant species react quickly with unoxidised or under-oxidised metal. When a disulphide is used, its mechanism of action has been explained in terms of the production of iron mercaptide $Fe(SR)_2$ **[65]**.

2.4.3.2 Mechanisms of action of disulphides with exoelectrons

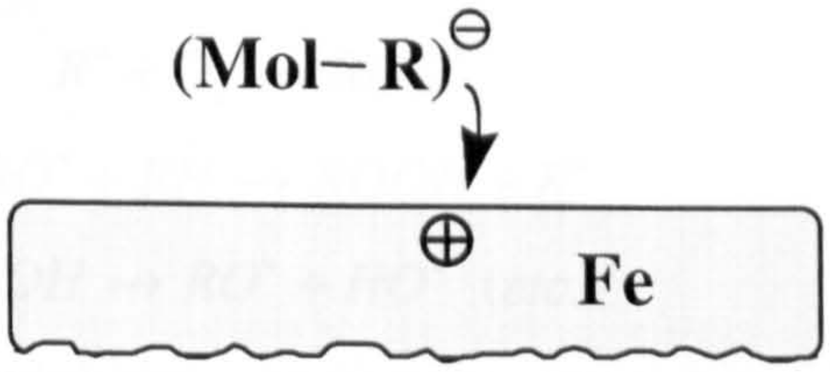
Kajdas proposed an action mechanism of organo-sulphides based on the concept of exoelectron emission **[37]**. In his model, additive molecules form negative ions which

are then chemisorbed on the positively charged areas of the rubbing metal surface. The following stages were considered:

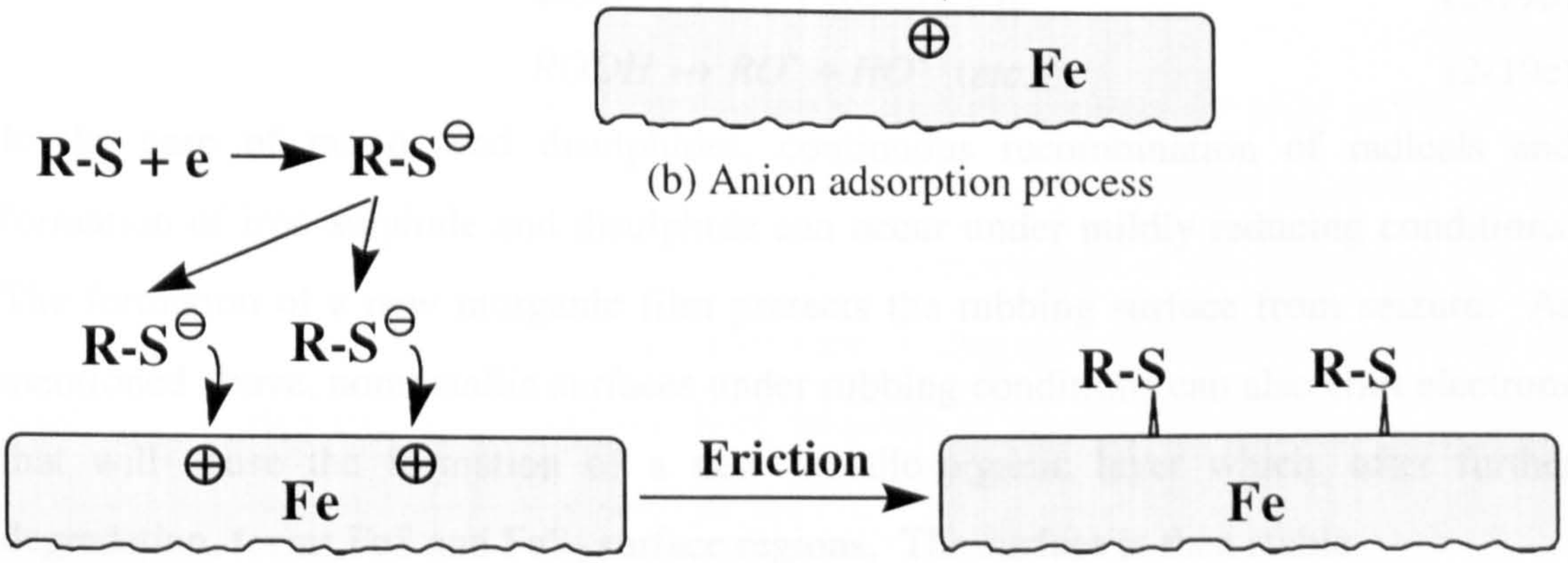
1. Low-energy (2–3 eV) electron emission creates positively charged spots, generally on asperities of metal surfaces, as shown schematically in Fig.2.11(a).



(a) Electron emission process



(b) Anion adsorption process



(c) Wear-preventing film forming process by sulphide iron under lubricated condition

Fig.2.11 Mechanism of extreme pressure additives' function involving exoelectron emission.

2. Action of the emitted electrons with additive molecules (or base oil components **[66]**), close to the rubbing surface, causing the formation of negative irons and radicals:

$$Mol + e \rightarrow (Mol - R)^{-} + R^{\bullet} \qquad (2\text{-}18)$$

(*Mol* is an additive molecule)

3. Reaction of negative irons $(Mol-R)^-$ with metal surfaces and other reactions, *e.g.*, radical $R^\bullet$ reactions causing formation of rubbing polymers forming a metallo-organic film, shown in Fig.2.11(b).

According to the above hypothesis, molecules close to the rubbing surfaces form negative ions which then react with positively charged parts of the metal surface. The kinetics of such reactions depend on the susceptibility of the additive molecule to anion formation. For examples, the RS^- should give a stable, wear-preventing film during boundary friction, shown in Fig.2.11(c).

If the shear strength is high (extreme pressure), it can cause cracking of chemical bonds producing further radicals $R^\bullet$. The radicals may form friction polymers and, in the presence of oxygen, they undergo oxidation:

$$R^\bullet + O_2 \rightarrow ROO^\bullet \qquad (2\text{-}19a)$$

$$ROO^\bullet + RH \rightarrow ROOH + R^\bullet \qquad (2\text{-}19b)$$

$$ROOH \rightarrow RO^\bullet + HO^\bullet \ (etc.) \qquad (2\text{-}19c)$$

In the case of mono- and disulphides, continuous recombination of radicals and formation of iron sulphide and disulphide can occur under mildly reducing conditions. The formation of a new inorganic film protects the rubbing surface from seizure. As mentioned above, nonmetallic surfaces under rubbing conditions can also emit electrons that will cause the formation of a new metallo-organic layer which, after further degradation, forms FeS and FeS_2 surface regions. The surface is then stable.

2.4.3.3 Effect of chemical structure on lubricity performance with the above model

It has been reported that extreme pressure (EP) performance of dibenzyl disulphide was much better than that of diphenyl disulphide **[65,67]**. Kajdas explained this difference in terms of the process in Fig.2.11.

Decomposition of sulphides containing benzyl groups results in the formation of both RS^+ ions and $(Ph\text{-}CH_2)^-$ ions. For example, benzyl phenyl sulphide yields PhS^+ and

$(Ph\text{-}CH_2)^-$ ions **[68]**, the latter decomposing further acetylene and $(C_5H_5)^-$ ions by the reaction:

$$(Ph-CH_2)^- \rightarrow (C_5H_5)^- + CH \equiv CH \qquad (2\text{-}20)$$

Acetylene can readily polymerise forming a protective polymer film on the rubbing surfaces.

2.4.3.4 Cathodic reactions of disulphide

The electrochemical reduction of disulphides produces thiolate anions, which may either be protonated, mainly in aqueous solution to give the corresponding mercapto derivative, or react with an appropriate electrophile present, thus creating a new C-S bond in reactions such as (2-21) **[69]**:

$$RS-SR+2e^- \rightarrow 2RS^- \qquad (2\text{-}21a)$$

$$2RS^- + 2H^+ \rightarrow 2RSH \qquad (2\text{-}21b)$$

$$2RS^- + 2R'X \rightarrow 2RS-R' + X^- \qquad (2\text{-}21c)$$

This reaction can be used in chemical synthesis in several ways. An alkyl halide which may be a good electrophile can be added to the solution to form mixed sulphides in high yield; the addition of an acylating agent to the solution results in the formation of thiol esters. If oxygen is bubbled through the solution during electrolysis, sulphinate salts are produced in excellent yield, and the final addition of an alkyl halide to the medium produces sulphones in 80-90% overall yield **[70]**:

$$RS^- + O_2 \rightarrow RSO_2^- \qquad (2\text{-}22a)$$

$$RSO_2^- + R'X \rightarrow RSO_2R' + X^- \qquad (2\text{-}22b)$$

2.4.3.5 Anodic reactions of disulphides

The oxidation products of these compounds depend markedly on the nature of the alkyl or aryl *R* group and the experimental conditions, as illustrated in Fig.2.12 **[71-76]**.

The oxidation of diphenyl disulphide by $AlCl_3$ in CH_2Cl_2 results in the formation of triantherene cation radicals, also shown in Fig.2.12 **[76]**. Cation radicals such as $RS^{+\bullet}-SR$ formed by oxidation of simple dialkyl, diaryl and di-phenyl disulphides are

too short-lived to be observed by voltammetry, although the existence of these species has been confirmed by pulse radiolysis **[71]** and ESR spectroscopy **[72]**.

On the other hand, aromatic compounds containing a disulphide linkage between two peri positions, such as NDS in Fig.2.13, give cation radicals which are sufficiently stable to be observed at the time scale of slow sweep voltammetry **[77]**.

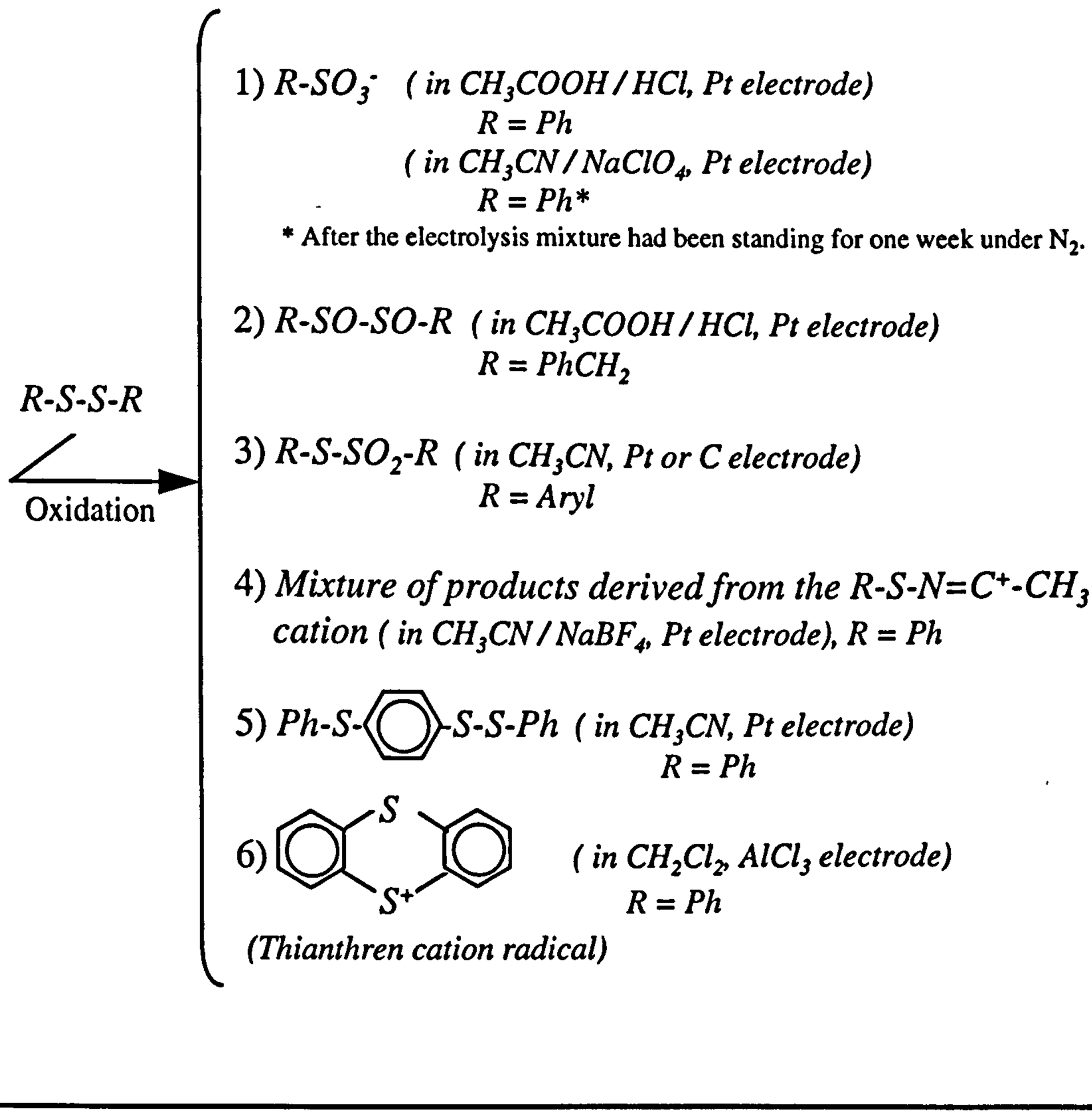
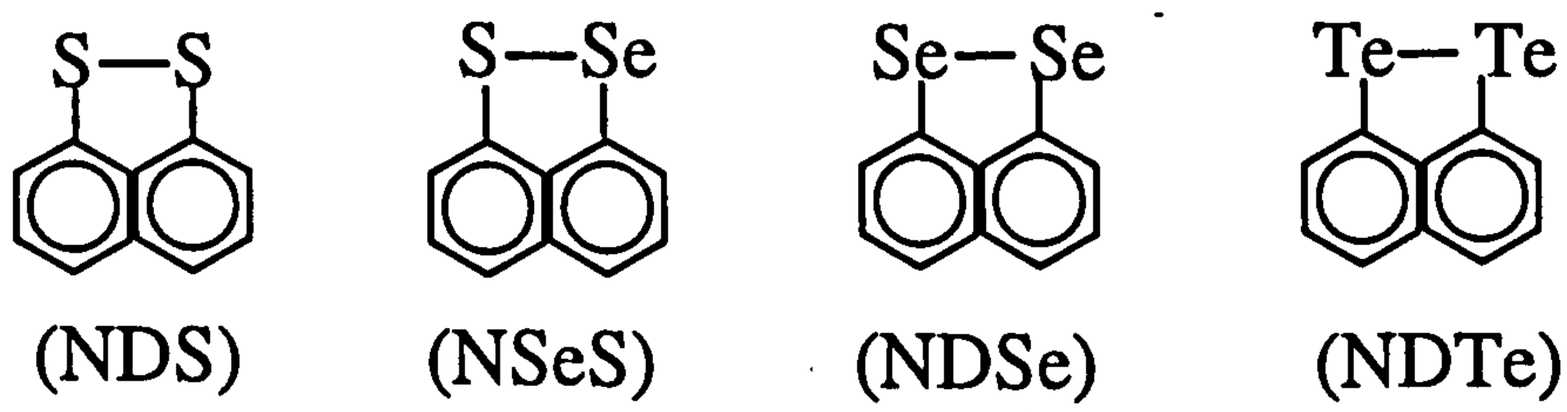


Fig.2.12 Possible electrochemical oxidative reactions of disulphides.

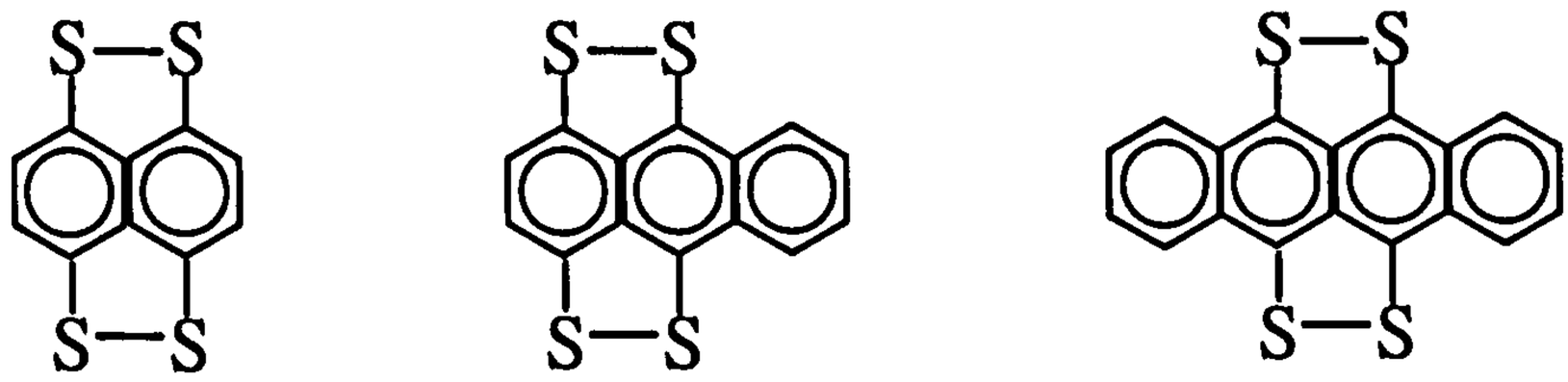
When two disulphide linkages are present in the molecule, as in TTN (see Fig.2.13), even the di-cations are stable **[77,78]**. The magnitudes of the oxidation potentials have been observed to vary with structure as follows:

(1) NDS > NSeS > NDSe > NDTe (2) TTN > TTA > TTT

Fig.2.13 indicates that the substitution of sulphur with the heavier selenium and tellurium, results in compounds that are increasingly more easily oxidised, and that the disulphides derived from extended aromatic systems are easier to oxidise that those derived from less extended aromatic structures.



E_1^{ox}	:	0.86	0.80	0.76	0.45



E_1^{ox}/E_2^{ox}	:	0.55/0.93	0.41/0.85	0.24/0.67

*These oxidation potentials were measured in benzonitrile.

Fig.2.13 Electrochemical oxidation potentials of donor molecules.

2.4.4 Carboxylic acids

2.4.4.1 Introduction

Alkyl carboxylic acids and derivatives are effective friction modifiers, because their adsorption on surfaces results in an adsorbed layer which is hard to compress, but easy to shear. As shown schematically in Fig.2.14, the adsorption is driven by cohesive, lateral van der Waals forces between the vertically-oriented hydrocarbon, and by either electro-static interactions of their anionic head groups with cationic metal sites **[48]** or by chemical reaction between iron oxide and free carboxylic acid or anions.

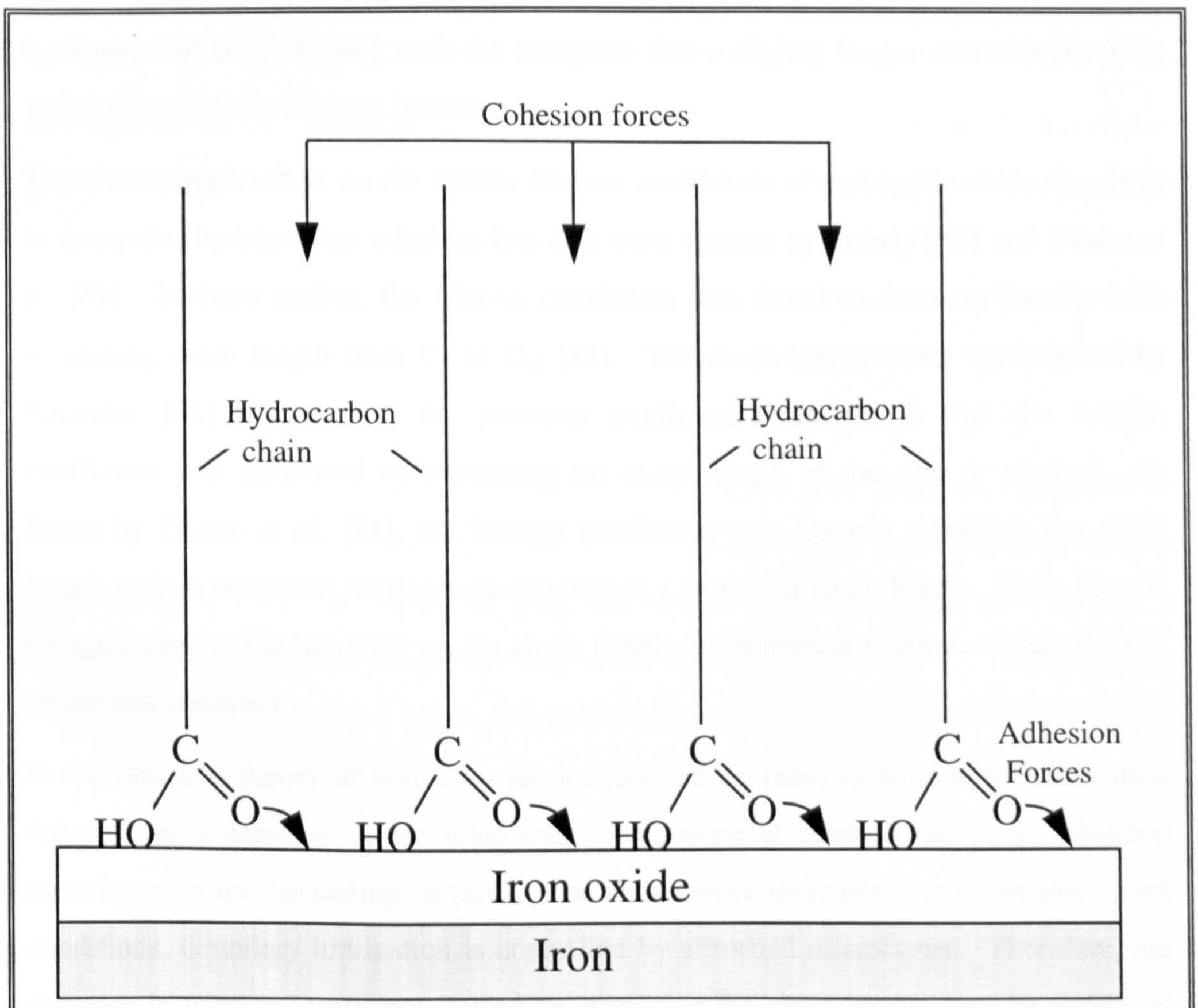


Fig.2.14 Schematic adsorption of carboxylic acids on iron-iron oxide substrate.

2.4.4.2 Effect of chain length of carboxylic acids on lubrication

It has been known for almost a century that the friction coefficient in boundary lubrication is influenced by the chain length and molecular weight of simple polar hydrocarbons such as carboxylic acids, normal alcohols and esters. Both the static and kinetic friction coefficients are lowered by increasing the chain length of its polar compound **[79-81]**.

The effect of chain length on the kinetic friction coefficient was studied by Bowden and co-workers **[81,83]**. The kinetic friction coefficient decreased linearly with the increase in chain length up to C_8 alkyl acid and alcohols. At higher molecular weights, the friction coefficient remained independent of chain length. Similar results were obtained by Murry and Burwell **[84]**, with the exception that a slightly longer chain length (C_{10}) was necessary for minimum friction.

The chain length effect on the kinetic friction coefficient of carboxylic acids dissolved in non-polar hydrocarbon solutions has also been studied by Pomey **[85]** and Okabe *et al.* **[81]**. In these studies, the friction coefficient was found to decrease linearly with increasing chain length from C_6 to C_{18} **[81]**. The chain length effect investigated by Jahanmir **[86]** agreed with the previous published literature, in that the friction coefficient was decreased by increasing the chain length of the acid or alcohol. As found by Okabe *et al.* **[81]**, the friction coefficient was linearly related to the chain length and no minimum friction was obtained at a particular chain length. Since there is no agreement in the literature on the chain length for minimum friction, it must depend on the test conditions.

In the classical theory of boundary lubrication, the decrease in friction by lubrication arises from a decrease in the total area of metal-metal contact due to an adsorbed monolayer on the contacting surfaces. The above work indicated that under low speed conditions, boundary lubrication is controlled by adsorbed monolayers. Therefore, the decrease in friction coefficient caused by increasing the chain length, may be attributed to the increased lateral cohesive interactions between the adsorbed molecules **[79]**. As is shown in Fig.2.14, these cohesive forces arise from intermolecular chain dispersion

forces, which depend on the number of methylene groups on the adsorbed molecules. Thus, surface films containing longer chain length molecules are more resistant to disruption by the higher temperatures and pressures at the asperity contacts. Hence, the total metal-metal contact area and the friction coefficient will be smaller.

2.4.4.3 Effect of carboxylic acids on forming mono-, or multi-molecular layers

The concept of ordered multi-molecular layers near a metallic surface dates back to the early 20th century **[87]**. However, this has been controversial, and most investigators have assumed that only the primary adsorbed monolayer survives a frictional contact and that other layers, being weakly bonded, will be removed **[88]**. Thus, there is still a question whether multi-molecular layers can be stable in high pressure contact conditions.

Although the EHD lubrication theory suggests that the viscous behaviour is dominated by the properties of the base oil, experimental observations have indicated the presence of long-range effects in EHD lubrication with lubricants containing long-chain polar additives. For instance, Beeck *et al.* **[89]** have shown that the transition to EHD lubrication is affected by long chain polar additives which adsorb strongly on the surface.

Another example was given by Smith and Cameron **[90]**, who observed experimental evidence on the formation of thick (2×10^{-7} m) and viscous layers on the surfaces when a polar compound, *e.g.*, octadecanoic acid, was present in the oil. Extensive evidence exists showing abnormally high viscosity under EHD lubrication **[91]**. The transition from disordered to ordered layers can occur as a result of high pressure under EHD condition.

The stability of thick multi-molecular layers may be affected by the high shear rate in EHD contact. According to Cameron **[92]**, these layers are fragile and do not contribute to the EHD film under high shear rate. Since the rate of shear is dependent upon the sliding speed, ordered multi-molecular layers may be stable only under low speeds, *i.e.*, partial EHD lubrication.

In fact, measurements of the shear properties of deposited multi-layers in the form of linear-alkyl chain carboxylic acids on mica substrates by Briscoe and Evans **[93]** have shown that these layers are extremely durable under low sliding speeds. In addition to being stable at low speeds, multi-molecular layers tend to promote fluid film lubrication **[92]** at speeds lower than the expected speed based on EHD lubrication.

The primary driving force for the formation of ordered multi-molecular layers of long-chain polar compounds is intermolecular dispersion interaction between hydrocarbon chains **[94]**. Thus, the disorientation energy increases with increasing chain length. Differences in the crystallographic structure of multi-layers of fatty acids, depending on their chain length, have been detected by X-ray diffraction on the metal surfaces **[88]**.

Short alkyl chain lengths produced layers with orthorhombic structures, in which carbon chains were normal to the metal surface **[88]**, whereas, with longer alkyl chain acids, the structure of the first mono-layer was orthorhombic, but subsequent layers crystallised into a monoclinic structure and the chains were inclined to the surface. The chain length at which the change in structure was observed depended on the metal substrate.

2.4.4.4 Cathodic reactions of carboxylic acids

The cathodic reduction of carboxylic acids can produce carboxylate anions, aldehydes, alcohols, or the hydrocarbon in a one-, two-, four-, or six- electron reduction process, respectively, as indicated by reactions (2-23) to (2-26), the last three reactions requiring that the proton reduction reaction be avoided (2-23).

$$RCOOH + e^- \rightarrow RCOO^- + \frac{1}{2}H_2 \qquad (2\text{-}23)$$

Iverson and Lund have shown that carboxylic acids may be converted into the corresponding aldehydes if the carbonyl group is activated by an electron-withdrawing group **[95]**. In general, cathodes with high hydrogen overpotentials (*e.g.*, mercury or lead) are used for converting acids to the corresponding alcohols **[95]**.

$$RCOOH + 2H^+ + 2e^- \rightarrow R(OH)_2H \rightarrow RCHO + H_2O \qquad (2\text{-}24)$$

$$RCOOH + 4H^+ + 4e^- \rightarrow RCH_2OH + H_2O \qquad (2\text{-}25)$$

$$RCOOH + 6H^+ + 6e^- \rightarrow RCH_3 + 2H_2O \quad (2\text{-}26)$$

Aliphatic and aromatic acids that are not strongly activated by electron-withdrawing groups and do not contain more easily reducible groups, give well-developed polarographic waves in aqueous **[96]** or non-aqueous **[97]** solvents, but this is usually due to the reduction of protons to hydrogen. For instance, the hydrogen evolution wave for acetic acid reduction in acetonitrile containing 0.1 M tetraethylammonium perchlorate appears at -2.0 V vs. S.C.E.

2.4.4.5 Anodic oxidation reactions of carboxylic acid

Oxidation of alkyl carboxylates with noble metal anodes at high anodic potentials results in the Kolbé electro-decarboxylation reaction **[98]**, by which alkyl radicals couple to give a dimer:

$$2RCOO^- \rightarrow R-R + 2CO_2 + 2e^- \quad (2\text{-}27)$$

Though the Kolbé reaction has a long history in electro-organic chemistry, it is still an important synthetic tool in organic synthesis. Electro-decarboxylation has been studied extensively as a function of solvent **[99-101]**, electrode material **[102,103]**, pH, electrolytes **[104,105]**, *etc.*

For metals such as iron, which form carboxylates at potentials less positive than the potential at which the Kolbé reaction occurs, the following reactions are possible in an aprotic electro-inactive solvent containing carboxylic acid:

(Anode) $$M + xRCOO^- \rightarrow M(RCOO)_x + xe^- \quad (2\text{-}28a)$$

(Cathode) $$RCOOH + e^- \rightarrow RCOO^- + \frac{1}{2}H_2 \quad (2\text{-}28b)$$

Metal carboxylates, $M(R\text{-}COO^-)_x$, which will be discussed in the next section, can be deposited on the working electrode surface, or dissolved into an electrolyte solution.

2.4.5 Metal carboxylate

Metal carboxylates are generally defined as the formula $M(R\text{-}COO^{-})_x$, where "*M*" is a metal in oxidation state "*x*", and "*R*" is an organic radical containing at least 6-7 carbon atoms. The term "metallic soaps" is restricted to salts of fatty acids, *i.e.*, those in which "*R*" is an aliphatic carbon structure.

The lubricating properties of metal carboxylates were noticed as early as 1,400 B.C., when lime soap thickened lubricants were used for the wheels of chariots **[106]**. However actual manufacture of lubricating greases involving lime soap started around 1854. A continuous search for better lubricants for the new and more complex mechanical devices being introduced after the Industrial Revolution, resulted in rapid progress in the field of metal carboxylates **[106]**.

2.4.5.1 Solubility of metal carboxylates in aqueous solution

The solubility of metal carboxylates depends upon many factors, such as temperature, nature of the fatty acid, the presence of some impurities and the nature of their cations. The solubility of some alkali metal carboxylates, such as lithium soaps, in aqueous and alcohol-mixed aqueous solutions have been studied by Mehrotra and his co-workers **[107,108]**. These workers reported **[109]** the solubilities and conductivities of metal carboxylates in aqueous solutions decreased with increasing length of their hydrocarbon chains, as expected.

Atter and Bech **[110]** reported a linear relationship, nearly independent of the nature of the cation in the metal carboxylate, between the pK_{sp} of several metal carboxylates and the number (n) of carbon atoms in the alkyl chain:

$$pK_{sp} = a + bn \qquad \text{(2-29a)}$$

Table 2.2 summarises their pK_{sp} data for several metal carboxylates. Kelsall *et al.* **[111]** calculated a and b values of the above equation for iron carboxylate with the pK_{sp} data of iron carboxylates **[112]**:

$$pK_{sp} = 1.2 + 0.9n \qquad \text{(2-29b)}$$

and calculated the aqueous activity-pH diagram of Fe(II)-octanoic acid, shown in Fig.2.15.

Similar work with ferrosilicides (Fe_xSi) **[113-115]** has been also carried out to investigate the electrochemical behaviour of these materials.

Table 2.2 Values of pK_{sp} of metal carboxylates.

n	H^+	Mg^{2+}	Ca^{2+}	Ba^{2+}
18	14.00 ± 0.17	18.33 ± 0.35	19.69 ± 0.34	1960 ± 0.35
16	12.73 ± 0.02	15.77 ± 0.05	17.42 ± 0.04	17.11 ± 0.06
14	11.29 ± 0.08	13.08 ± 0.17	14.66 ± 0.15	14.15 ± 0.17
13	10.49 ± 0.08	NA	13.30 ± 0.15	NA
12	9.97 ± 0.22	10.48 ± 0.05	12.16 ± 0.04	11.46 ± 0.05
11	9.48 ± 0.09	NA	10.90 ± 0.18	NA
10	8.51 ± 0.08	NA	9.32 ± 0.15	NA
9	8.44 ± 0.03	NA	9.10 ± 0.06	NA

2.4.5.2 Solubility of metal carboxylates in non-aqueous solution

Metal carboxylate of alkali metals, Cr, Mn, Ni, Co, Cu and Fe have been prepared electrochemically in non-aqueous solvents containing various carboxylic acids including long chain fatty acids **[116]**. Small amounts of electrolyte were added to enhance the conductivity of the media to accelerate the formation of the metal carboxylate. Palit and McBain **[117]** studied the solubility of alkali metal soaps in chloroform and propylene glycol, and reported an increased solubility in the mixed solvent mixture.

The solubility of various bivalent metallic soaps in different organic solvents, has been observed to increase at a particular temperature range **[118]**. This temperature was called the critical solution temperature (CST). These workers reported CST values of a number of soaps and found that the zinc soaps were insoluble in benzene due to their CST, but were soluble in dioxane, toluene, etc.

These authors reached the conclusion that the increased solubility at the CST was not due to an alteration in the degree of aggregation of the soap in solution, but resulted

from mesomorphic changes in the solid soaps. Copper and nickel stearates and palmitates were found to be quite soluble in pyridine because they form stable crystalline addition products **[119]**. Cluster complexes are usually insoluble in organic solvents.

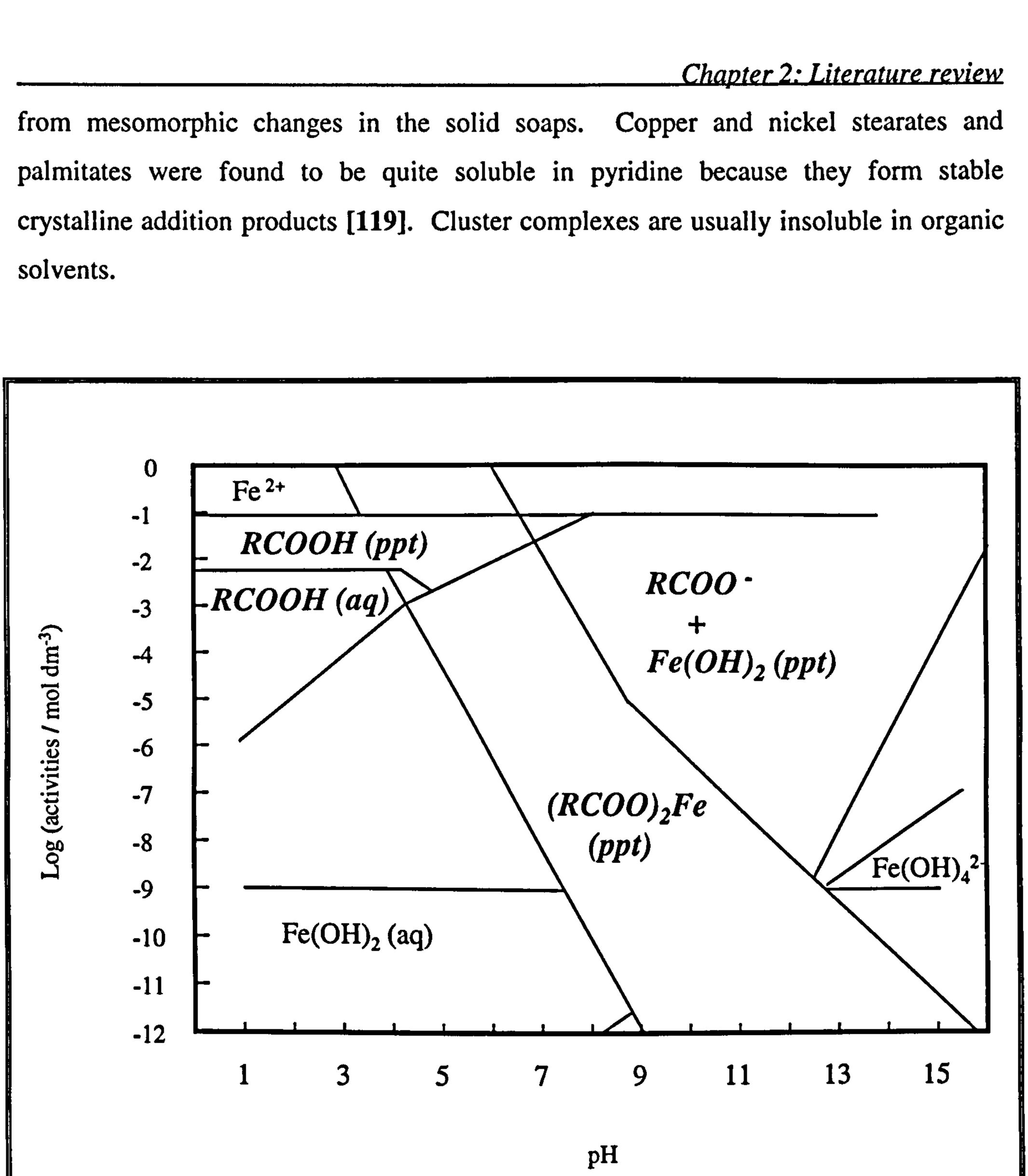


Fig.2.15 Calculated Fe(II)-octanoic acid activity-pH diagram for aqueous solutions.

In general, derivatives of lower carboxylic acids are mostly insoluble or sparingly soluble in non-aqueous solvents, while those of higher carboxylic aids are readily soluble in common organic solvents **[120]**.

2.5 Recent electrochemical studies using aqueous lubricated systems

Potentiostats, developed in the late 1950s, made it possible to study friction and wear of metals under controlled electrode potential conditions, although usually in highly conducting aqueous lubricated systems. This enabled classical electrochemical methods to be employed to tribological systems.

2.5.1 Effect of types of metals on friction and wear

Reports about triboelectrochemical behaviour of aqueous lubricated systems have been concerned mainly with the effect of electrode potential on the corrosive wear of metals **[121-128]**. In all cases, corrosion was shown to make a large contribution to total wear.

2.5.1.1 Behaviour of nickel

Naerheim and Kendig **[121]** reported the influence of applied electrode potential over the range -1.4 to 1.2 V vs. S.C.E. on the wear rate of nickel in aerated 1 M aqueous $NaClO_4$ solution. Wear tests were conducted with a sliding pin (Al_2O_3)-on-disc (nickel) machine. The volume of material removed at each potential was related to the potential *vs.* log(current density) behaviour. A marked increase in wear rate was observed over the potential range -1.0 to -0.2 V vs. S.C.E., attributed to a transition from purely mechanical to mechanical and electrochemical wear mechanisms.

Later, Pearson *et al.* **[122]** suggested that the wear of nickel and of steel in 1 M aqueous $NaClO_4$ solution under controlled electrode potential could be interpreted in terms of the electrochemical formation of an oxide film within the wear scar and its subsequent removal by mechanical action. They also discussed that the potential range over which transitions to an increased wear rate, is related to the Tafel slope associated with metal dissolution reaction.

2.5.1.2 *Behaviour of steel and stainless steel*

El-Raghy *et al.* **[123]** observed that, for a low alloy steel in NaCl and NaOH solutions, pure mechanical wear progresses towards a process of both mechanical wear and electrochemical corrosion with increasingly oxidising applied potential. Their observations for 18Cr-10Ni stainless steel **[124]** indicated that the transition potential is a function for wear and environmental conditions, particularly pH value. A typical example is shown in Fig.2.16.

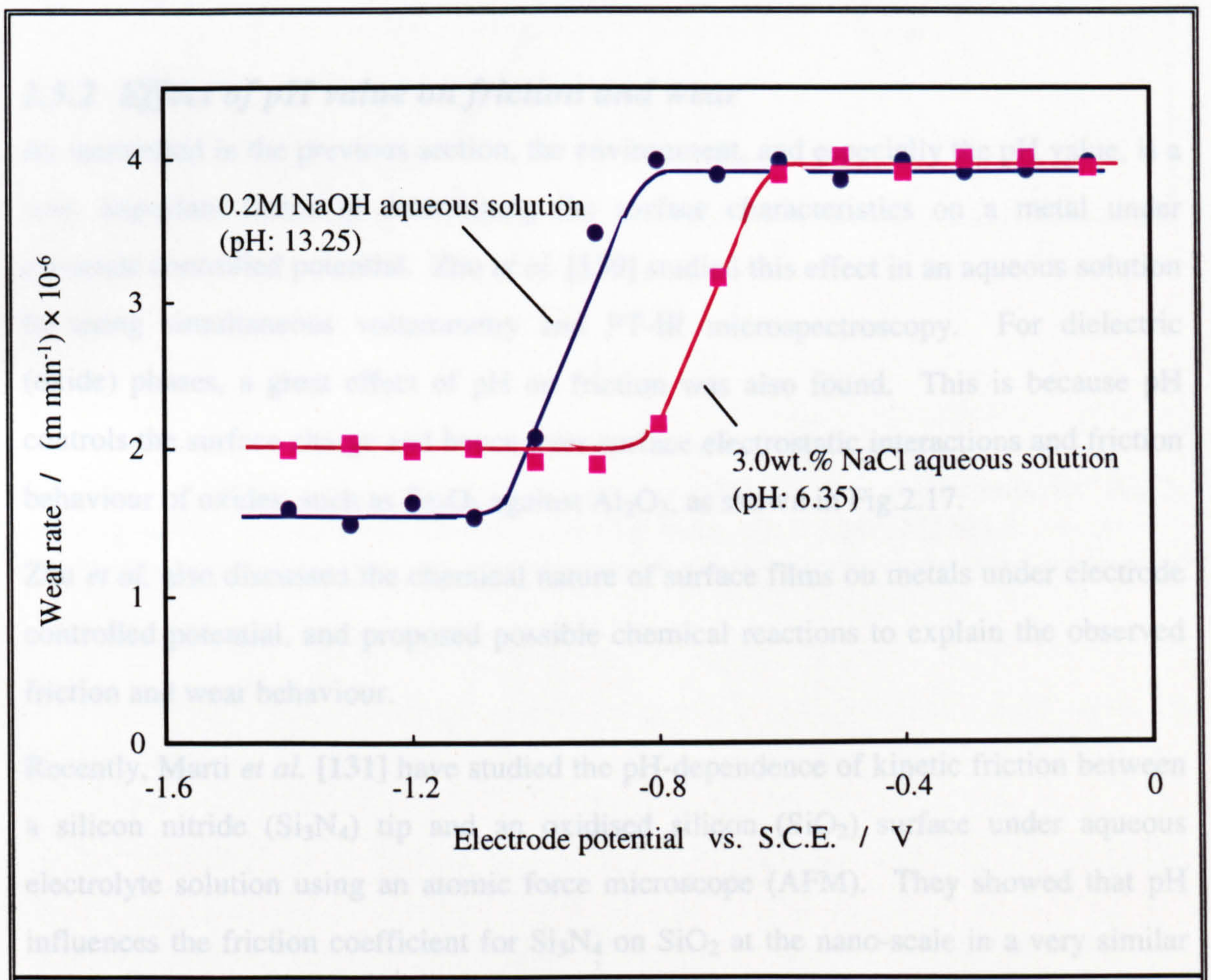


Fig.2.16 Wear rate against electrode potential for 18Cr-10Ni stainless steel in aqueous solutions of different pH, at a load of 71.6 g cm^{-2}.

Brigham **[125]** modified a four ball apparatus to allow electrode potential control, and observed maximum friction between type 302 stainless steel balls in an aqueous solution with 0.3 M Na_2SO_4 and 0.05 M NaCl as supporting electrolytes, at a potential of around -0.2 V vs. S.H.E. He also suggested that the stability of metal against crevice corrosion could be related to the resistivity of the hydrogen evolution reaction in the crevice.

Other tests have been carried out into the corrosive wear of cast iron in sulphuric acid **[126]**, die steel in sodium sulphate **[127]**, mild steel in sodium octanoate **[128,47]** and mild steel in drilling mud **[129]**.

2.5.2 Effect of pH value on friction and wear

As mentioned in the previous section, the environment, and especially the pH value, is a very important factor in determining the surface characteristics on a metal under electrode controlled potential. Zhu *et al.* **[130]** studied this effect in an aqueous solution by using simultaneous voltammetry and FT-IR microspectroscopy. For dielectric (oxide) phases, a great effect of pH on friction was also found. This is because pH controls the surface charge and hence inter-surface electrostatic interactions and friction behaviour of oxides, such as Fe_2O_3 against Al_2O_3, as shown in Fig.2.17.

Zhu *et al.* also discussed the chemical nature of surface films on metals under electrode controlled potential, and proposed possible chemical reactions to explain the observed friction and wear behaviour.

Recently, Marti *et al.* **[131]** have studied the pH-dependence of kinetic friction between a silicon nitride (Si_3N_4) tip and an oxidised silicon (SiO_2) surface under aqueous electrolyte solution using an atomic force microscope (AFM). They showed that pH influences the friction coefficient for Si_3N_4 on SiO_2 at the nano-scale in a very similar fashion to that described above with macro-contacts. This study also showed that there was a strong correlation over the pH range 3.5 to 8.5 between friction measurements using AFM and the adhesive hysteresis observed using normal force AFM measurements. This lends support to a recent model of boundary friction based upon the concept that the energy dissipation process involves adhesion hysteresis **[132]**.

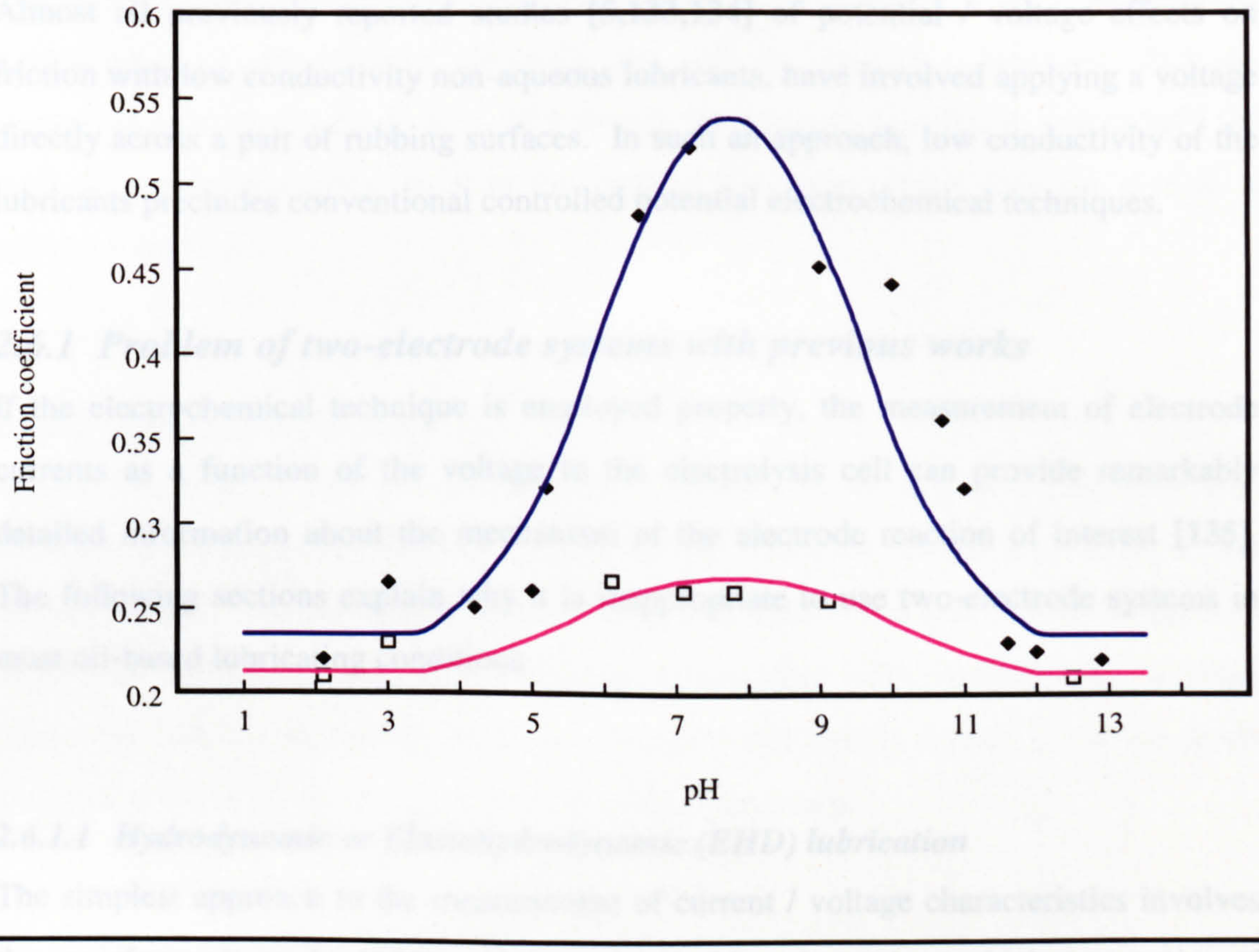


Fig.2.17 Comparison of theoretical and measured friction coefficients for Al_2O_3 rubbing on Fe_2O_3 at different pH values (◆: 2.6 MPa, □: 7.8 MPa) **[130]**.

2.6 Recent studies using non-aqueous lubricated systems

Almost all previously reported studies **[5,133,134]** of potential / voltage effects on friction with low conductivity non-aqueous lubricants, have involved applying a voltage directly across a pair of rubbing surfaces. In such an approach, low conductivity of the lubricants precludes conventional controlled potential electrochemical techniques.

2.6.1 Problem of two-electrode systems with previous works

If the electrochemical technique is employed properly, the measurement of electrode currents as a function of the voltage to the electrolysis cell can provide remarkably detailed information about the mechanism of the electrode reaction of interest **[135]**. The following sections explain why it is inappropriate to use two-electrode systems in most oil-based lubricating conditions.

2.6.1.1 Hydrodynamic or Elastohydrodynamic (EHD) lubrication

The simplest approach to the measurement of current / voltage characteristics involves the use of two electrodes **[136]**, one being the working electrode at which the reaction of interest occurs, and the other is a reference-counter electrode which should provide a counter-reaction to that of the working electrode, as shown schematically in Fig.2.18 for ball-on-plate type friction tester. In EHD lubricating conditions, a thin oil film is present between two electrodes **[137]**. The total cell voltage (U) of such an electrochemical cell is related to the Faradaic current (I) by:

$$U = E_a + \eta_a + E_c - \eta_c + \sum_i \frac{Id_i}{\overline{\sigma}_i A_i} \qquad (2\text{-}30)$$

where E signifies a thermodynamic potential against an appropriate reference electrode, η the overpotential, providing the driving force for electrochemical reaction, dependent on the current density, at anode (a) and cathode (c), A_i the area and d_i the distance of the current path through the ionically-conducting phase(s) i, of mean conductivity $\overline{\sigma}_i$. In

this equation, (E_a + η_a) and (E_c - η_c) are the electrode potentials at the anode and cathode, respectively.

The aim of many electrochemical experiments is to measure I as a function of overpotential at the working electrode, the ball in Fig.2.18. However, with an increasing working electrode area, IR becomes increasingly significant, particularly for high resistivity lubricants, so then the counter electrode cannot function also as a reference electrode.

2.6.1.2 Boundary lubrication

In this lubricating condition, direct metal / metal contact will occur between two electrode materials **[138]**, causing short-circuit electronic currents to flow between the metal surfaces. The currents are not due to the electrochemical reaction on the surface. It can be concluded that two electrode experiments with macroscopic working electrodes will be impossible, since the current is not readily related to the electrode potential at the working electrode (ball) / lubricant interface.

2.6.1.3 Experiments with three-electrode systems

To circumvent this problem, it is usual to conduct electrochemical experiments using a three-electrode system in which the reference and counter electrode functions are separated, as shown schematically in Fig.2.19. In this case, the plate and ball are electronically connected, both function as working electrodes and their electrode potential (E_A) is controlled relative to a reference electrode, by a potentiostat, current flowing only between the working and counter electrodes.

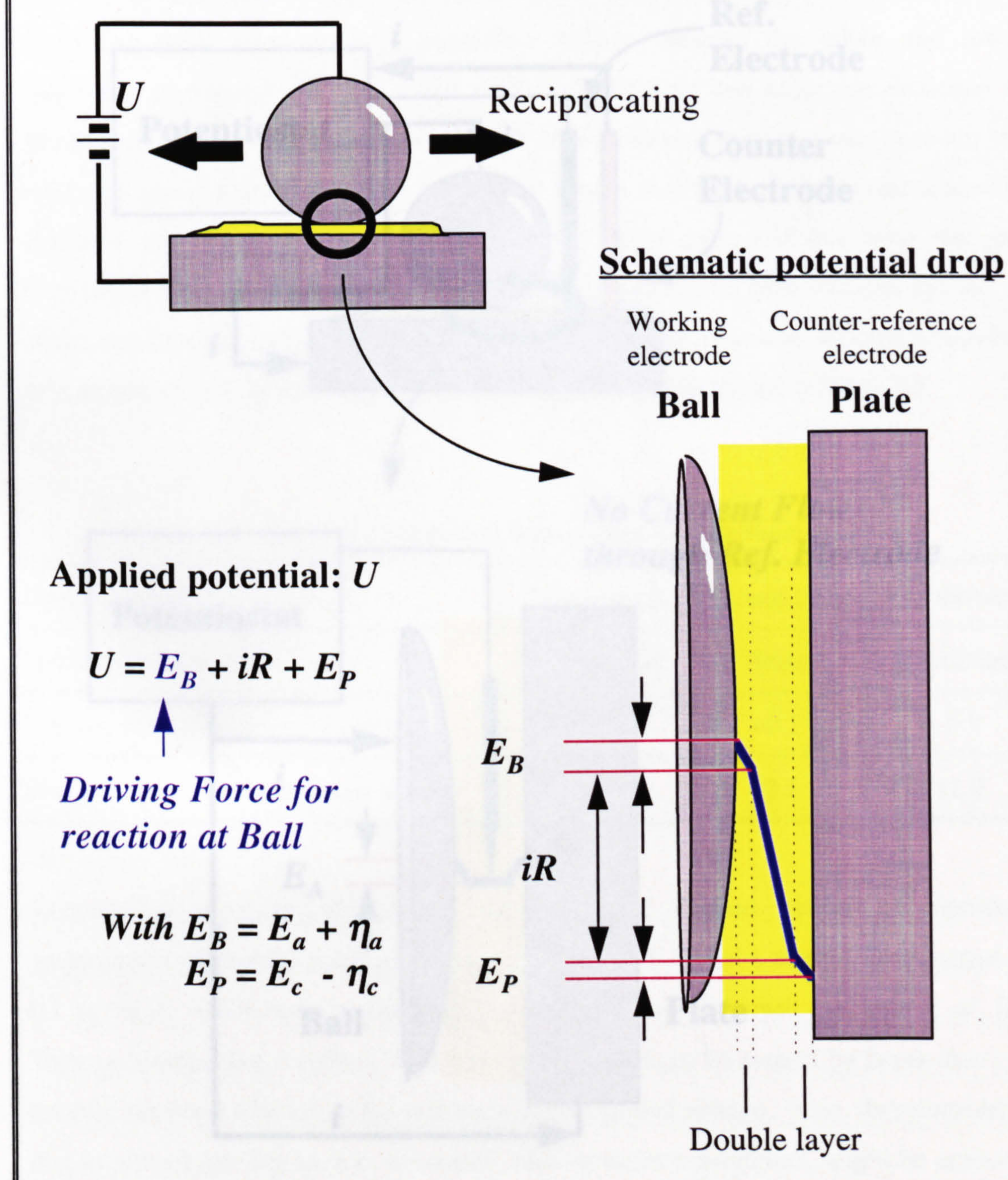


Fig.2.18 Schematic potential drop between ball and plate as a two-electrode system.

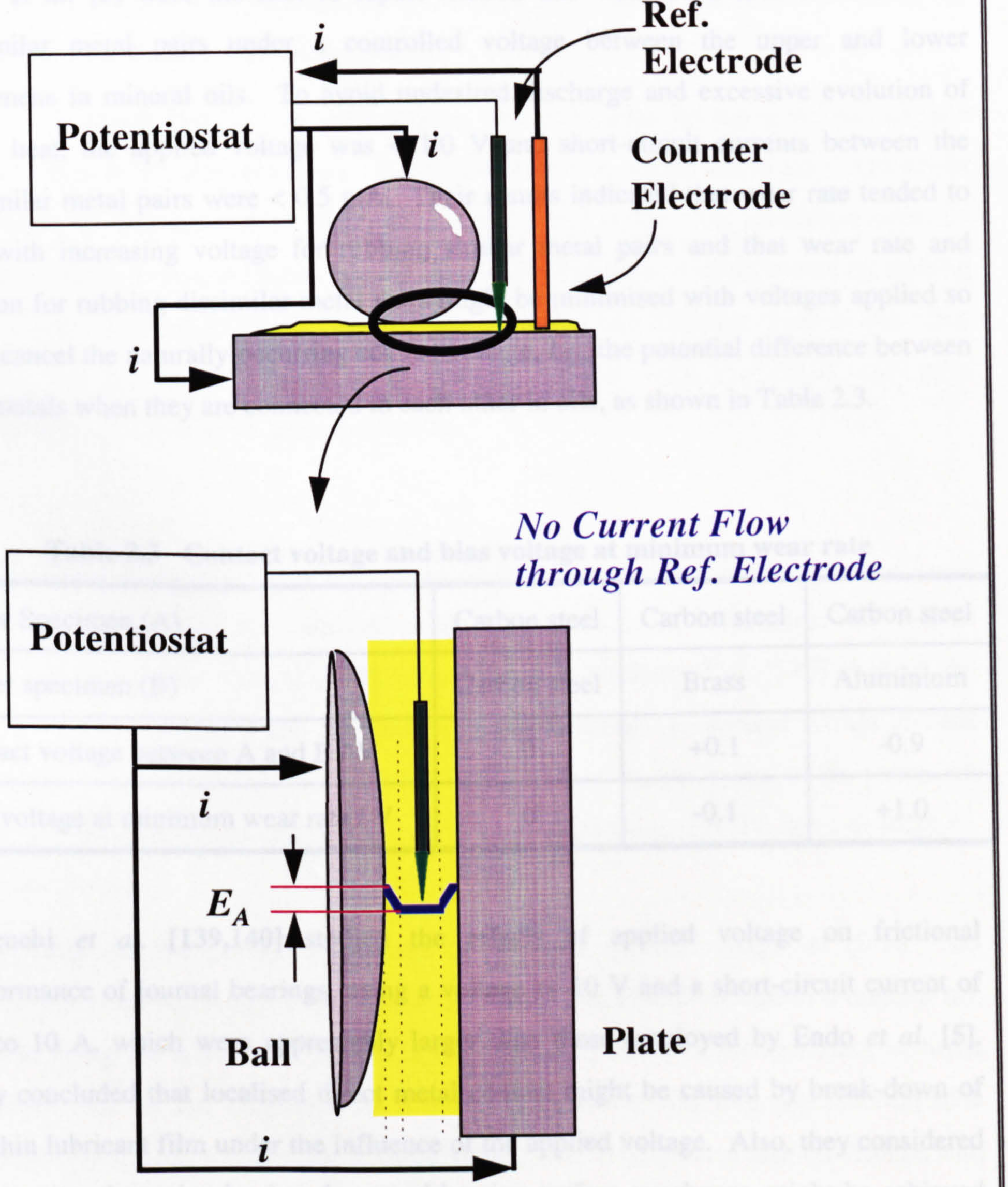


Fig.2.19 Schematic three-electrode system with independent reference electrode.

2.6.2 Using mineral oil as a lubricant

2.6.2.1 Effect of application of voltage on friction and wear

Endo *et al.* **[5]** were the first to report friction and wear behaviour of metals and dissimilar metal pairs under a controlled voltage between the upper and lower specimens in mineral oils. To avoid undesired discharge and excessive evolution of Joule heat, the applied voltage was < 1.0 V and short-circuit currents between the dissimilar metal pairs were < 0.5 mA. Their results indicated that wear rate tended to rise with increasing voltage for rubbing similar metal pairs and that wear rate and friction for rubbing dissimilar metal pairs might be minimised with voltages applied so as to cancel the naturally-occurring contact voltage, *i.e.*, the potential difference between two metals when they are connected to each other in oils, as shown in Table 2.3.

Table 2.3 Contact voltage and bias voltage at minimum wear rate

Upper Specimen (A)	Carbon steel	Carbon steel	Carbon steel
Lower specimen (B)	Carbon steel	Brass	Aluminium
Contact voltage between A and B / V	0	+0.1	-0.9
Bias voltage at minimum wear rate / V	0	-0.1	+1.0

Takeuchi *et al.* **[139,140]** studied the effects of applied voltage on frictional performance of journal bearings, using a voltage of 10 V and a short-circuit current of 0.1 to 10 A, which were appreciably larger than those employed by Endo *et al.* **[5]**. They concluded that localised direct metal contact might be caused by break-down of the thin lubricant film under the influence of the applied voltage. Also, they considered that improved running-in, *i.e.*, decreased bearing surface roughness, might be achieved by promotion of oxide film formation on the shaft by making it the anode under severe lubricating conditions.

Yamamoto *et al.* **[141]** investigated the effect of the applied voltages of -8.0 to 8.0 V on friction and wear performance using a ball / disc friction tester. The test specimens were bearing steel balls (Vickers hardness, Hv 786) and carbon steel disc (Hv 180). With the disc as the anode, the inherently soft steel carbon substrate was protected by a passive surface film of enhanced hardness, so that low friction was achieved, but at the expense of considerable wear of the ball.

It was also found that friction performance was influenced by the dissolved oxygen concentration in the lubricating oil. Yamamoto's results, which are in good agreement with those of Takeuchi *et al.* **[139,140]**, showed that oxide film formation over the rubbing surface in discontinuous contact with another surface, was promoted by making it an anode. Consequently, the surface was protected and abrasive wear of the other surface was promoted, smoothing it quickly, so that both running-in and mild lubricating conditions were achieved rapidly.

2.6.2.2 Effect of application of voltage on additive performance for friction and wear

Adsorption or reaction of additives on rubbing surfaces in lubricating oils is also influenced by applied voltage **[142]**. For example, Morizur *et al.* **[143]** showed the influence of the magnitude and direction of an electric field, *i.e.*, applied voltage divided by a nominal separation distance between metal surface, on the extent of the formation of surface films and wear rate using a paraffin oil containing ZnDTP (zinc di-alkyl di-thio phosphate).

Later, Tung and Wang **[19]** investigated the effect of applied voltages of 10-20 V on friction and wear in tool steel ball / disk type tests with ZnDTP added to a mineral oil, the disc being the anode. As shown in Fig.2.20, their results indicated that disc wear decreased due to the formation of a yellow protective film and that friction also decreased by 35 %, whereas the applied voltage had negligible effect on friction and wear in the absence of ZnDTP.

Tung and Wang **[144]** also showed that lower friction and wear performance in mineral oil resulted from pre-treating steel by the application of external voltages against a counter electrode in phosphoric acid-blended oils. This indicated that the iron

phosphate coatings could be deposited with phosphoric acid-blended oils by application of the voltage, and this formation of coatings resulted in low friction and wear.

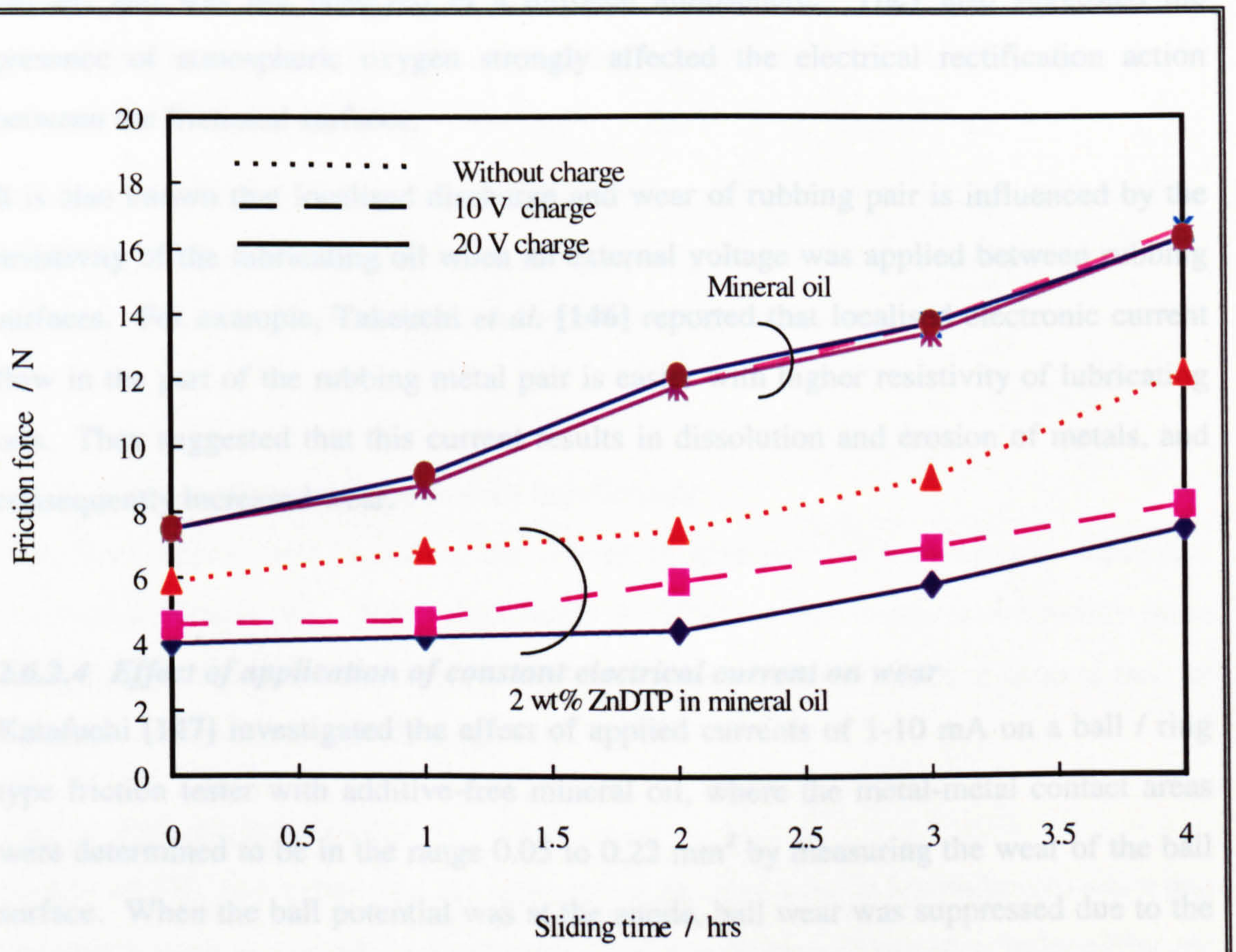


Fig.2.20 Comparison of sliding friction between steel surfaces uncharged and *in-situ* charged at 20 V, with / without ZnDTP in mineral oil **[19]**.

2.6.2.3 Effect of application of voltage on lubricating film properties

When oil film thicknesses between two rubbing surfaces are very small, electron tunnelling and dielectric break-down through the film must be considered when external voltages are applied. According to Kawamura **[145]**, electron tunnelling is negligible for oil film thicknesses > 0.5 nm between a pair of opposing surfaces, and dielectric break-down under the application of external voltage of 0.1 V will occur when the oil film thickness is < 2.0 nm, *i.e.*, the length of a typical lubricating oil molecule.

Katafuchi and Takano **[17]** found evidence of electrical rectification in current-voltage curves obtained by the application of an external voltage between a pair of rubbing steel surfaces, lubricated by mineral oil. However, this phenomenon was observed only in the air, and was not observed in a nitrogen atmosphere. They also suggested the presence of atmospheric oxygen strongly affected the electrical rectification action between the frictional surfaces.

It is also known that localised discharge and wear of rubbing pair is influenced by the resistivity of the lubricating oil when an external voltage was applied between rubbing surfaces. For example, Takeuchi *et al.* **[146]** reported that localised electronic current flow in the part of the rubbing metal pair is easier with higher resistivity of lubricating oils. They suggested that this current results in dissolution and erosion of metals, and consequently increased wear.

2.6.2.4 Effect of application of constant electrical current on wear

Katafuchi **[147]** investigated the effect of applied currents of 1-10 mA on a ball / ring type friction tester with additive-free mineral oil, where the metal-metal contact areas were determined to be in the range 0.05 to 0.22 mm^2 by measuring the wear of the ball surface. When the ball potential was at the anode, ball wear was suppressed due to the protective oxide formation. The ball surface also became smooth and exhibited metallic lustre. By contrast, wear was promoted when the ball potential was at the cathode.

This was explained in terms of the insolubility of anodically-formed metal ions in non-polar lubricating oil, resulting in their reaction with oxygen present in the oil to form surface oxide; conversely, cathodic treatment was supposed to result in oxide reduction of the ball. Actually, the ball was in continuous contact with the ring during the test, so the change of the chemical properties on the ball surface could strongly influence wear behaviour.

Goldblatt **[148]** proposed that substantial electronic activation accompanies the surface distress caused during wear. This electronic activation increases the mobility of electrons at the surface and near-surface, and stimulates electron emission from the

metal. As a consequence, electron transfer may occur between metal and adsorbate. This possibility has been supported by the measurement of self-generated voltages between rubbing two iron surfaces under boundary lubrication **[149,150]**. Dissimilar surfaces would be expected to generate voltages when in rubbing contact as inhibiting product layers are removed. Even oxide-covered steel in contact with bare iron would be expected to exhibit potential differences.

Katafuchi **[147]** also discussed the effect of the self-generated voltage, proposed by Goldblatt **[148]**, due to oxidation reactions, giving rise to electron transport processes, between rubbing surfaces under boundary lubricating conditions.

2.6.3 Using other non-aqueous lubricants

Very few studies have examined the triboelectrochemistry of non-aqueous lubricants other than mineral oils. Since such fluids are likely to be simpler and possibly more easily interpreted than mineral oils, the lack of such studies reflects a general lack of rigorous fundamental research in the field.

2.6.3.1 With phosphate ester

Beck *et al.* **[151]** proposed that the major cause of valve wear in hydraulic systems using phosphate ester as a working fluid must be electrochemical corrosion induced by the flow of the working fluid. Later, he reported significant currents in bearings, by using an electrometer connecting two metal surfaces immersed in phosphate ester **[152]**. One surface was the rubbing journal used as a working electrode, and the other one was the same kind of metal separated from the rubbing surfaces, as a counter-reference electrode. This current caused corrosion and electro-polymerisation deposits, and Beck also showed that the current induced by the flow of working fluid, *i.e.*, wear rate, was largely dependent on the electric conductivity of the fluid. Both of his studies were, however, performed to investigate the relationship between redox systems and the electrical current flow due to the rubbing surfaces, without applying external potential.

Yamamoto *et al.* **[18]** showed that applied external voltages across a rubbing ball and ring contact in tricresyl phosphate (TCP), promoted protective film formation (iron

phosphate) to prevent scuffing under severe lubricating condition. However, application of an excessive external voltage (> 100mV) between the surfaces resulted in the decrease of scuffing resistance, as such voltages prevented the formation of surface films.

2.6.3.2 With DMF or acetonitrile

Dubois and Lacaze *et al.* **[153-155]** showed that oxides, polymers or other species electrochemically-deposited on metal surfaces could be detected by the measurement of the friction coefficient of metals such as gold or platinum in DMF with BTAP (benzyltrimethyl-ammonium perchlorate), or in acetonitrile solution with 0.1 M $NaClO_4$. It was a pity perhaps that noble metals were employed as rubbing surfaces in this study, since these are not generally realistic for practical uses in examining tribological phenomena.

2.7 Conclusions

One conclusion that can be drawn at the end of this review is that there is still a lack of work which effectively correlates lubricating properties with electrochemical phenomena for non-aqueous lubricated systems, *i.e.*, investigating the influence of redox systems induced by applying potential. Although many models of redox systems have been proposed, these have not been sufficient to explain the effect of applied potentials on friction and wear, mainly because of poor electrochemical experimentation.

Almost all work in the field has simply studied the effect of applied voltage on friction across a pair of rubbing surfaces because of the low conductivity of non-aqueous lubricants precluding three electrode electrochemical techniques. The selection of an appropriate supporting electrolyte for such lubricants is indispensable to enable carrying out such experiments, as described in the next chapter.

CHAPTER 3

3. Experimental techniques

3.1 Introduction

This chapter describes the main experimental techniques used in this study to measure the effect of electrode potential on the properties of metal surfaces and on friction and wear characteristics. It also describes the techniques and apparatus used to measure film thicknesses under controlled surface-potential.

3.2 Electrochemical techniques

3.2.1 Voltammetry

3.2.1.1 Transport processes in electrochemical system

As electrode reactions involve electron transfer usually at the interface between an electronically conducting solid and an ionically conducting electrolyte, reactants and products have to be transported to and from such interfaces [1]. When the transfer of reactants to, or products from electrodes becomes slow, compared with the inherent electron transfer rate at the interface, the mass transport step in the overall electrode process may limit the reaction rate. It is thus important to be able to predict the mass transport rate to enable the maximum (transport limited) rate of electrode reaction to be calculated.

The flux (N_i) of charged electro-active solute species i with mobility u_i ($u_i = 0$ for uncharged species) to an electrode surface, is due to the vectorial sum of:

a) (first term) their migration in an electric field ($\nabla\phi$);

b) (second term) diffusion in a concentration (C) / activity gradient;

c) (third term) convection due to the local fluid velocity (v):

$$N_i = -u_i C_i \nabla\phi - D_i \nabla C_i + C_i v \tag{3-1}$$

The current density in solution is a vector (i) perpendicular to equipotential surfaces in solution, and according to Faraday's law is given by:

$$i = F\sum_i z_i N_i \tag{3-2}$$

When concentration gradients in the solution can be ignored (*i.e.*, at current densities well below the mass transport limited rate), substitution of Eq.(3-1) into Eq.(3-2) gives:

$$i = -\kappa \nabla\phi \tag{3-3a}$$

where

$$\kappa = F\sum_i z_i u_i C_i \tag{3-3b}$$

Eq.(3-3b) is the specific conductivity of the solution, and where the convective terms sum up to zero by the electro-neutrality requirement:

$$\sum_i z_i C_i = 0 \tag{3-4}$$

The electro-neutrality condition holds in the bulk solution, but is violated in the electric double layer, since the intense electric field across the electrode/electrolyte interface causes a separation of charge between the two phases, although the system as a whole is electro-neutral.

The differential conservation law, Eq.(3-5) arises from a material balance on a small electrolyte volume element:

$$\frac{\partial C_i}{\partial t} = -\nabla N_i \pm H_i \tag{3-5}$$

The last term H_i is the rate of homogeneous chemical reaction involving species i, occurring simultaneously with its electrochemical reaction. This is often zero, so that substitution of Eq.(3-1) into Eq.(3-5), then gives:

$$\frac{\partial C_i}{\partial t} = D_i \nabla^2 C_i - u_i \nabla(C_i \nabla\phi) - v \nabla C_i \tag{3-6}$$

When excess supporting electrolyte is present, the migrational term can be neglected, as can the convection term over short periods. The resulting simplified form of Eq.(3-7) is then Fick's second law, which in one dimension is:

$$\frac{\partial C_i}{\partial t} = D_i \frac{\partial^2 C_i}{\partial x^2} \tag{3-7}$$

With appropriate boundary conditions, this equation can be used, for example, to predict the time dependence of the current transient in response to a step in potential during which a reaction is transport controlled. This indicates that the current will decay linearly with time$^{-0.5}$ over short periods, prior to convective processes contributing to the overall transport rate.

3.2.1.2 Cyclic voltammetry

Cyclic voltammetry is often the first technique employed in an electrochemical investigation, since it is easy to perform and rapidly provides qualitative kinetic information about the system under investigation **[2]**. It can also yield quantitative information, though it is less often used to do so. The experiments are normally conducted in stationary solutions and so rely on diffusion to transport materials to the electrode surface. Assuming that an electrolyte solution contains an electroactive species *A* which can undergo a simple one-electron ($z = 1$) oxidation to form *B*:

$$A(aq) \xrightarrow{k_{ox}} B(aq) + e^-(m) \tag{3-8a}$$

$$B(aq) + e^-(m) \xrightarrow{k_{red}} A(aq) \tag{3-8b}$$

The time dependence of the mass transport of the species *A* to the electrode can be predicted using Eq.(3-7):

$$\frac{\partial C_A}{\partial t} = D_A \frac{\partial^2 C_A}{\partial x^2} \tag{3-9}$$

The potential of the working electrode is swept from an electrode potential E_1 at which *A* cannot undergo oxidation, to a potential E_2, at which electron transfer is driven rapidly, then the scan direction is reversed and the potential scanned back to the original value, E_1, as shown in Fig.3.1. This gives a triangular-shaped potential cycle and the technique is termed *cyclic voltammetry*.

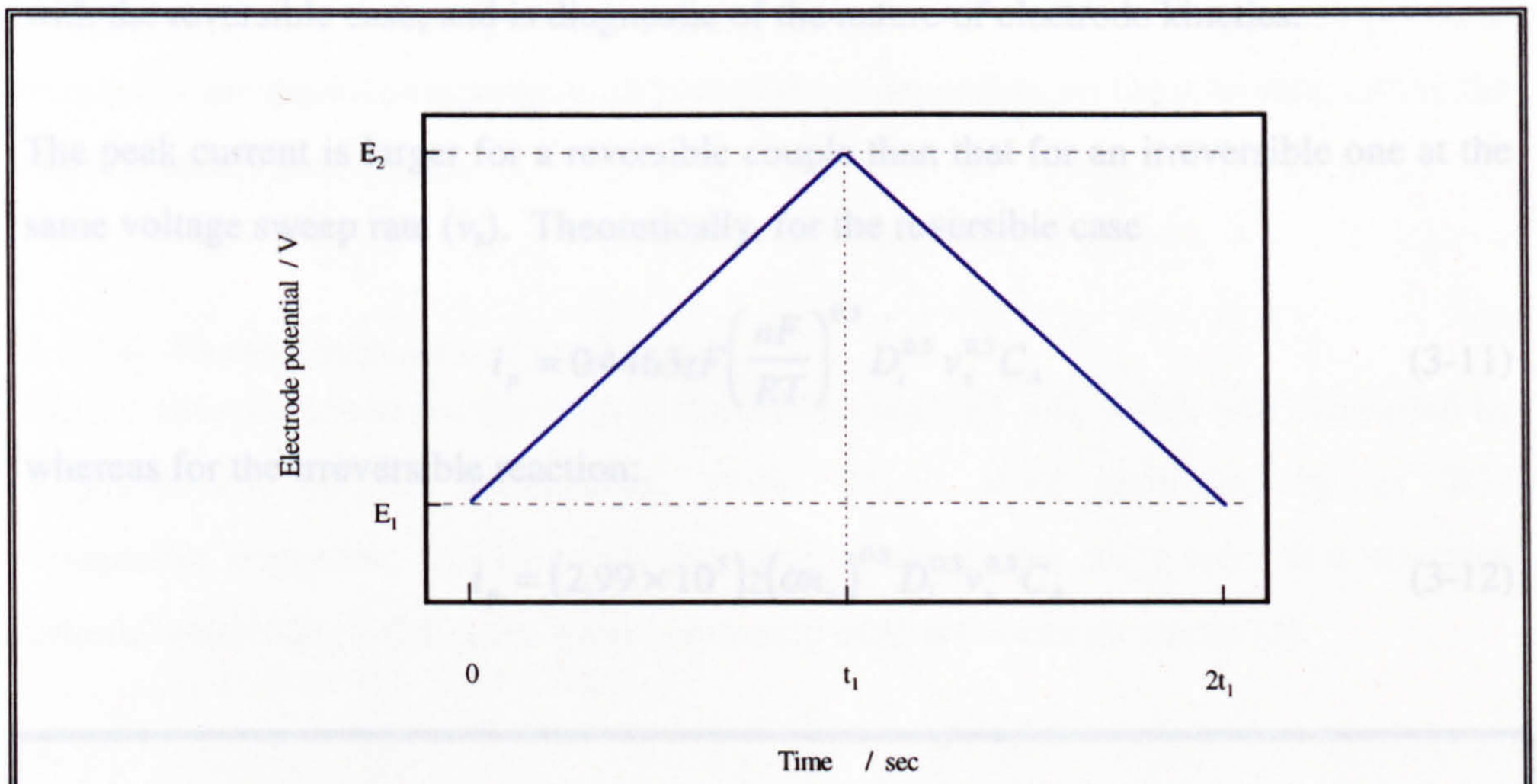


Fig.3.1 Time dependence of the applied potential in cyclic voltammetry.

3.2.1.3 Reversible and irreversible electron transfer reaction

The shape of the voltammogram, especially the peak potential or peak current, depends on the kinetics of the *A/B* redox couple. Fig.3.2 compares the cyclic voltammetric behaviour for a "reversible" (*i.e.*, for which the kinetics are so fast that local concentrations are those corresponding to the Nernst equation at any potential) and an "irreversible" electrode couple. In the case of a reversible couple, the magnitudes of the current peaks on the positive-going and negative-going potential sweeps are the same, and the peaks are separated by a potential difference (E_p^{ox} - E_p^{red}) which is independent of the scan rate. If z electrons are transferred in a reversible electrode process, the separation of these peak-potentials is:

$$\left|E_p^{ox} - E_p^{red}\right| = 2.218 \times (RT / zF) \qquad (3\text{-}10)$$

On the other hand, in the case of an irreversible couple, an appreciable over-potential is required for *B* to be converted into *A*, and the current peak for the reverse reaction appears at more negative potential than that for the reversible case. The potentials of

both the forward and reverse peaks are dependent on the potential sweep rate, in contrast with the reversible case, and is diagnostic of the nature of electrode kinetics.

The peak current is larger for a reversible couple than that for an irreversible one at the same voltage sweep rate (v_s). Theoretically, for the reversible case

$$i_p = 0.4463zF\left(\frac{nF}{RT}\right)^{0.5} D_i^{0.5} v_s^{0.5} C_A \qquad (3\text{-}11)$$

whereas for the irreversible reaction:

$$i_p = \left(2.99\times10^5\right)z\left(\alpha n_a\right)^{0.5} D_i^{0.5} v_s^{0.5} C_A \qquad (3\text{-}12)$$

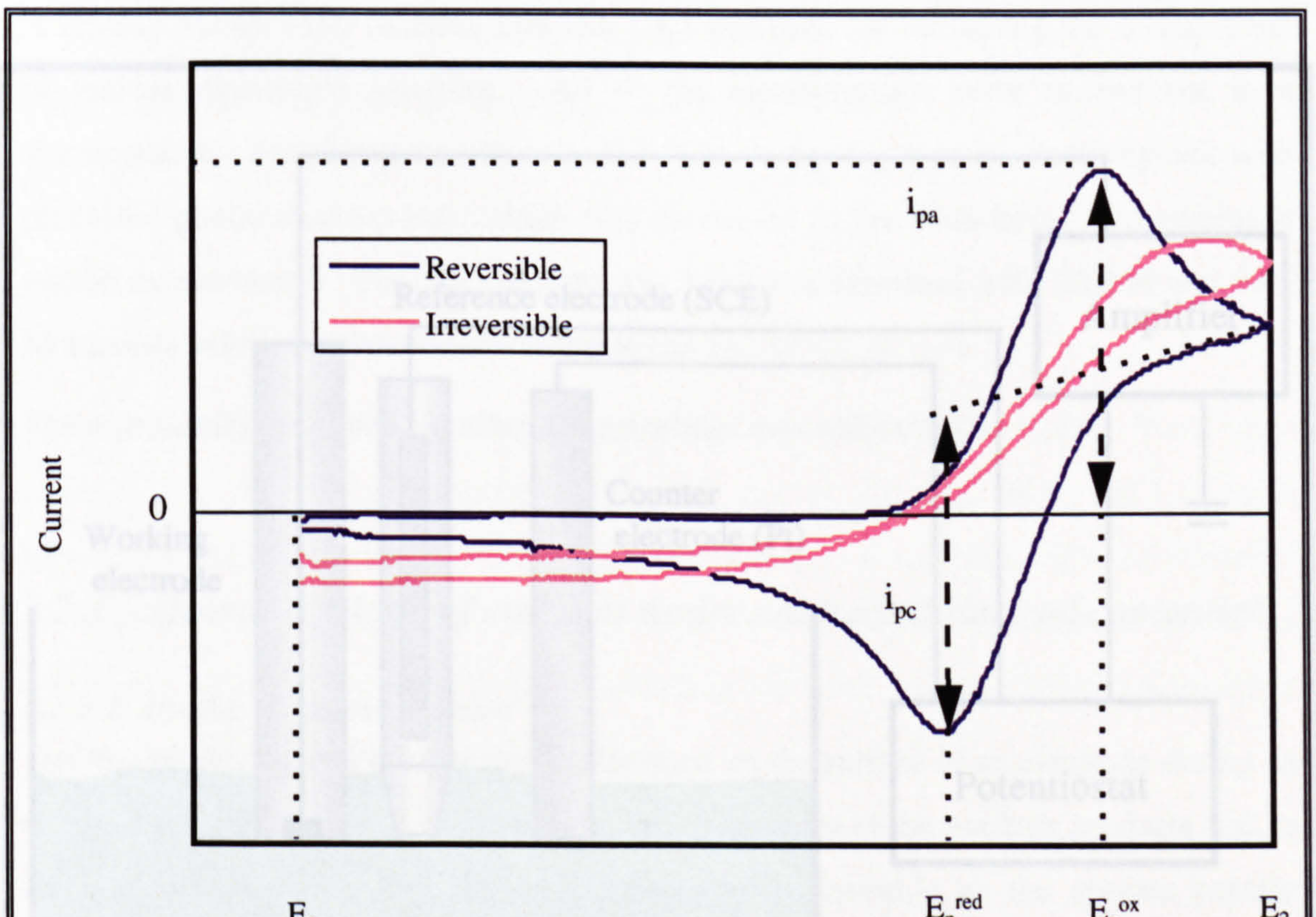


Fig.3.2 Typical cyclic voltammograms for reversible and irreversible electron transfer reactions.

For systems with partially irreversible kinetics, a current peak for the reverse reaction of similar magnitude to that for the forward reaction, is observed on the reverse potential sweep but the potential separation of two peaks is dependent on the scan rate, unlike the case for reversible kinetics.

3.2.1.4 Electrochemical cell used

Fig.3.3 shows a schematic diagram of the electrochemical cell, which was controlled by a potentiostat (EG&G Instruments, model 273A), itself controlled by an IBM compatible computer. All electrode potential values in this study refer to a saturated calomel electrode (S.C.E.), the most commonly used reference electrode **[3]**.

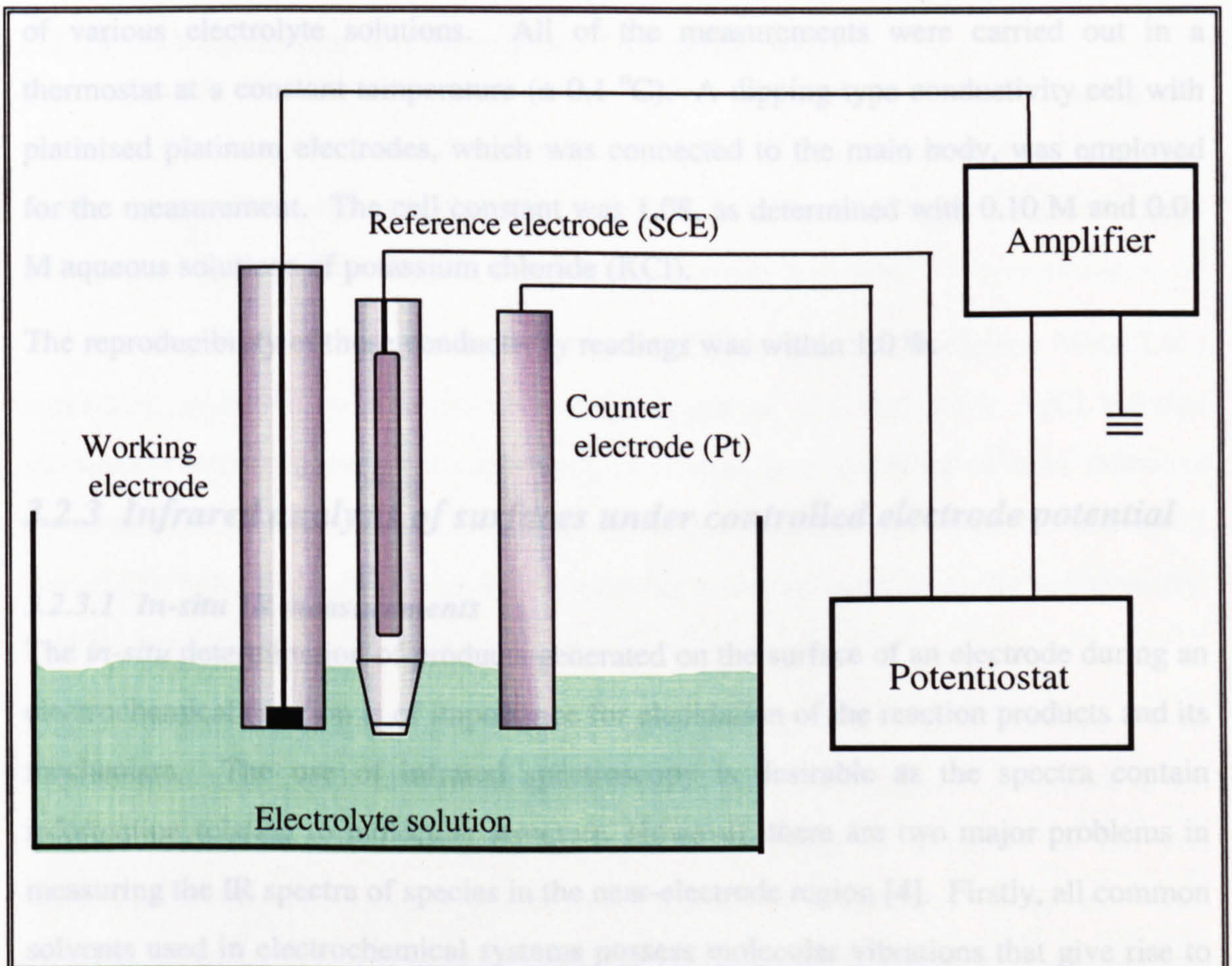


Fig.3.3 Schematic diagram of the electrochemical cell.

A 1 mm diameter of iron disc (99.99 % purity from Goodfellow Metal Ltd.) or a 0.5 mm diameter of Pt wire (99.99+% purity from the same company) was embedded in PTFE or glass, and was used as a working electrode. Its surface was polished with 0.3 and 0.075 μm Al_2O_3 particles dispersed in high purity water before each measurement. A rectangular Pt foil (0.8 cm^2, 99.99% purity) was used as a counter electrode. Dissolved oxygen and water were removed from the electrolyte solution (base oil and supporting electrolyte) by bubbling high purity nitrogen gas (from boiling liquid nitrogen, its purity of 99.99+ %) for at least two hours.

3.2.2 Conductivity determination

A Jenway Model 4150 (Jenway Limited, UK) was used for measuring the conductivity of various electrolyte solutions. All of the measurements were carried out in a thermostat at a constant temperature (± 0.1 °C). A dipping type conductivity cell with platinised platinum electrodes, which was connected to the main body, was employed for the measurement. The cell constant was 1.08, as determined with 0.10 M and 0.01 M aqueous solutions of potassium chloride (KCl).

The reproducibility of those conductivity readings was within 1.0 %.

3.2.3 Infrared analysis of surfaces under controlled electrode potential

3.2.3.1 In-situ IR measurements

The *in-situ* determination of products generated on the surface of an electrode during an electrochemical reaction is of importance for elucidation of the reaction products and its mechanism. The use of infrared spectroscopy is desirable as the spectra contain information relating to molecular structure. However, there are two major problems in measuring the IR spectra of species in the near-electrode region **[4]**. Firstly, all common solvents used in electrochemical systems possess molecular vibrations that give rise to strong absorption bands in the mid-IR range. Secondly, there is a problem of overall sensitivity, which is lower than that with UV-visible spectroscopy.

To overcome these limitations, subtractively normalised Fourier transform infrared spectroscopy (SNFTIRS) was used, in which infrared radiation is reflected from the surface of an electrode contained in a thin layer cell, as shown schematically in Fig.3.4. The short path length of the analysing beam in the solution of the thin layer cell decreases absorption by the bulk electrolyte species **[5]**. In this study, the spectra obtained were examined by a potential modulation method, *i.e.*, subtraction of spectra obtained at potentials at which product species form close to, or are adsorbed on, the electrode surface from a reference spectrum determined at a potential (-2.0 V) at which no such products are formed. This enables information about their chemical nature to be determined from the "difference spectra".

3.2.3.2 Electrochemical cell for in-situ FT-IR spectroscopy

The influence of electrode potential on surface products was studied using the electrochemical cell shown schematically in Fig.3.4 **[6]**, in which a metal electrode surface under electrode-controlled potential could be monitored by external reflection-absorption infrared spectroscopy through a non-aqueous lubricant.

A 5 mm diameter iron disc electrode (purity of 99.99+ % from Goodfellow Metal Ltd.) embedded in PTFE, was positioned within 2 μm of a 2 mm thick AgCl infrared transparent window, and a potential applied relative to a saturated calomel reference electrode (S.C.E.). The surface of the electrode had been polished with 0.3 and 0.075 μm Al_2O_3 in the same manner as for the working electrode used for cyclic voltammetry. A Pt wire was used as a counter electrode.

The infrared measurements were carried out by using a FTS-60A Bio-Rad FT-IR spectrometer equipped with an external reflection unit. The angle of incidence at the window was about 60°, leading to an angle of incidence of about 41° at the iron electrode surface. The infrared spectra were recorded from 4000 cm^{-1} to 400 cm^{-1} with a resolution of 4 cm^{-1}. All measurements for FT-IR spectroscopy were conducted at a room temperature of 25 ± 2 °C.

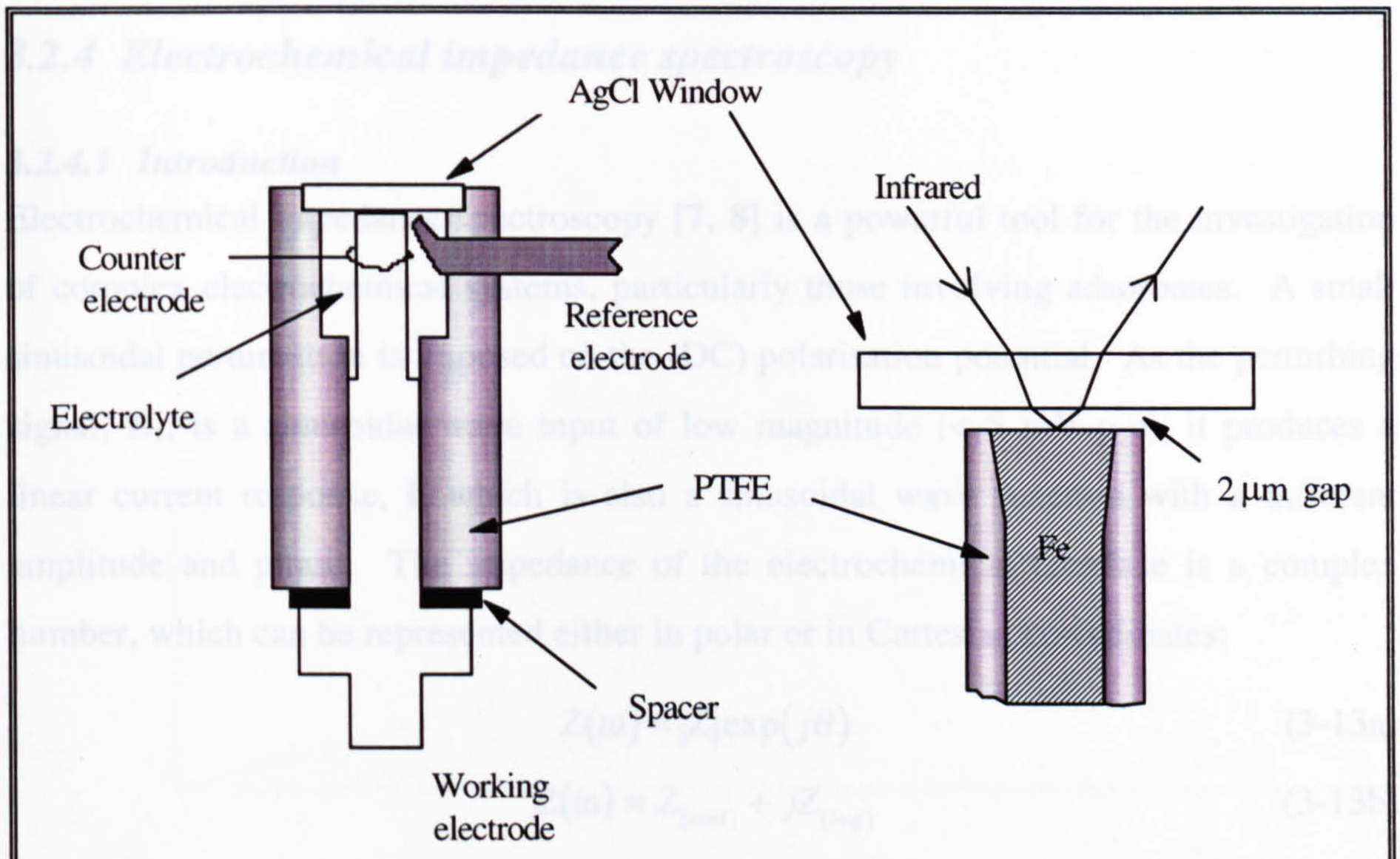


Fig.3.4 Spectro-electrochemical cell to study the surface of an electrode using infrared spectroscopy.

3.2.3.3 Test procedure

Before the start of each *in-situ* experiment, the potential of the working electrode was held for 20 minutes at -2.7 V vs. S.C.E., with the electrode drawn away from the window. This was to reduce any air-formed iron oxides or other spontaneously-formed oxidation products. The working electrode was then positioned within 2 μm of the AgCl window **[6].** A reference interferogram / spectrum was determined at -2.0 V vs. S.C.E., at which it was considered that the working electrode would have a clean iron surface. Then FT-IR spectra were collected while scanning the electrode potential to less negative potentials at which oxidation currents were observed. Different spectra at various potentials were obtained in non-real time by subtracting the original spectrum obtained at -2.0 V vs. S.C.E.

3.2.4 Electrochemical impedance spectroscopy

3.2.4.1 Introduction

Electrochemical impedance spectroscopy **[7, 8]** is a powerful tool for the investigation of complex electrochemical systems, particularly those involving adsorbates. A small sinusoidal perturbation is imposed on the (DC) polarisation potential. As the perturbing signal, E_1, is a sinusoidal wave input of low magnitude (< 5 mV p-p), it produces a linear current response, I, which is also a sinusoidal wave function with a different amplitude and phase. The impedance of the electrochemical interface is a complex number, which can be represented either in polar or in Cartesian co-ordinates:

$$Z(\omega) = |Z|\exp(j\theta) \tag{3-13a}$$

$$Z(\omega) = Z_{(real)} + jZ_{(img)} \tag{3-13b}$$

$$\omega = 2\pi f \tag{3-13c}$$

The components of $Z_{(img)}$ are assigned as imaginary and are multiplied by $\sqrt{-1}$. The relationship between these quantities is:

$$|Z|^2 = \left(Z_{(real)}\right)^2 + \left(Z_{(img)}\right)^2 \tag{3-14}$$

$$\theta = Arc\tan\frac{Z_{(real)}}{Z_{(img)}} \tag{3-15}$$

Therefore, the impedance data can be described conveniently by a plot such as Fig.3.5 in which the quantities $Z_{(real)}$ and $-Z_{(img)}$ appear on the *x*- and *y*-axes, respectively. These components are handled mathematically as "real" and "imaginary", but both types are real in the sense of being measurable by a phase angle.

Typically, the impedance *Z*, at each frequency is plotted as a point with co-ordinates $\left(Z_{(real)} - Z_{(img)}\right)$. The resulting vector from the origin to this point represents the impedance. It has a magnitude equal to the length of this vector and the phase difference between the current and voltage is given by θ.

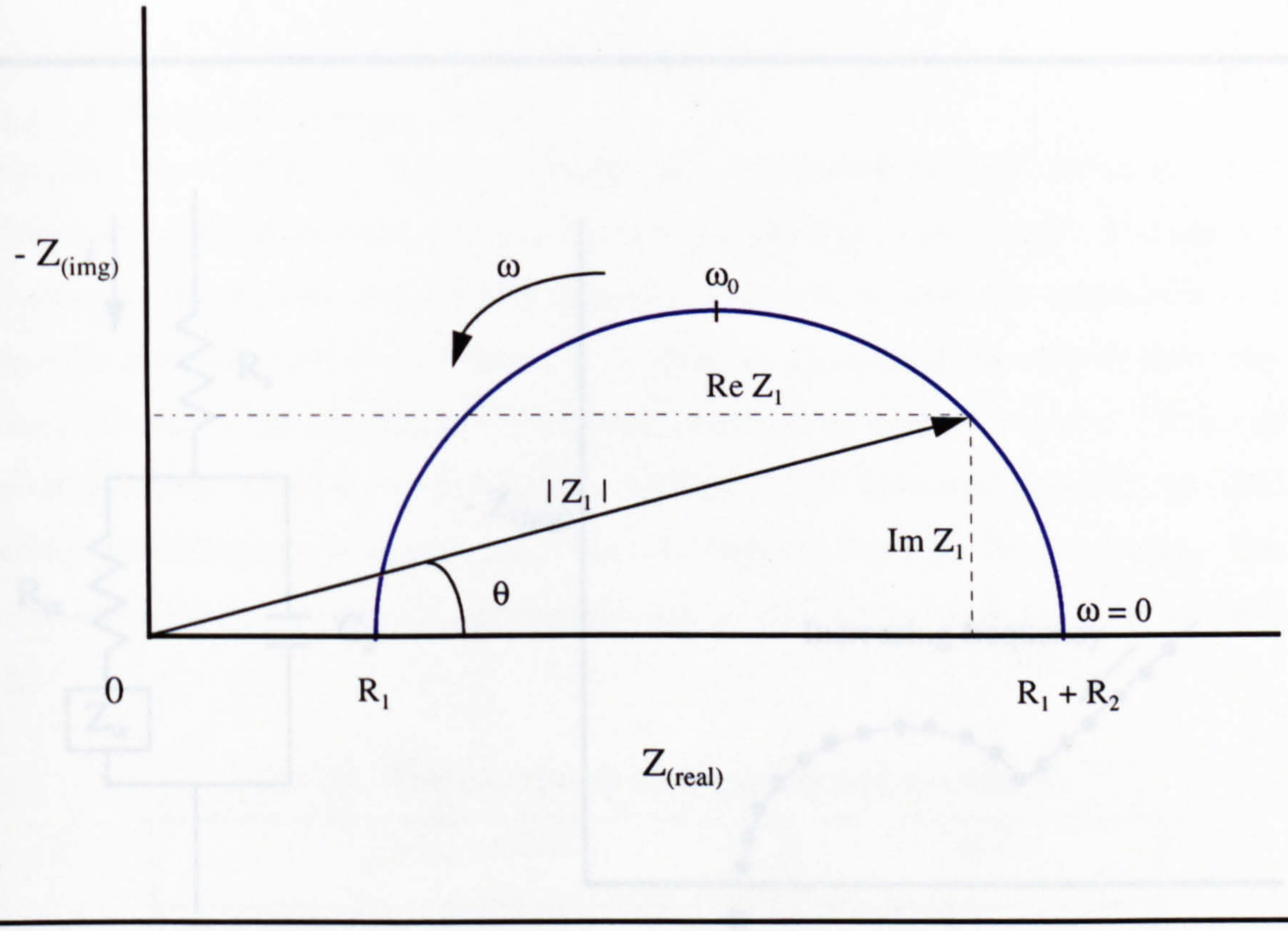


Fig.3.5 Typical impedance plots described in a complex plane.

3.2.4.2 Equivalent circuits for the interpretation of electrochemistry

In a general sense, an electrochemical cell is simply an impedance to a small sinusoidal excitation; hence its performance should be able to be represented by an equivalent circuit of resistors and capacitors that pass current with the same amplitude and phase angle that the real cell does, under a given excitation. A typical circuit and its corresponding complex plane are shown in Fig.3.6.

This may be understood as a so-called "Randles circuit", which is used for the conditions when an electrolytic reaction is taking place at the electrode **[8]**. The parallel elements are introduced because the total current through the working interface is the sum of distinct contributions from the faradaic process i_f and double-layer charging i_c.

In this circuit, all the current must pass through the uncompensated solution resistance, and therefore R_s is inserted as a series element to represent this effect.

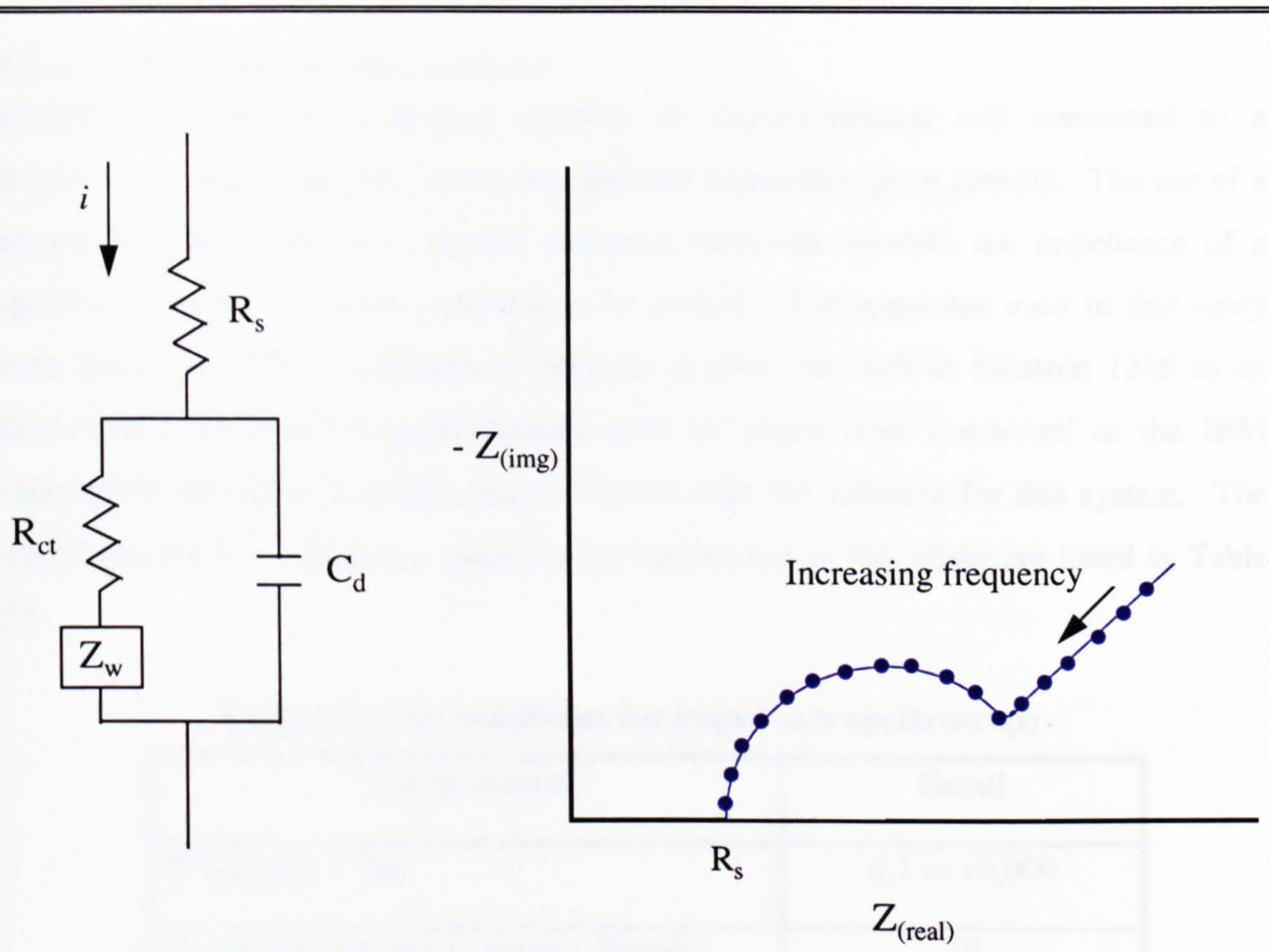


Fig.3.6 Electrochemical interface represented by an equivalent circuit (Randles circuit) and a corresponding complex plane diagram.

Warburg impedance (Z_w), allows for the frequency dependence of diffusive transport to the electrode. At high frequency, the impedance plot shows that the dominant contribution to the total impedance is simply that of the solution resistance, since the double layer provides a path of negligible resistance to the current. It follows that no electrolysis takes place at high frequency.

However, as the frequency is reduced, this is no longer the case, and the effect of resistance in parallel with the capacitance gives rise to the characteristic semicircular part of the plot. Finally, the impedance shows a large rise, modelled by the Warburg impedance (Z_w), as lower frequencies are reached. This is due to significant

concentration changes induced by the A.C. current which becomes increasingly difficult to replenish by diffusion as the frequency decreases.

3.2.4.3 Frequency response analyser

Modern experimental techniques employ an electrochemical cell connected to a frequency response analyser which can generate impedance plots directly. The use of a three-electrode system and suitable reference electrode, permits the impedance of a specific electrode / solution interface to be probed. The apparatus used in this study were Solatron 1250 as a frequency response analyser, as well as Solatron 1286 as an electrochemical interface (potentiostat), both of which were connected to the IBM compatible computer to enable remote control with the software for this system. The conditions for the impedance spectroscopy carried out in this study are listed in Table 3.1.

Table 3.1 Test conditions for impedance spectroscopy.

Test condition	Detail
Frequency / Hz	0.1 to 10,000
Frequency interval / (points /decade)	10
P-P amplitude of sinusoidal wave / mV	10
Imposed DC potential / V vs. S.C.E.	-2.0 to 1.5

3.3 Friction and wear test methods

3.3.1 High Frequency Reciprocating (HFR) rig

3.3.1.1 Introduction

Frictional and wear characteristics were determined at room temperature (25 ± 1 °C) using a high frequency reciprocating (HFR) rig, shown schematically with the electrochemical instruments in Fig.3.7 **[9]**.

A 6.0 mm diameter steel ball was held in a chuck and loaded downwards on the flat face of a 10.0 mm diameter disc. Both ball and disc were cleaned thoroughly before a test in an ultrasonic bath using toluene and analytical grade acetone respectively.

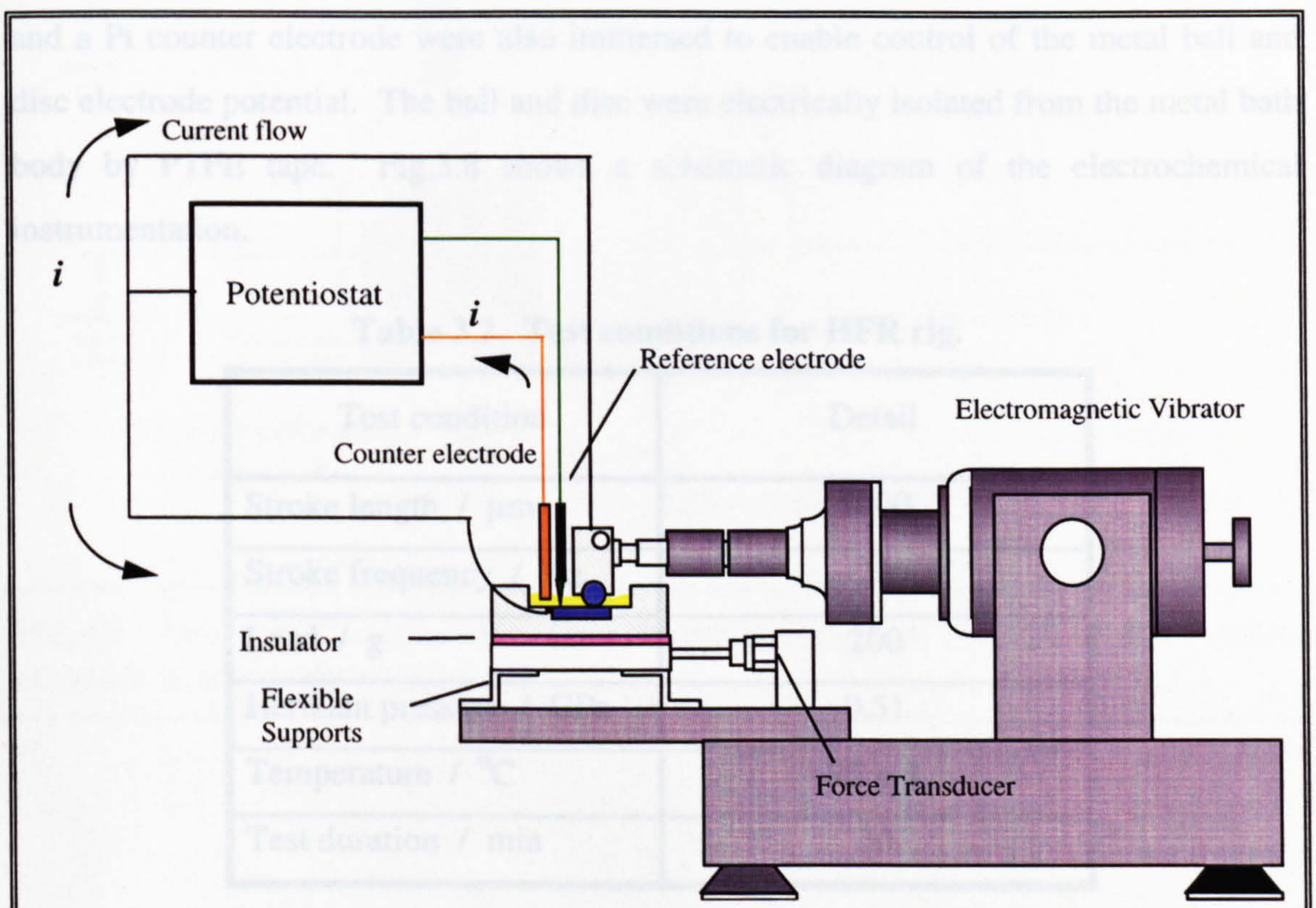


Fig.3.7 HFR rig for friction and wear measurements under controlled electrode potential.

3.3.1.2 Test conditions and method

The tests in this study were generally carried out under the conditions listed in Table 3.2.

The bath has a heater and a control system so that the temperature can be set at any value between room temperature and 200 °C. During each measurement, an electrical vibrator was employed to oscillate the ball backwards and forwards in contact with the disc at a stroke length and frequency that can be set by the user. A control circuit maintained constant stroke length regardless of the friction value. Friction between the ball and disc was measured with a load cell attached to the lower specimen holder.

The contact between the ball and disc was fully immersed in a bath, two-thirds filled with an electrolyte solution, in which a saturated calomel reference electrode (S.C.E.) and a Pt counter electrode were also immersed to enable control of the metal ball and disc electrode potential. The ball and disc were electrically isolated from the metal bath body by PTFE tape. Fig.3.8 shows a schematic diagram of the electrochemical instrumentation.

Table 3.2 Test conditions for HFR rig.

Test condition	Detail
Stroke length / μm	1000
Stroke frequency / Hz	20
Load / g	200
Hertzian pressure / GPa	0.51
Temperature / °C	25 ± 1
Test duration / min	30

3.3.1.3 Estimation of lubricating condition in HFR tests

In oil film lubrication, the extent to which the total load carried is shared between the oil and the larger surface asperities, depends upon the relative height of the asperities and

the oil film thickness which is often described in terms of the "specific film thickness" or *Lambda ratio* (λ). This relates the minimum oil film thickness in the contact, h_{min} to the composite surface roughness, R_{qc}, as in the following formula:

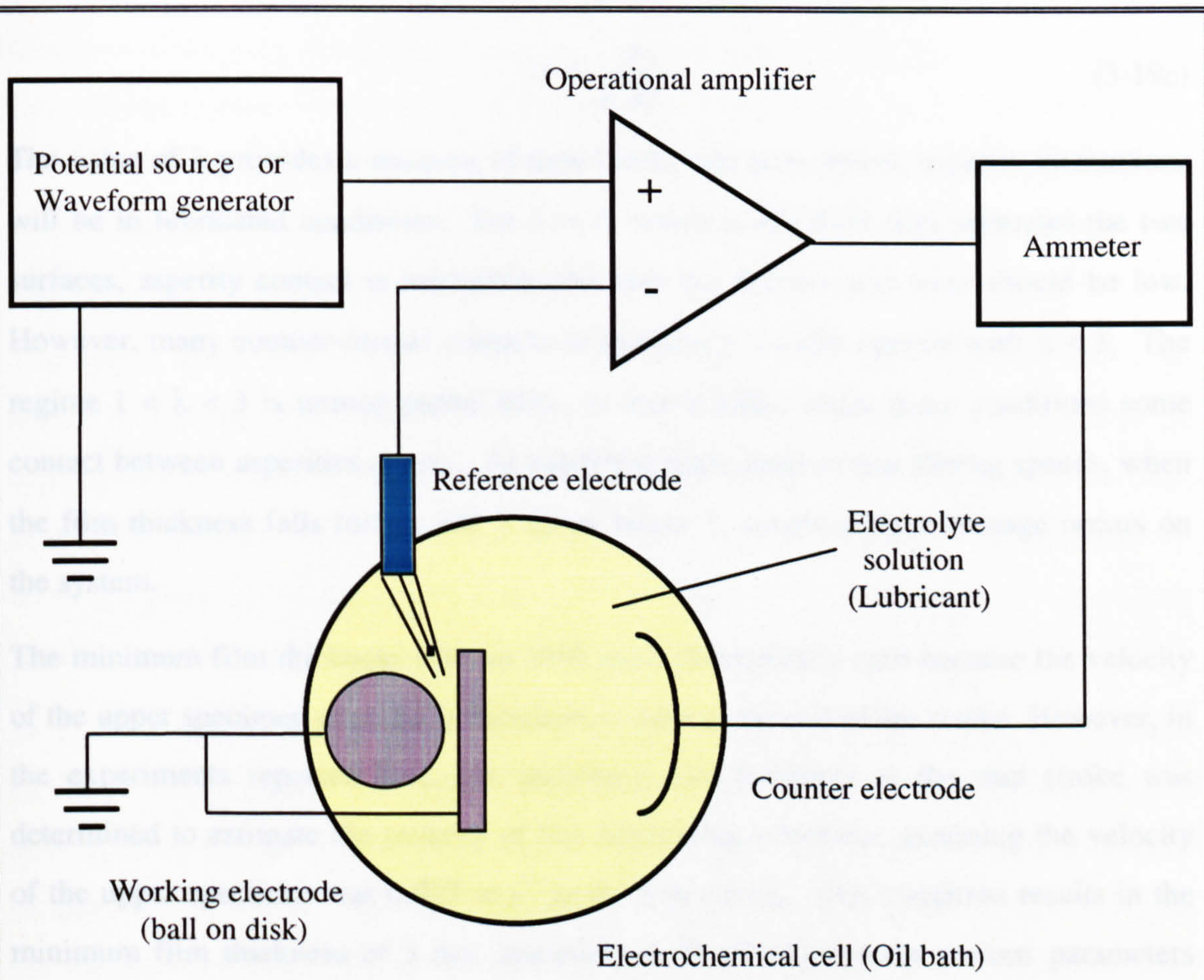


Fig.3.8 Schematic diagram of the potentiostatic control of the ball-on-disc working electrode in an electrochemical cell.

$$\lambda = \frac{h_{min}}{R_{qc}} \tag{3-16}$$

with
$$R_{qc} = \sqrt{R_{q1}^2 + R_{q2}^2} \tag{3-17}$$

where R_{q1} and R_{q2} are the root mean square (RMS) roughnesses of the two metal surfaces, and h_{min} is derived from Dowson-Hamrock's equations **[10]** as below:

$$\frac{h_{min}}{R_r}\left(\frac{W}{U}\right)^2 = 3.42\times(1-e^{-0.68})\times\left(\frac{GW^3}{U^2}\right)^{0.49}\left(\frac{W^{8/3}}{U^2}\right)^{0.17} \quad (3\text{-}18)$$

with $$G = \alpha_p E \quad (3\text{-}19a)$$

$$U = \frac{\eta_0 u}{E' R_r} \quad (3\text{-}19b)$$

$$W = \frac{w}{E' R_r^2} \quad (3\text{-}19c)$$

The value of λ provides a measure of how likely, and how severe, asperity interactions will be in lubricated conditions. For $\lambda > 3$, where a full fluid film separates the two surfaces, asperity contact is negligible and both the friction and wear should be low. However, many counter-formal contacts in machinery usually operate with $\lambda < 3$. The regime $1 < \lambda < 3$ is termed partial EHL, or mixed EHL; under these conditions some contact between asperities occurs. At extremely high loads or low sliding speeds, when the film thickness falls further and λ drops below 1, severe surface damage occurs on the system.

The minimum film thickness with an HFR rig is theoretically zero because the velocity of the upper specimen eventually decreases to zero at the end of the stroke. However, in the experiments reported here, the minimum film thickness at the mid stroke was determined to estimate the severity of this lubricating condition, assuming the velocity of the upper specimen was 0.025 m s^{-1} at the mid stroke. This condition results in the minimum film thickness of 3 nm, according to Eq.(3-18) and the various parameters used in Tables 3.2 and 4.4. The λ value was also determined as 0.1, by using Eq.(3-16) and the parameters in Table 4.4. These are summarised in Table 3.3. The result indicates that the metal-metal contact should occur during testing, even at the mid stroke, and the behaviour of the lubricating system depends critically upon the boundary lubricant film properties and the redox conditions at the metal surface.

Table 3.3 The minimum film thickness and λ value at the mid stroke.

G	U	W	h_{min} / nm	λ
4.28×10^{3}	4.03×10^{-13}	9.57×10^{-7}	3	0.1

3.3.2 Nano-probe spectroscopy

3.3.2.1 Introduction

Scanning probe microscopy refers to a family of techniques which enable three-dimensional imaging of topography and some physical and chemical properties surfaces from atomic to micro-metre scales to be measured. The first member of that family was the scanning- tunnelling microscope (STM), which maps topography by measuring the "tunnelling" current flowing between a sharp metal tip rastered across the surface of an electronically conducting substrate **[11]**.

The atomic force microscope (AFM), which followed a few years later, measures the attractive or repulsive forces between tip and substrate **[12]**. AFM greatly expanded the applications of scanning probe microscopy, since it can be used for conductive or non-conductive samples. In its most basic form, AFM measures topography by mechanically moving a sharp probe across the sample to "feel" the contours of the surface in a manner similar to a phonograph stylus tracing the grooves of a record.

In the few years of its existence, the technology of scanning probe microscopy has been extended to encompass the measurement of other sample characteristics using newly developed probes and signal processing techniques **[13]**. The common thread among all of these techniques is that a sharp probe is rastered across a substrate surface mapping the spatial distribution of some substrate property. A typical schematic instrumentation is described in Fig.3.9.

3.3.2.2 STM / AFM system

A conventional STM system was employed (Oxysys Ltd., Oxford) which was able to produce 2D topographical scanned images of surfaces with a vertical resolution of 0.01 nm **[14]**. This was augmented using a home-built AFM head, as shown schematically in Fig.3.10, the bending and twisting of the cantilever holding the tip being measured separately using a four-quadrant photodiode detector, to enable simultaneous measurement of the spatial distribution of normal and lateral (friction) forces.

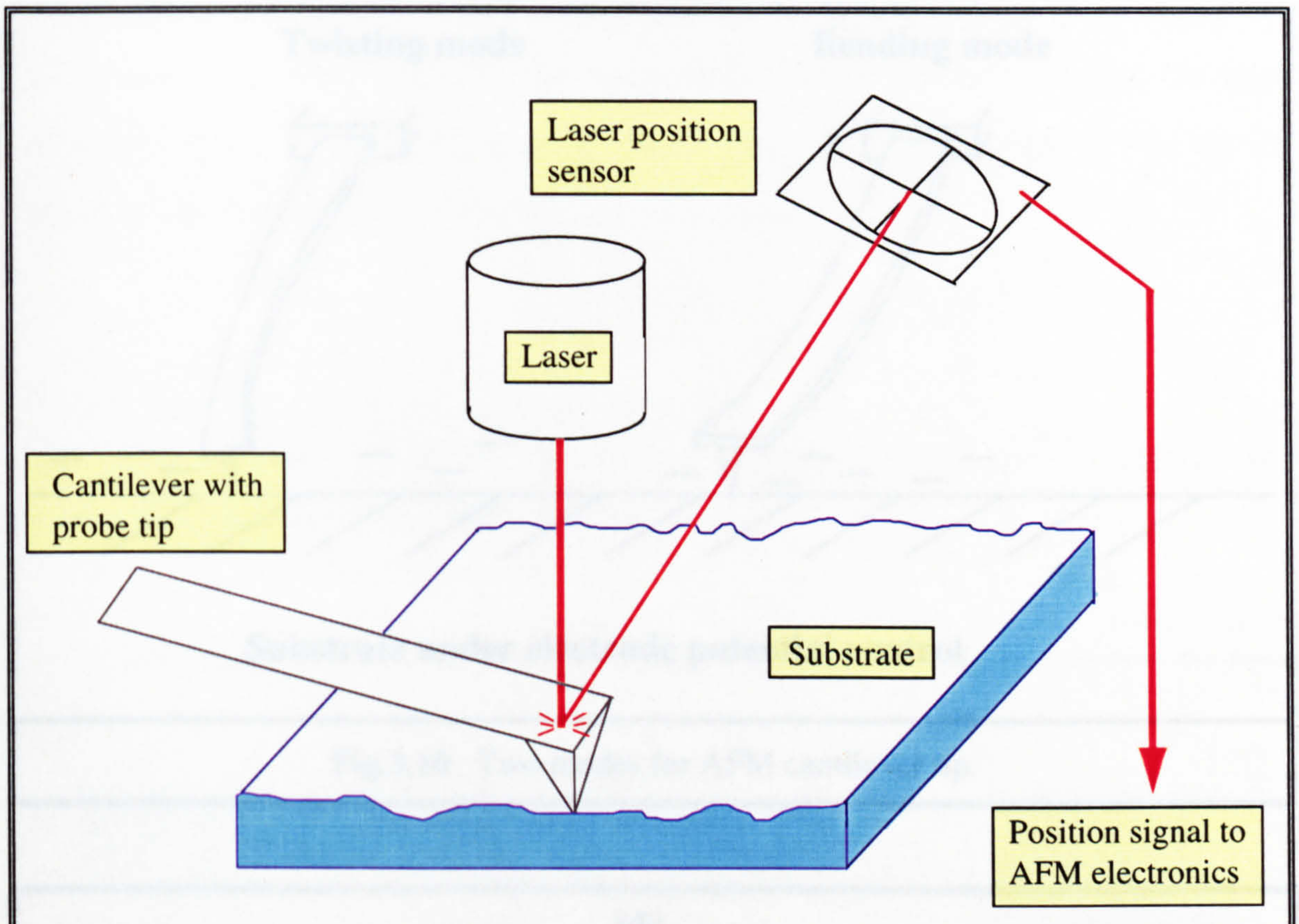


Fig.3.9 Operating principles of the atomic force microscope (AFM).

These forces contain a component of the surface geometry.

Fig.3.11 shows a free body diagram of the forces on the AFM tip. Resolving these gives:

$$F = L\cos\theta + W\sin\theta \tag{3-20a}$$

$$N = W\cos\theta + L\sin\theta \tag{3-20b}$$

$$\mu = \frac{\mu_m - \rho}{1 + \mu_m \rho} \tag{3-21}$$

$$\mu = \frac{1}{2}(\bar{\mu}_m + \bar{\mu}_m) \tag{3-22}$$

where F and N are the true frictional and normal forces, μ_m is the measured horizontal force coefficient and ρ is the slope (dz/dx).

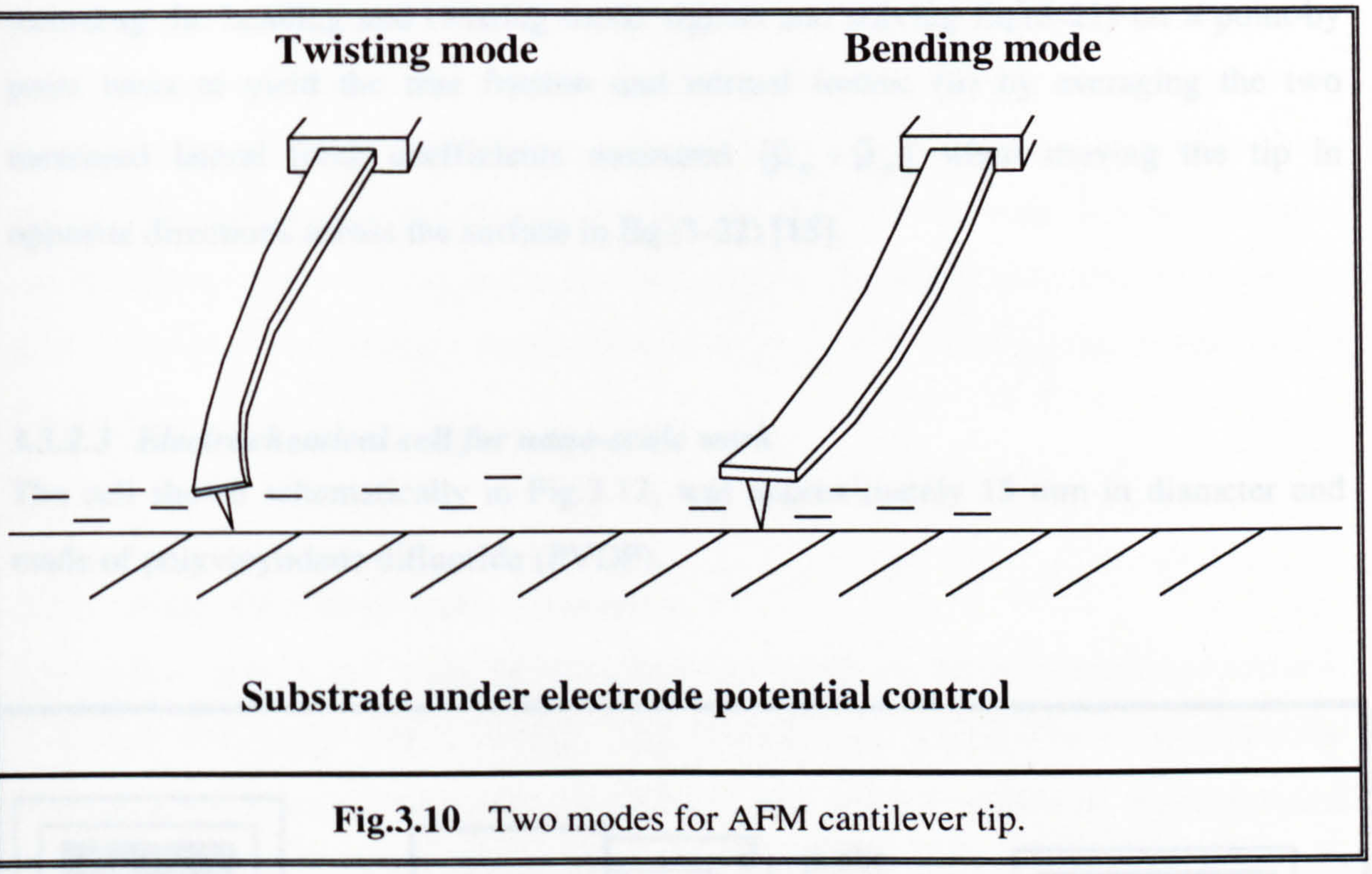


Fig.3.10 Two modes for AFM cantilever tip.

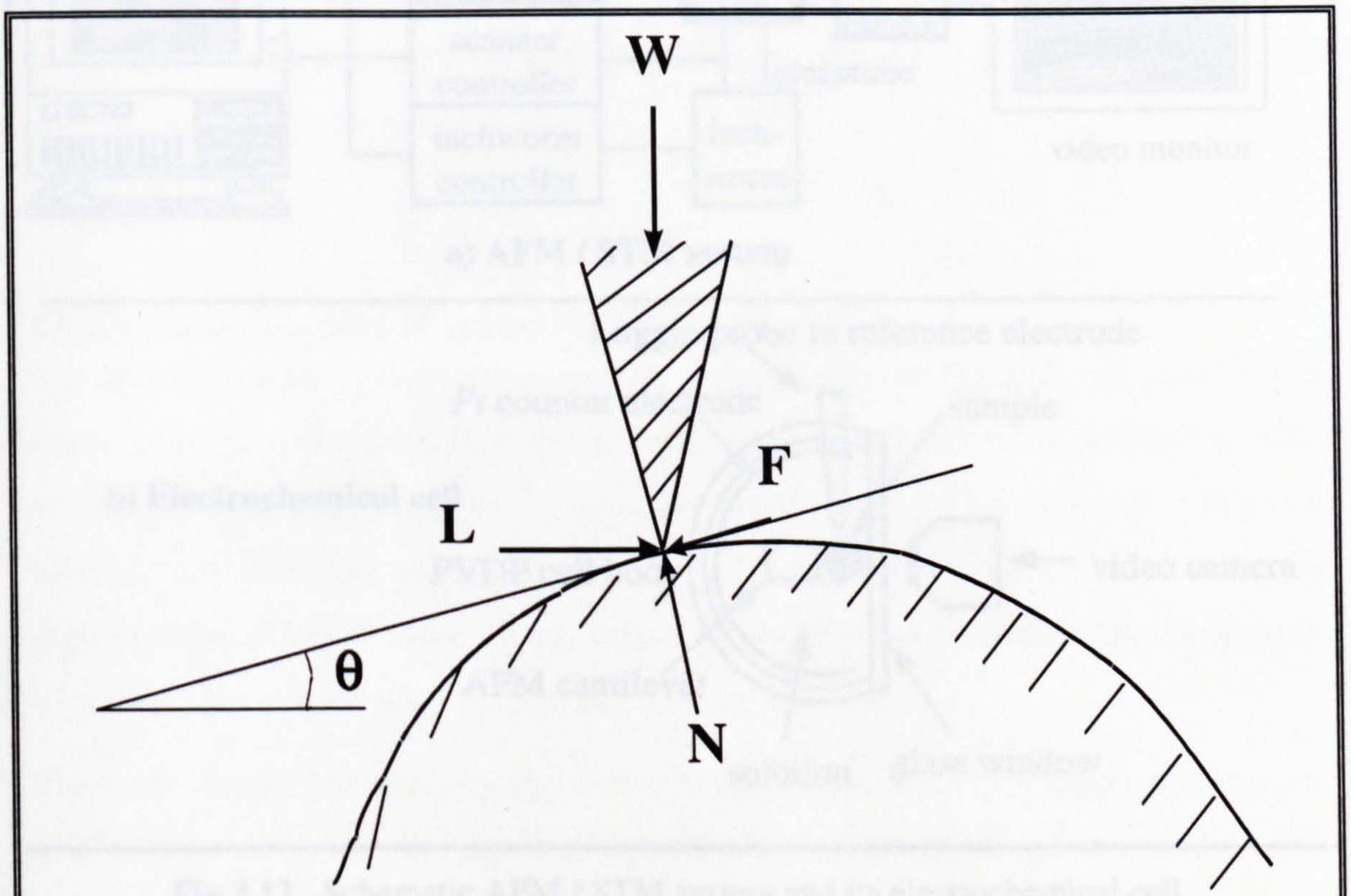
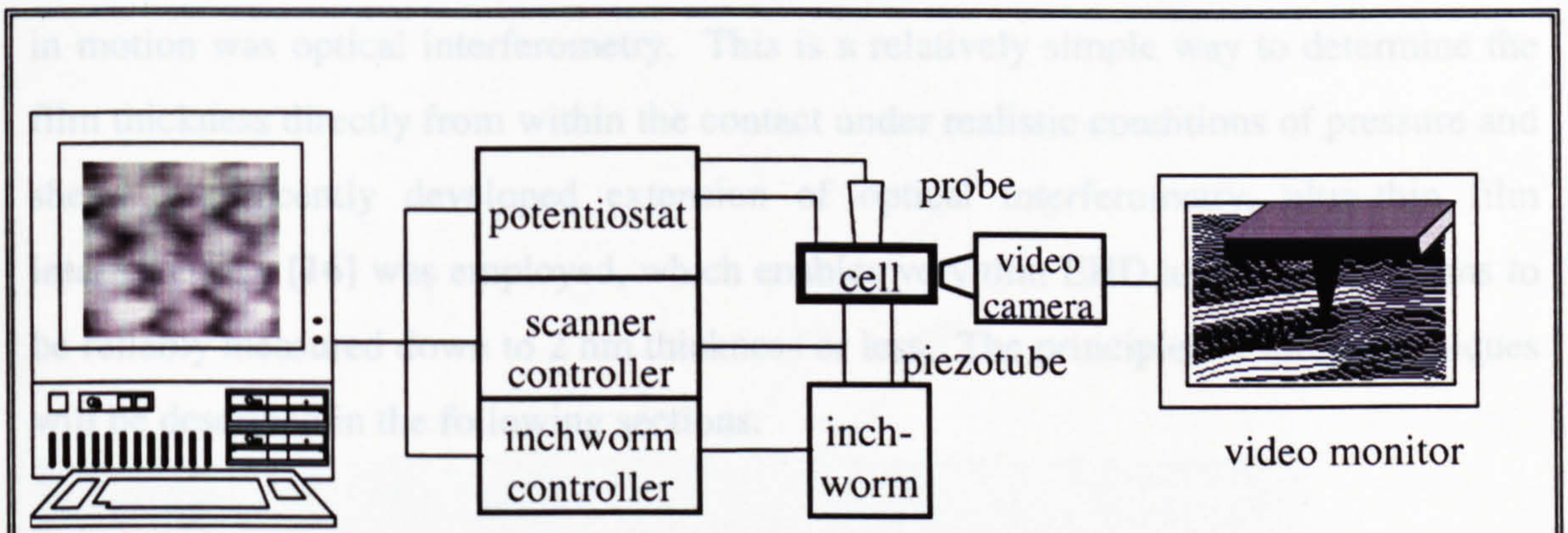


Fig.3.11 A free body diagram of the forces on the AFM tip.

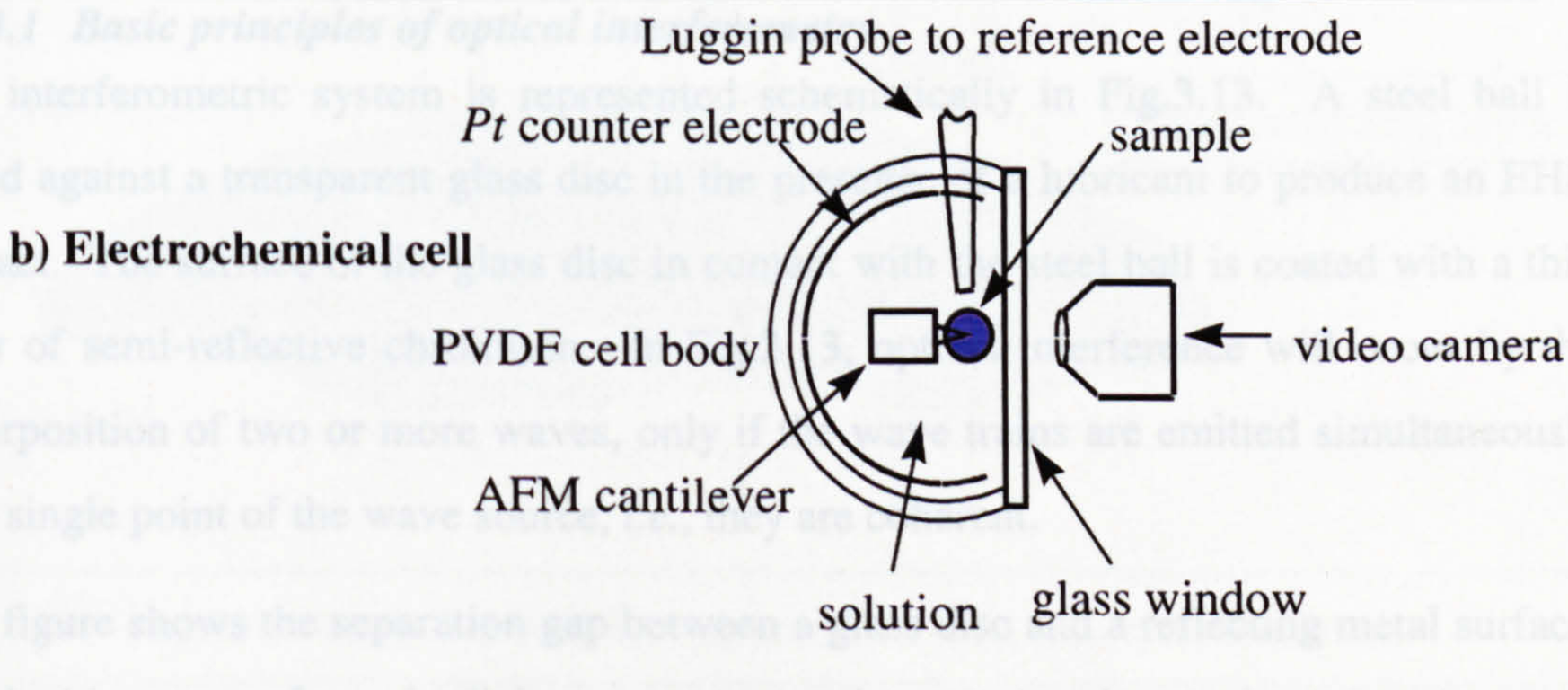
The ratio of *F/N*, the friction coefficient (μ), was determined in two ways: (i) by recording the bending and twisting mode signals and solving Eq.(3-21) on a point-by point basis to yield the true friction and normal forces; (ii) by averaging the two measured lateral force coefficients measured $(\bar{\mu}_m + \bar{\mu}_m)$ when moving the tip in opposite directions across the surface in Eq.(3-22) **[15]**.

3.3.2.3 Electrochemical cell for nano-scale work

The cell shown schematically in Fig.3.12, was approximately 15 mm in diameter and made of polyvinylidene difluoride (PVDF).



a) AFM / STM system



b) Electrochemical cell

Fig.3.12 Schematic AFM / STM system and its electrochemical cell.

One side was cut away and a glass window inserted so that the fully immersed tip / sample contact region could be imaged using a microscope / video camera system. The cell contained a 1 cm^2 Pt foil counter electrode and a glass Luggin probe containing a saturated calomel referenced electrode (S.C.E.) was inserted into the solution from above. The cell was moved upward against the cantilever tip under computer control and the applied potential and lateral scanning motion of the cell were also controlled by microcomputer. A schematic control system for the AFM / STM is also represented in Fig.3.12.

3.3.3 Film thickness measurement

The method used in this study for measuring the separation between lubricated surfaces in motion was optical interferometry. This is a relatively simple way to determine the film thickness directly from within the contact under realistic conditions of pressure and shear. A recently developed extension of optical interferometry, ultra-thin film interferometry **[16]** was employed, which enables very thin EHD and boundary films to be reliably measured down to 2 nm thickness or less. The principles of these techniques will be described in the following sections.

3.3.3.1 Basic principles of optical interferometry

The interferometric system is represented schematically in Fig.3.13. A steel ball is rolled against a transparent glass disc in the presence of a lubricant to produce an EHD contact. The surface of the glass disc in contact with the steel ball is coated with a thin layer of semi-reflective chromium. In Fig.3.13, optical interference will occur by the superposition of two or more waves, only if the wave trains are emitted simultaneously by a single point of the wave source, *i.e.*, they are coherent.

The figure shows the separation gap between a glass disc and a reflecting metal surface. The incident wave from the light source passes through the glass and reaches the semi-reflecting layer deposited on the lower surface of the glass. Here it is divided by partial reflection into two waves; one wave is transmitted further through the gap and being

reflected by the reflecting metal surface, and the second is reflected directly by the semi-reflecting layer. The resulting wave front maintains its original width but has reduced amplitude. On recombining, the resulting intensity depends on the phase difference which in its turn, is a function of the actual path difference between the two waves since they have travelled different distances. For oblique incidence, the path difference d depends on the refraction angle r and on the "optical path difference", $2nh$, shown by the formula:

$$d = 2nh\ \cos r + \phi\lambda \tag{3-23}$$

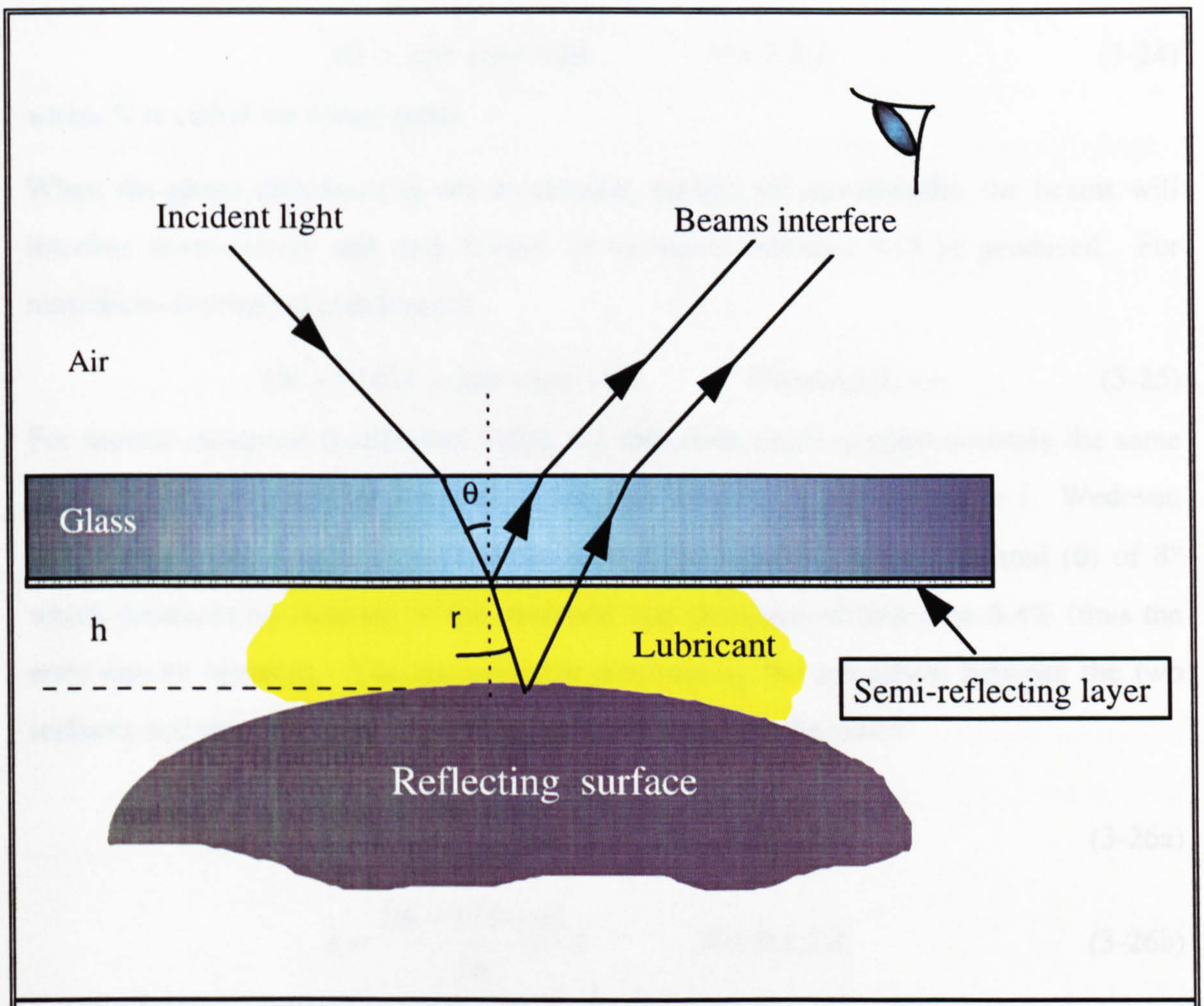


Fig.3.13 Basic interferometric system for thin film measurements.

where n is the refractive index of the separation medium, h is the physical gap thickness, ϕ is a phase change due to reflection and is taken to be 0.28 for film thickness calculations **[16]**.

For reflection on dielectric surfaces, the phase change ϕ is equal to π from a rare to dense medium and zero from dense to rare medium. With metal reflections, the situation is more complex and the phase change lies somewhere between 0 and π **[17]**.

If the two waves are in phase, they will interfere constructively and the phase difference will be an integral number of wavelengths, $N\lambda$. Thus, the condition for constructive interference will be:

$$N\lambda = 2nh\ \cos r + \phi\lambda \qquad N = 1,2,3, \cdots\cdots \tag{3-24}$$

where N is called the fringe order.

When the phase difference is not an integral number of wavelengths, the beams will interfere destructively and dark fringes of minimum intensity will be produced. For maximum destructive interference,

$$(N + 1/2)\lambda = 2nh\ \cos r + \phi\lambda \qquad N = 0,1,2,3, \cdots\cdots \tag{3-25}$$

For normal incidence (collimated light), the refraction angle is approximately the same to the incident one and for low values, the cosine can be approximated to 1. Wedeven **[17]** showed that a typical commercial source has a deviation from normal (θ) of 8° which produces an increase in the observed film thickness of less than 0.4% (thus the error can be ignored). The formulae for determining the separation between the two surfaces and thus, the thickness of the lubricant film, then becomes:

$$h = \frac{(N - \phi)}{2n}\lambda \qquad N = 1,2,3, \cdots\cdots \tag{3-26a}$$

$$h = \frac{(N + 1/2 - \phi)}{2n}\lambda \qquad N = 0,1,2,3, \cdots\cdots \tag{3-26b}$$

for constructive and destructive interference, respectively.

3.3.3.2 Ultra-thin film technique

There are two major limitations of classical optical interferometry for studying lubricant films. Firstly, the minimum measurable film thickness is large compared with many films of practical value. Even with a fringe order N is equal to 1, the smallest wavelength detectable by human eye is violet (approximately 400 nm), so for a refractive index of 1.4 (for standard mineral oil), a normal incident light and a phase change upon reflection of 0.28, equation (3-26) predicts a film thickness of *ca.* 100 nm. The second limitation of conventional interferometry is the resolution of the technique which relies on the human eye to distinguish the interferometric fringes. Thus on one hand, the measurable thicknesses are only possible in steps of 50 nm and on the other, the resolution depends on the ability of human eye to distinguish colours accurately, typically 1/8 of the wavelength of light, *i.e.*, approximately 50 to 90 nm.

In order to overcome these limitations, two main improvements have been made. One is a "spacer layer" in Fig.3.14, initially introduced by Westlake **[18]** in 1967. A transparent layer of silicon dioxide (SiO_2) is deposited on top of the chromium semi-reflecting layer on one side of the glass disc. SiO_2 was found to have suitable qualities for an efficient spacer layer since it has a refractive index which is very close to that of most lubricants, and also has a negligible absorption and gives a durable coating. This added layer with a thickness comparable to the wavelength of light, acts like a solid layer of oil which gives a measurable film thickness even in static contact. This is measured at the beginning of the test on a dry contact and the value is then subtracted from each reading to give the real film thickness. Thus, when constructive interference takes place, the film thickness is calculated from:

$$N_{sp}\lambda_{sp} = 2h_{sp}n_{sp} + \phi\lambda_{sp} \qquad (3\text{-}27a)$$

$$N_{sp+oil}\lambda_{sp+oil} = 2h_{sp}n_{sp} + \phi\lambda_{sp+oil} + 2n_{oil}h_{oil} \qquad (3\text{-}27b)$$

$$h_{oil} = \frac{(N_{sp+oil} - \phi)\lambda_{sp+oil} - (N_{sp} - \phi)\lambda_{sp}}{2n_{oil}} \qquad N = 1,2,3,\cdots\cdots \qquad (3\text{-}27c)$$

since n_{oil} and n_{sp} are very similar in practice.

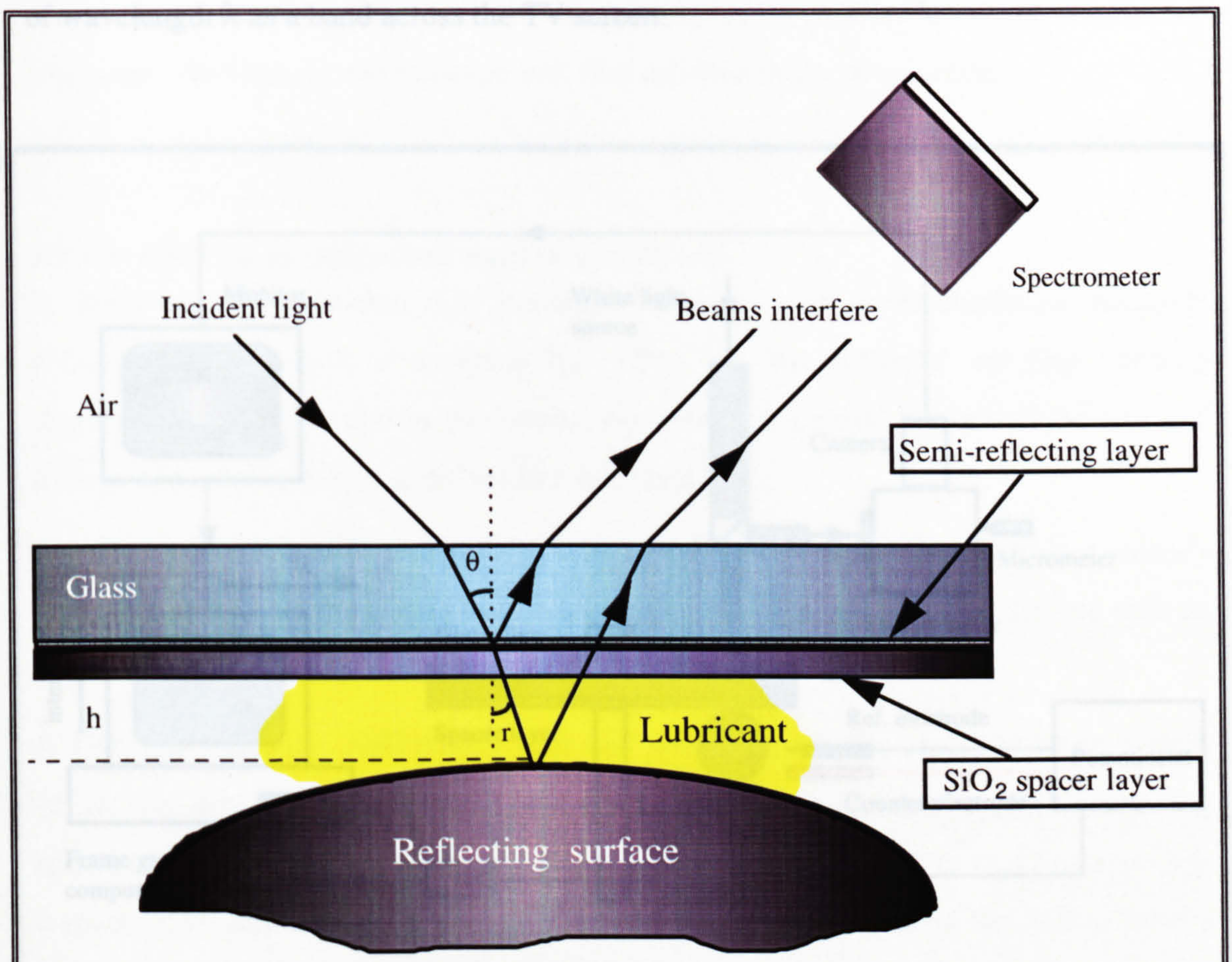


Fig.3.14 Schematic of ultra-thin film thickness measurement technique.

A major advance was made in 1990 by Johnston **[16]** when a spectrometer was introduced to accurately determine which particular wavelengths have constructively interfered and, consequently, calculate the film thickness value. A schematic design of the instrumentation is shown in Fig.3.15.

The spectrometer contains a grating that can pivot about an axis. The light reflected from the centre of the contact and subject to interference, is directed into the spectrometer, in which the fine grating grooves disperse the light into its component wavelengths. The spectrometer is connected to a 50 images / second black and white video camera and a monitor which displays part of the spectrum (typically over a wavelength range of 80 to 100 nm). The spectrometer grating can be rotated by the use

of a micrometer to scan the whole spectrum. The spectral intensity is displayed in terms of wavelength λ as a band across the TV screen.

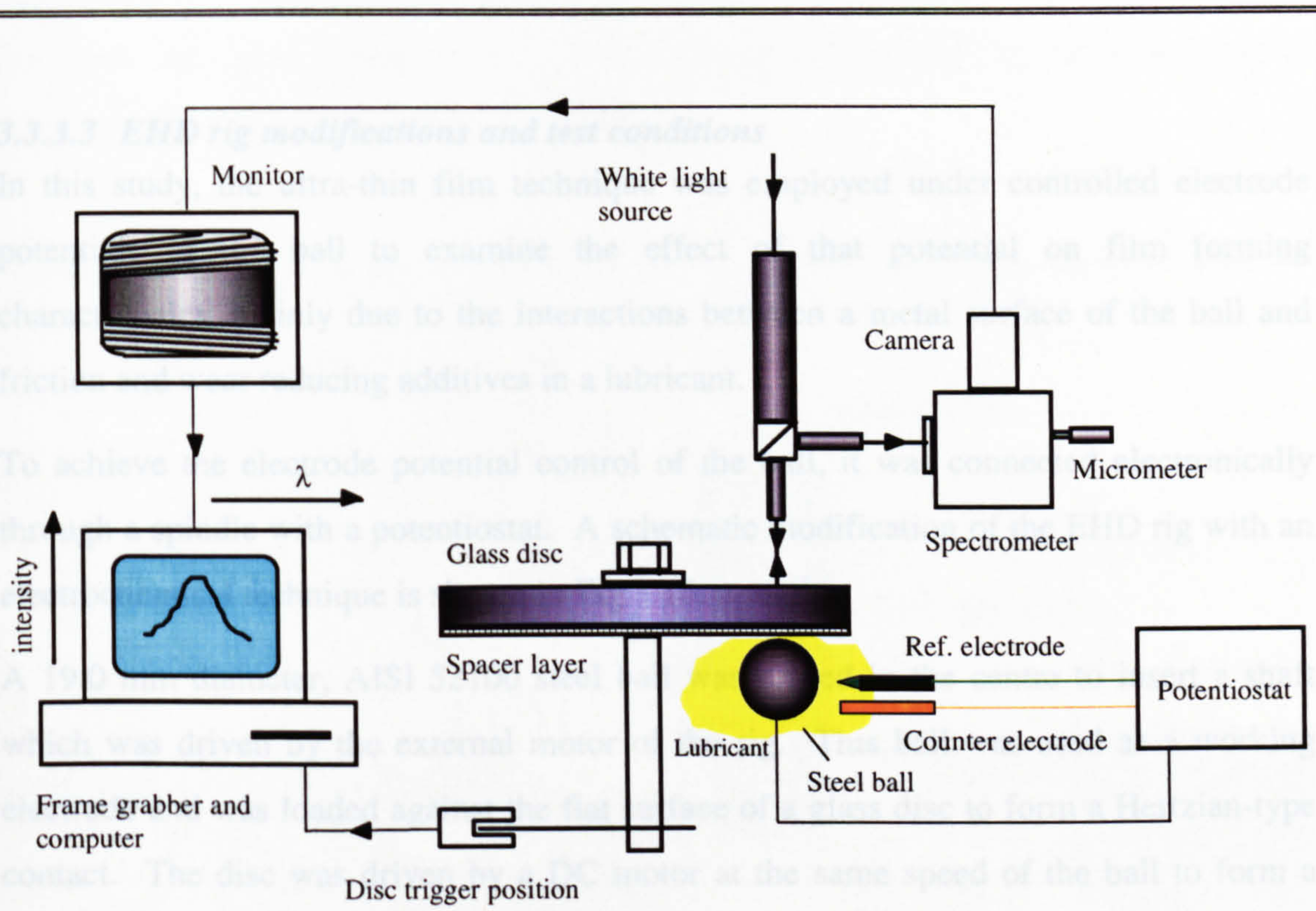


Fig.3.15 Schematic representation of spectrometric film thickness measurement system.

By identifying the wavelength at which maximum constructive interference occurs, it is possible to determine the separation. In order to enable this, the system incorporates a frame grabber and a computer. Two calibrations are necessary: one of the spectrometer with respect to the micrometer reading by using the light from a mercury lamp with known wavelength emission, and the second calibration of the spectrometer with respect to the screen position, which is made by noting the variation in screen position for each spectral line, as a function of micrometer setting. With these improvements the ultra-thin film technique enables films down to less than 5 nm thick to be measured with an accuracy of ± 2 nm **[19]**.

There is also a major modification in Fig.3.15, that of including two electrodes connecting to a potentiostat, to control the potential of the ball surface versus a reference electrode. This test rig modification will be explained in the next section.

3.3.3.3 EHD rig modifications and test conditions

In this study, the ultra-thin film technique was employed under controlled electrode potentials of the ball to examine the effect of that potential on film forming characteristics, mainly due to the interactions between a metal surface of the ball and friction and wear reducing additives in a lubricant.

To achieve the electrode potential control of the ball, it was connected electronically through a spindle with a potentiostat. A schematic modification of the EHD rig with an electrochemical technique is shown in Fig.3.16.

A 19.0 mm diameter, AISI 52100 steel ball was drilled in the centre to insert a shaft which was driven by the external motor of the rig. This ball was used as a working electrode and was loaded against the flat surface of a glass disc to form a Hertzian-type contact. The disc was driven by a DC motor at the same speed of the ball to form a nominally pure rolling contact. A two-speed gear-box allowed a speed variation from 10^{-3} to 5 m s^{-1}.

For electrochemical control of the steel ball in the EHD test rig, a platinum plate and a silver wire, both which were located at very close to the ball (less than 1 mm away), were employed as counter and reference electrodes, respectively. The equilibrium potential of silver wire (Ag^{+}/Ag) was measured as -0.188 V vs. S.C.E., in the 0.01 M $(Et)_4NBF_4$ PC electrolyte solution.

The ball was two-thirds-immersed in test lubricant, and the ball, disc and lubricant were contained in a stainless steel chamber, which was provided with electric heaters so that the temperature could be maintained within ± 1°C. The bulk lubricant temperature, as well as the temperature close to the contact inlet, which is controlled by a local thermocouple, were measured during the test.

Film thickness was measured using ultra-thin film interferometry; to enable this, the disc surface was coated with a 20 nm thick chromium layer, covered by a 600 nm thick silica layer, as described in the previous section. Both ball and glass had a roughness of approximately 11 nm rms and Young's moduli of the two surfaces were 210 and 75 GPa for steel and glass, respectively. The load applied was 20 N, corresponding to maximum Hertz contact pressure of 0.54 GPa.

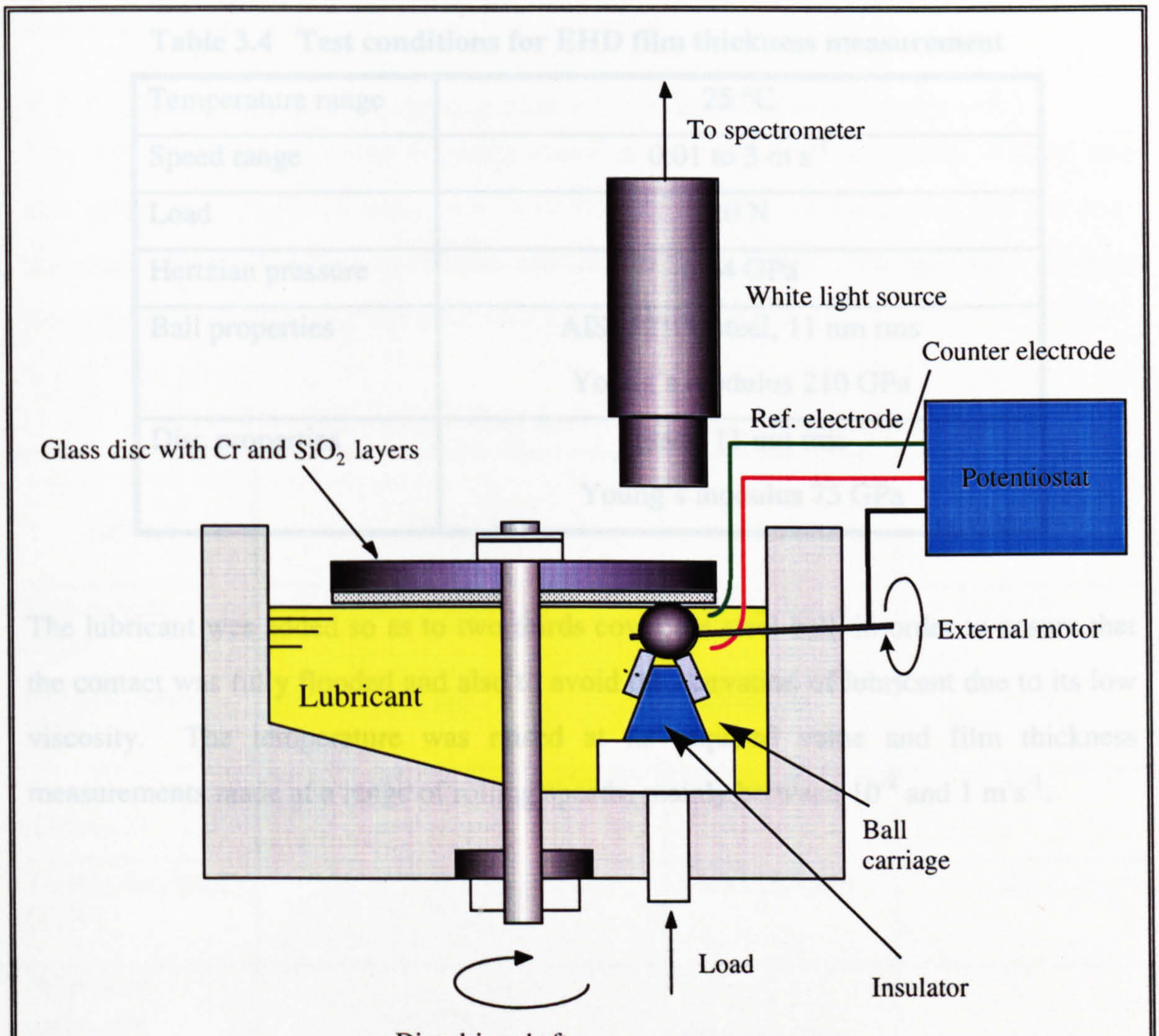


Fig.3.16 EHD rig modified to enable control of the ball electrode potential.

The test conditions employed in most of the current work are summarised in Table 3.4.

The experimental protocol was as follows. A new steel ball was used for each test. The test rig, glass disc and steel ball were cleaned thoroughly using toluene and analytical grade acetone and the rig assembled. Before lubricant was added, the thickness of the spacer layer was measured in dry loaded contact. This value was subtracted from the overall film thickness measured when oil was present, in order to give the true value of the oil film.

Table 3.4 Test conditions for EHD film thickness measurement

Temperature range	25 °C
Speed range	0.01 to 3 m s^{-1}
Load	20 N
Hertzian pressure	0.54 GPa
Ball properties	AISI 52100 steel, 11 nm rms Young's modulus 210 GPa
Disc properties	glass, 11 nm rms Young's modulus 75 GPa

The lubricant was added so as to two-thirds cover the steel ball, in order to ensure that the contact was fully flooded and also to avoid the starvation of lubricant due to its low viscosity. The temperature was raised at its required value and film thickness measurements made at a range of rolling speeds, mainly between 10^{-2} and 1 m s^{-1}.

CHAPTER 4

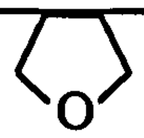
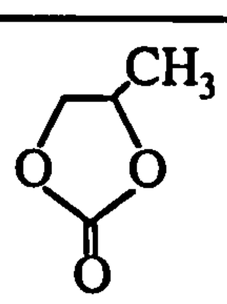
4. Chemicals and materials used

4.1 Chemicals

4.1.1 Chemicals as supporting electrolytes and solvents(base oils)

Five solvents listed in Table 4.1 were examined as lubricant base fluids, divided into two categories: (i) fluids analogous to conventional lubricant base oils, and (ii) non-aqueous solvents in which to conduct electrochemical studies. The first three solvents lie in the first category and the other two lie in the second one.

Table 4.1 Solvents used as a base oil. (A.G. : Analytical Grade)

Solvent	Formula	Detail	Kinematic viscosity @25 °C / $mm^2\ s^{-1}$
Hexadecane (HD)	CH_3-$(CH_2)_{14}$-CH_3	Aldrich Inc.	3.69
Butylbenzene (BB)	Ph-$(CH_2)_3$-CH_3	Aldrich Inc.	1.09
Diethyl-adipate (DEA)	$C_2H_5OCHO_2(CH_2)_4CO_2C_2H_5$	Aldrich Inc.	3.06
Tetrahydrofuran (THF)		Fluka (A.G.)	0.57
Propylene carbonate (PC)		Fluka (A.G.)	2.00

An appropriate supporting electrolyte was selected to enhance the conductivity of a lubricant, to enable electrode potential control.

The salts listed in Table 4.2 were screened as supporting electrolytes, initially determining their solubility in the non-aqueous solvents described in Table 4.2. All of them except propylene carbonate (PC) were used as received, without further purification. To remove dissolving water, molecular sieves (BDH Chemical Ltd. Type 4A) were mixed with PC, and left at least one night before use.

Table 4.2 Salts used as supporting electrolytes. (A.G. : Analytical Grade)

Supporting electrolyte	Formula	Detail
Tetrahexylammonium perchlorate [$(Hx)_4NClO_4$]	$[CH_3(CH_2)_5]_4N$-ClO_4	Fluka (A.G.)
Tetrabutylammonium bromide [$(Bu)_4NBr$]	$[CH_3(CH_2)_3]_4N$-Br	Fluka (A.G.)
Tetraethylammonium tetrafluoroborate [$(Et)_4NBF_4$]	$[CH_3CH_2]_4N$-BF_4	Fluka (A.G.)
Sodium tetraphenylborate	$Na[(Ph)_4B]$	Fluka (A.G.)
Lithium tetrafluoroborate	$LiBF_4$	Aldrich Inc.
Lithium perchlorate	$LiClO_4$	Aldrich Inc.

4.1.2 Other chemicals and additives for friction and wear reduction

Before using conventional lubricant additives, preliminary voltammetric experiments were carried out using ferrocene as a 'model' fast redox couple in various combinations of supporting electrolyte and solvent, to investigate the reversibility or otherwise of the ferrocene / ferrocinium couple **[1,2]**. This was a useful model redox couple for this study because of its good solubility in most non-aqueous solvents as well as the ease of interpretation of its electrochemical behaviour, based on previous work **[3-5]**.

$$\left(\pi - C_5H_5\right)_2 Fe \leftrightarrow \left(\pi - C_5H_5\right)_2 Fe^+ + e^- \qquad (4\text{-}1)$$

Dibenzyl disulphide and organic acids were selected as anti-seizure and wear additives and friction modifiers, respectively, because these are widely used for this purpose in commercial lubricants, and have relatively simply chemical structures, as indicated in Table 4.3.

Table 4.3 Chemicals and additives used in this study.

Chemical /Additive	Formula	Detail
Ferrocene	$(\pi\text{-}C_5H_5)_2\text{-}Fe$	Fluka (Analytical Grade)
Dibenzyl disulphide	$Ph\text{-}CH_2\text{-}S\text{-}S\text{-}CH_2\text{-}Ph$	Koch-Light Limited
Octanoic acid	$CH_3(CH_2)_6\text{-}COOH$	Fluka (Analytical Grade)
Dodecanoic acid	$CH_3(CH_2)_{10}\text{-}COOH$	Fluka (Analytical Grade)
Hexadecanoic acid	$CH_3(CH_2)_{14}\text{-}COOH$	Fluka (Analytical Grade)
Octadecanoic acid	$CH_3(CH_2)_{16}\text{-}COOH$	Fluka (Analytical Grade)

4.2 Materials

All the solid materials used in this study are listed in Table 4.4.

A platinum wire or an iron rod was used as a working electrode for the voltammetry, FT-IR spectroscopy and impedance spectroscopy, with a platinum foil as a counter electrode.

Friction and wear measurements were conducted in a high frequency reciprocating (HFR) rig, with a 6.0 mm diameter steel ball on a 10.0 mm diameter steel disc. The average surface roughnesses of disc and ball were approximately 30 nm and 11 nm, respectively. The hardnesses of these specimens are described in Table 3.6.

For the film thickness measurement using ultra-thin film interferometry, the glass disc surface was coated with a 20 nm thick chromium layer covered by a 600 nm thick silica layer. Both ball and glass had a roughness of approximately 11 nm in root mean square value (rms) and the Young's moduli of the two surfaces are 210 and 75 GPa for steel and glass, respectively. The load applied was 20 N, corresponding to maximum Hertz contact pressure of 0.54 GPa.

Table 4.4 Solid materials used.

Purpose of use	Material	Detail
Electrode materials for voltammetry	Platinum wire	Diameter = 0.5 mm
	Iron rod	Diameter = 1 mm
	Platinum plate	Area of plate = 0.8 cm^2
Specimens for HFR rig	Steel ball (AISI 52100)	Surface roughness = 30 nm Hardness (Hv) = 850 Diameter = 6.0 mm
	Steel disc (AISI 52100)	Surface roughness = 11 nm Hardness (Hv) = 190 - 210 Diameter = 10 mm
Electrode materials for infrared spectroscopy	Iron rod	Diameter = 5 mm
	Platinum wire	Length = 30 mm
Materials for ultra-thin film thickness technique	Glass disc	Cr layer = 20 nm SiO_2 layer = 600 nm Surface roughness = 11 nm Diameter = 100 mm
	Ball (AISI 52100)	Surface roughness = 11 nm Hardness (Hv) = 190 - 210 Diameter = 19 mm
	Platinum plate	Area of plate = 1.2 cm^2
	Silver wire	Diameter = 1 mm
Electrode materials for AFM measurement	Iron rod	Diameter = 1 mm
	Platinum plate	Area of plate = 0.8 cm^2

For electrochemical control of the steel ball in the EHD test rig, a platinum plate and a silver wire were employed as counter and reference electrodes, respectively. The equilibrium potential of silver wire (Ag^+/Ag) was measured as -0.188 V vs. S.C.E., in the 0.01 M $(Et)_4NBF_4$ PC electrolyte solution.

The test rig, glass disc and steel ball were cleaned thoroughly using toluene and analytical grade acetone in an ultrasonic bath.

For AFM measurement, the iron electrode (99.99%, Goodfellow Metals Ltd.) was polished firstly with various grades of SiC paper, then finally with an aqueous dispersion of nominally 15 nm alumina powder. The AFM tip was Si_3N_4 with an applied load on the cantilever.

CHAPTER 5

5. Selection of non-aqueous systems for electrochemical work

5.1 Introduction

This chapter describes the selection of appropriate non-aqueous electrolyte systems for subsequent tribological measurements as a function of electrode potential. This selection process involved solubility and conductivity measurements, and determination of the electrochemical behaviour of the model redox couple ferrocinium (Fc^+) / ferrocene (Fc)", in a range of organic solvents to which various supporting electrolytes were added.

5.2 Solubility test of electrolytes with non-aqueous solvents

It was necessary to identify appropriate supporting electrolytes which provided sufficient conductivity for the determination of the voltammetric behaviour of additives in non-aqueous lubricants. This is mainly because ionic strength, depending on the type of electrolyte, will influence the diffuse double layer thickness, and hence the potential across the Helmholtz layer will be varied due to the change of uncompensated ohmic potential losses when a potential is applied between working and reference electrodes.

5.2.1 Estimation of polarities for non-aqueous lubricants

Generally, according to the theory of regular solutions, the closer the polarity of a compound to that of the solvent, the more facile its dissolution **[1]**. The polarity of an organic compound can be quantified as a solubility parameter (δ) by Fedor's method **[2]**, in which an organic compound is divided into basic molecular groups, the contributions from which can be determined by their molar volumes (v_m) and their energies of vaporisation (E_v), according to Eq.(5-1).

$$\delta = \left(\frac{E_v}{v_m}\right)^{0.5} = \left(\frac{\sum_i \Delta E_{vi}}{\sum_i \Delta v_{mi}}\right)^{0.5} \qquad (5\text{-}1)$$

where ΔE_{vi} and Δv_{mi} correspond to the energy of vaporisation and molar volume of each basic molecular group. The solubility parameters of non-aqueous solvents used in this study were determined by that method and are summarised in Table 5.1.

Table 5.1 Solubility parameters for non-aqueous solvents

Non-aqueous solvent	Solubility parameter/ $(MJ\ m^{-3})^{1/2}$
Di-ethyl adipate (DEA)	19.39
Butyl benzene (BB)	18.32
Hexadecane (HD)	16.38
Propylene carbonate (PC)	23.54
Tetrahydrofuran (THF)	18.41

5.2.2 Solubility test results

The electrolytes listed in Table 4.2 in Chapter 4 were added individually to the solvents listed in Table 5.1 at various temperatures to determine whether they were sufficiently soluble to form a 0.1 M solution. This was because the electrolyte concentration of 0.1 M had been used as a standard in previous non-aqueous work **[3-5]**. The results, summarised in Table 5.2, indicate that the higher the polarity (solubility parameter) of the solvent, the greater the number of electrolytes that can be dissolved, and the more facile their dissolution. Consequently, the solvents PC and THF, frequently used in non-aqueous electrochemical studies, were the best of the five solvents for the chosen electrolytes. The other three, HD, BB and DEA intended as solvents to represent lubricant base oils, had limited solubilities for the chosen electrolytes. Among those three, DEA was the most promising because it could dissolve both $LiClO_4$ and $LiBF_4$ at room temperature, partly due to its relatively high polarity. Hence, this ester was also chosen for further study.

Table 5.2 Test result of the solubility of electrolytes in non-aqueous solvents.

Types of electrolytes	Non-aqueous solvents				
	DEA	BB	HD	PC	THF
$(Hx)_4NClO_4$	×	$\triangle^1$	×	△	$\times^1$
$(Bu)_4NBr$	×	×	×	△	△
$(Et)_4NBF_4$	×	×	×	○	×
$Na[(Ph)_4B]$	△	×	×	○	△
$LiClO_4$	△	×	×	△	△
$LiBF_4$	△	×	×	○	○

○ : Soluble after stirred magnetically
△ : Soluble after heated up, or soluble above 100 °C ($\triangle^1$)
× : Insoluble or colour of the solvent changed ($\times^1$)

On the other hand, high temperatures were required to dissolve $(Hx)_4NClO_4$ in BB, which is less polar than DEA, and led to volatility losses. Even at high temperatures, no electrolyte could be dissolved in HD at the 0.1 M level, because of the latter's non-polar nature.

A lack of solubility parameter information for Na^+, Li^+, ClO_4^- *etc.* in previous work **[2]**, precluded calculation of the solubility parameters for the electrolytes used. However, all of the electrolytes dissolved in PC, as indicated in Table 5.2. Thus, these parameters can be estimated as ≥ *ca.* 23, if the theory of regular solutions can be applied.

5.3 Prediction of the suitability of non-aqueous systems

An appropriate supporting electrolyte and concentration in DEA, PC and THF, were chosen by measuring the behaviour of the ferrocinium ion / ferrocene redox couple in terms of the deviation from its model voltammetric behaviour, which is an indication of complications induced by the electrolyte.

5.3.1 Electrochemical behaviour of DEA electrolyte solutions

The suitability of electrolytes found to be soluble in DEA, *i.e.*, $Na[(Ph)_4B]$, $LiClO_4$ and $LiBF_4$ was investigated by voltammetric experiments.

5.3.1.1 Electrochemical behaviour of electrolytes in DEA

Fig.5.1 shows cyclic voltammograms of Pt / DEA with three types of electrolytes. With $Na[(Ph)_4B]$ supporting electrolyte, the oxidation current increased rapidly at electrode potentials > 0.4 V on the positive-going potential sweep, due to the oxidation of $[(Ph)_4B]^-$ to $[(Ph)_4{}^+B]^-$ **[6]**, the currents at such potentials being approximately proportional to the electrolyte concentration.

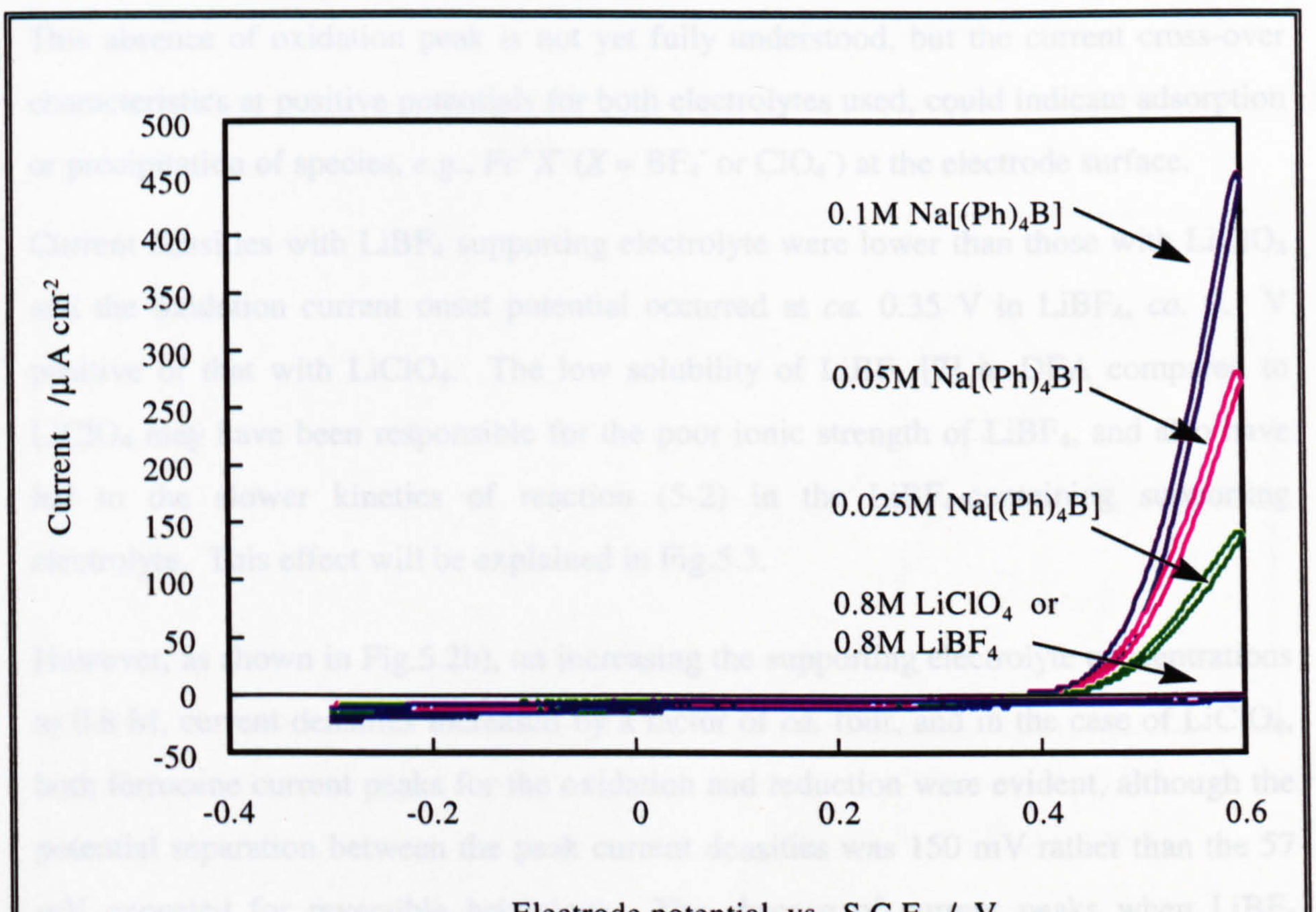


Fig.5.1 Effect of electrolyte type and concentration on the voltammetric behaviour of a Pt electrode in DEA, obtained at a scan rate of 100 mV s^{-1}.

On the other hand, no such oxidation currents were observed with $LiClO_4$ or $LiBF_4$ electrolytes, implying both were stable in DEA over the electrode potential range studied.

5.3.1.2 Voltammetric behaviour of ferrocene in DEA

The cyclic voltammetric behaviour of ferrocene in DEA was studied to investigate the suitability of $LiClO_4$ and $LiBF_4$ as supporting electrolytes. Fig.5.2a) shows the voltammogram of a Pt electrode in 4 mM ferrocene with 0.1 M $LiClO_4$ and $LiBF_4$, respectively, indicating the absence of a transport controlled ferrocene oxidation current peak, although the subsequent reduction peak was better defined:

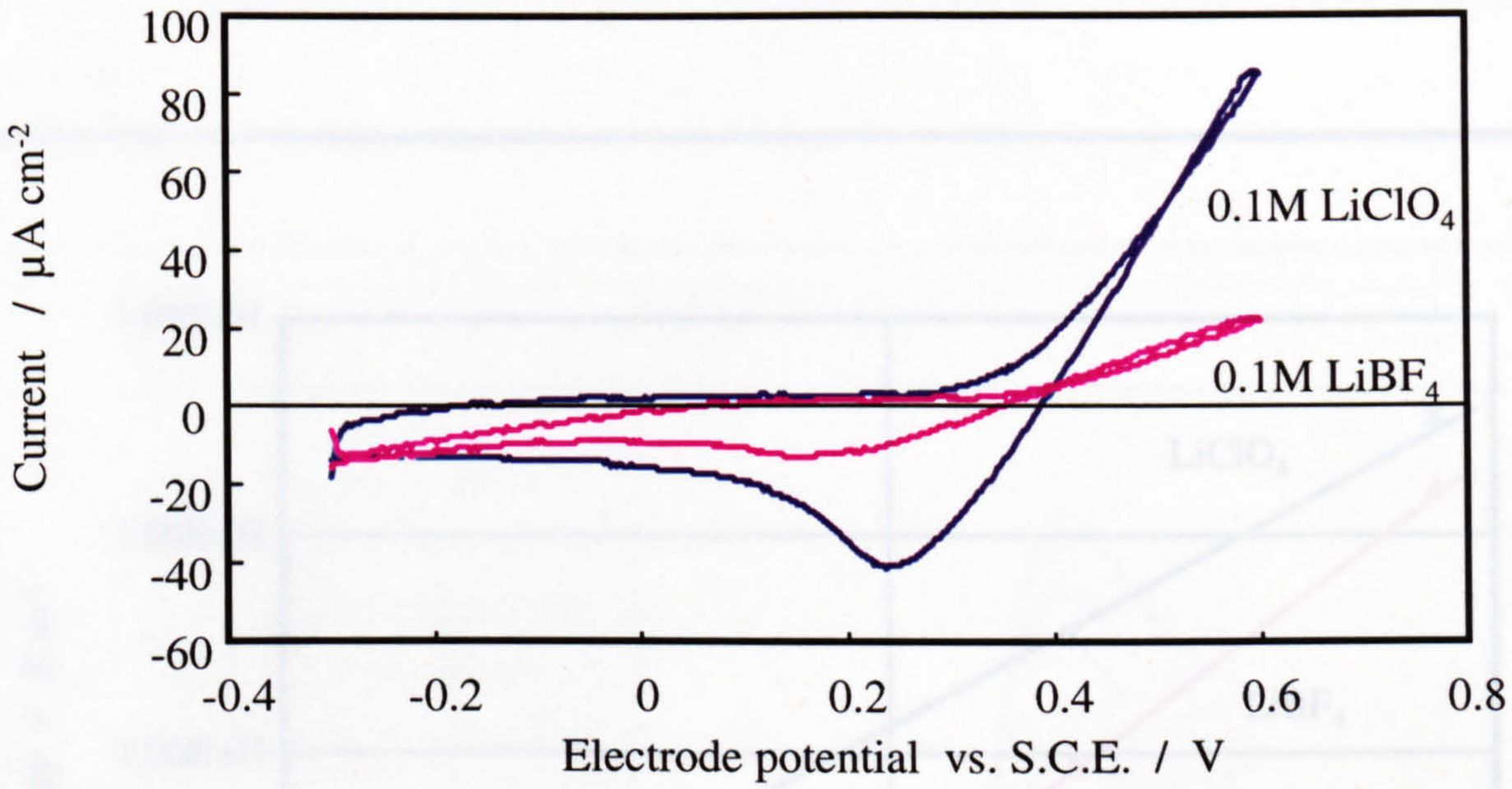
$$\left(\pi - C_5H_5\right)_2 Fe \leftrightarrow \left(\pi - C_5H_5\right)_2 Fe^+ + e^- \qquad (5\text{-}2)$$

This absence of oxidation peak is not yet fully understood, but the current cross-over characteristics at positive potentials for both electrolytes used, could indicate adsorption or precipitation of species, *e.g.*, Fc^+X^- ($X = BF_4^-$ or ClO_4^-) at the electrode surface.

Current densities with $LiBF_4$ supporting electrolyte were lower than those with $LiClO_4$ and the oxidation current onset potential occurred at *ca.* 0.35 V in $LiBF_4$, *ca.* 0.1 V positive of that with $LiClO_4$. The low solubility of $LiBF_4$ **[7]** in DEA compared to $LiClO_4$ may have been responsible for the poor ionic strength of $LiBF_4$, and also have led to the slower kinetics of reaction (5-2) in the $LiBF_4$-containing supporting electrolyte. This effect will be explained in Fig.5.3.

However, as shown in Fig.5.2b), on increasing the supporting electrolyte concentrations to 0.8 M, current densities increased by a factor of *ca.* four, and in the case of $LiClO_4$, both ferrocene current peaks for the oxidation and reduction were evident, although the potential separation between the peak current densities was 150 mV rather than the 57 mV expected for reversible behaviour. The absence of current peaks when $LiBF_4$ supporting electrolyte was used, may reflect adsorption blocking the electrode surface.

a) Electrolyte concentration: 0.1 M



b) Electrolyte concentration: 0.8 M

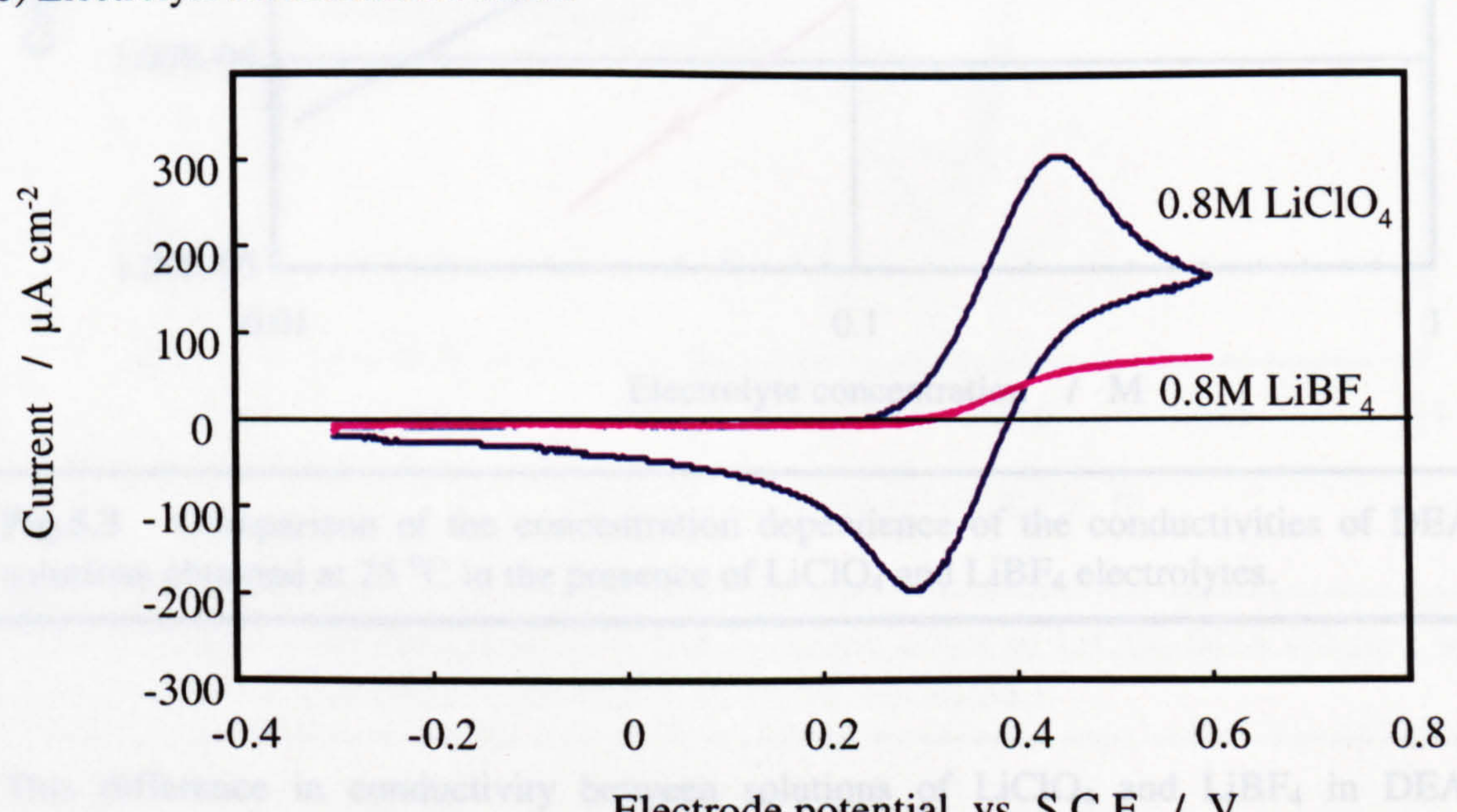


Fig.5.2 Cyclic voltammograms of Pt / 4 mM ferrocene at a scan rate of 100 mV s^{-1}, in DEA containing $LiClO_4$ and $LiBF_4$ supporting electrolytes, at concentrations of a) 0.1M and b) 0.8M.

The influence of electrolyte concentration on the voltammetric behaviour could be due to its effect on the conductivity of $LiClO_4$ and $LiBF_4$ in DEA, as shown in Fig.5.3, DEA with $LiClO_4$ having higher conductivities than DEA with $LiBF_4$.

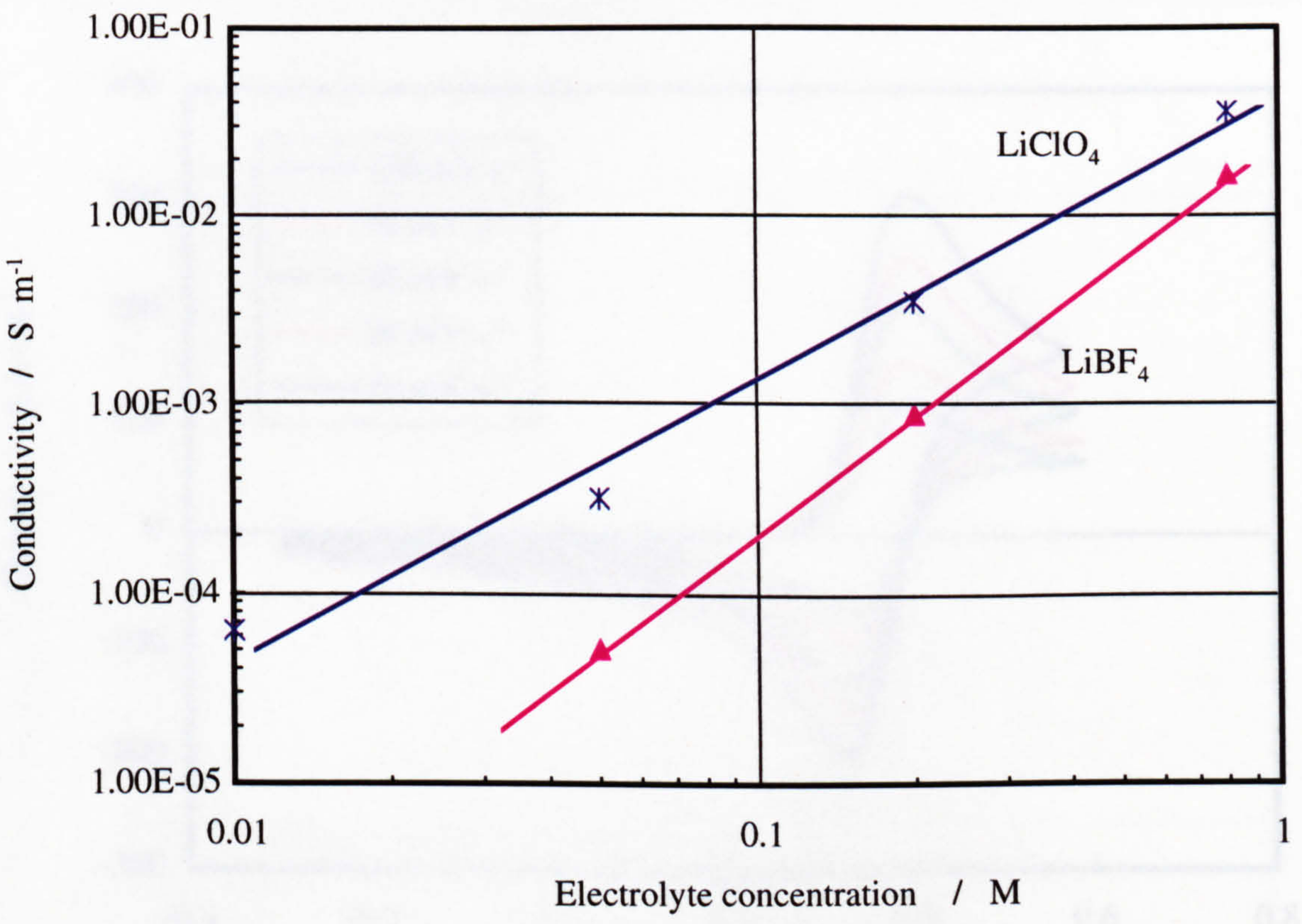


Fig.5.3 Comparison of the concentration dependence of the conductivities of DEA solutions obtained at 25 °C in the presence of $LiClO_4$ and $LiBF_4$ electrolytes.

This difference in conductivity between solutions of $LiClO_4$ and $LiBF_4$ in DEA, presumably reflects differences in the interactions between the anions and / or cations **[8]**, which in turn depend on the properties of the solvent.

5.3.1.3 Analysis of the voltammetry with ferrocene in DEA electrolyte solutions

Figs.5.4 and 5.5 show the effect of potential scan rate (v) on the cyclic voltammograms of Pt / ferrocene in DEA with 0.8 M $LiClO_4$ and 0.8 M $LiBF_4$ as supporting electrolyte, respectively.

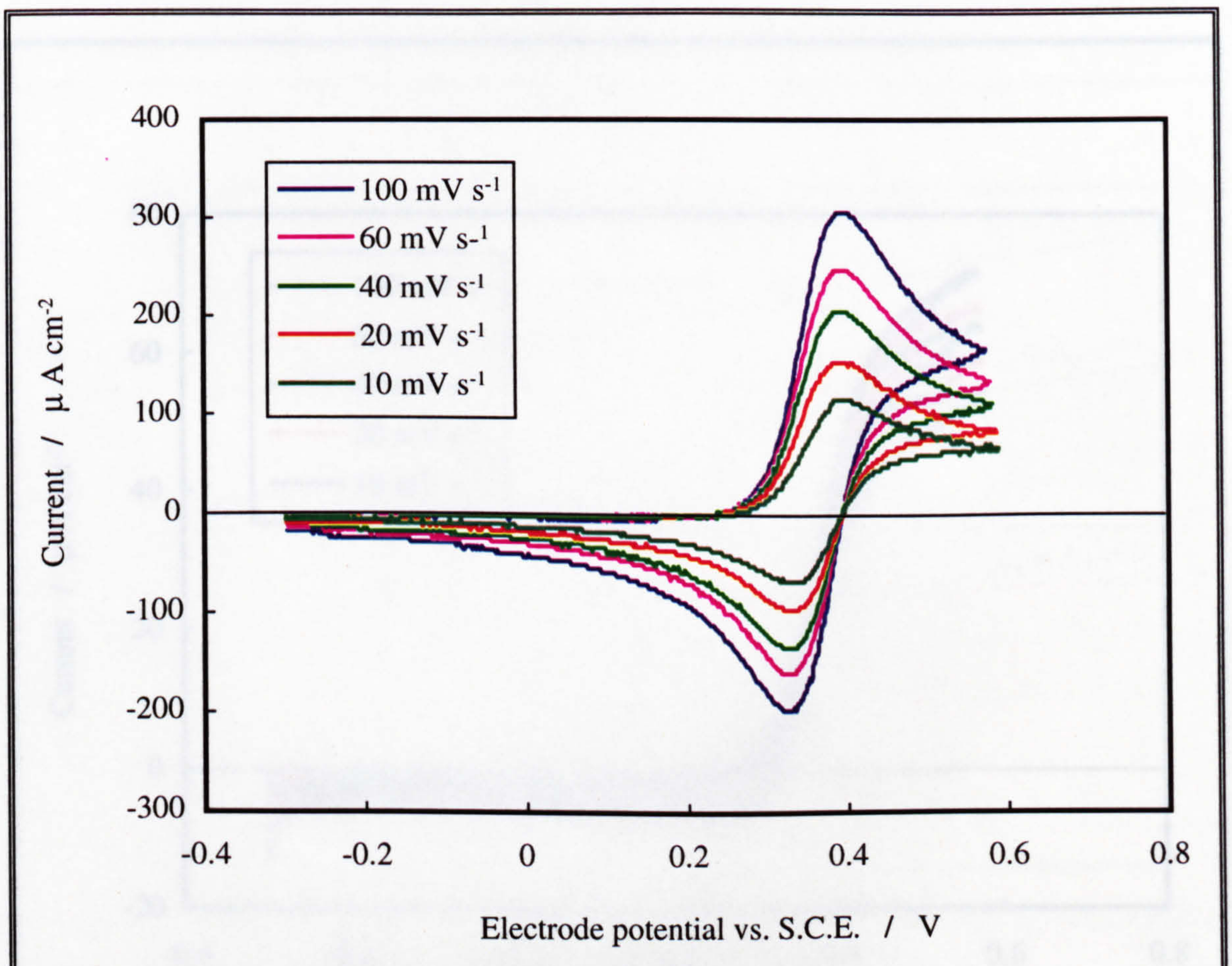


Fig.5.4 Cyclic voltammograms of 4 mM ferrocene in 0.8 M $LiClO_4$ DEA solution, at various potential scan rates. (The data were not IR-corrected.)

All the voltammograms were modified with the subtraction of IR potential drop between working and reference electrodes, which was calculated from the electrolysis current values and the conductivities of the solutions according to the results in Fig.5.3.

As described in Chapter 3, for the case of 'reversible' electron transfer, the peak current density (i_p / A cm^{-2}) is predicted theoretically to increase with the square root of the potential sweep rate (v_s / V s^{-1}), according to the equation **[9,10]**:

$$i_p = 0.4463 zF\left(\frac{zF}{RT}\right)^{0.5} D_i^{0.5} v_s^{0.5} C_A \qquad (3\text{-}11)$$

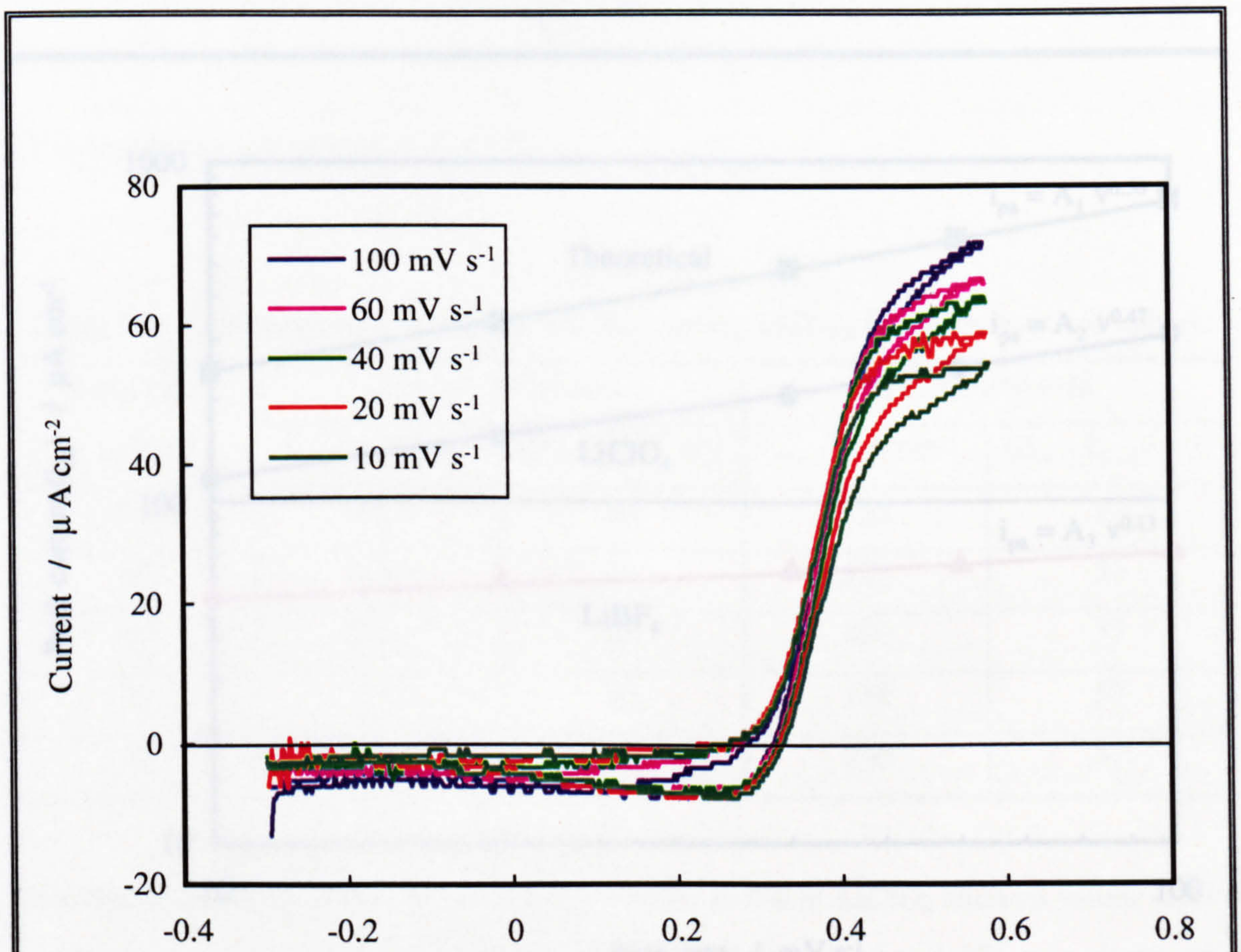


Fig.5.5 Cyclic voltammograms of 4 mM ferrocene in 0.8 M $LiBF_4$ DEA solution, at various potential scan rates. (The data were not IR-corrected.)

whereas for 'irreversible' reactions:

$$i_p = \left(2.99 \times 10^5\right) z\left(\alpha z_a\right)^{0.5} D_i^{0.5} v_s^{0.5} C_A \qquad (3\text{-}12)$$

where z_a corresponds to the number of electrons involved in the rate-determining step.

As shown in Fig.5.6, experimental values of i_{pa} varied linearly with $v^{0.48}$ in $LiClO_4$ supporting electrolyte, and with $v^{0.13}$ in $LiBF_4$, indicating that solution phase diffusion was not the rate-determining step in the latter electrolyte, possibly due to the presence of an adsorbed layer of $FcBF_4$ ions on the Pt electrode, hindering ferrocene oxidation in $LiBF_4$.

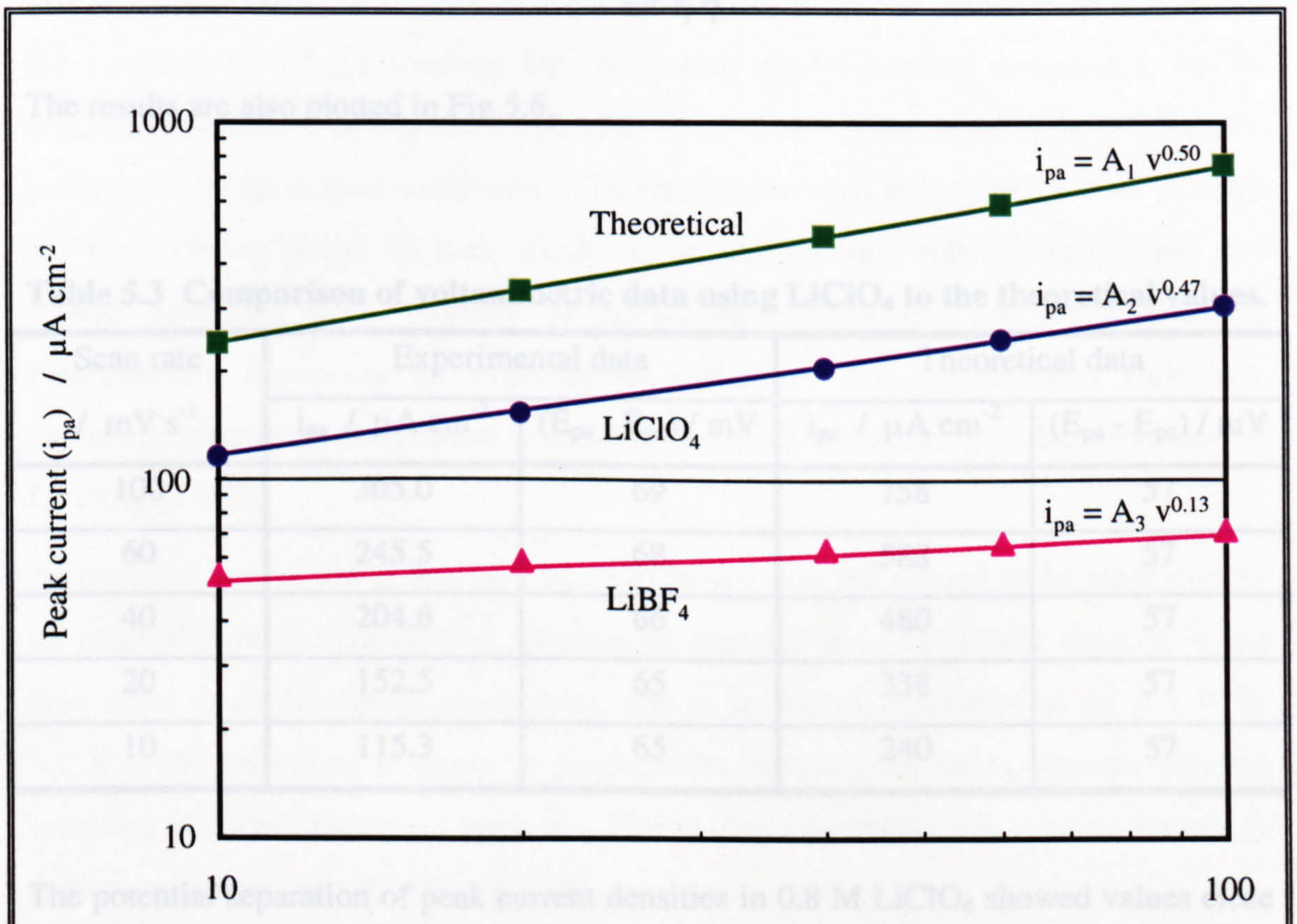


Fig.5.6 Relationship between cyclic voltammetric anodic peak current densities (i_{pa}) and potential scan rate (v) for ferrocene oxidation in DEA electrolyte solutions.

Table 5.3 summarises experimental values of the oxidation peak current densities (i_{pa}) and separation of the potentials corresponding to the oxidation and reduction peak current densities (E_{pa} - E_{pc}) for ferrocene in 0.8 M $LiClO_4$.

Theoretical values predicted by Eqs.(3-11) and (3-12) are also tabulated, assuming a diffusion coefficient (D_i) of 5.7×10^{-10} m^2 s^{-1} **[11]**, which was obtained in di-methyl sulphoxide (DMSO), chosen because DMSO and DEA have a similar viscosity (η), so that for the same effective hydrodynamic radius (r_s) of the diffusing electro-active species, D_i would have a similar value in the two solvents. D_i can be expressed according to the Stokes-Einstein equation:

$$D_i = \frac{k_B T}{6\pi r_s \eta} \qquad (5\text{-}3)$$

The results are also plotted in Fig.5.6.

Table 5.3 Comparison of voltammetric data using $LiClO_4$ to the theoretical values.

Scan rate / mV s^{-1}	Experimental data		Theoretical data	
	i_{pa} / μA cm^{-2}	$(E_{pa} - E_{pc})$ / mV	i_{pa} / μA cm^{-2}	$(E_{pa} - E_{pc})$ / mV
100	305.0	69	758	57
60	245.5	68	588	57
40	204.6	66	480	57
20	152.5	65	338	57
10	115.3	65	240	57

The potential separation of peak current densities in 0.8 M $LiClO_4$ showed values close to the theoretical ones, the high potential drop between working and reference electrodes having been eliminated using the measured electrolyte solution, *i.e.*, conductivity for electrolyte solutions. However, peak current densities were approximately half of the theoretical values. This indicates that ferrocene exhibits only quasi-reversible electron transfer behaviour in DEA containing 0.8 M $LiClO_4$, though this electrolyte showed the fastest kinetics of those studied in DEA, and hence it was chosen as one of the non-aqueous systems for further investigation.

5.3.2 *Electrochemical behaviour of PC and THF electrolyte solutions*

Compared to DEA for which choices of supporting electrolytes were limited, according to the solubility test results, PC and THF have a wide range of possible supporting electrolytes.

5.3.2.1 Pre-selection of electrolytes for triboelectrochemistry with PC and THF

The practical reason for using a supporting electrolyte for this project was to enhance the conductivity of the solution for conducting electrochemical techniques, but its concentration should be the lowest possible to minimise interactions with the electrode surfaces under lubricated conditions. The electrolytes used for solubility tests in Table 5.2 were chosen based on their suitability in non-aqueous solvents **[3-5]**, and they should generally work properly as supporting electrolytes for electro-chemical measurement, depending on experimental conditions and compatibility with iron. However, pre-testing was needed to examine the relative suitability of these electrolytes for PC and THF.

As reported previously in this chapter, $Na[(Ph)_4B]$ was considered to be least suitable for electrochemical investigation, because its potential limit for anodic reaction is less than other those of organic electrolytes, due to its radical formation at *ca.* 0.4 V vs. S.C.E. The behaviour is likely to preclude the detection of redox systems between lubricant additives and metal surfaces. Hence, this electrolyte was omitted for use in further investigations with PC and THF.

$(Hx)_4NClO_4$ and $LiClO_4$ were also less favoured for this study, because perchlorate is thermodynamically predicted to be a powerful oxidant. Chloride ion reduction products could also be aggressive towards iron if they behaved as in aqueous electrolytes. These chemicals might then influence the redox system under dynamic lubricated conditions, both as oxygen providers and anti-wear agents, and could lead to a change in tribological properties **[12]**. Thus, both of these supporting electrolytes were not favoured for further electrochemical studies.

Hence, the subsequent electrochemical studies were carried out mainly with supporting electrolytes, $(Bu)_4NBr$, $(Et)_4NBF_4$ and $LiBF_4$, and the suitability for their use in electrochemistry was determined.

5.3.2.2 Conductivity measurements of non-aqueous electrolyte solutions

Fig.5.7 shows the concentration dependencies of the conductivities of various electrolytes at 25 °C. These results show that the conductivity of the electrolyte solutions increases dramatically with increase of the molar concentration of the electrolytes. This behaviour conforms well with previous work **[13]**.

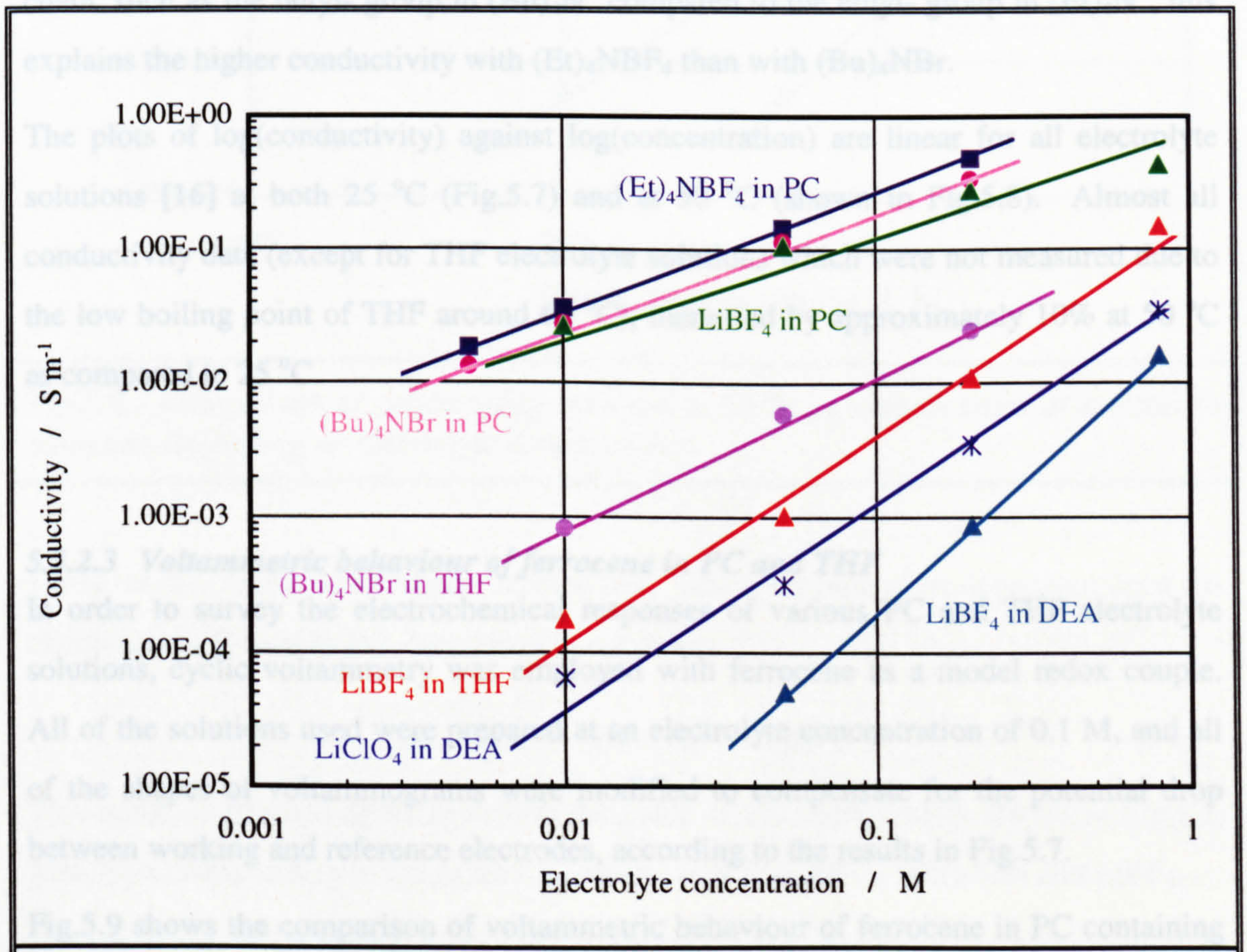


Fig.5.7 Concentration dependencies of the conductivities obtained at 25 °C in various types of electrolyte solutions.

In terms of conductivity, electrolytes and solvents obeyed the following order:

$(Et)_4NBF_4$ in PC > $(Bu)_4NBr$ in PC > $LiBF_4$ in PC >> $(Bu)_4NBr$ in THF >

$LiBF_4$ in THF > $LiClO_4$ in DEA >> $LiBF_4$ in DEA (5-4)

This means that the ability to ionise and to stabilise a supporting electrolyte strongly corresponds to the polarity of the solvent employed **[14]**. This also implies differences are due to effective ionic concentrations and activities.

The type of electrolyte also influences the conductivity, even in the same solvent. Differences of conductivity could be due to the size, geometry and distribution of charge on the anion and /or cation of the electrolyte employed **[15]**. These physical properties would be expected to yield an ion of enhanced stability in a solvent. For instance, the localised charge of the tetra-alkyl ammonium ion would be hindered by a longer alkyl chain, such as the butyl- group in $(Bu)_4N^+$ compared to the ethyl- group in $(Et)_4N^+$, this explains the higher conductivity with $(Et)_4NBF_4$ than with $(Bu)_4NBr$.

The plots of log(conductivity) against log(concentration) are linear for all electrolyte solutions **[16]** at both 25 °C (Fig.5.7) and at 50 °C (shown in Fig.5.8). Almost all conductivity data (except for THF electrolyte solutions which were not measured due to the low boiling point of THF around 66 °C), increased by approximately 10% at 50 °C as compared to 25 °C.

5.3.2.3 Voltammetric behaviour of ferrocene in PC and THF

In order to survey the electrochemical responses of various PC and THF electrolyte solutions, cyclic voltammetry was employed with ferrocene as a model redox couple. All of the solutions used were prepared at an electrolyte concentration of 0.1 M, and all of the shapes of voltammograms were modified to compensate for the potential drop between working and reference electrodes, according to the results in Fig.5.7.

Fig.5.9 shows the comparison of voltammetric behaviour of ferrocene in PC containing these different electrolytes, which was obtained at 100 mV s^{-1}. All of three show very similar characteristics, and also clear oxidation and reduction peaks.

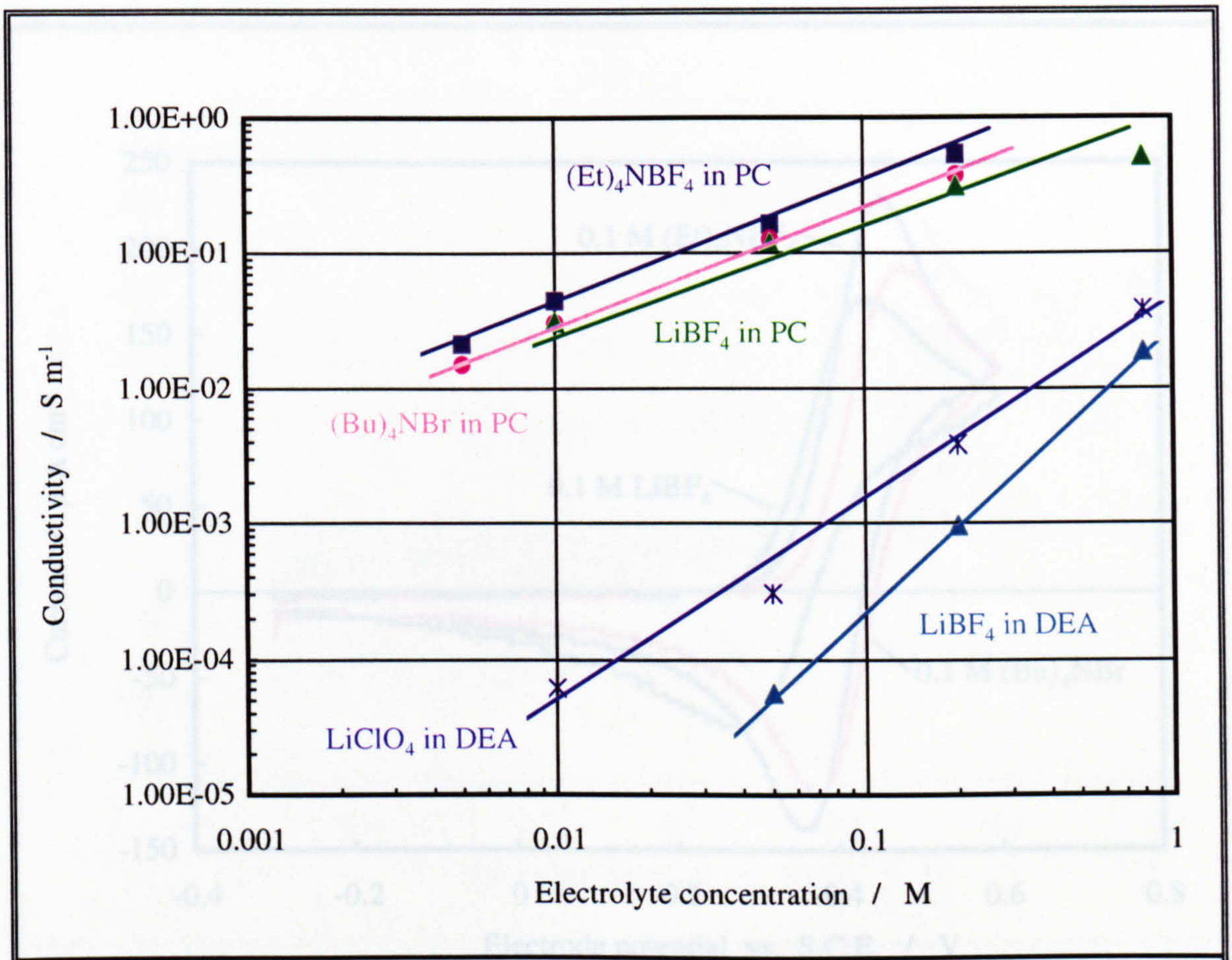


Fig.5.8 Comparison of conductivity obtained at 50 °C in various types of electrolyte solutions, depending on electrolyte concentration.

However, the anodic and cathodic current peak values are seen to be dependent upon the electrolyte **[17]** used in PC, increasing in the order:

$$(Et)_4NBF_4 > (Bu)_4NBr > LiBF_4 \qquad (5\text{-}5)$$

This result is in good agreement with the order of the conductivity shown in Fig.5.7, possibly corresponding to the extent of ionisation of $(Et)_4NBF_4$, $(Bu)_4NBr$ and $LiBF_4$.

As shown in Fig.5.10, the voltammetric behaviour of ferrocene in THF electrolyte solutions was very different to that in PC. The anodic and cathodic peak values were decreased and were not clearly recognisable as reversible voltammetric behaviour

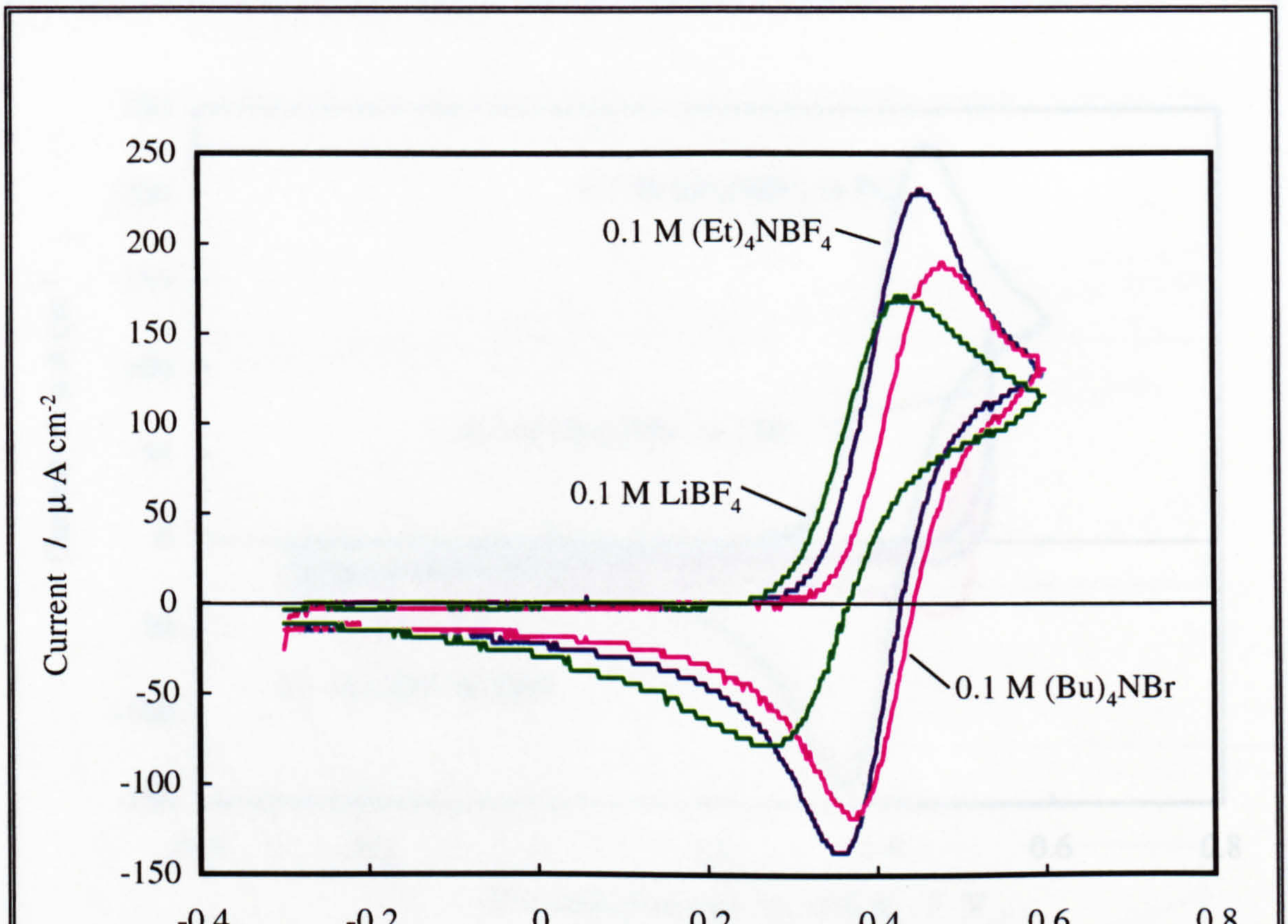


Fig.5.9 Comparison of cyclic voltammetry of ferrocene in various electrolyte PC solutions obtained at the scan rate of 100 mV s^{-1}.

This is probably due to the low conductivity of the electrolyte in THF. As was indicated in Fig.5.3 with DEA electrolyte solutions, clear oxidation and reduction peaks in voltammetry were observed with 0.8 M $LiClO_4$, whose conductivity in DEA was measured as 0.036 S m^{-1}. Based on this value, a concentration of 0.4 M of $(Bu)_4NBr$ or $LiBF_4$ in THF would be required to obtain clear redox peaks of ferrocene. This result suggests that THF is not as suitable as non-aqueous system in this study as PC.

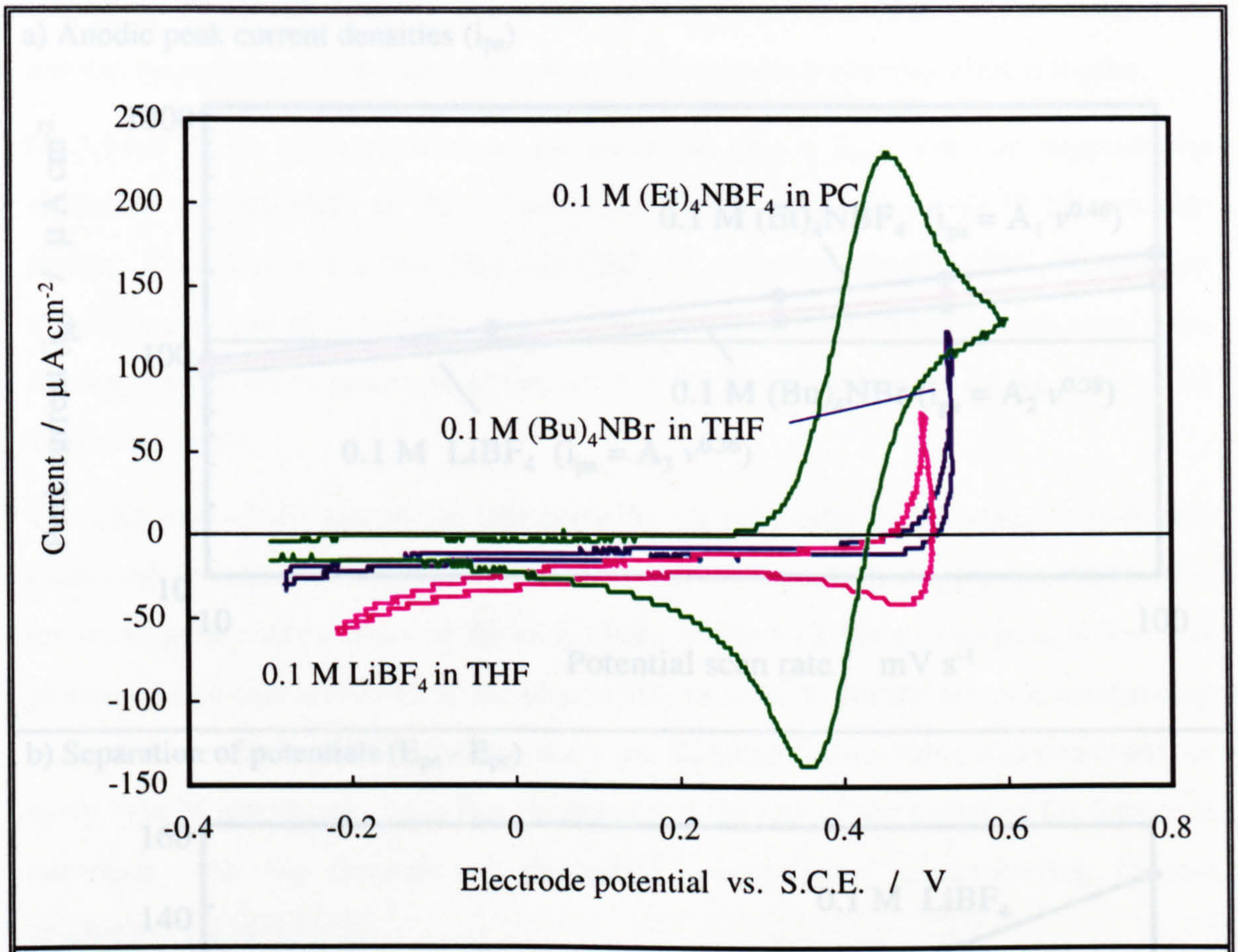


Fig.5.10 Comparison of voltammetry of ferrocene in 0.1 M $LiBF_4$ in THF, $(Bu)_4NBF_4$ in THF, and $(Et)_4NBF_4$ in PC, obtained at the potential scan rate of 100 mV s^{-1}.

5.3.2.4 Analysis of the voltammetry with ferrocene in PC electrolyte solutions

Fig.5.11 shows a comparison of experimental values of anodic peak current densities (i_{pa}) and separation of potentials corresponding to the oxidation and reduction of peak current densities (E_{pa} - E_{pc}) for ferrocene in 0.1 M electrolyte PC solutions. The peak current densities and the separation of potentials were plotted against the potential scan rate in Fig.5.11a) and Fig.5.11b), respectively.

In Fig.5.11a), all of three i_{pa} values varied linearly with $v^{0.46}$ in $(Et)_4NBF_4$, with $v^{0.38}$ in $(Bu)_4NBr$, and with $v^{0.36}$ in $LiBF_4$.

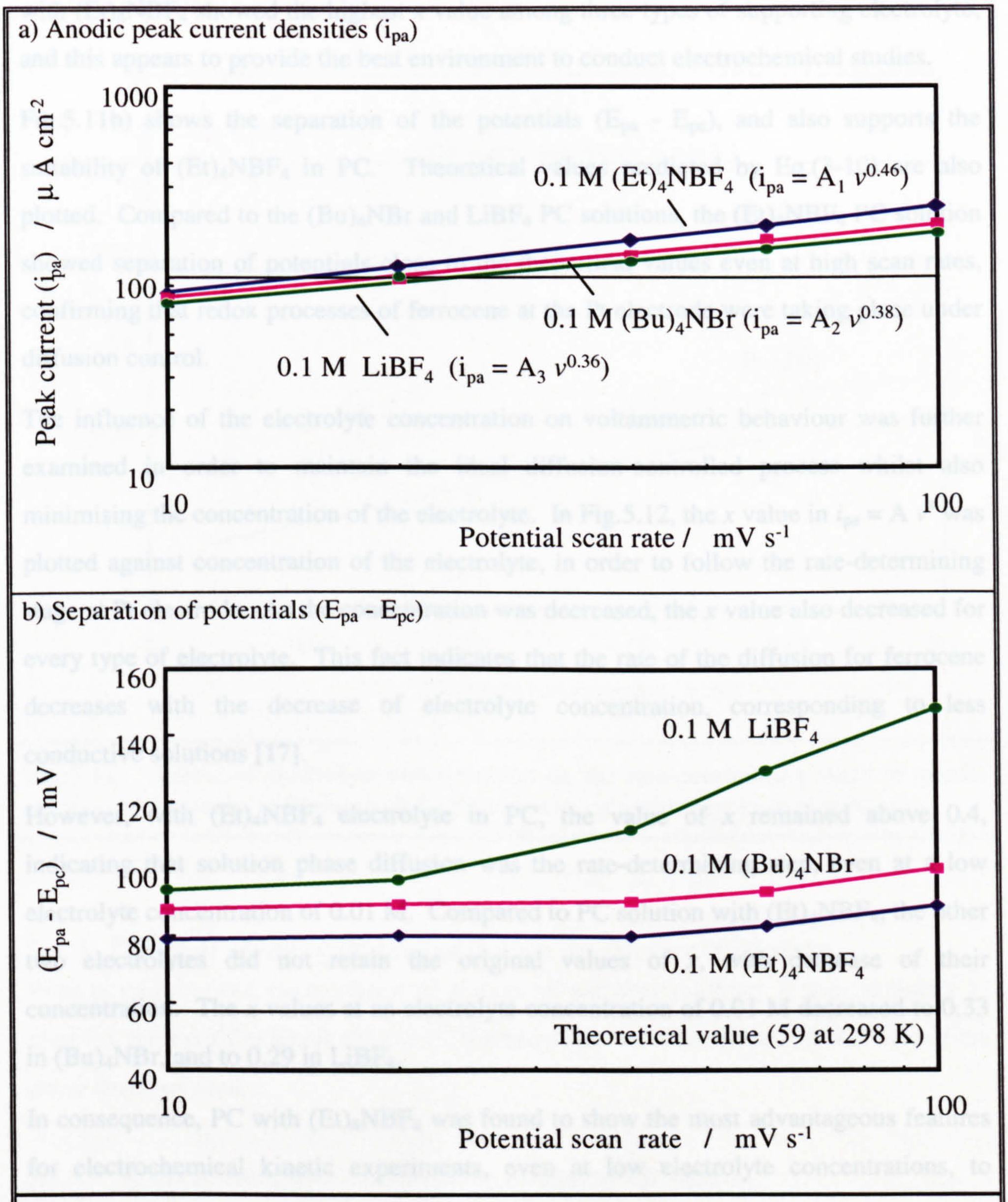


Fig.5.11 Relationship between potential scan rate (ν) and a) cyclic voltammetric peak current densities (i_{pa}). b) potential scan rate and separation of potentials (E_{pa} - E_{pc}).

This result indicates that the value x in the equation ($i_{pa} = A\ \nu^x$) became higher and closer to 0.50, the value expected for a diffusion-controlled process, with increase of the

conductivity for the electrolyte solution employed. Thus, the PC electrolyte solution with $(Et)_4NBF_4$ showed the highest x value among three types of supporting electrolyte, and this appears to provide the best environment to conduct electrochemical studies.

Fig.5.11b) shows the separation of the potentials (E_{pa} - E_{pc}), and also supports the suitability of $(Et)_4NBF_4$ in PC. Theoretical values predicted by Eq.(3-10) are also plotted. Compared to the $(Bu)_4NBr$ and $LiBF_4$ PC solutions, the $(Et)_4NBF_4$ PC solution showed separation of potentials close to the theoretical values even at high scan rates, confirming that redox processes of ferrocene at the Pt electrode were taking place under diffusion control.

The influence of the electrolyte concentration on voltammetric behaviour was further examined in order to maintain the ideal diffusion-controlled process whilst also minimising the concentration of the electrolyte. In Fig.5.12, the x value in $i_{pa} = A\ v^x$ was plotted against concentration of the electrolyte, in order to follow the rate-determining stage at Pt electrode. As the concentration was decreased, the x value also decreased for every type of electrolyte. This fact indicates that the rate of the diffusion for ferrocene decreases with the decrease of electrolyte concentration, corresponding to less conductive solutions **[17]**.

However, with $(Et)_4NBF_4$ electrolyte in PC, the value of x remained above 0.4, indicating that solution phase diffusion was the rate-determining step, even at a low electrolyte concentration of 0.01 M. Compared to PC solution with $(Et)_4NBF_4$, the other two electrolytes did not retain the original values of x, with decrease of their concentration. The x values at an electrolyte concentration of 0.01 M decreased to 0.33 in $(Bu)_4NBr$, and to 0.29 in $LiBF_4$.

In consequence, PC with $(Et)_4NBF_4$ was found to show the most advantageous features for electrochemical kinetic experiments, even at low electrolyte concentrations, to minimise interactions between $(Et)_4NBF_4$ and the electrode surfaces under dynamic lubricated conditions.

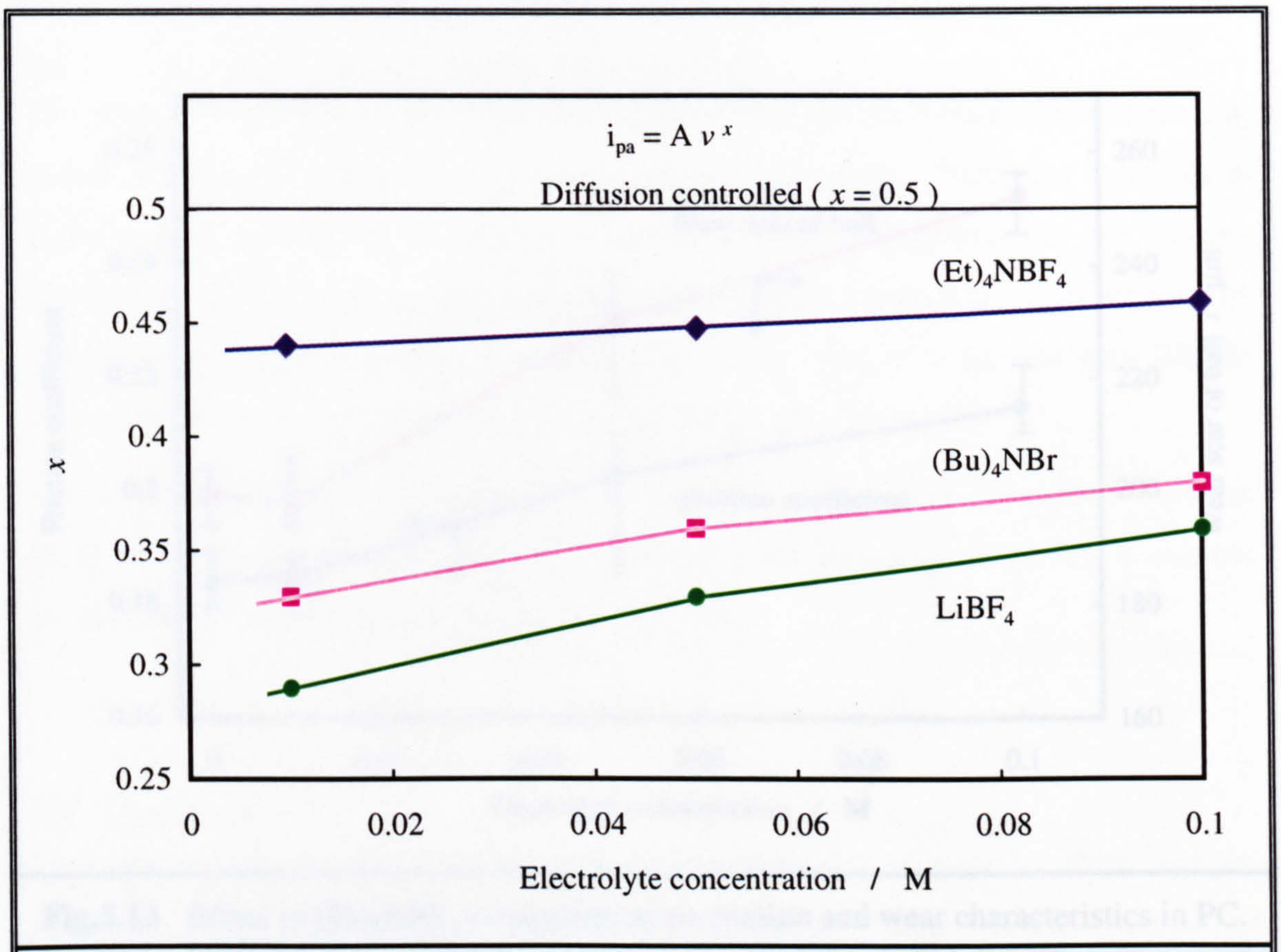


Fig.5.12 Effect of electrolyte concentration on the rate-determining stage of anodic reaction of ferrocene at Pt electrode in the presence of various types of electrolyte.

5.3.3 Effect of electrolyte concentration on friction and wear

Prior to carrying out electrochemical studies on additive solutions it was necessary to establish the extent to which the electrolyte employed influenced friction and wear at the concentrations used.

5.3.3.1 Effect of electrolyte concentration on dynamic friction

Fig.5.13 shows the effect of $(Et)_4NBF_4$ concentration on friction and wear properties, obtained by HFR rig with $(Et)_4NBF_4$-PC solutions as a lubricant. Each frictional data point represents an average of the root mean square friction value, over a rubbing test of 30 min duration at a constant load (0.2 kg). Each test was carried out at least three times under the same conditions to confirm repeatability.

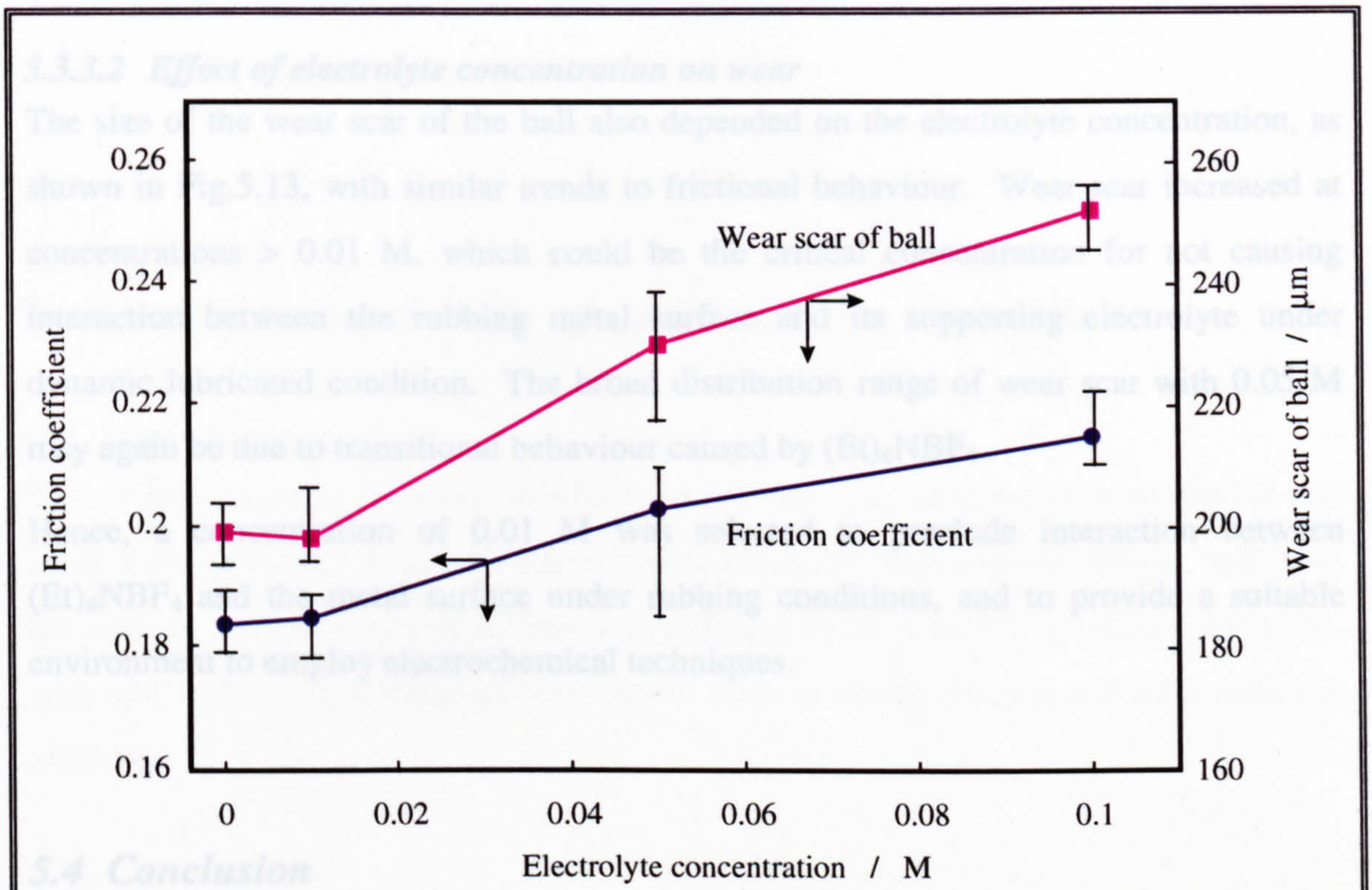


Fig.5.13 Effect of $(Et)_4NBF_4$ concentration on friction and wear characteristics in PC.

It was found that the friction coefficient increased with increasing electrolyte concentration. However, 0.01 M $(Et)_4NBF_4$ PC has no significant effect on friction. Fig.5.13. indicates that $(Et)_4NBF_4$ as a supporting electrolyte in PC plays a negative role on dynamic friction coefficient under rubbing conditions, *i.e.*, inhibiting effective lubricating performance by PC, although this effect is negligible if its concentration is less than *ca.* 0.01M.

It should also be noted that the range of friction values obtained with concentrations of zero, 0.01 and 0.1 M showed narrower distribution, *i.e.*, good repeatability, compared to that of a concentration of 0.05 M. This suggests that frictional behaviour with 0.05 M is a transitional response between no-electrolyte and high electrolyte concentration. Hence the concentration of 0.05 M resulted in poor repeatability of friction behaviour and the distribution of friction coefficient showed a broad range of measured values.

5.3.3.2 Effect of electrolyte concentration on wear

The size of the wear scar of the ball also depended on the electrolyte concentration, as shown in Fig.5.13, with similar trends to frictional behaviour. Wear scar increased at concentrations > 0.01 M, which could be the critical concentration for not causing interaction between the rubbing metal surface and its supporting electrolyte under dynamic lubricated condition. The broad distribution range of wear scar with 0.05 M may again be due to transitional behaviour caused by $(Et)_4NBF_4$.

Hence, a concentration of 0.01 M was selected to preclude interaction between $(Et)_4NBF_4$ and the metal surface under rubbing conditions, and to provide a suitable environment to employ electrochemical techniques.

5.4 Conclusion

This chapter has examined the electrochemical behaviour of a model redox couple, ferrocene, in a range of organic solvents, to try to detect suitable lubricant systems for subsequent electrochemical studies. According to the investigation, two non-aqueous systems have been selected. One is 0.8 M $LiClO_4$-DEA solution, in which DEA has a realistic chemical structure to represent typical synthetic lubricant base oils. The other one is 0.01 M $(Et)_4NBF_4$-PC solution, which showed the most ideal electrochemical behaviour even with low electrolyte concentrations, which minimise the influence of electrolyte on tribological performance.

CHAPTER 6

6. Electrochemical study of metal-additive interactions

6.1 Introduction

This chapter explains the basis on which the non-aqueous lubricant systems used in this study were selected. It then describes electrochemical experimental results, mainly in the form of voltammograms, of iron and platinum in DEA or PC electrolyte solutions, with and without disulphide and carboxylic acids as model friction and wear reducing additives.

6.2 Metal-additive interactions in DEA

The electrochemical behaviour of platinum and iron in DEA containing 0.8 M $LiClO_4$ was determined prior to carrying out dynamic friction and wear testing of iron surfaces under controlled electrode potential, which is described in Chapter 7.

6.2.1 Interactions without lubricant additives in DEA

6.2.1.1 Determination of range of electrode potentials to be studied

Fig.6.1 shows cyclic voltammograms at a scan rate of 100 mV s^{-1} for a Pt electrode in DEA containing 0.8 M $LiClO_4$. The voltammogram with a positive potential limit of 1.2 V showed several oxidation / reduction peaks, due to Pt oxidation [1] and / or the oxidative dimerisation of the ester [2], both of which were absent if that limit was 0.6 V. On the subsequent negative-going potential sweep, the reverse of the reaction (6-1) produced reduction current peaks at -0.5, -0.9 and -1.2 V. With increasingly negative electrode potentials, a reduction of lithium ions from the supporting electrolyte may also have occurred [2], leading to hydrogen abstraction and subsequent oxidative coupling of the carbanion:

(Pt oxidation) $$Pt + xH_2O \leftrightarrow PtO_x + 2xH^+ + 2xe^- \quad (6\text{-}1)$$

(Dimerisation) $$Li^+ + e^- \rightarrow Li^\bullet \quad (6\text{-}2a)$$

$$Li^\bullet + R_1CH_2COOR_2 \rightarrow R_1C(Li)HCOOR_2 + \frac{1}{2}H_2 \quad (6\text{-}2b)$$

$$R_1C(Li)HCOOR_2 \rightarrow R_1(C^-)HCOOR_2 + Li^+ \quad (6\text{-}2c)$$

$$R_1(C^-)HCOOR_2 \rightarrow \frac{1}{2}\begin{matrix} R_1CHCOOR_2 \\ | \\ R_1CHCOOR_2 \end{matrix} + e^- \quad (6\text{-}2d)$$

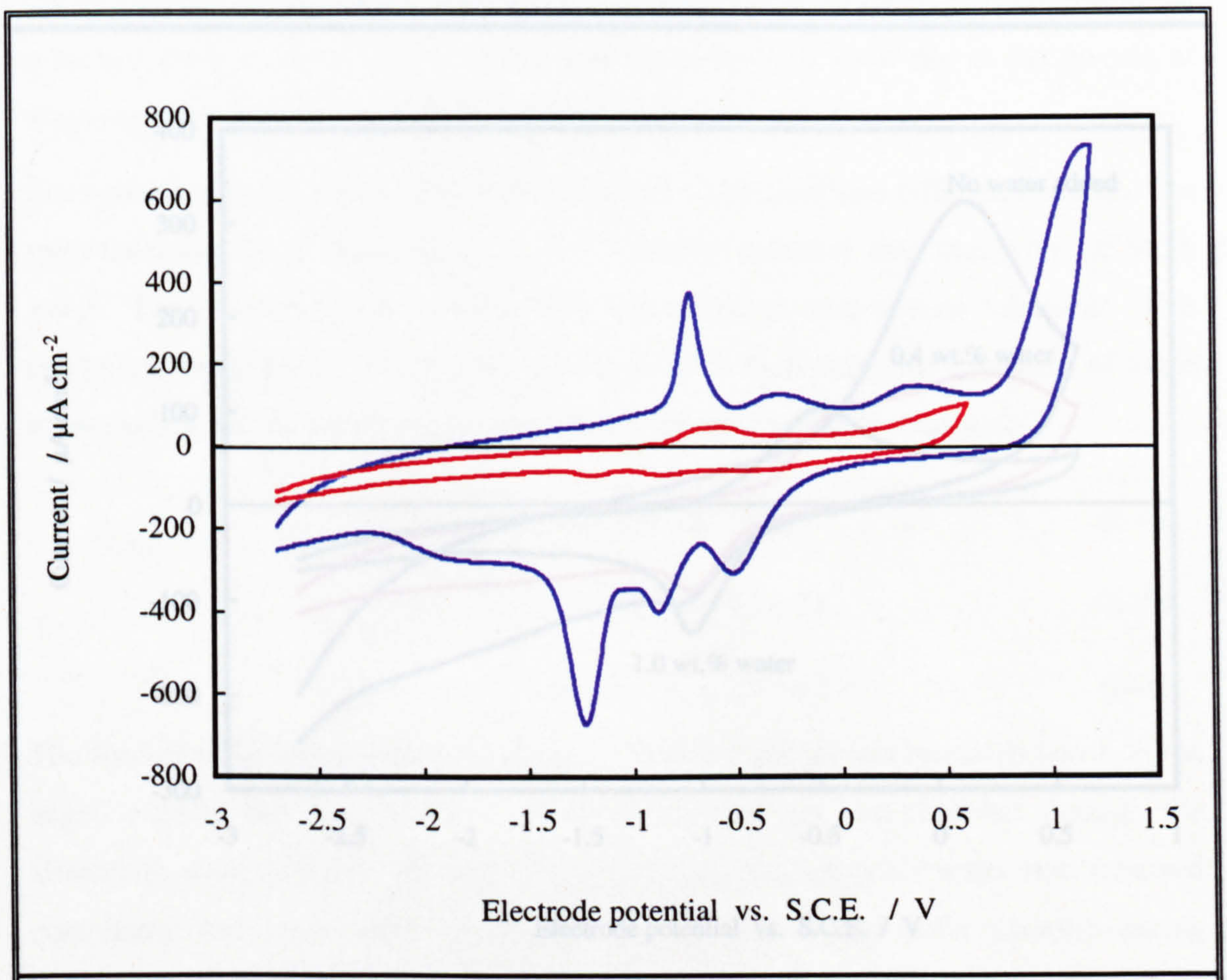


Fig.6.1 Cyclic voltammograms of Pt in DEA containing 0.8 M $LiClO_4$ at the potential scan rate of 100 mV s^{-1}.

The scanning potential range for subsequent voltammetry was constrained between -2.7 and 0.6 V, to minimise the effect of the solvent decomposition on the voltammetric

behaviour, and to maximise the detection of the reactions of additives which were added subsequently.

6.2.1.2 Voltammetric behaviour of iron in ester

Fig.6.2 shows voltammograms of an iron electrode in DEA containing 0.8 M $LiClO_4$, with and without 0.4 wt.% and 1.0 wt.% water. An investigation of the effect of water was important since commercially-available esters usually contain *ca.* 0.1 wt.% water.

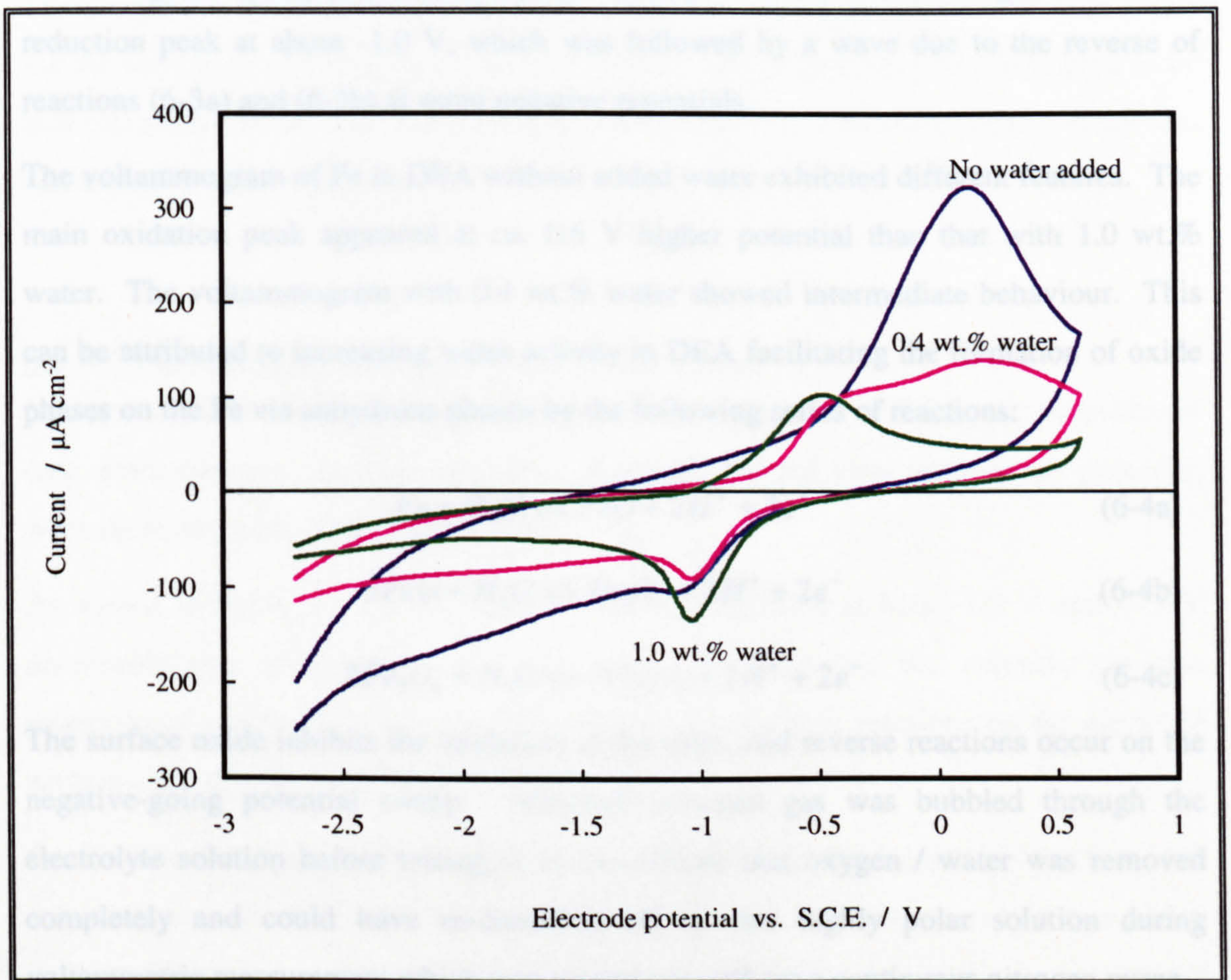


Fig.6.2 Cyclic voltammograms of iron in DEA containing 0.8 M $LiClO_4$, to which 0.4 wt.% and 1.0 wt.% water were added subsequently.

The voltammogram for Fe with 1.0 wt.% water shows similar features to those reported for Fe in aqueous solutions of 0.1 M NaOH **[3]**, exhibiting the onset of oxidation current

at *ca.* -1.0 V on the positive-going potential scan and a current peak at *ca.* -0.6 V. This behaviour is due to a complex oxidation process **[3,4]** which in the low water activity conditions of these experiments may form hydrous oxides via the following series of reactions:

$$Fe + OH^- \leftrightarrow FeOH_{ads} + e^- \qquad (6\text{-}3a)$$

$$Fe + 2OH^- \leftrightarrow Fe(OH)_{2(ads)} + 2e^- \qquad (6\text{-}3b)$$

$$Fe(OH)_{2(ads)} + OH^- \leftrightarrow Fe(OH)_{3(ads)} + e^- \rightarrow H_2O + FeOOH \qquad (6\text{-}3c)$$

On the negative-going potential sweep, the reverse of the reaction (6-3c) gave rise to the reduction peak at about -1.0 V, which was followed by a wave due to the reverse of reactions (6-3a) and (6-3b) at more negative potentials.

The voltammogram of Fe in DEA without added water exhibited different features. The main oxidation peak appeared at *ca.* 0.6 V higher potential than that with 1.0 wt.% water. The voltammogram with 0.4 wt.% water showed intermediate behaviour. This can be attributed to increasing water activity in DEA facilitating the formation of oxide phases on the Fe via anhydrous phases by the following series of reactions:

$$Fe + H_2O \leftrightarrow FeO + 2H^+ + 2e^- \qquad (6\text{-}4a)$$

$$3FeO + H_2O \leftrightarrow Fe_3O_4 + 2H^+ + 2e^- \qquad (6\text{-}4b)$$

$$2Fe_3O_4 + H_2O \leftrightarrow 3Fe_2O_3 + 2H^+ + 2e^- \qquad (6\text{-}4c)$$

The surface oxide inhibits the oxidation of the ester, and reverse reactions occur on the negative-going potential sweep. Although nitrogen gas was bubbled through the electrolyte solution before testing, it is improbable that oxygen / water was removed completely and could have re-dissolved **[5]** in this highly polar solution during voltammetric measurement which was carried out without a continuous nitrogen purge.

The data for onset (E_{onset}) and peak (E_{pa}) potentials as a function of water concentration from the voltammograms are summarised in Table 6.1. E_{onset} and E_{pa} showed more negative potential with higher water concentration, implying that water can provide an environment for iron to be oxidised easily.

Table 6.1 E_{onset} and E_{pa} as a function of water concentration

Water concentration / wt.%	E_{onset} vs. S.C.E. / V	E_{pa} vs. S.C.E. / V
0	-0.6	0.1
0.4	-0.75	-0.4
1.0	-1.0	-0.5

The lower peak current for the voltammogram with 1.0 wt.% water could be responsible for the formation of $Fe(OH)_x$ on the electrode surface, which may be considered to be less conductive rather than iron oxide, and hence acted as a blocking barrier to prevent subsequent oxidative process.

6.2.1.3 Chronoamperometry with 0.8 M $LiClO_4$ DEA

In order to further investigate the electrochemical behaviour of DEA, the time-current data under constant electrode controlled potential, stepped from open-circuit potential, were measured with 0.8 M $LiClO_4$ DEA.

As shown in Fig.6.3a), the electrolysis currents controlled at both -1.0 V and -0.1 V decreased, and approached zero with time. In Fig.6.3b), the currents are also proportional to time$^{(-0.5)}$, indicating that the electrochemical reactions on the electrode surface obey simple diffusion-controlled kinetics.

On the other hand, the currents at 0.3 V and 1.2 V in Fig.6.3a) increased with time, due to pitting, *i.e.*, dissolution of the iron electrode causing an active electrode area which increased with time reaching a quasi-steady state. At both the anodic potentials, the current-time$^{(-0.5)}$ plots in Fig.6.3b) did not form straight lines, implying that the electrochemical reactions at the electrode did not correspond to a diffusion-controlled process.

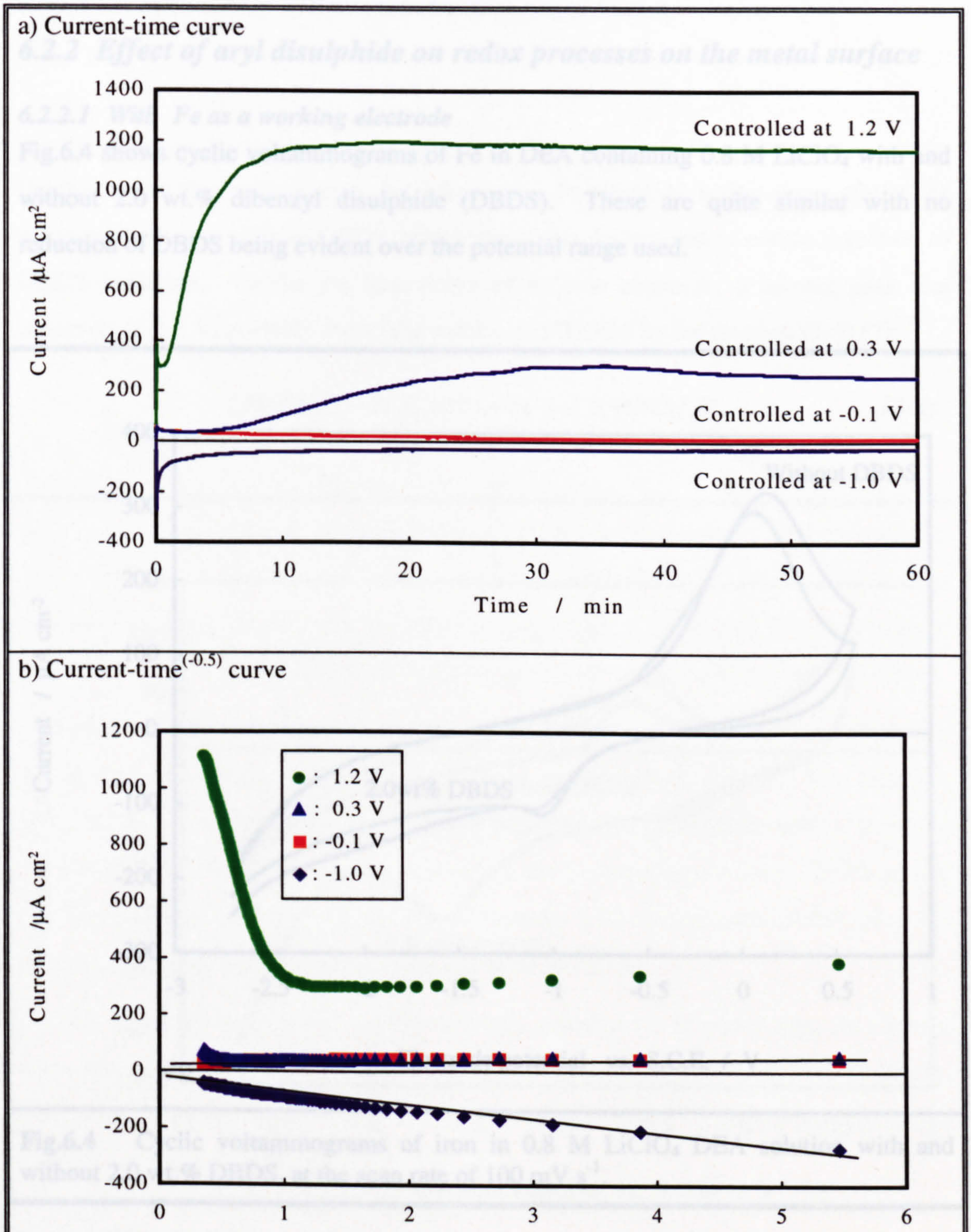


Fig.6.3 The electrolysis current of iron measured against a) time, b) time$^{(-0.5)}$ in 0.8 M $LiClO_4$ DEA, obtained at various electrode potentials.

6.2.2 Effect of aryl disulphide on redox processes on the metal surface

6.2.2.1 With Fe as a working electrode

Fig.6.4 shows cyclic voltammograms of Fe in DEA containing 0.8 M $LiClO_4$ with and without 2.0 wt.% dibenzyl disulphide (DBDS). These are quite similar with no reduction of DBDS being evident over the potential range used.

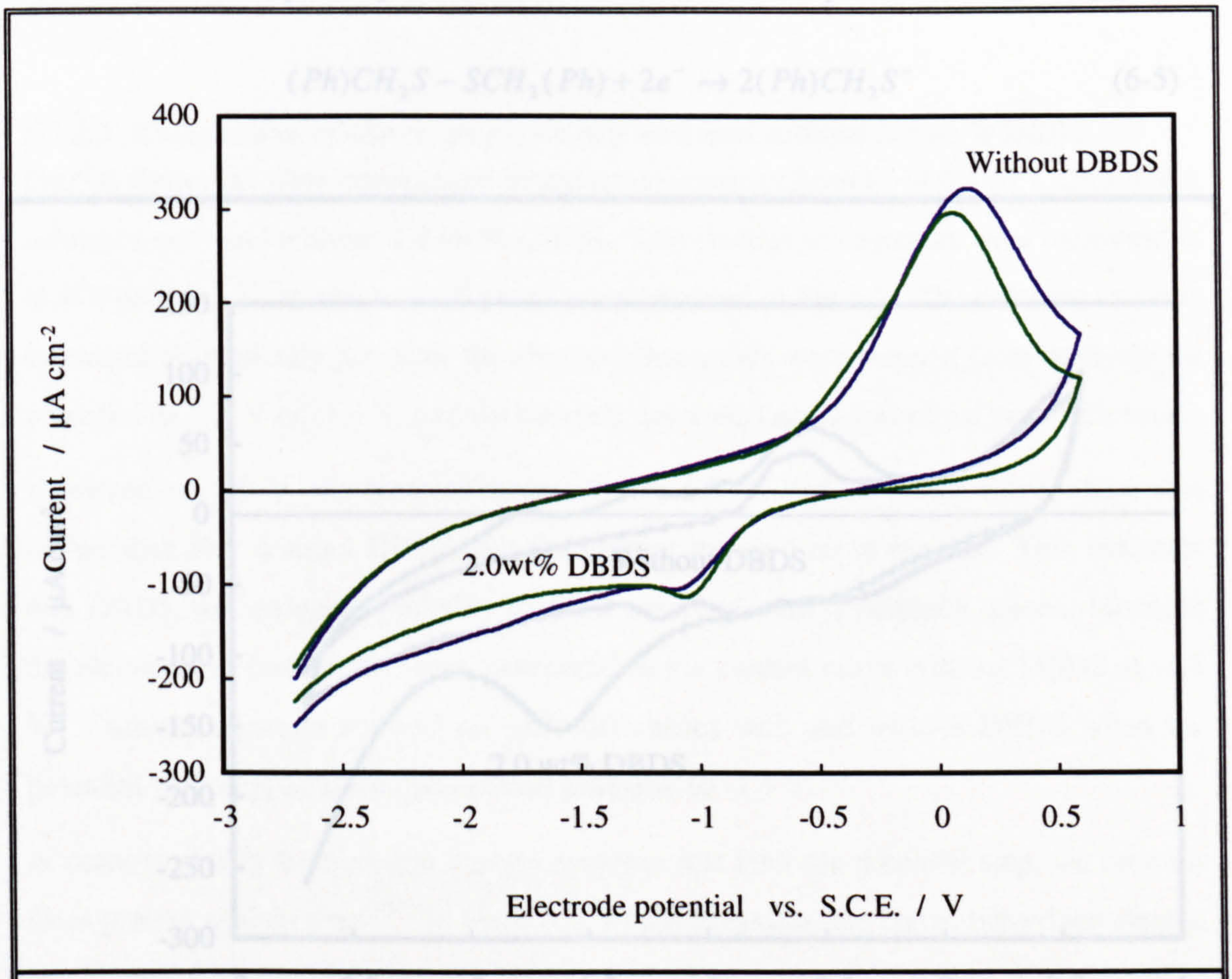


Fig.6.4 Cyclic voltammograms of iron in 0.8 M $LiClO_4$ DEA solution with and without 2.0 wt.% DBDS, at the scan rate of 100 mV s^{-1}.

However, previous work **[6]** has shown that DBDS can be reduced at less than -1.0 V vs. S.C.E. in DMF electrolyte solutions, using a graphite electrode. This indicates that

the reduction of DBDS on the Fe surface could be masked by the simultaneous reduction of iron oxides on the negative-going potential sweep.

6.2.2.2 With Pt as a working electrode

Fig.6.5 shows the voltammetric behaviour of a Pt electrode in the same electrolyte solutions with and without DBDS, which were also determined to enable detection of DBDS reduction. Unlike the behaviours of an iron electrode, a current peak was observed at -1.6 V, possibly due to the reduction of DBDS by the reaction (6-5) **[7]**:

$$(Ph)CH_2S - SCH_2(Ph) + 2e^- \rightarrow 2(Ph)CH_2S^- \qquad (6\text{-}5)$$

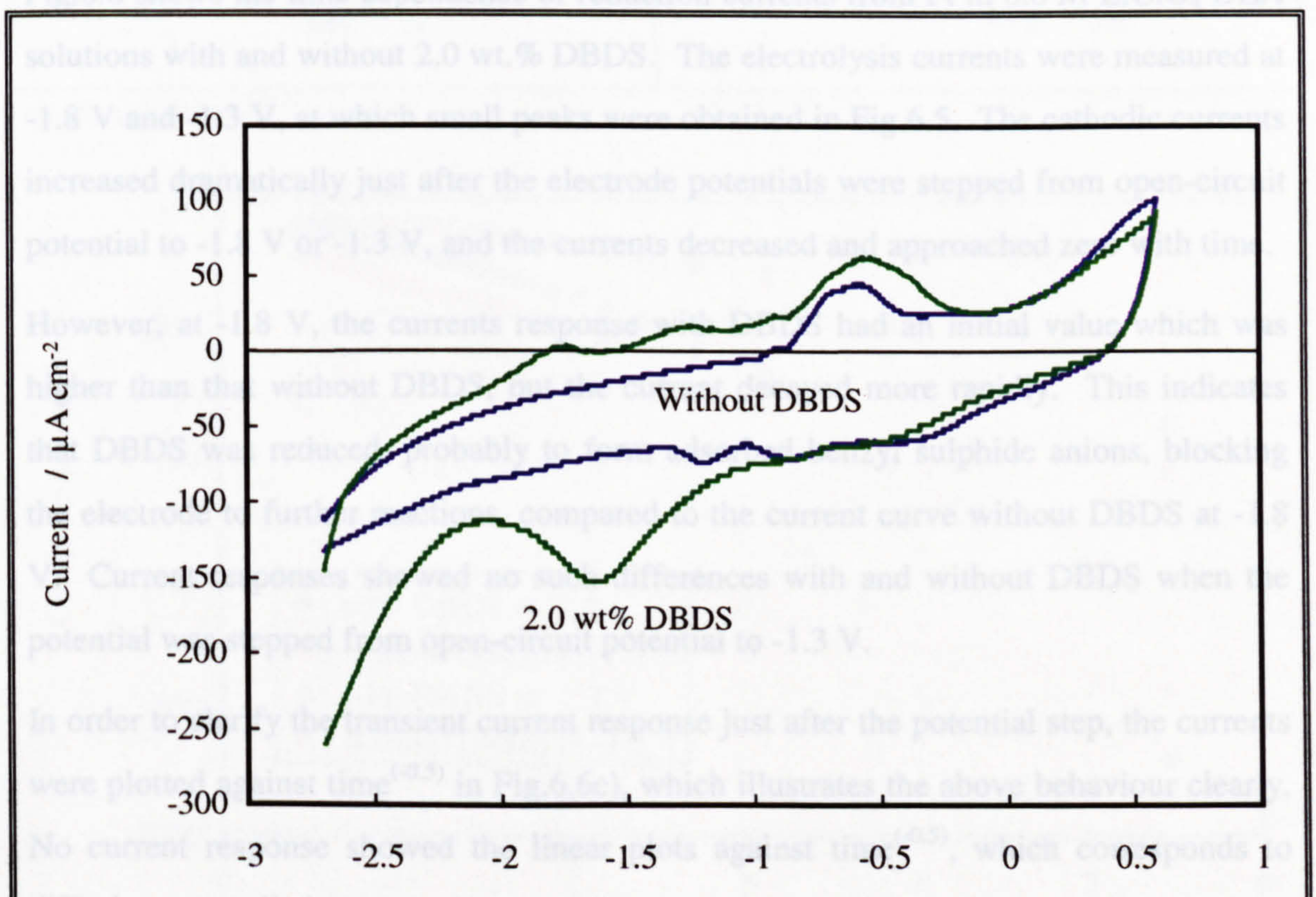


Fig.6.5 Cyclic voltammograms of Pt in 0.8 M $LiClO_4$ DBDS solution with / without 2.0 wt.% DBDS, obtained at the scan rate of 100 mV s^{-1}.

The potential range over which a reduction occurred was in agreement with that reported previously **[6,8]**, using DMF electrolyte solutions. On the positive-going potential sweep, the voltammograms with and without 2.0 wt.% DBDS exhibited similar features, although the one with 2.0 wt.% DBDS showed small oxidation peaks at -1.8 V and -1.3 V, and significantly greater oxidation current between -2.5 V and -0.3 V, possibly due to the re-oxidation of adsorbed benzyl sulphide anions from reaction (6-5) or the oxidation of DBDS itself **[9]** as follows:

$$(Ph)CH_2S - SCH_2(Ph) \rightarrow (Ph)CH_2S^{\bullet+} - SCH_2(Ph) + e^- \qquad (6\text{-}6)$$

6.2.2.3 Comparison of chronoamperometry with and without 2.0 wt.% DBDS

Fig.6.6 shows the time dependence of reduction currents from Pt in 0.8 M $LiClO_4$ DEA solutions with and without 2.0 wt.% DBDS. The electrolysis currents were measured at -1.8 V and -1.3 V, at which small peaks were obtained in Fig.6.5. The cathodic currents increased dramatically just after the electrode potentials were stepped from open-circuit potential to -1.8 V or -1.3 V, and the currents decreased and approached zero with time. However, at -1.8 V, the currents response with DBDS had an initial value which was higher than that without DBDS, but the current decayed more rapidly. This indicates that DBDS was reduced, probably to form adsorbed benzyl sulphide anions, blocking the electrode to further reactions, compared to the current curve without DBDS at -1.8 V. Current responses showed no such differences with and without DBDS when the potential was stepped from open-circuit potential to -1.3 V.

In order to clarify the transient current response just after the potential step, the currents were plotted against time$^{(-0.5)}$ in Fig.6.6c), which illustrates the above behaviour clearly. No current response showed the linear plots against time$^{(-0.5)}$, which corresponds to diffusion-controlled process.

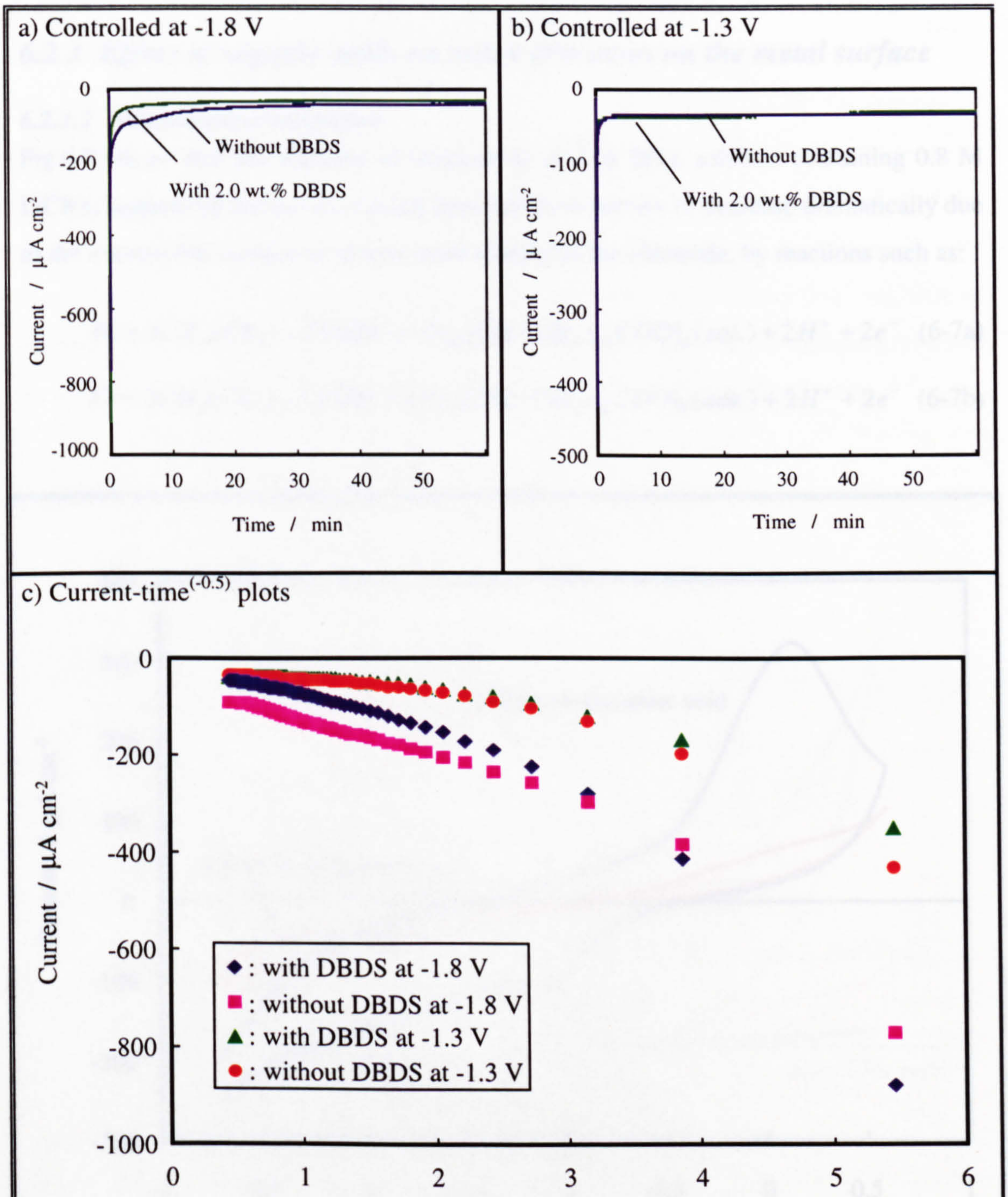


Fig.6.6 Time dependence of the currents of Pt obtained at a) -1.8 V, b) -1.3 V, in 0.8 M $LiClO_4$ DEA with / without 2.0 wt.% DBDS; c) replots of currents against time$^{(-0.5)}$.

6.2.3 Effect of organic acids on redox processes on the metal surface

6.2.3.1 Voltammetric behaviour

Fig.6.7 shows that the addition of dodecanoic acid in DEA solution containing 0.8 M $LiClO_4$ supporting electrolyte caused iron oxidation current to decrease dramatically due to the irreversible formation of iron dodecanoate on the electrode, by reactions such as:

$$Fe + 2CH_3(CH_2)_{10}COOH \rightarrow Fe_{II}[CH_3(CH_2)_{10}COO]_2(sol.) + 2H^+ + 2e^- \quad (6\text{-}7a)$$

$$Fe + 2CH_3(CH_2)_{10}COOH \rightarrow Fe_{II}[CH_3(CH_2)_{10}COO]_2(ads.) + 2H^+ + 2e^- \quad (6\text{-}7b)$$

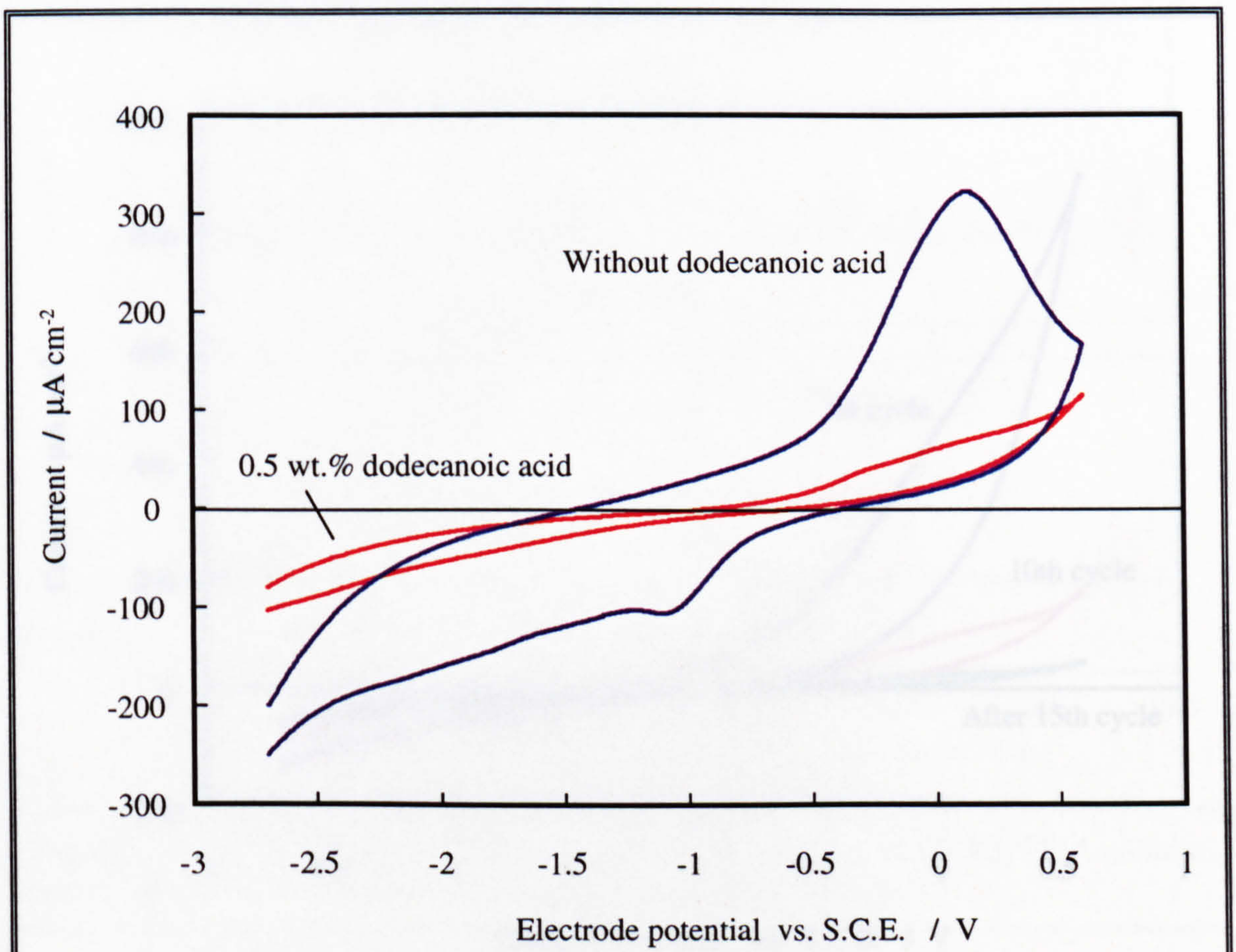


Fig.6.7 Typical cyclic voltammograms of iron in DEA containing 0.8 M $LiClO_4$ with and without 0.5 wt.% dodecanoic acid, obtained at the scan rate of 100 mV s^{-1}.

$$Fe[CH_3(CH_2)_{10}COO]_2 + CH_3(CH_2)_{10}COOH$$

$$\rightarrow Fe[CH_3(CH_2)_{10}COO]_3 + H^+ + e^- \qquad (6\text{-}7c)$$

Fig.6.8 shows that the oxidation and reduction currents decayed with the number of cycles when the potential was scanned from -2.7 V to 0.6 V, with an iron electrode in DEA electrolyte solution containing 0.5 wt.% dodecanoic acid, but stabilised after the 15th cycle. Even with a negative potential limit of -2.7 V, cathodic currents were very small and the ratio of oxidation to reduction current densities indicated that very little of the oxidation product was reduced. This behaviour indicates that the surface is blocked by a dielectric iron carboxylate compound accumulating on the electrode surface.

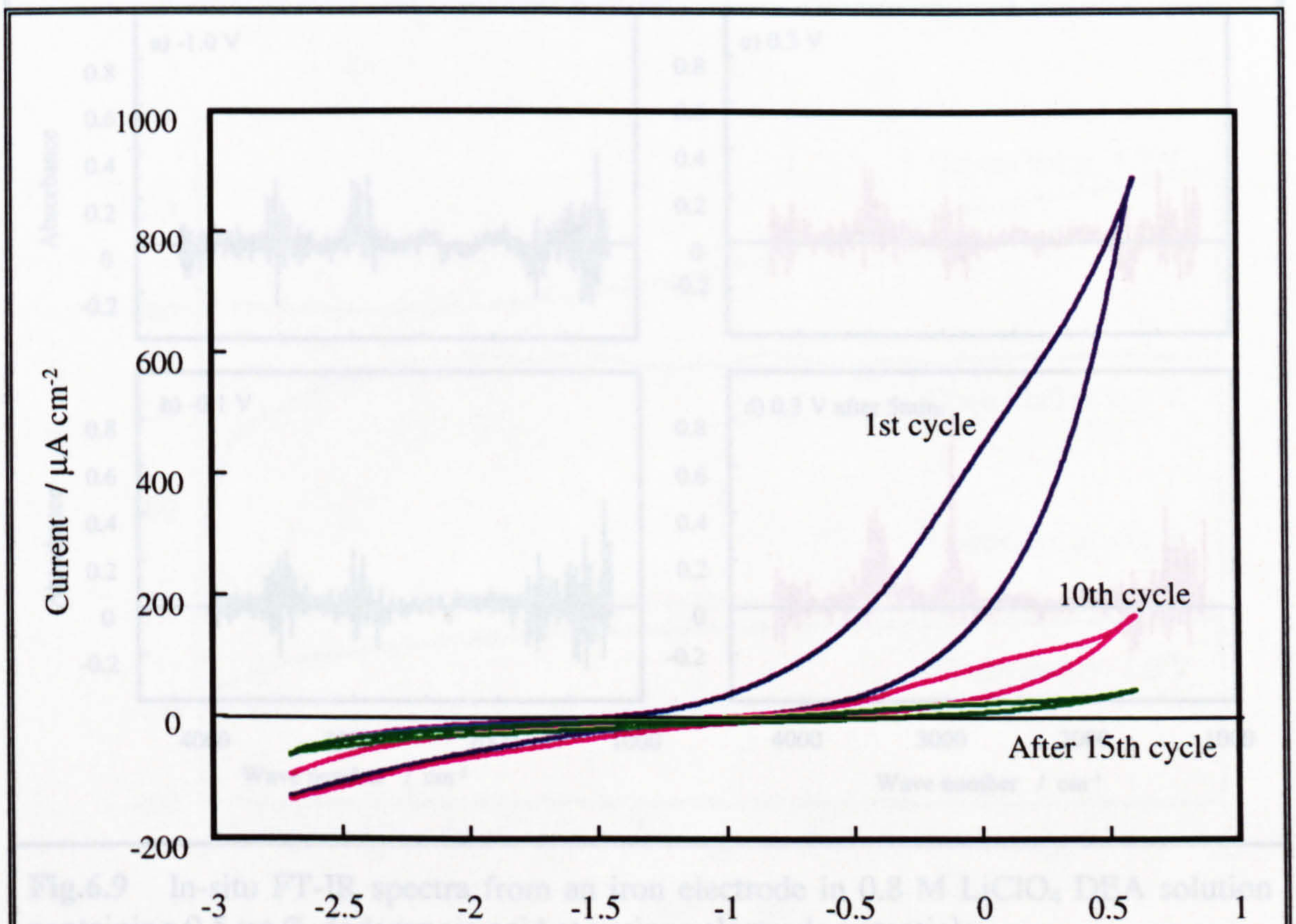


Fig.6.8 Dependence on cyclic number of voltammetric behaviour of iron in DEA containing 0.8 M $LiClO_4$ and 0.5 wt.% dodecanoic acid, at the scan rate of 100 mV s^{-1}.

6.2.3.2 *In-situ FT-IR measurement*

Fourier transform infrared (FT-IR) reflection-absorption spectroscopy was used in an attempt to characterise the product phase(s) formed on an iron electrode in DEA containing 0.5 wt.% dodecanoic acid electrolyte solution. Fig.6.9 shows a series of spectra for different electrode potentials from -1.0 V to 0.3 V, obtained by the subtraction of a reference spectrum initially obtained at -2.0 V, at which no oxidative product is considered to be formed on the electrode surface.

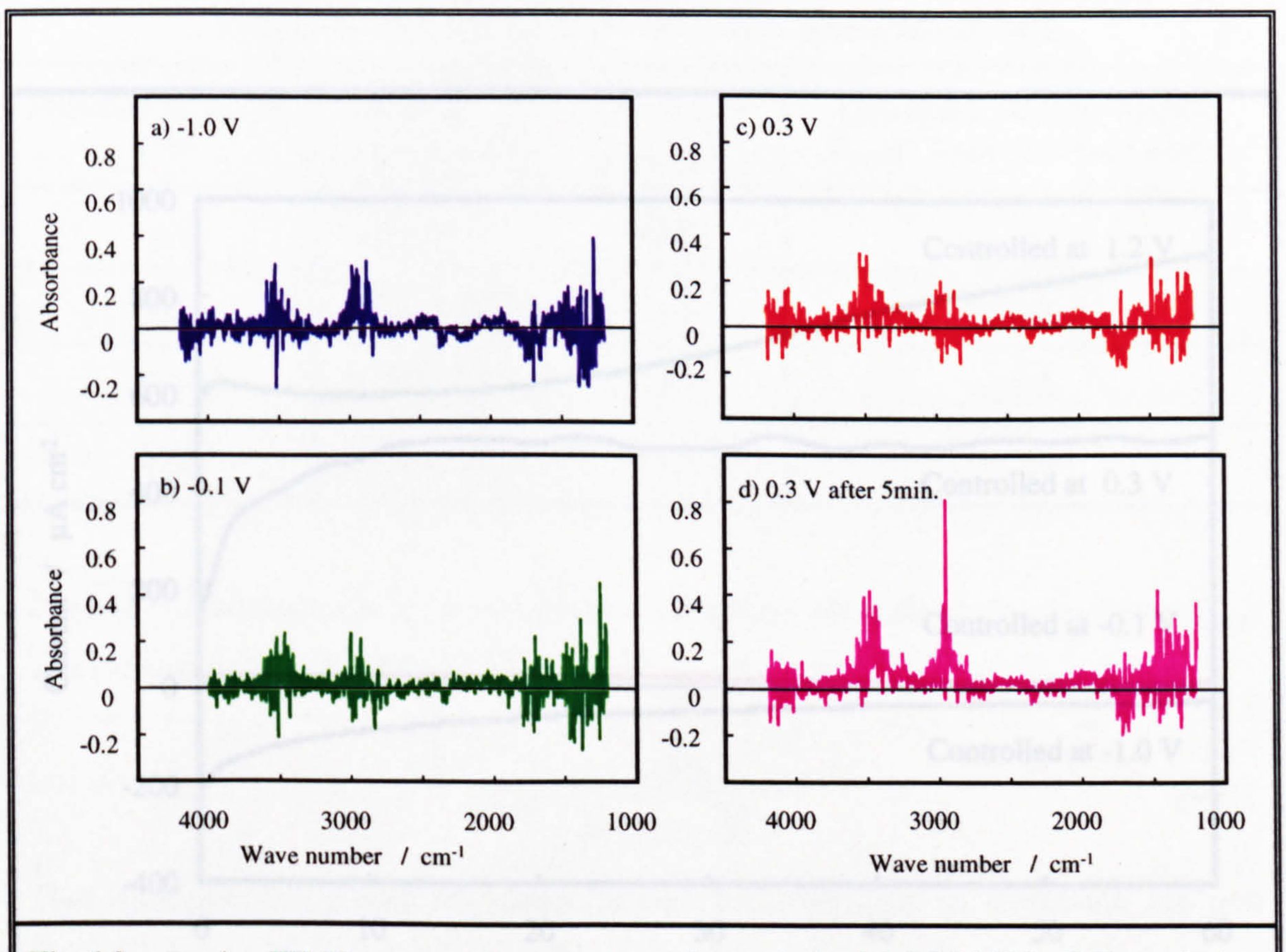


Fig.6.9 In-situ FT-IR spectra from an iron electrode in 0.8 M $LiClO_4$ DEA solution containing 0.5 wt.% dodecanoic acid at various electrode potentials.

At electrode potentials below -0.1 V, the spectra obtained show similar features. However, when the potential was controlled at 0.3 V for 5 minutes, absorption increased at *ca.* 3000 cm^{-1}. This can be attributed to the asymmetric and symmetric stretching of

hydrocarbon groups **[10]** such as CH_3- (2970, 2870 cm^{-1}) and -CH_2- (2930, 2860 cm^{-1}) associated with the formation of iron dodecanoate on the electrode surface. However, a small peak at *ca.* 3000 cm^{-1}, which might be due to as the adsorption of dodecanoic acid or ester itself, was also evident at potentials < 0.3 V.

6.2.3.3 Chronoamperometry with 0.8 M $LiClO_4$ DEA + 0.5 wt.% dodecanoic acid

In order to investigate the adsorption of dodecanoic acid on the electrode surface, and the formation of iron dodecanoate, the time dependence of the current at a constant electrode potential was measured in Fig.6.10.

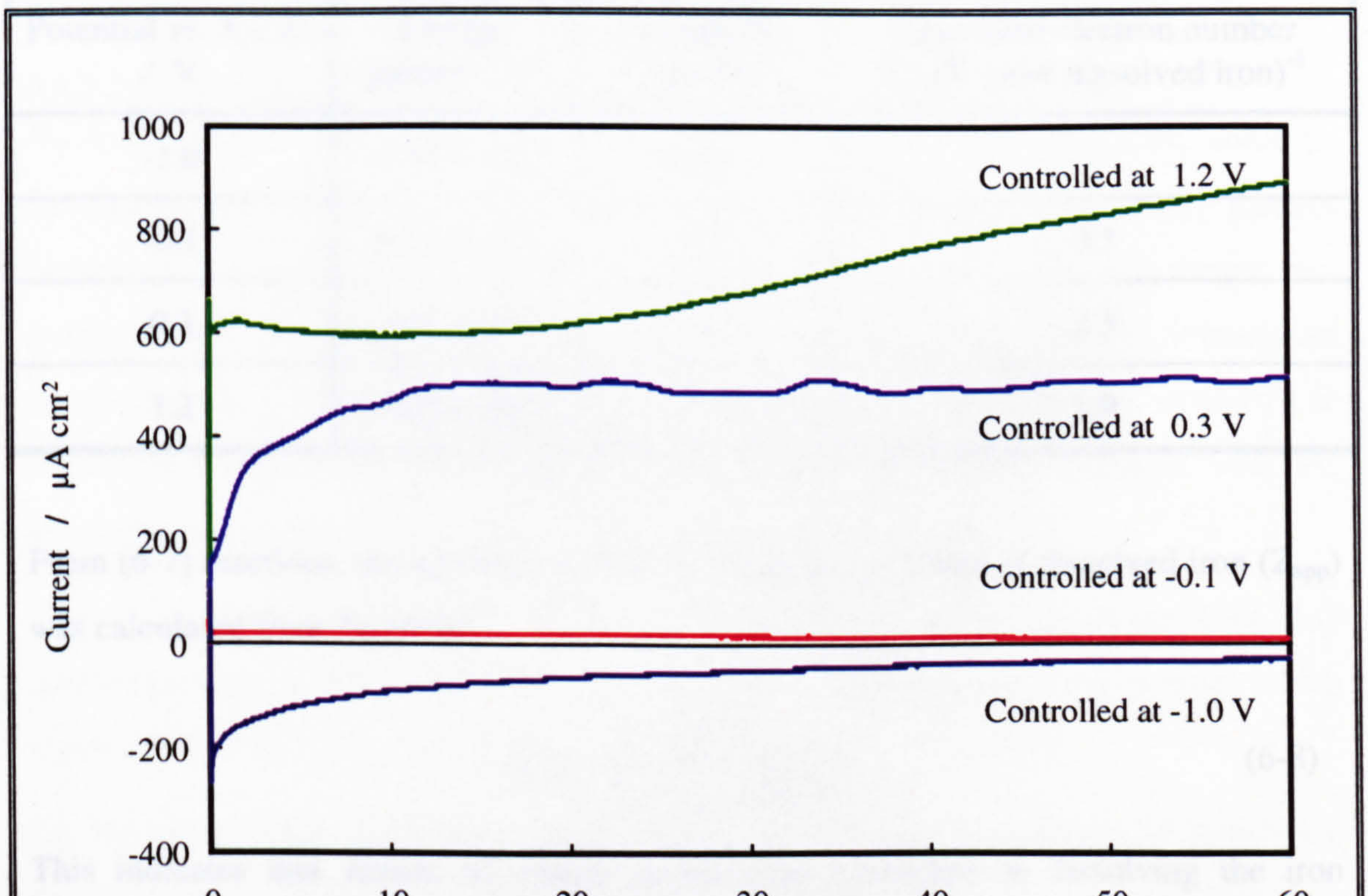


Fig.6.10 Time dependence of currents from Fe in 0.8 M $LiClO_4$ DEA containing 0.5 wt.% dodecanoic acid, at various controlled potentials.

Currents at -1.0 V and -0.1 V decreased and approached zero with increasing time, indicating that dodecanoic acid were adsorbed on the metal surface and blocked further reactions on electrode surfaces.

On the other hand, currents at 0.3 V and 1.2 V initially increased with time, and oxidation currents in quasi-steady state were achieved after 45 minutes. This indicates that electrode dissolution of metal or iron dodecanoate occurred at these potentials.

To correlate the charge passed with adsorption and metal dissolution, ICP (inductive coupled plasma emission) spectroscopy was used to determine the iron concentrations in these electrolyte solutions, the results of which are listed in Table 6.2.

Table 6.2 Metal dissolution at various potentials in DEA.

Potential vs. S.C.E. / V	Charge passed / C	[iron(II/III)] / mg dm^{-3}	Calculated electron number Z_{app}/F (mol dissolved iron)$^{-1}$
-1.0	-4.17×10^{-2}	< 0.02	-
-0.1	2.97×10^{-4}	0.05	0.3
0.3	3.40×10^{-1}	7.19	2.5
1.2	5.01×10^{-1}	9.13	2.9

From (6-7) reactions, the apparent number of Faradays per mole of dissolved iron (Z_{app}) was calculated from Eq.(6-8):

$$Z_{app} = \frac{Q M_{Fe}}{\left[iron_{(II/III)}\right] F V} \qquad (6\text{-}8)$$

This indicates that almost all charge passed was consumed in dissolving the iron electrode, at 0.3 V and 1.2 V. Deviation from values of Z_{app} in the range of 2-3 may be attributed to a proportion of the charge passed resulting in adsorbed species in accordance with (6-7) reactions.

6.3 Metal-additive interactions in PC

The use of PC electrolyte solutions made it possible to use much lower electrolyte concentrations for electrochemical kinetic experiments than in DEA. The electrochemical behaviour of platinum and iron in 0.01 M $(Et)_4NBF_4$ PC was determined to understand the redox processes of alkyl carboxylic acids, before performing dynamic friction / wear testing of iron surfaces under controlled electrode potential, as described in Chapter 7.

6.3.1 Interactions without additives in PC

6.3.1.1 Voltammetry of Pt in PC electrolyte solution

Fig.6.11 shows typical cyclic voltammograms of Pt in 0.01 M $(Et)_4NBF_4$ PC solution, for various negative and positive potential limits. These voltammograms show distinct cathodic peaks at *ca.* -1.0 V and anodic peaks at *ca.* 0.8 V. The anodic peak current was independent of the positive potential limit, as shown in Fig.6.11a); however, it increased as the preceding negative potential limit was made increasingly negative, as shown in Fig.6.11b). This behaviour conforms with the previous results obtained with PC electrolyte solution containing 0.05 M $(Bu)_4NClO_4$ **[11]**.

The origin of the anodic peaks on the voltammograms is not yet clear; however, it is likely that these peaks could correspond to the oxidation process of the product which was formed below -1.5 V on the negative going potential.

On the other hand, the cathodic peaks at *ca.* -1.0 V, the magnitudes of which are independent on both the positive and negative potential limit, could be attributed to water reduction **[12]**:

$$H_2O + e^- \rightarrow \frac{1}{2}H_2 + OH^- \qquad (6\text{-}9)$$

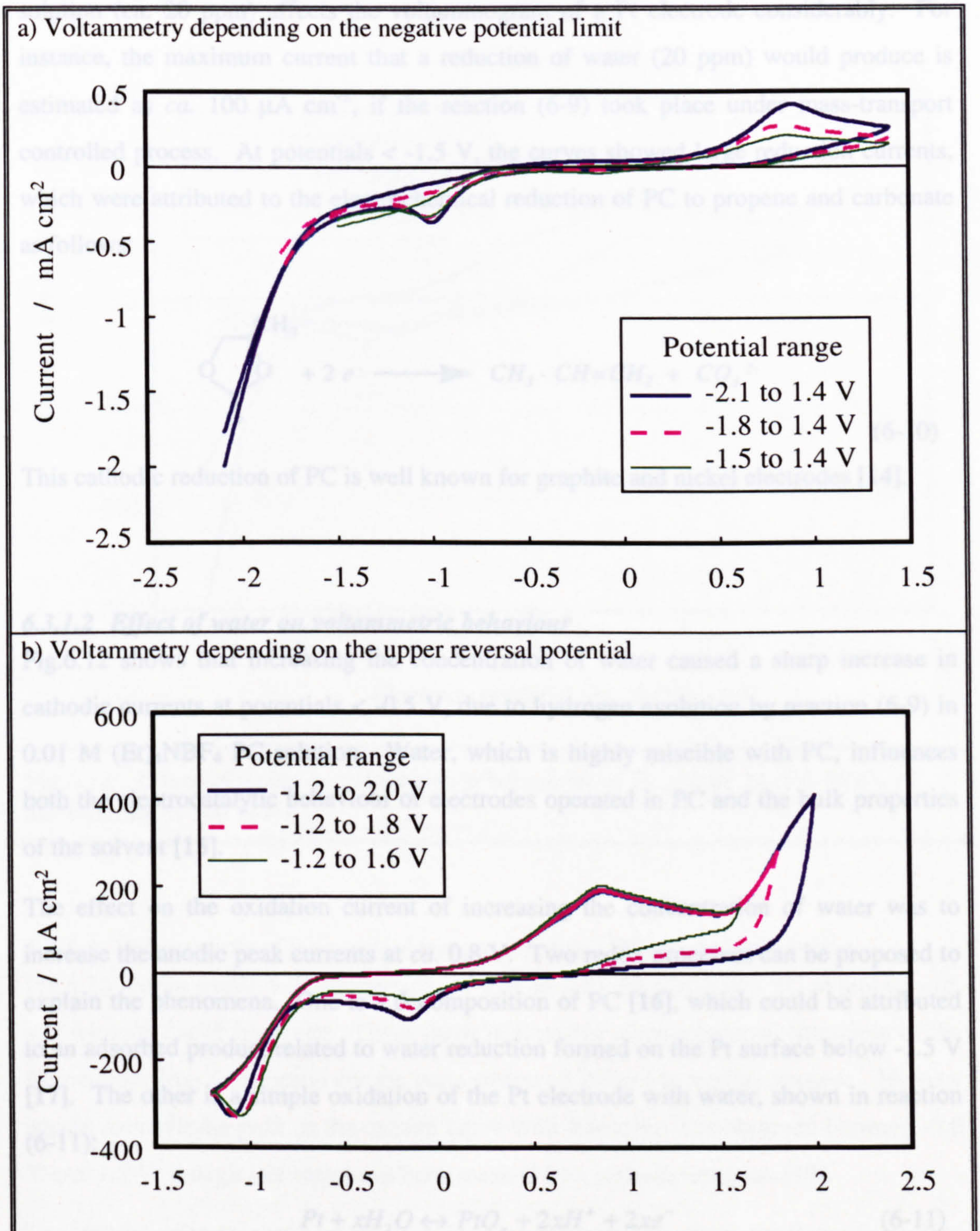
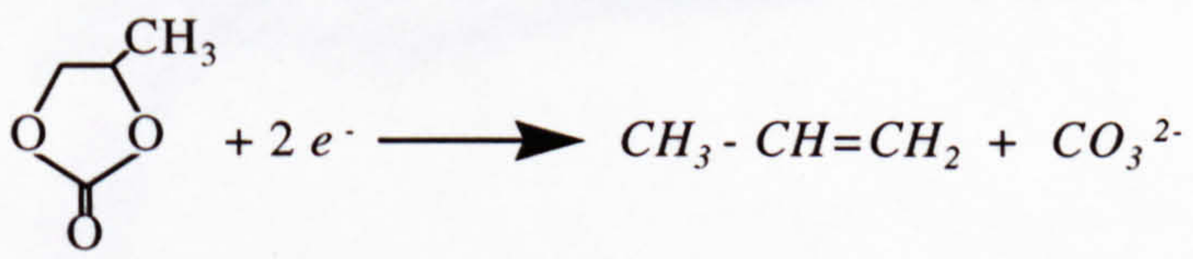


Fig.6.11 Cyclic voltammograms of Pt in 0.01 M $(Et)_4NBF_4$ PC solution, depending on a) negative potential limit, b) positive potential limit.

According to previous work **[13]**, the addition of even tiny amounts of water to the PC solution (*ca.* 20 ppm) affects the voltammogram of a Pt electrode considerably. For instance, the maximum current that a reduction of water (20 ppm) would produce is estimated as *ca.* 100 μA cm^{-2}, if the reaction (6-9) took place under mass-transport controlled process. At potentials < -1.5 V, the curves showed large reduction currents, which were attributed to the electrochemical reduction of PC to propene and carbonate as follows:



$$+ 2\,e^{-} \longrightarrow CH_3\text{-}CH{=}CH_2 + CO_3^{2-} \qquad (6\text{-}10)$$

This cathodic reduction of PC is well known for graphite and nickel electrodes **[14]**.

6.3.1.2 Effect of water on voltammetric behaviour

Fig.6.12 shows that increasing the concentration of water caused a sharp increase in cathodic currents at potentials < -0.5 V, due to hydrogen evolution by reaction (6-9) in 0.01 M $(Et)_4NBF_4$ PC solution. Water, which is highly miscible with PC, influences both the electrocatalytic behaviour of electrodes operated in PC and the bulk properties of the solvent **[15]**.

The effect on the oxidation current of increasing the concentration of water was to increase the anodic peak currents at *ca.* 0.8 V. Two redox processes can be proposed to explain the phenomena. One is a decomposition of PC **[16]**, which could be attributed to an adsorbed product related to water reduction formed on the Pt surface below -1.5 V **[17]**. The other is a simple oxidation of the Pt electrode with water, shown in reaction (6-11):

$$Pt + xH_2O \leftrightarrow PtO_x + 2xH^+ + 2xe^- \qquad (6\text{-}11)$$

The presence of water in PC makes electrochemical redox processes complicated, and the details of the processes are still not yet understood.

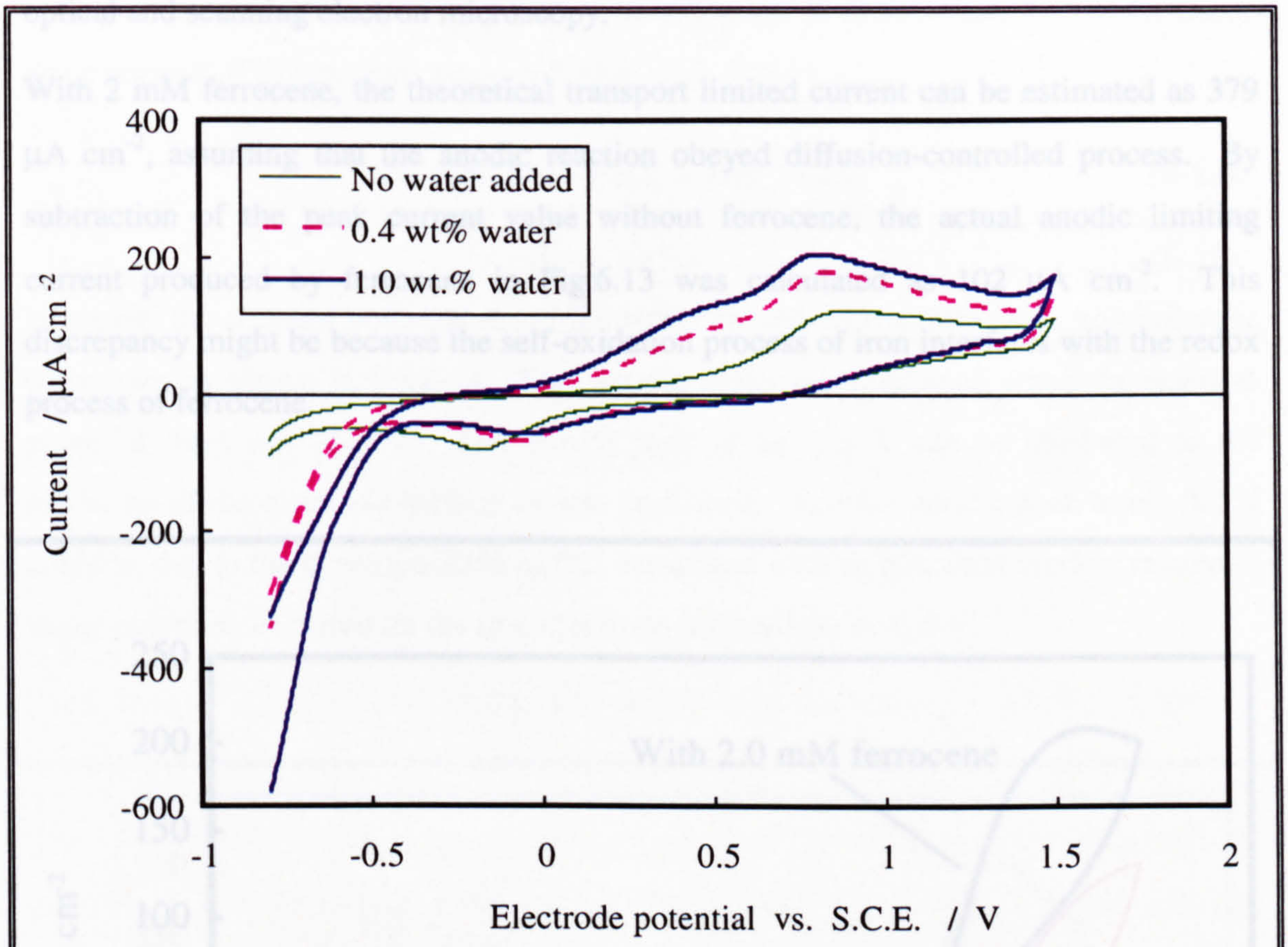


Fig.6.12 Effect of water on voltammetric behaviour of Pt in 0.01 M $(Et)_4NBF_4$ PC, at the scan rate of 100 mV s^{-1}.

6.3.1.3 Voltammetry of iron in ferrocene-containing PC electrolyte solution

Fig.6.13 shows cyclic voltammograms of iron in 0.01 M $(Et)_4NBF_4$ PC solution, with and without 2 mM ferrocene. These show irreversible electrochemical behaviour of the ferrocinium iron / ferrocene couple were observed in an irreversible manner. No new anodic /or cathodic peak in the current curve with ferrocene was observed between -0.8 V and 1.5 V, though one may have been masked by a cathodic reaction **[18]**.

The anodic current peaks at *ca.* 1.2 V were attributed to the oxidation of the iron electrode to iron oxide, on which oxidation of 2.0 mM ferrocene also occurred. At potentials > 1.5 V, an activation-controlled process was taking place on the iron

electrode, *i.e.*, a pitting of the iron electrode surface **[19]**, which has been confirmed by optical and scanning electron microscopy.

With 2 mM ferrocene, the theoretical transport limited current can be estimated as 379 μA cm^{-2}, assuming that the anodic reaction obeyed diffusion-controlled process. By subtraction of the peak current value without ferrocene, the actual anodic limiting current produced by ferrocene in Fig.6.13 was calculated as 102 μA cm^{-2}. This discrepancy might be because the self-oxidation process of iron interferes with the redox process of ferrocene.

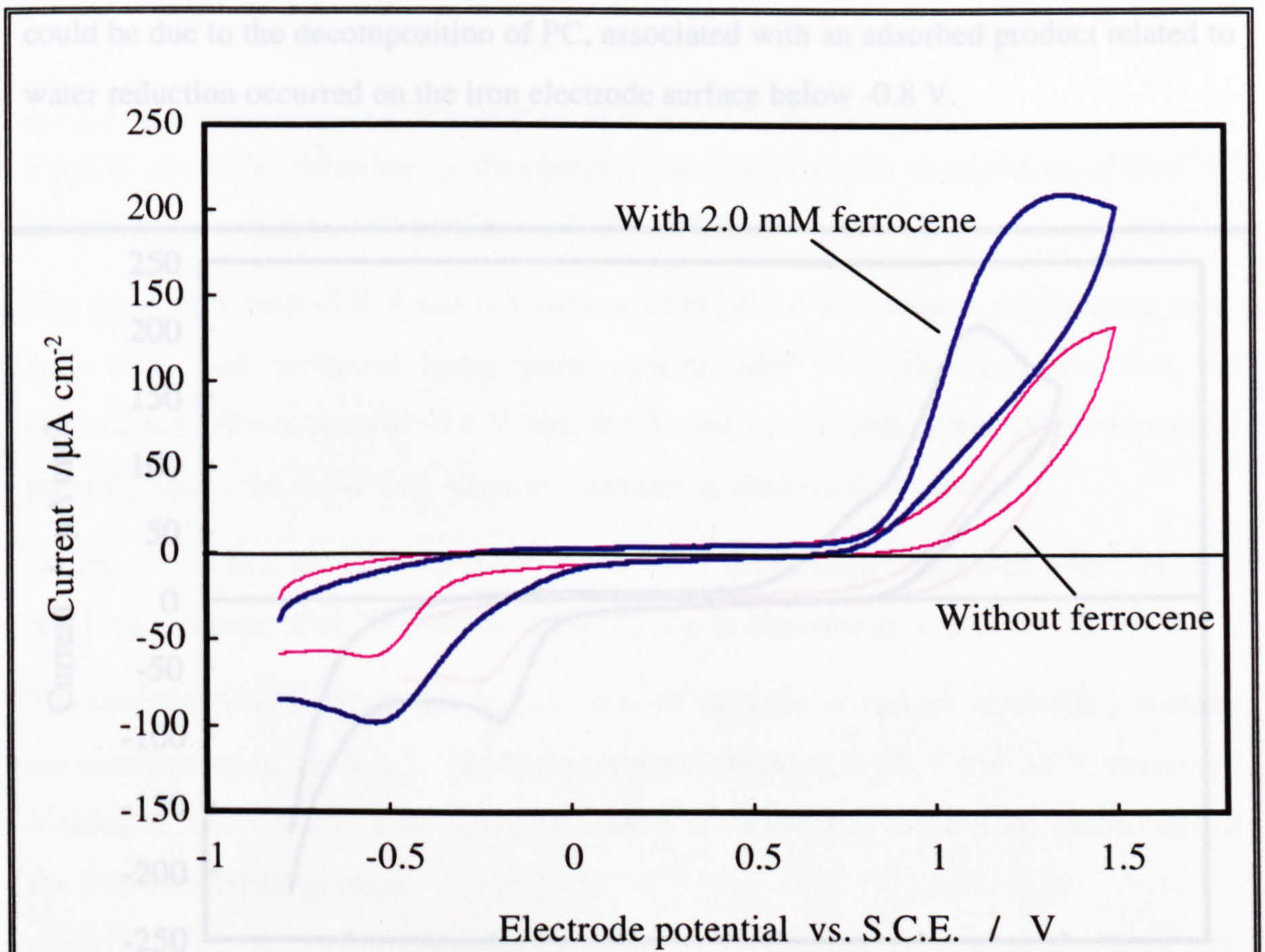


Fig.6.13 Comparison of cyclic voltammograms of iron in 0.01 M $(Et)_4NBF_4$ PC solution, with and without 2.0 mM ferrocene, obtained at the scan rate of 100 mV s^{-1}.

The cathodic current peaks at *ca.* -0.5 V were assumed to be due to the reduction of iron oxide on the electrode surface, and also the reduction of ferrocinium ions to ferrocene when present. The reactions are as follows:

$$Fe + xH_2O \leftrightarrow FeO_x + 2xH^+ + 2xe^- \quad (6\text{-}12)$$

$$Fc \leftrightarrow Fc^+ + e^- \quad (6\text{-}13)$$

However, the scanned potential range for voltammetric curves influenced voltammetric behaviour, as shown in Fig.6.14. Two anodic peaks were obtained when the negative potential limit was -1.2 V. The anodic peak at *ca.* 1.2 V can be attributed to the oxidation of the electrode surface as was explained. Another anodic peak at *ca.* 0.7 V could be due to the decomposition of PC, associated with an adsorbed product related to water reduction occurred on the iron electrode surface below -0.8 V.

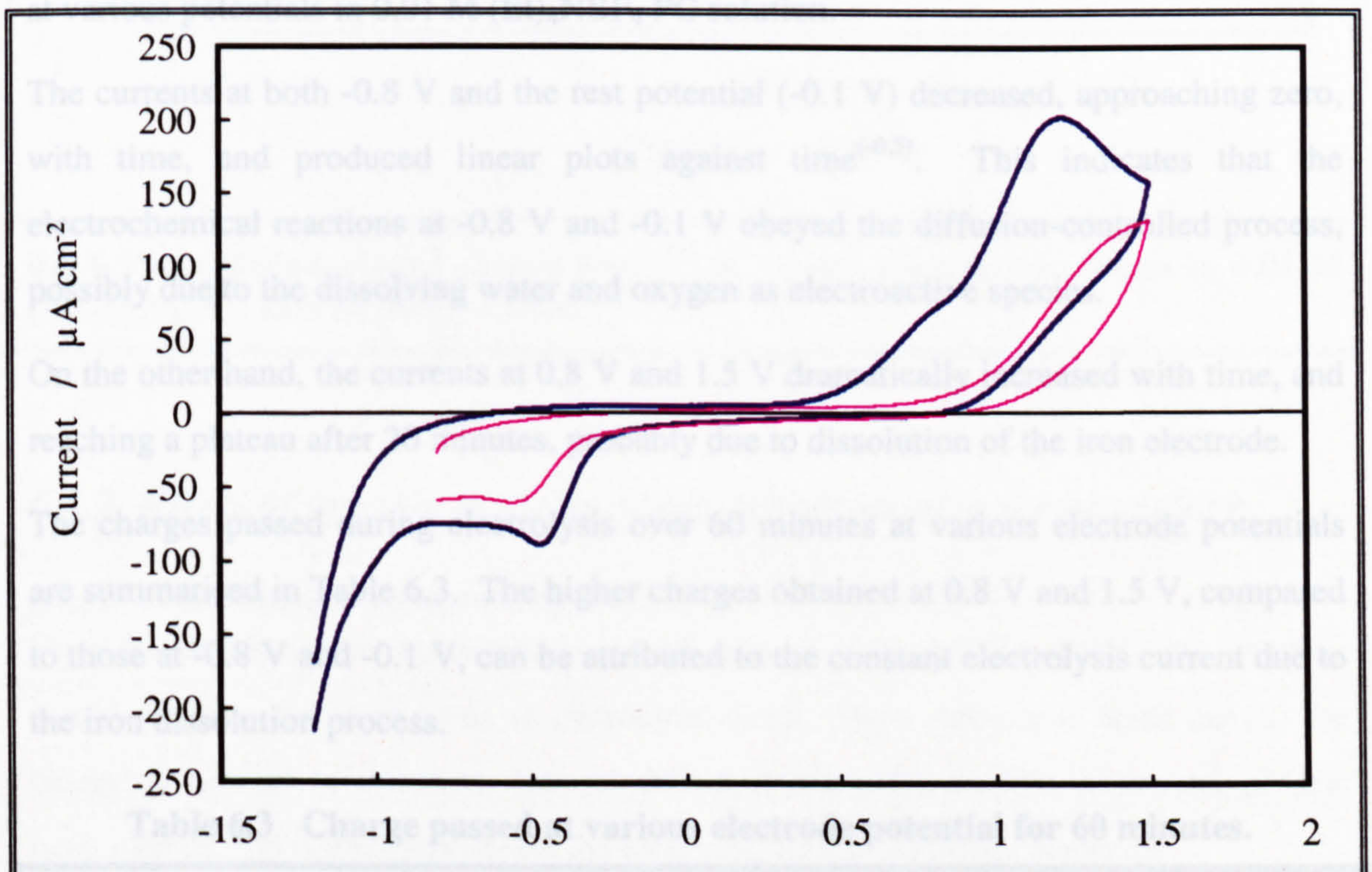


Fig.6.14 Comparison of cyclic voltammograms of iron obtained at the potential scan rate of 100 mV s^{-1}, in 0.01 M $(Et)_4NBF_4$ PC, depending on the scanned potential range.

This oxidation process was assumed to involve the formation of CO_2 and other organic products of as yet unknown composition **[16]**. The potential for decomposition of PC at 0.7 V conforms closely with the previously reported behaviour of iron in 0.5 M $LiClO_4$ PC solution **[19]**.

The cathodic current peaks at *ca.* -0.5 V were attributed mainly to the reduction of iron oxide to iron. The cathodic current below *ca.* -1.0 V dramatically increased, probably due to the reduction of water, and decomposition of PC to CO_2 and propene, as was explained earlier in discussing Fig.6.11. This decomposition and the oxidation of PC are totally irreversible and lead to the imbalance between anodic and cathodic charges.

6.3.1.4 Chronoamperometry with 0.01 M $(Et)_4NBF_4$ PC solution

Fig.6.15 shows the behaviour of the current of an iron electrode as a function of time$^{(-0.5)}$ at various potentials in 0.01 M $(Et)_4NBF_4$ PC solution.

The currents at both -0.8 V and the rest potential (-0.1 V) decreased, approaching zero, with time, and produced linear plots against time$^{(-0.5)}$. This indicates that the electrochemical reactions at -0.8 V and -0.1 V obeyed the diffusion-controlled process, possibly due to the dissolving water and oxygen as electroactive species.

On the other hand, the currents at 0.8 V and 1.5 V dramatically increased with time, and reaching a plateau after 20 minutes, probably due to dissolution of the iron electrode.

The charges passed during electrolysis over 60 minutes at various electrode potentials are summarised in Table 6.3. The higher charges obtained at 0.8 V and 1.5 V, compared to those at -0.8 V and -0.1 V, can be attributed to the constant electrolysis current due to the iron dissolution process.

Table 6.3 Charge passed at various electrode potential for 60 minutes.

Potential vs. S.C.E / V	-0.8	-0.1	0.8	1.5
Charge passed / C	-1.2×10^{-2}	7.9×10^{-3}	0.72	1.75

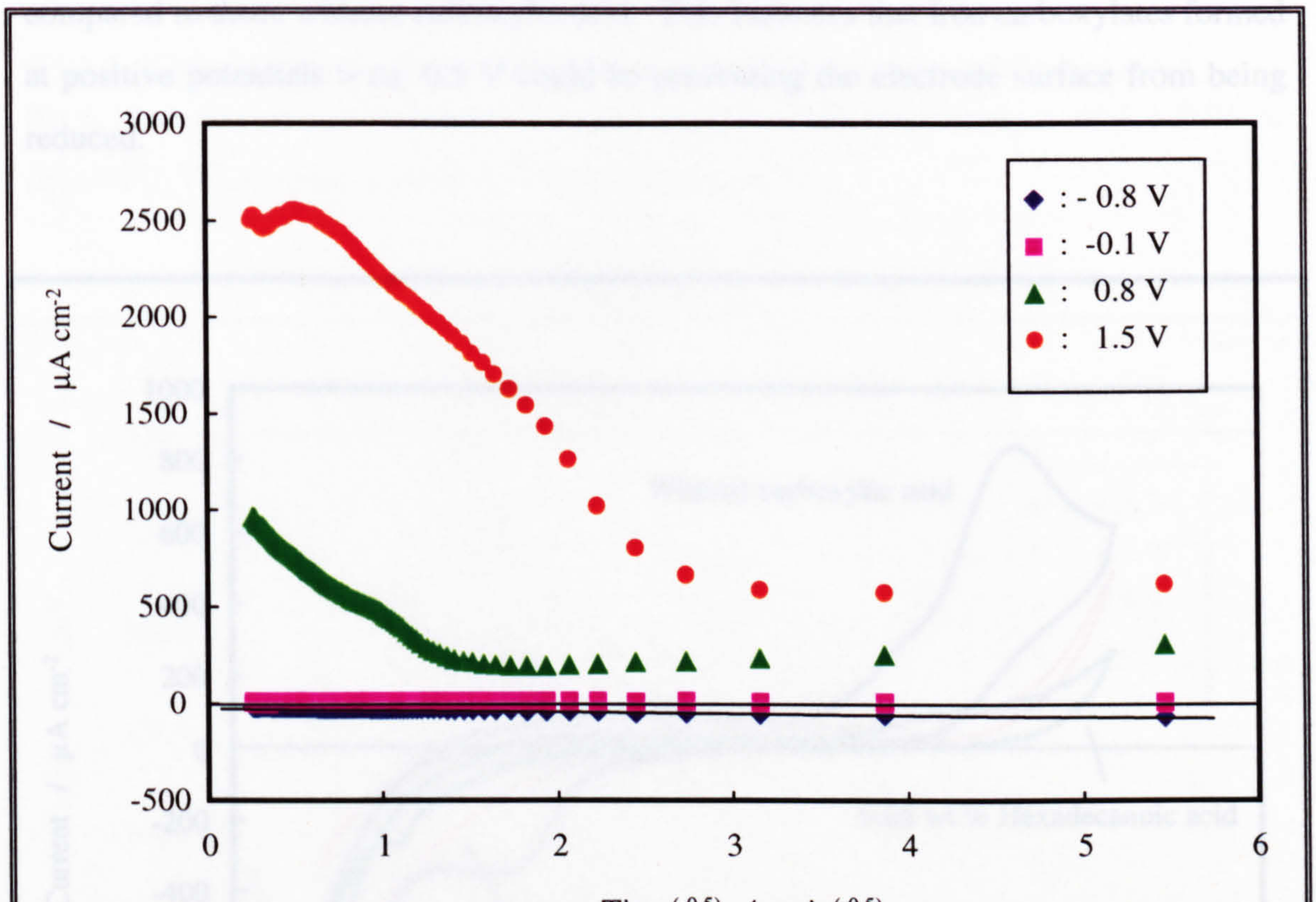


Fig.6.15 Currents plotted against time$^{(-0.5)}$ at various electrode potentials in 0.01 M $(Et)_4NBF_4$ PC, with an iron electrode.

6.3.2 Effect of organic acids on redox processes on a metal surface

6.3.2.1 Voltammetric behaviour of iron

Fig.6.16 shows cyclic voltammograms of iron in 0.01 M $(Et)_4NBF_4$ PC solution containing two different types of carboxylic acids. Both carboxylic acids caused the oxidation current to decrease dramatically due to the irreversible formation of iron octanoate or iron hexadecanoate on the electrode, by the following reactions:

$$Fe + 2RCOOH \rightarrow Fe[RCOO]_2 + 2H^+ + 2e^- \qquad (6\text{-}14a)$$

$$Fe[RCOO]_2 + RCOOH \rightarrow Fe[RCOO]_3 + H^+ + e^- \qquad (6\text{-}14b)$$

Octanoic acid: $R = CH_3(CH_2)_6$, Hexadecanoic acid: $R = CH_3(CH_2)_{14}$

Fig.6.16 also shows that cathodic currents with carboxylic acids at *ca.* -0.5 V are lower, compared to those without carboxylic acid. This indicates that iron carboxylates formed at positive potentials > *ca.* 0.5 V could be preventing the electrode surface from being reduced.

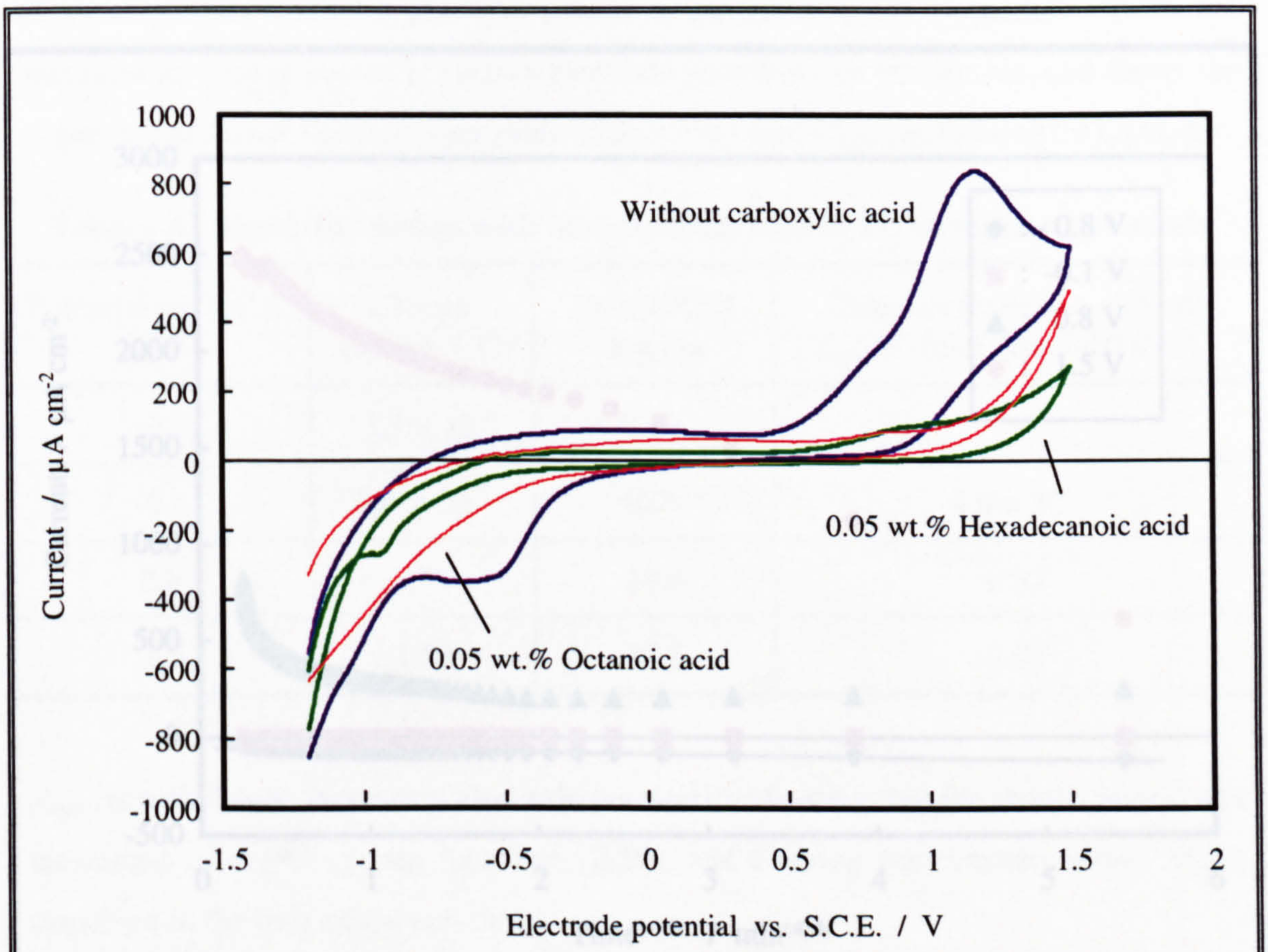


Fig.6.16 Typical cyclic voltammograms of iron in 0.01 M $(Et)_4NBF_4$ PC solution, with and without 0.5 wt.% octanoic and hexadecanoic acids.

When the electrode was controlled at potentials < -1.2 V, the cathodic current increased even in the presence of carboxylic acid. This indicates that some of the iron carboxylate on the electrode surface was reduced to iron and carboxylate anions, with the resulting iron electrode surface then reducing PC into CO_2 and propene **[19]**. This interpretation suggests that the thin friction-reducing layer formed by carboxylic acid might not function effectively at potentials < -1.0 V.

6.3.2.2 Chronoamperometry with 0.05wt.% hexadecanoic acid + PC electrolyte

Fig.6.17 shows current behaviour for iron in 0.05 wt.% hexadecanoic acid + 0.01 M $(Et)_4NBF_4$ PC solution, plotted as a function of time$^{(-0.5)}$.

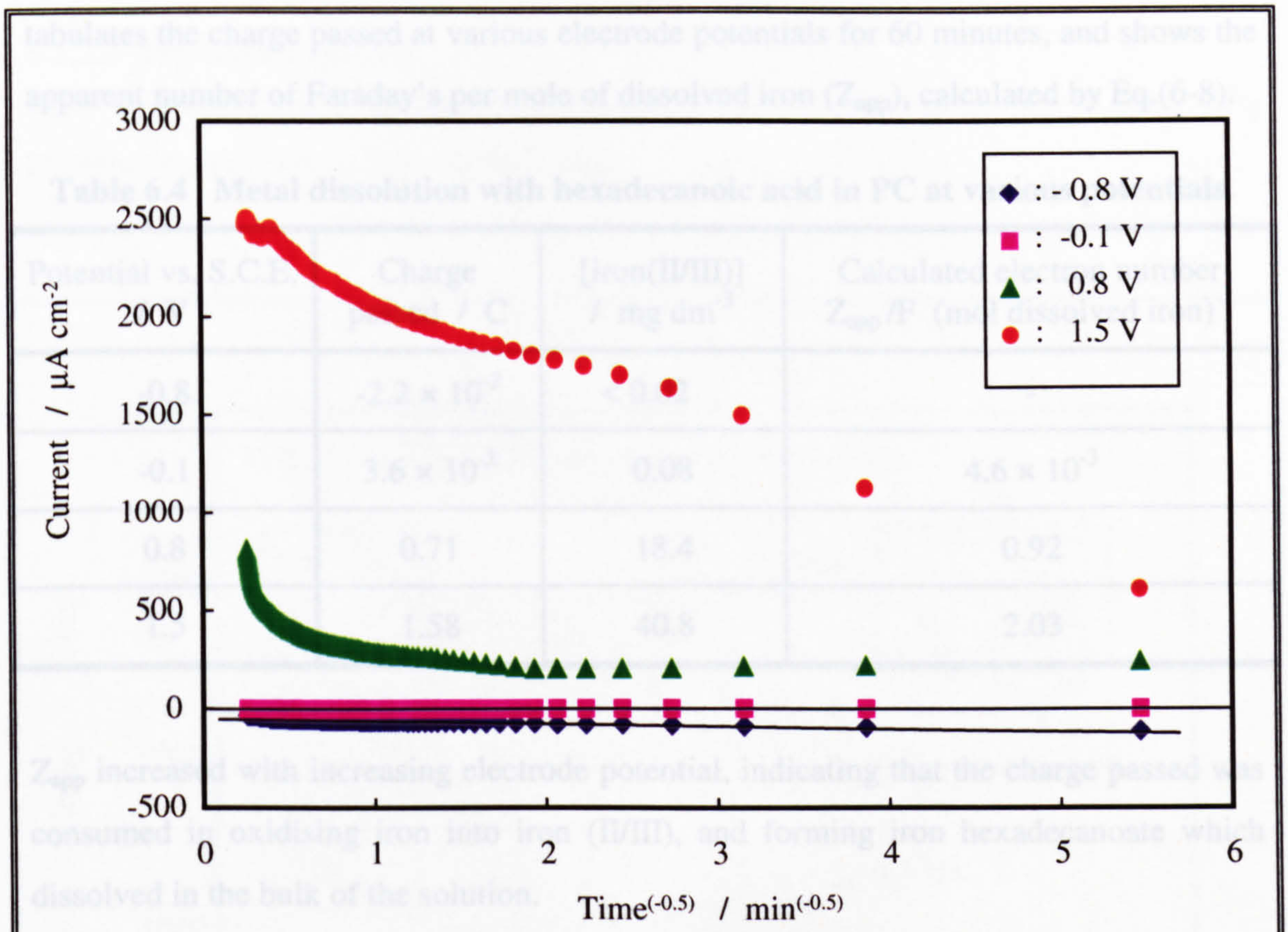


Fig.6.17 Current behaviour for iron plotted against time$^{(-0.5)}$ at various electrode potentials in 0.01 M $(Et)_4NBF_4$ PC containing 0.05 wt.% hexadecanoic acid.

This result showed similar features to Fig.6.15 which was obtained without carboxylic acid. Currents at -0.8 V and -0.1 V (rest potential) decreased and approached zero with time, and formed straight paths against time$^{(-0.5)}$, indicating that hexadecanoic acid or oxygen / water, obeying diffusion-controlled process, were adsorbed on the electrode surface, blocking further reaction.

Currents at 0.8 V and 1.5 V initially increased dramatically, and levelled off with time. This result indicates that the dissolution of metal or iron hexadecanoate occurred at both these potentials.

To correlate the charge passed with metal dissolution, ICP (inductive coupled plasma emission) spectroscopy was used to investigate the iron concentration [iron(II/III)] in these electrolyte solutions after electrolysis at various electrode potentials. Table 6.4 tabulates the charge passed at various electrode potentials for 60 minutes, and shows the apparent number of Faraday's per mole of dissolved iron (Z_{app}), calculated by Eq.(6-8).

Table 6.4 Metal dissolution with hexadecanoic acid in PC at various potentials.

Potential vs. S.C.E. / V	Charge passed / C	[iron(II/III)] / mg dm^{-3}	Calculated electron number Z_{app}/F (mol dissolved iron)$^{-1}$
-0.8	-2.2×10^{-2}	< 0.02	-
-0.1	3.6×10^{-3}	0.08	4.6×10^{-3}
0.8	0.71	18.4	0.92
1.5	1.58	40.8	2.03

Z_{app} increased with increasing electrode potential, indicating that the charge passed was consumed in oxidising iron into iron (II/III), and forming iron hexadecanoate which dissolved in the bulk of the solution.

The charge passed with hexadecanoic acid at the negative potential of -0.8 V showed a lower value than that with dodecanoic acid in DEA at -1.0 V, shown in Table 6.2. This is partly because the concentration of dodecanoic acid in DEA was ten times higher than that of hexadecanoic acid in PC. It is also generally assumed that the adsorption of carboxylic acids on metal surfaces can take place in a more orderly way when molecules have shorter alkyl-chains **[20]**, and hence the dodecanoate anions enable the formation of more packed molecular adsorption layers.

6.3.3 Impedance spectra analysis of iron in PC electrolyte solutions

Electrochemical impedance spectroscopy was used to obtain further information about the interfacial properties of iron as a function of electrode potential in PC electrolyte solution with and without 0.05 wt.% hexadecanoic acid.

6.3.3.1 Impedance spectra

Fig.6.18 shows typical impedance spectra using an iron electrode in 0.01 M $(Et)_4NBF_4$ PC solution, at various electrode potential.

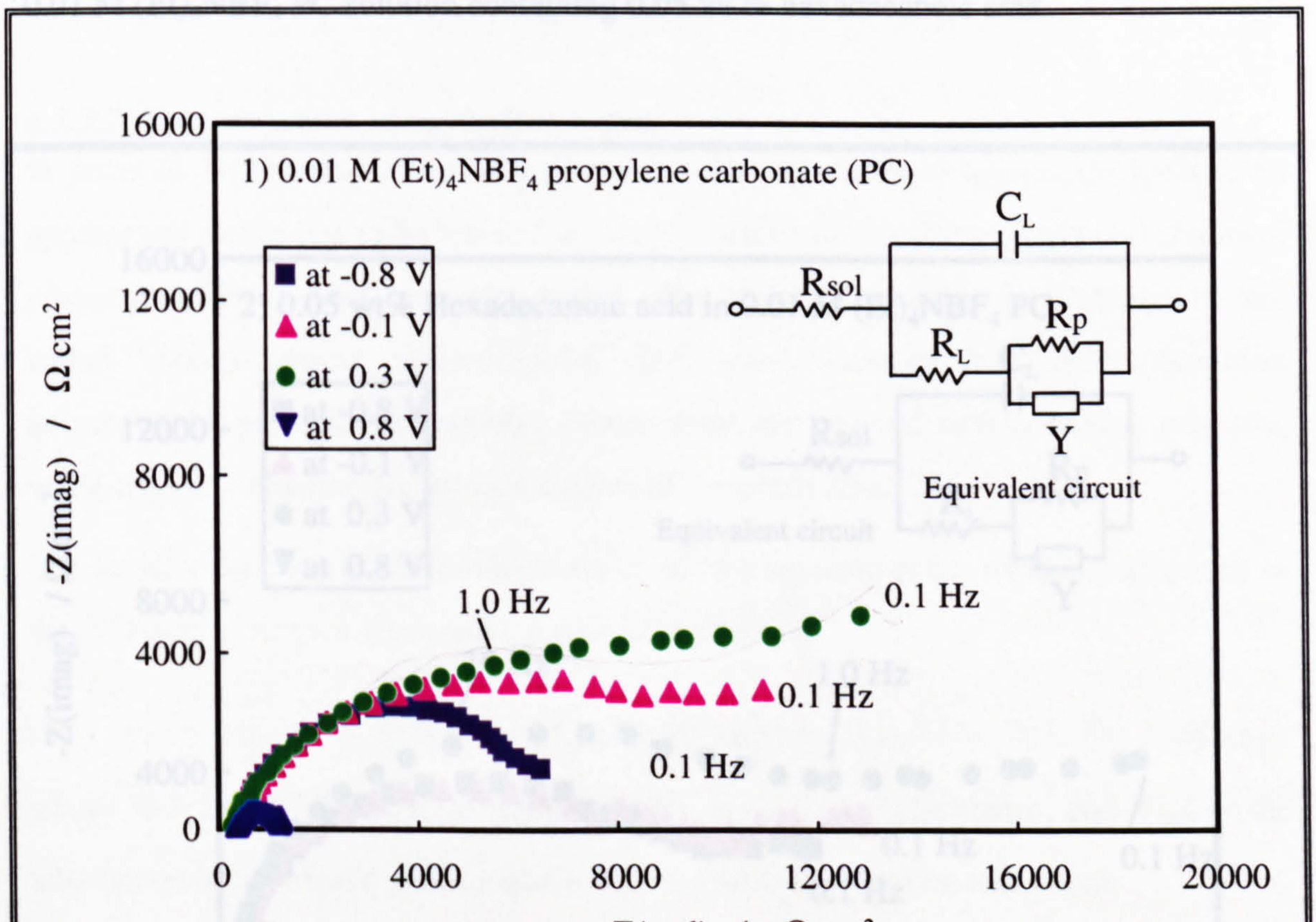


Fig.6.18 Impedance spectra for iron electrode obtained at various controlled electrode potentials in 0.01 M $(Et)_4NBF_4$ PC solution.

The total electrode impedance initially increased with increasing electrode potential (reaction resistance of the iron electrode corresponds to the diameter of semicircle). This result suggests that an iron oxide layer formed on the electrode surface at positive potentials causes the electrical resistance, and hence the total impedance, to be higher. This is consistent with the voltammetric behaviour and the result shown in Fig.6.15.

As expected from the voltammogram in Fig.6.13, the reaction resistance decreased dramatically when the electrode potential was controlled at 0.8 V. This suggests that some parts of the iron oxide layer on the electrode dissolve into the bulk electrolyte solution.

Fig.6.19 shows impedance spectra at various electrode potentials for an iron electrode in 0.01 M $(Et)_4NBF_4$ PC solution containing 0.05 wt.% hexadecanoic acid.

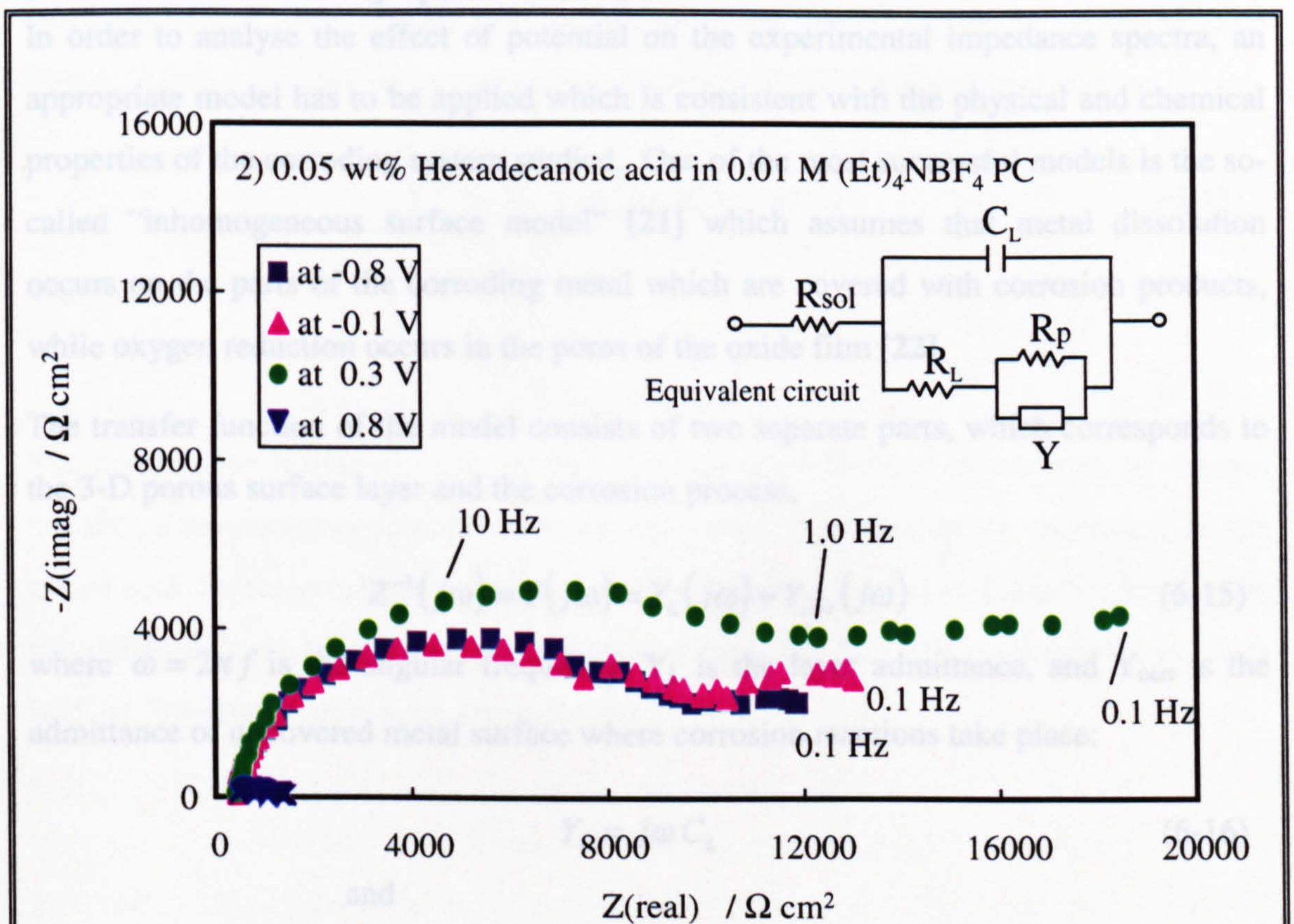


Fig.6.19 Impedance spectra for iron electrode obtained at various controlled potential in 0.05 wt.% hexadecanoic acid + 0.01 M $(Et)_4NBF_4$ PC solution.

Focusing on the total electrode impedance of an iron electrode, the impedance controlled at -0.8 V to 0.3 V did not show large difference compared to the results obtained in PC electrolyte solution without hexadecanoic acid. This result indicates that the adsorption of hexadecanoic acid on the electrode surface caused the impedance to increase slightly at -0.8 V, and maintained high values up to an electrode potential of 0.3 V.

At 0.8 V, however, the total impedance shows a drastic decrease, with the radius of the semicircle becoming small at 0.8 V. This feature, similar to that obtained in the PC electrolyte solution without hexadecanoic acid, is assumed to result from the dissolution taking place at high anodic potentials.

6.3.3.2 Determination of equivalent circuit

In order to analyse the effect of potential on the experimental impedance spectra, an appropriate model has to be applied which is consistent with the physical and chemical properties of the corroding system studied. One of the most successful models is the so-called "inhomogeneous surface model" **[21]** which assumes that metal dissolution occurs on the parts of the corroding metal which are covered with corrosion products, while oxygen reduction occurs in the pores of the oxide film **[22]**.

The transfer function of the model consists of two separate parts, which corresponds to the 3-D porous surface layer and the corrosion process,

$$Z_p^{-1}(j\omega) = Y(j\omega) = Y_L(j\omega) + Y_{corr}(j\omega) \qquad (6\text{-}15)$$

where $\omega = 2\pi f$ is the angular frequency, Y_L is the layer admittance, and Y_{corr} is the admittance of uncovered metal surface where corrosion reactions take place:

$$Y_L = j\omega C_L \qquad (6\text{-}16)$$

and

$$Y_{corr}^{-1} = R_L + R_p\left(1 + j\omega R_p C_{dl}\right)^{-1} \qquad (6\text{-}17)$$

where C_L characterises the properties of the inhomogeneous surface layer, R_L stands for the resistance of the electrolyte within the pores, and C_{dl} constitutes the double-layer capacitance in parallel with the polarisation resistance characterising the surface reaction.

Kendig [23] introduced another approach for interpreting corrosion data by the modification of the corrosion impedance Z_{corr}, replacing the double-layer capacitance with a constant phase element (CPE), which can represent surface inhomogeneities in detail, given by:

$$Z_{corr} = \frac{1}{Y_0(j\omega)^{\alpha}} \tag{6-14}$$

The coefficient Y_0 is a simple function coupling polarisation resistance to capacitance and α is a measure of the deviation from the ideal RC behaviour due to the surface inhomogeneities [24]. Using this modification, the model circuit is shown in both Figs.6.18 and 6.19, and the corresponding expression of corrosion impedance is:

$$Y_{corr}^{-1} = R_L + R_p\left[1 + R_p Y_0(j\omega)^{\alpha}\right]^{-1} \tag{6-15}$$

where

$$R_p Y_0 = \left(R_p C_{dl}\right)^{\alpha} \tag{6-16}$$

The polarisation resistance is in general a complicated function determined by charge-transfer, mass-transport and chemical reaction rates. The quantitative analysis to fit the above equivalent circuit was performed and the results tabulated in Table 6.5 for 0.01 M $(Et)_4NBF_4$ PC without hexadecanoic acid, and Table 6.6 for 0.01 M $(Et)_4NBF_4$ PC with 0.05 wt.% hexadecanoic acid, respectively.

Table 6.5 Parameters of equivalent model for PC without hexadecanoic acid.

Potential vs. S.C.E. / V	-0.8	-0.1	0.3	0.8
R_{sol} / $\Omega\,cm^2$	370	376	351	344
R_L / $\Omega\,cm^2$	65	60	60	54
R_p / $\Omega\,cm^2$	7320	12214	17029	893
C_L / $\mu F\,cm^{-2}$	4.6	4.7	3.7	1.2
Y_0 / $\mu F\,cm^{-2}$	30	31	35	110
α	0.63	0.62	0.57	0.57

Table 6.6 Parameters of equivalent model for PC with hexadecanoic acid.

Potential vs. S.C.E. / V	-0.8	-0.1	0.3	0.8
R_{sol} / $\Omega\,cm^2$	375	382	373	353
R_L / $\Omega\,cm^2$	77	76	83	77
R_p / $\Omega\,cm^2$	10697	11706	18040	689
C_L / $\mu F\,cm^{-2}$	0.17	0.26	0.56	1.2
Y_0 / $\mu F\,cm^{-2}$	4.0	4.4	4.5	780
α	0.75	0.66	0.65	0.77

6.3.3.3 Analysis of parameters for the equivalent model

Among the model parameters given in Tables 6.5 and 6.6, only C_L, R_p and Y_0 showed significant variations with increasing electrode potential. C_L obtained in 0.01 M $(Et)_4NBF_4$ PC solution containing 0.05 wt.% hexadecanoic acid showed smaller values at electrode potentials from -0.8 V to 0.3 V, compared to those obtained in the PC solution without hexadecanoic acid. This indicates that adsorbed dielectric layers, such

as the hexadecanoate anion film, gave rise to a capacitance whose inverse is proportional to film thickness, and hence showed small capacitance values **[25]**. The thickness of the adsorbed film of hexadecanoate at negative potentials can be estimated as 5-10 nm.

At 0.8 V, corroding processes are assumed to become dominant on the electrode surface, in the presence and absence of hexadecanoic acid, and resulted in the same values of C_L.

On the other hand, the second low frequency parameter Y_0 produced similar values at the electrode potentials between -0.8 V and 0.3 V, and increased at 0.8 V, for PC electrolyte solutions with and without hexadecanoic acid. This result indicates that the charge-transfer reaction changes at the electrode potential of 0.8 V, probably due to the increase in dissolution reaction rates.

The polarisation resistance R_p without hexadecanoic acid gradually increased with increasing electrode potential between -0.8 V and 0.3 V, because of the formation of an iron oxide layer, and hence increase of charge-transfer reaction rates **[26]**. The R_p with hexadecanoic acid also showed the same trends, probably due to the formation of hexadecanoate film, as well as iron oxide layers.

Following electrolysis at constant potentials, during which the current-time response was integrated, the electrolyte solution was analysed for dissolved iron species by ICP spectroscopy. Depending on whether iron(II) or iron(III) species were assumed to be formed, almost all the charge passed could be accounted for in terms of the iron dissolved, probably as iron hexadecanoate species. Hence, addition of hexadecanoic acid at 0.8 V had no effect on the capacitance values and decreased the values of R_p slightly, compared to the values obtained in the electrolyte without hexadecanoic acid.

6.4 Conclusion

This chapter has investigated the electrochemical kinetics of iron and platinum in DEA and PC electrolyte solutions, mainly by determination of voltammograms with and without DBDS and alkyl-carboxylic acids, to infer their interactions with electrode

surfaces. For the iron electrode, adsorption densities and dissolution processes on the iron electrode, resulting from the formation of iron carboxylates with alkyl-carboxylic acids, were determined as a function of electrode potential. The interactions between DBDS and iron in DEA electrolyte solution are still not fully understood, probably due to the simultaneous reduction of iron oxide which masks the reduction of DBDS on the iron surface.

CHAPTER 7

7. Effect of electrode potential on friction and wear

7.1 Introduction

This chapter describes the tribological behaviour of steel as a function of electrode potential in both DEA and propylene carbonate(PC), with and without aryl disulphides and organic acid additives. HFR tests are used to measure friction and wear. This chapter also relates the observed tribological performance with the electrochemical studies described in the previous chapters.

7.2 Tribological behaviour of steel under controlled potential in DEA

7.2.1 Effect of electrode potential on dynamic friction

7.2.1.1 Average friction values

Fig.7.1 shows measured dynamic friction coefficient, with and without additives present as a function of electrode potential. Each data point represents a root mean square friction value during a rubbing test of 30 minutes in duration at a constant electrode potential. The rest potential (-0.1 V) corresponds to the 'rest' potential of iron in the electrolyte with no externally applied potential.

The friction in 0.8 M $LiClO_4$ without any friction or wear-reducing additive present, decreases on the positive-going potential scan, due mainly to the formation of iron oxide on the electrode surface, as shown in the voltammogram in Fig.6.2. The same frictional features can be recognised in previously published data **[1,2]** for iron friction in aqueous systems, in which the oxidised iron showed less surface roughness and also a reduced adhesive contribution to friction compared to reduced iron surfaces.

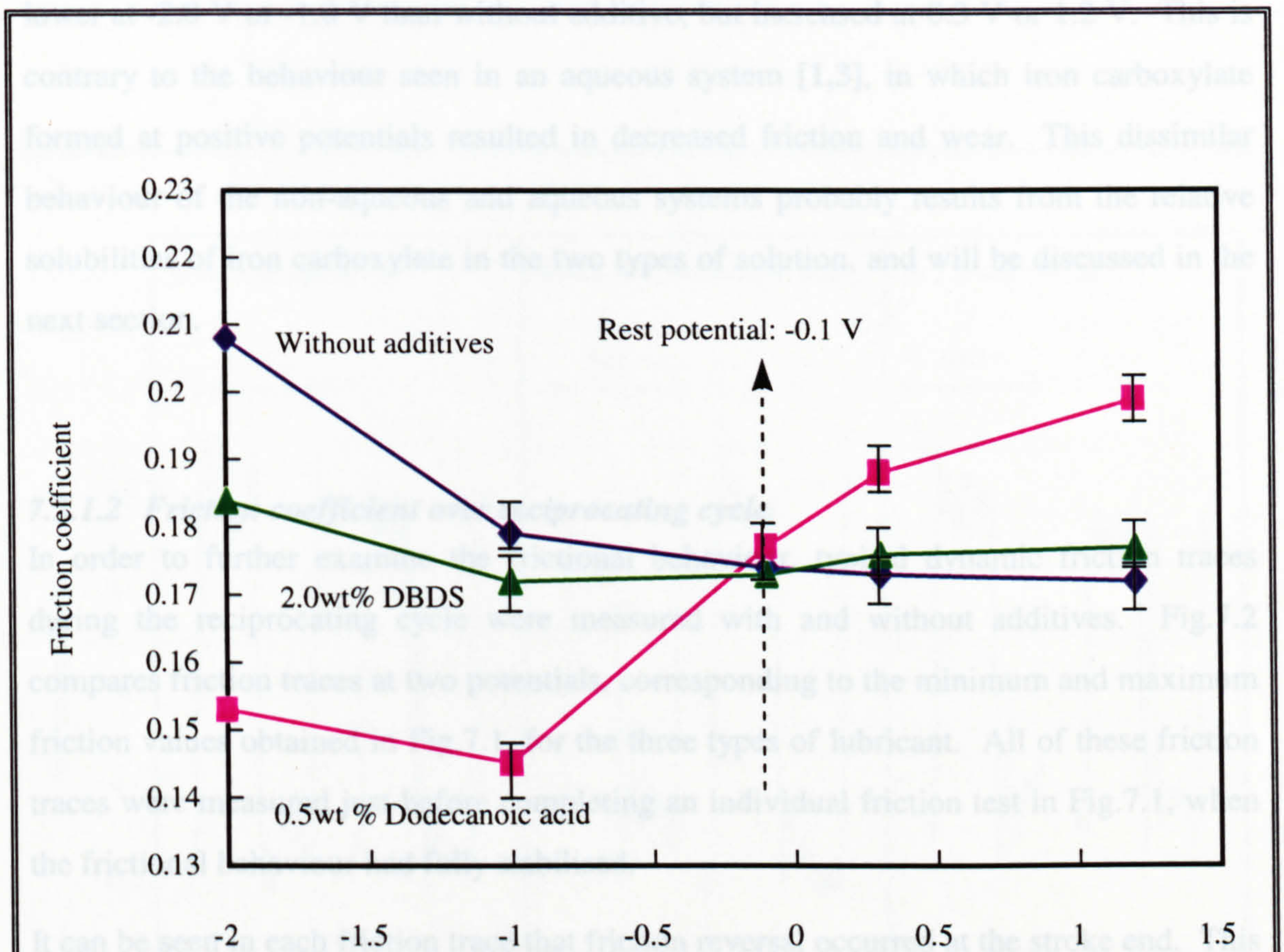


Fig.7.1 Effect of electrode potential on dynamic friction of iron-on-iron in 0.8 M $LiClO_4$ in DEA with and without 2.0 wt.% DBDS and 0.5 wt.% dodecanoic acid.

The friction coefficient at -1.0 V or -2.0 V in the presence of 2.0 wt.% DBDS in 0.8 M $LiClO_4$ DEA was slightly lower than in the absence of DBDS, probably due to the formation of iron mercaptide on the electrode surface. As shown in Fig.6.4 and reaction (6-5), DBDS can be reduced at potentials < -0.9 V by reactions such as:

$$Fe_2O_3 + 3(PhCH_2S)_2 + 6H^+ + 6e^- \leftrightarrow 2Fe(PhCH_2S)_3 + 3H_2O \qquad (7\text{-}1a)$$

$$Fe(PhCH_2S)_2 + 2e^- \rightarrow Fe + 2PhCH_2S^-_{(ads)} \qquad (7\text{-}1b)$$

The formation of iron mercaptide also resulted in low wear, which will be discussed in the next section.

In the presence of 0.5 wt.% dodecanoic acid, the friction coefficient was considerably lower at -2.0 V or -1.0 V than without additive, but increased at 0.3 V or 1.2 V. This is contrary to the behaviour seen in an aqueous system **[1,3]**, in which iron carboxylate formed at positive potentials resulted in decreased friction and wear. This dissimilar behaviour of the non-aqueous and aqueous systems probably results from the relative solubilities of iron carboxylate in the two types of solution, and will be discussed in the next section.

7.2.1.2 Friction coefficient over reciprocating cycle

In order to further examine the frictional behaviour, typical dynamic friction traces during the reciprocating cycle were measured with and without additives. Fig.7.2 compares friction traces at two potentials, corresponding to the minimum and maximum friction values obtained in Fig.7.1, for the three types of lubricant. All of these friction traces were measured just before completing an individual friction test in Fig.7.1, when the frictional behaviour had fully stabilised.

It can be seen in each friction trace that friction reversal occurred at the stroke end. This may result in part from a reversal effect. When the friction coefficient reaches its maximum value corresponding to zero velocity, slip may occur and energy be released from the deflected arm of the HFR rig connecting the main body and the head. This could cause the ball to accelerate its movement as it attempted to "catch up" with the driving head, giving some overshoot in the friction coefficient trace. This is a typical characteristic of stick-slip phenomena.

However, it can also be seen that, for the same lubricant, the sharpness of friction reversal varied markedly when the electrode potential at the metal surface was changed. With DBDS and dodecanoic acid under reducing conditions, friction appeared largely speed-independent, suggestive of a solid-like adsorbed or reacted layer. With dodecanoic acid under oxidising conditions, friction tended to fall in mid stroke but rise to a high value at the stationary ends of the stroke. This may indicate the presence of viscous material in the vicinity of the contact, able to augment the hydrodynamic film

but unable to form a film in stationary conditions. This is in accord with the expected electrochemical reactions, as discussed in Figs.6.5 and 6.7.

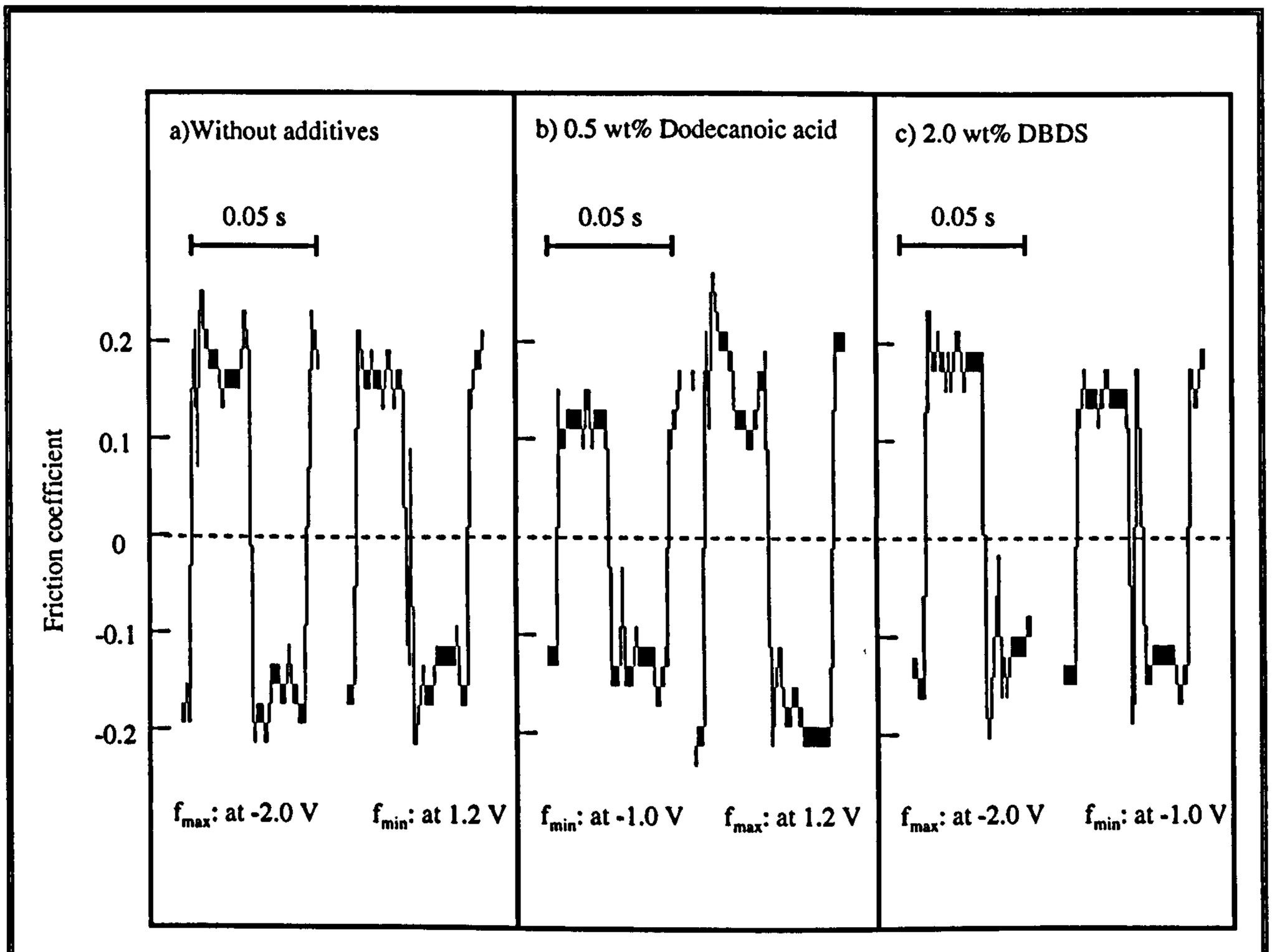


Fig.7.2 Typical friction coefficient traces between reciprocating contact at electrode potentials corresponding to the minimum and maximum friction coefficients in a) 0.8 M $LiClO_4$ DEA solutions containing b) 0.5 wt.% dodecanoic acid :c) 2.0 wt.% DBDS.

It should be noted that, with macro-contact systems such as the HFR rig, no information is obtained about the spatial distribution of the electrochemically-formed product on the rubbing surfaces. This distribution, due for example to two-dimensional phase nucleation and growth or pitting processes, may have a large effect on friction and wear.

Such distributions may be determined by combining electrochemical techniques with nano-probe techniques, such as atomic force microscopy (AFM) or scanning tunnelling microscopy (STM), as will be described in Chapter 9.

7.2.2 Effect of electrode potential on wear of ball

Fig.7.3 shows the effect of electrode potential on the ball wear scar, measured using an optical microscope after a 30 minutes test. In all cases, with and without friction and wear reducing additives, it is evident that the wear scars increase at potentials > -1.0 V and reach plateaux values at 0.3 V.

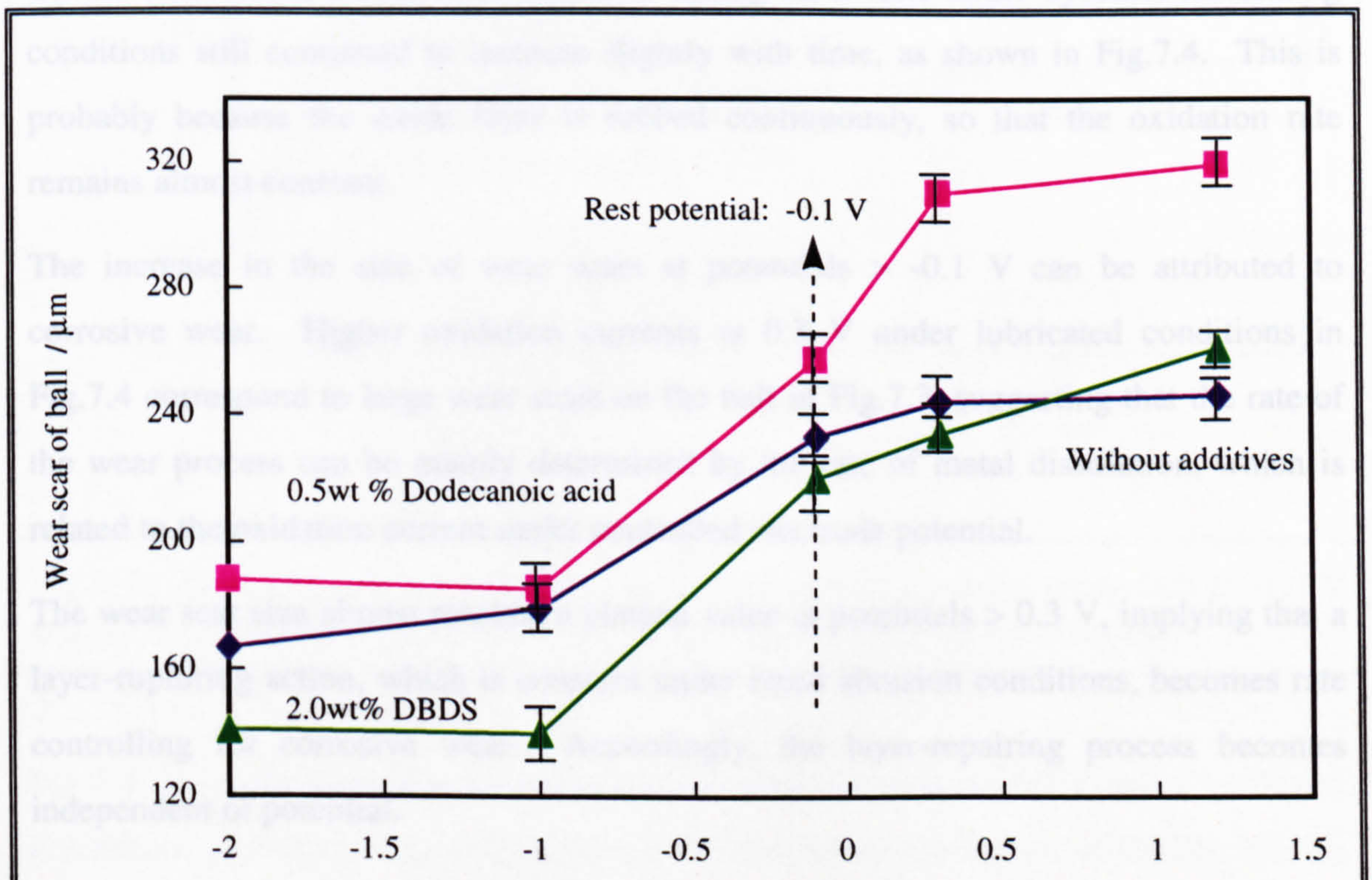


Fig.7.3 Effect of electrode potential on the ball's wear scar in 0.8 M $LiClO_4$ DEA solutions with and without 2.0 wt.% DBDS and 0.5 wt.% dodecanoic acid.

7.2.2.1 Wear of ball without friction and wear reducing additives

At very low potentials such as -1.0 V or -2.0 V, the ball and disc specimens are likely to have been subjected only to an adhesive wear mechanism. When the electrode potential is increased to > -0.6 V, a passive oxidation film should form on the iron surface, according to the voltammogram in Fig.6.2. In the static oxidation in Fig.6.3, the oxide film formed acted as a barrier between the base metal and the lubricant, and the rate of oxidation, as measured by the oxidation current at -0.1 V, decreased. The oxidation currents at > 0.3 V increased with time, before reaching a steady-state oxidative dissolution rate.

On the other hand, the currents measured during HFR tests under dynamic lubricating conditions still continued to increase slightly with time, as shown in Fig.7.4. This is probably because the oxide layer is rubbed continuously, so that the oxidation rate remains almost constant.

The increase in the size of wear scars at potentials > -0.1 V can be attributed to corrosive wear. Higher oxidation currents at 0.3 V under lubricated conditions in Fig.7.4 correspond to large wear scars on the ball in Fig.7.3, suggesting that the rate of the wear process can be mainly determined by the rate of metal dissolution, which is related to the oxidation current under controlled electrode potential.

The wear scar size almost reached a plateau value at potentials > 0.3 V, implying that a layer-rupturing action, which is constant under fixed abrasion conditions, becomes rate controlling for corrosive wear. Accordingly, the layer-repairing process becomes independent of potential.

7.2.2.2 Wear of ball with DBDS

The wear scars formed with DBDS at electrode potentials < -1.0 V are smaller than those with the base oil alone, due to the formation of protective iron mercaptide films on the metal surface, as discussed above. At reducing potentials in the absence of DBDS,

no adsorbed lubricating film was present, so direct metal-metal contact occurred between ball and disc, leading to high friction and adhesive wear.

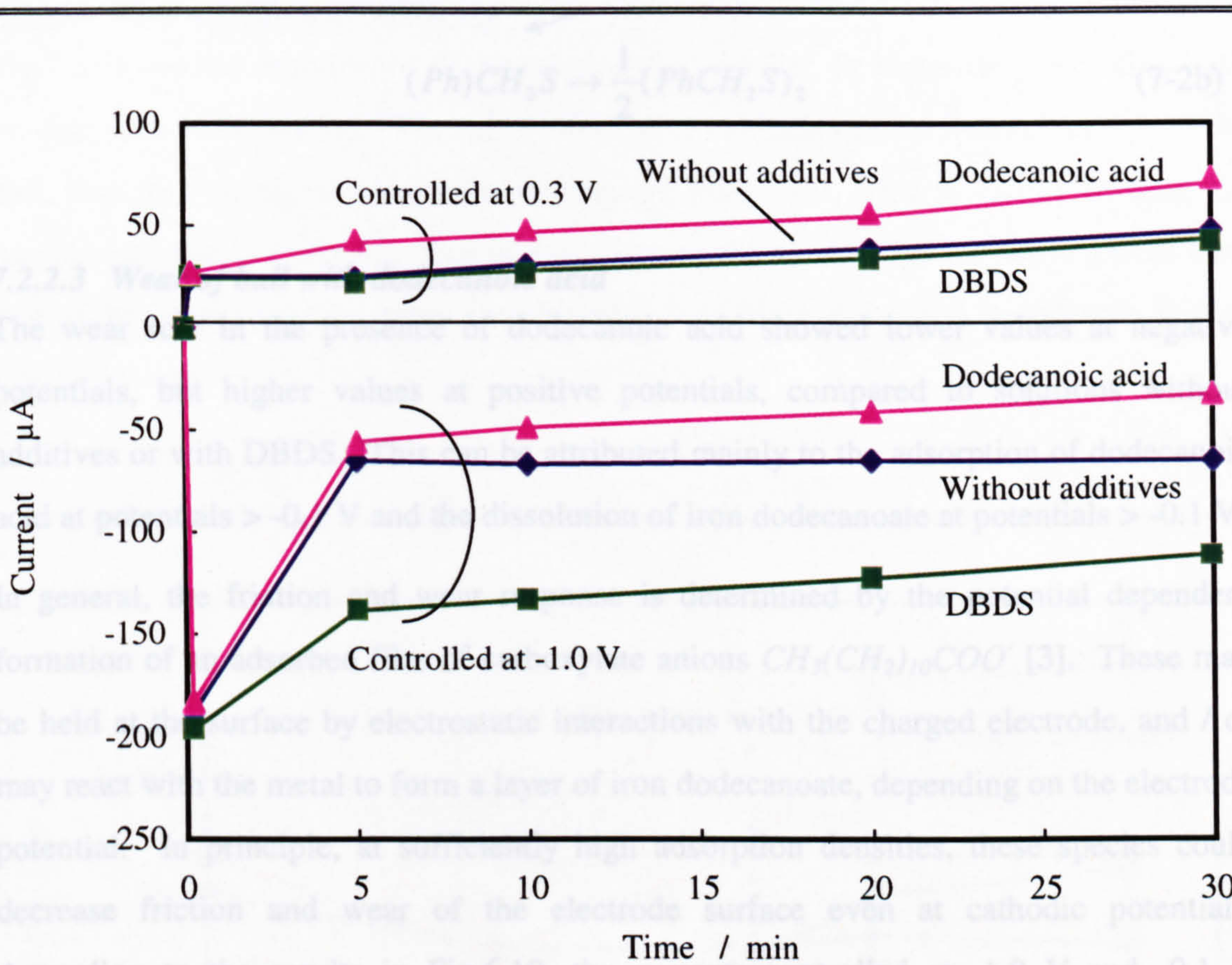


Fig.7.4 Time dependence of the anodic and /or cathodic current controlled at -1.0 V and 0.3 V, under lubricated conditions, using three different types of lubricants.

Fig.7.4 shows the time dependence of the reduction currents at -1.0 V under lubricated conditions, providing supporting evidence for the cathodic reduction of DBDS. Unlike the oxidative currents at 0.3 V, all the initial currents at -1.0 V showed high values and decreased immediately. After 5 minutes, the current in the presence of DBDS was more negative than in its absence, indicating that DBDS was still being reduced. In addition to the formation of iron mercaptide by reaction (7-1), other possible reactions to be considered could involve the formation of benzyl sulphonic acid by reaction (7-2a) and /

or the homogeneous re-formation of the DBDS by reaction (7-2b), if dissolved oxygen were present **[4]**:

$$(Ph)CH_2S^- + O_2 \rightarrow (Ph)CH_2S + O_2^- \rightarrow (Ph)CH_2SO_2^- \qquad (7\text{-}2a)$$

$$(Ph)CH_2S \rightarrow \frac{1}{2}(PhCH_2S)_2 \qquad (7\text{-}2b)$$

7.2.2.3 Wear of ball with dodecanoic acid

The wear scar in the presence of dodecanoic acid showed lower values at negative potentials, but higher values at positive potentials, compared to solutions without additives or with DBDS. This can be attributed mainly to the adsorption of dodecanoic acid at potentials > -0.1 V and the dissolution of iron dodecanoate at potentials > -0.1 V

In general, the friction and wear response is determined by the potential dependent formation of an adsorbed film of carboxylate anions $CH_3(CH_2)_{10}COO^-$ **[3]**. These may be held at the surface by electrostatic interactions with the charged electrode, and / or may react with the metal to form a layer of iron dodecanoate, depending on the electrode potential. In principle, at sufficiently high adsorption densities, these species could decrease friction and wear of the electrode surface even at cathodic potentials. According to the results in Fig.6.10, the currents controlled at -1.0 V and -0.1 V decreased and tended to zero with increasing time.

The high friction and high wear at high potentials (0.3 V and 1.2 V) is likely to result from a higher solubility of iron dodecanoate in the DEA **[5]**, compared with that in aqueous solutions, so that the iron carboxylate formed will not remain on the rubbing surfaces, particularly in the presence of imposed mechanical stress. This is likely to result in high rates of corrosive wear, and also cause friction coefficients to increase because of lower adsorption densities of iron dodecanoate. This oxidative metal dissolution under non-lubricated conditions has already been identified from dissolved iron concentrations measurements as listed in Table 6.1.

7.2.3 Effect of electrode potential on wear of disc

7.2.3.1 Wear of disc with HFR rig

Fig.7.5 shows the dependence of the wear of the iron disc on electrode potential in ball-on-disc wear experiments. The rate of disc wear exhibits similar features to that of the ball, though with higher wear rates at negative potentials. This is mainly because the hardness of disc is lower than that of ball. Hence, the wear of the former is greater than that of the latter under the same experimental conditions, even with dodecanoic acid or DBDS present.

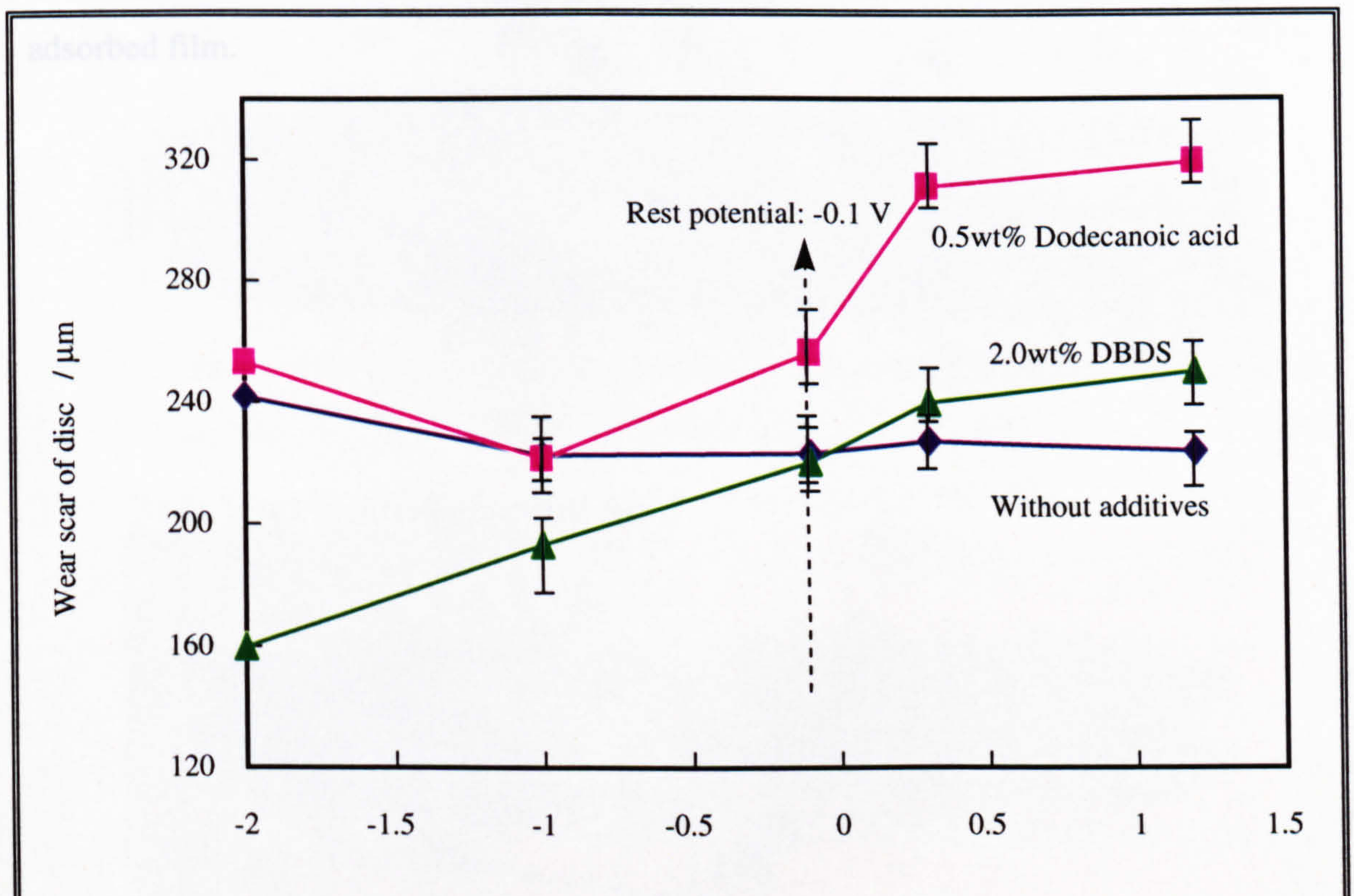


Fig.7.5 Effect of electrode potential on wear scar of disc in 0.8 M $LiClO_4$ solutions with and without 2.0 wt.% DBDS and 0.5 wt.% dodecanoate acid.

7.2.3.2 Wear scar appearance at anodic potential

Fig.7.6 shows the appearance of disc wear scars after wear tests conducted at 0.3 V. It is evident that the disc wear scars without additives and with 2.0 wt.% DBDS become black in colour as a result of the formation of an iron oxide film with dissolved oxygen in DEA or the formation of iron mercaptide with DBDS. However, the wear scar obtained in the presence of dodecanoic acid does not exhibit such an appearance.

This indicates that dodecanoic acid can protect the iron surface and prevent the surface from being oxidised with dissolved oxygen in DEA. In this case, dodecanoic acid would selectively react with the iron surface at positive potentials, and form iron dodecanoate which would simultaneously dissolve into the solution through the adsorbed film.

Fig.7.6 Comparison of the appearances of wear scars of discs after wear tests conducted at the electrode potential of 0.3 V.

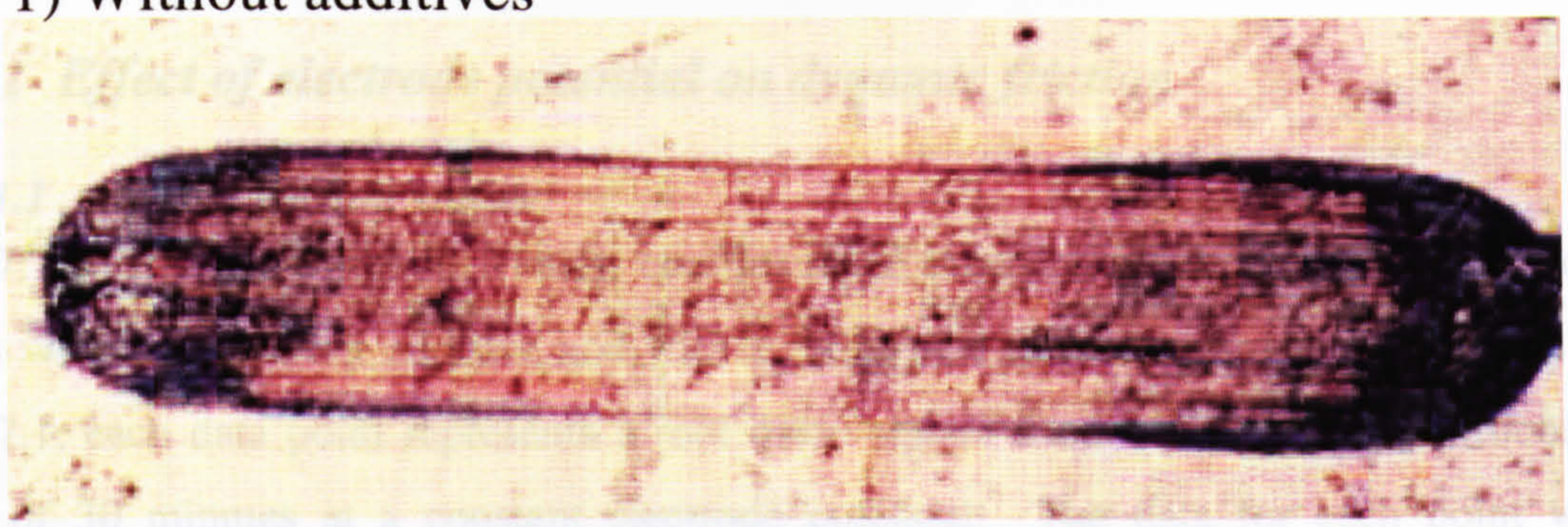


Fig.7.6 Comparison of the appearances of wear scars of discs after wear tests conducted at the electrode potential of 0.3 V.

7.3 Tribological behaviour of steel under controlled potential in PC

7.3.1 Effect of electrode potential on dynamic friction

7.3.1.1 Average friction values

Fig.7.7 shows the dynamic friction coefficient of propylene carbonate (PC) solution, both without any other additive and with a range of different carboxylic acids. As in Fig.7.1, each data point represents a root mean square friction value during a rubbing test of 30 minutes at a constant electrode potential. The data for each point was measured at least three times and was also calculated as an average friction coefficient. The rest potential (-0.1 V) shown in Fig.7.7 corresponds to the open-circuit potential of iron in the electrolyte solution with no externally applied potential, but at which a net reaction could still have been occurring.

PC without any carboxylic acid did not exhibit any significant change in friction coefficient between -1.5 V and 1.5 V. The iron oxide formed on the electrode surface at 0.8 V and 1.5 V, as implied by Fig.6.16, may have caused the decrease in friction. However, the oxidative dissolution of iron(II/III), which also occurred at 0.8 V and 1.5 V, should have increased friction. Thus the two effects of the chemical reactions on the electrode might well cancel any significant change in dynamic friction coefficient of iron in 0.1 M $(Et)_4NBF_4$ PC electrolyte solution, over the electrode potential ranges.

In the presence of carboxylic acids, all the friction coefficients between -1.5 V and -0.1 V were lower than those without carboxylic acids, and decreased markedly with increasing alkyl-chain length. However, they rose sharply at 0.8 V and 1.5 V. This behaviour at negative potentials is good evidence of the effectiveness of carboxylic acids as oiliness additives **[6]**.

These features of lower friction at negative potentials and higher friction at positive potentials are also in good agreement with the previous results using DEA electrolyte solutions. They can be explained by the adsorption of carboxylic acids on iron surfaces at the negative potentials and the dissolution of iron carboxylates into the bulk of PC electrolyte solutions, respectively. The longer the alkyl-chain length, the greater the

adsorption densities at low potentials and thus the lower the boundary friction. However, the longer the chain length, the greater the solubility in organic media when the potential is raised to produce oxidative dissolution of carboxylates.

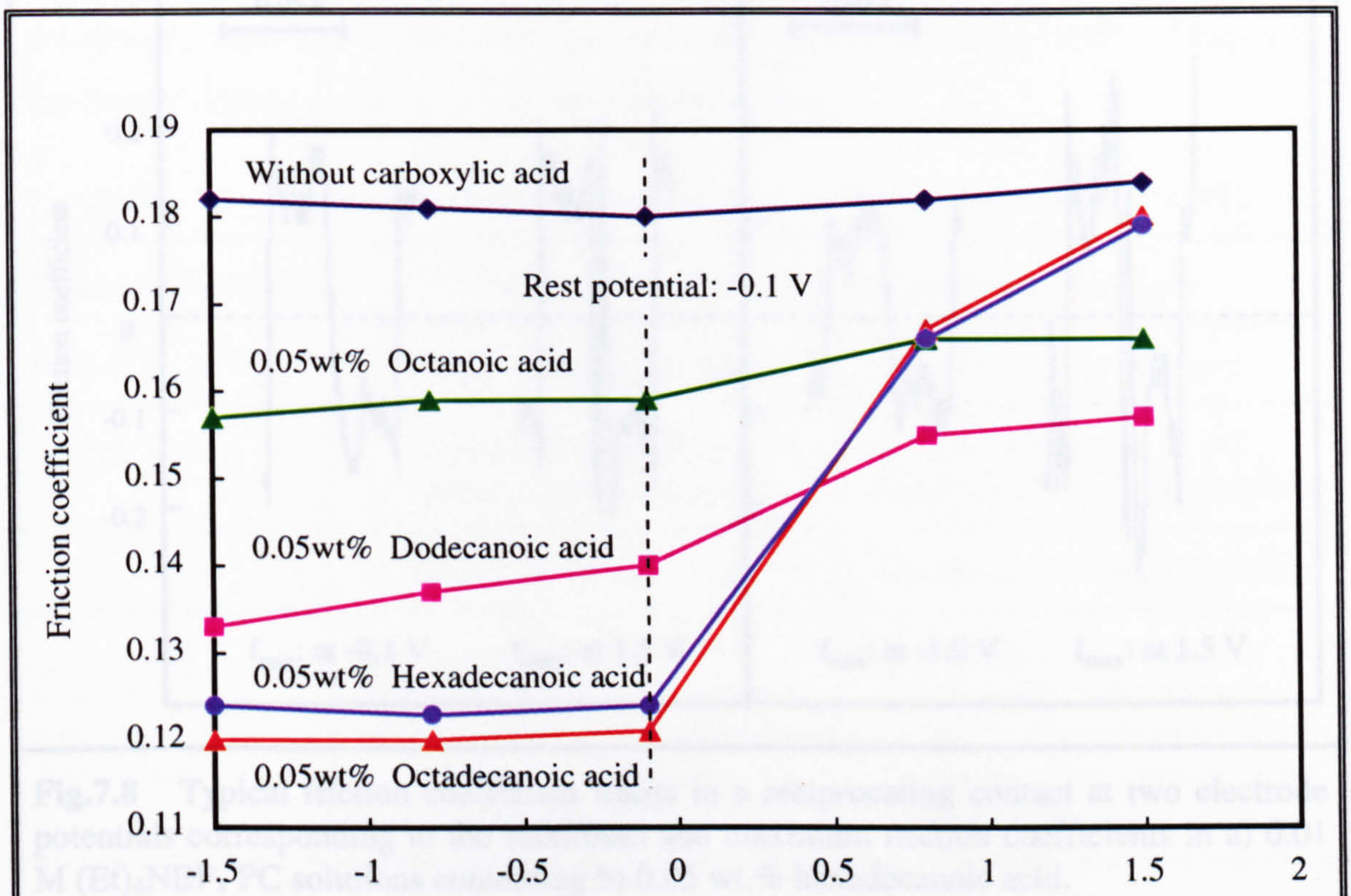


Fig.7.7 Effect of electrode potential on dynamic friction of iron-on-iron in 0.01 M $(Et)_4NBF_4$ PC solutions with and without various types of 0.05 wt.% carboxylic acid as a function of alkyl-chain length.

7.3.1.2 Friction coefficient over reciprocating cycle

Fig.7.8 compares friction traces observed at two potentials, corresponding to the minimum and maximum friction values measured in Fig.7.7, with and without hexadecanoic acid. As in Fig.7.2, all the friction traces were obtained just before finishing the individual friction testing in Fig.7.7, when the frictional behaviours had stabilised.

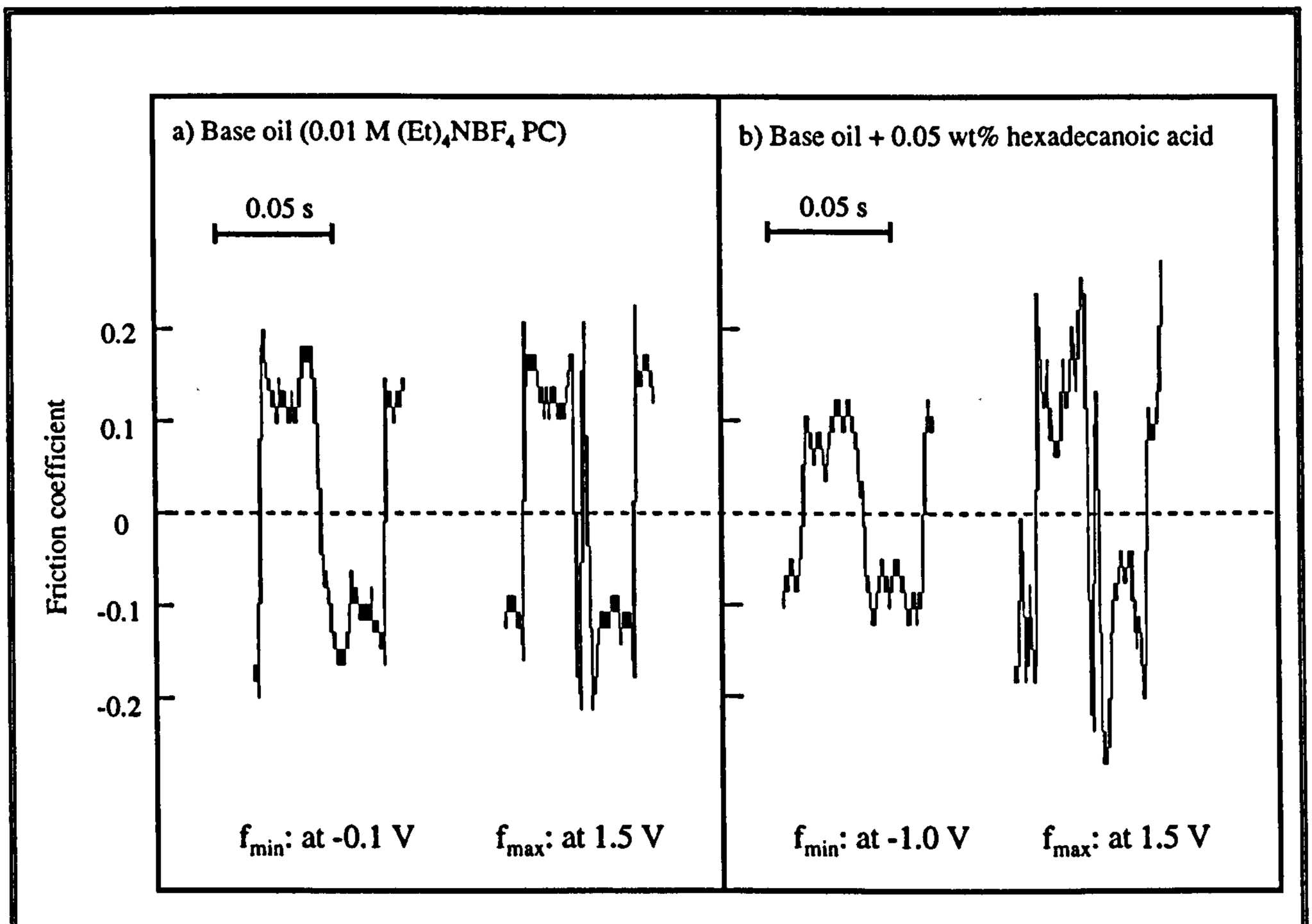


Fig.7.8 Typical friction coefficient traces in a reciprocating contact at two electrode potentials corresponding to the minimum and maximum friction coefficients in a) 0.01 M $(Et)_4NBF_4$ PC solutions containing b) 0.05 wt.% hexadecanoic acid.

The friction reversal in each friction trace can be seen at the stroke end. The sharpness of friction reversal varies when the electrode potential is changed, in spite of the use of the same electrolyte solution or additive. This sharpness can be seen most clearly with hexadecanoic acid at the electrode potential of 1.5 V, implying that the dissolution of iron hexadecanoate enhances the chances of metal-metal contact occurring under slow-speed lubrication conditions.

At the electrode potential of -0.1 V, the friction reversal without hexadecanoic acid became sharper compared to the result with the acid, indicating that the hexadecanoic acid gives "solid-like" protection against metal-metal contact and thus high friction under low speed lubrication conditions.

7.3.1.3 Analysis of the charge passed during friction testing

The charge passed with and without carboxylic acid in PC solutions during friction testing can be attributed to electrochemical adsorption and dissolution reactions, which are strongly dependent on the electrode potentials. According to the result in Chapter 6, the details of these would be expected to be as follows:

Table 7.1 Electrochemical reactions at various electrode potentials in PC.

Electrode potential vs. S.C.E. / V	Electrochemical reactions on the electrode surface	
	Without carboxylic acid	With carboxylic acid
-1.5	Decomposition of PC Reduction of iron oxide	Decomposition of PC Adsorption of carboxylic acids
-0.8	Reduction of iron oxide	Adsorption of carboxylic acids
0.8	Decomposition of PC Oxidative dissolution of iron(II)	Oxidative dissolution of iron(II) carboxylate
1.5	Oxidative dissolution of iron(II/III)	Oxidative dissolution of iron iron(II/III) carboxylate

At electrode potentials of 0.8 V and 1.5 V, the oxidation of iron into iron(II), or iron(II/III) can be determined by the electron number (Z_{app}) in Table 6.4, which can be calculated by the total number of Faradays per molar concentration of the dissolved iron.

At the electrode potential of -0.8 V, the charge densities in the presence of carboxylic acids in Table 7.2 were greater than in their absence, indicating that adsorption of carboxylic acids occurred on the iron electrode surface, in addition to the reduction of iron oxide, though the steady-state adsorption density may depend on the mechanical stress under boundary lubrication. The charge passed during friction testing at -0.8 V was used to calculate the amount of carboxylic acids produced by reaction (7-5), assuming it to be the sole reaction at that potential:

$$RCOOH + e^- \rightarrow RCOO^-_{(ads)} + \frac{1}{2}H_2 \qquad (7\text{-}5)$$

At -1.5 V, decomposition of PC predominated on the iron electrode, precluding such calculations.

Table 7.2 Charge passed depending on electrode potential over 30 minutes.

Types of oils	Potential vs. S.C.E. / V	Charge passed / mC	Adsorption density of carboxylic acid / mol m^{-2}
0.01 M $(Et)_4NBF_4$ PC without carboxylic acid	-0.8	-24	-
	0.8	111	-
	1.5	293	-
0.01 M $(Et)_4NBF_4$ PC containing 0.05 wt.% octanoic acid	-0.8	-30	1.4×10^{-3}
	0.8	60	-
	1.5	223	-
0.01 M $(Et)_4NBF_4$ PC containing 0.05 wt.% dodecanoic acid	-0.8	-39	1.8×10^{-3}
	0.8	68	-
	1.5	230	-
0.01 M $(Et)_4NBF_4$ PC containing 0.05 wt.% hexadecanoic acid	-0.8	-42	1.9×10^{-3}
	0.8	109	-
	1.5	278	-
0.01 M $(Et)_4NBF_4$ PC containing 0.05 wt.% octadecanoic acid	-0.8	-83	3.8×10^{-3}
	0.8	114	-
	1.5	288	-

At the negative potential, carboxylate anions could adsorb on the iron electrode surface, but some of them might be removed by mechanical stress under boundary lubricating conditions. Hence, the charge passed during friction testing could be translated into the total molar number of carboxylate anions produced from reaction (7-5).

At the electrode potential of -0.8 V, all the charges passed with carboxylic acid present were higher than that without carboxylic acid, indicating that the adsorption of carboxylate anions was taking place in addition to the reduction of iron oxide. The charge passed at -0.8 V also increased with increase of the alkyl-chain length of carboxylic acid, indicating that a higher density of adsorption with longer alkyl-chain length of carboxylic acids may be attributed to greater lateral interaction between the vertically oriented alkyl-chains.

At the positive electrode potentials of 0.8 V and 1.5 V, the charges passed during friction measurements were due to the oxidative dissolution of iron(II/III), as iron carboxylate in the presence of carboxylic acid, possibly reflecting increased solubility of iron carboxylates with increasing alkyl-chain length

This would explain why at positive electrode potentials, friction coefficients increased, as shown in Fig.7.7 because the solubility of iron carboxylates presumably increased with alkyl-chain length, resulting in their being inefficient friction modifying agents under oxidising conditions.

7.3.2 Effect of electrode potential on wear of ball

Fig.7.9 shows the effect of electrode potential on the ball wear scar, which was measured after friction testing by using an optical microscope. In all cases, especially with carboxylic acids, it was evident that the wear scars increased at potentials > -0.8 V, and reached plateaux values at 0.8 V.

7.3.2.1 Wear of ball without carboxylic acids

The increase in the size of wear scars at potentials > -0.1 V in the absence of carboxylic acids can be attributed to corrosive wear, whereas at -1.5 V and -0.8 V, the ball and disc specimens were likely to be subject to an adhesive wear mechanism.

At potentials > -0.1 V, the corrosive nature of wear can be inferred by comparing the observed level of wear with the measured charge passed during friction testing shown in Table 7.1. Both wear (Fig.7.9) and the amount of the charge passed show the same

dependence on electrode potential, indicating that the rate of loss of materials, *i.e.*, iron dissolution into the bulk of PC solution, is controlled by an electrochemical process.

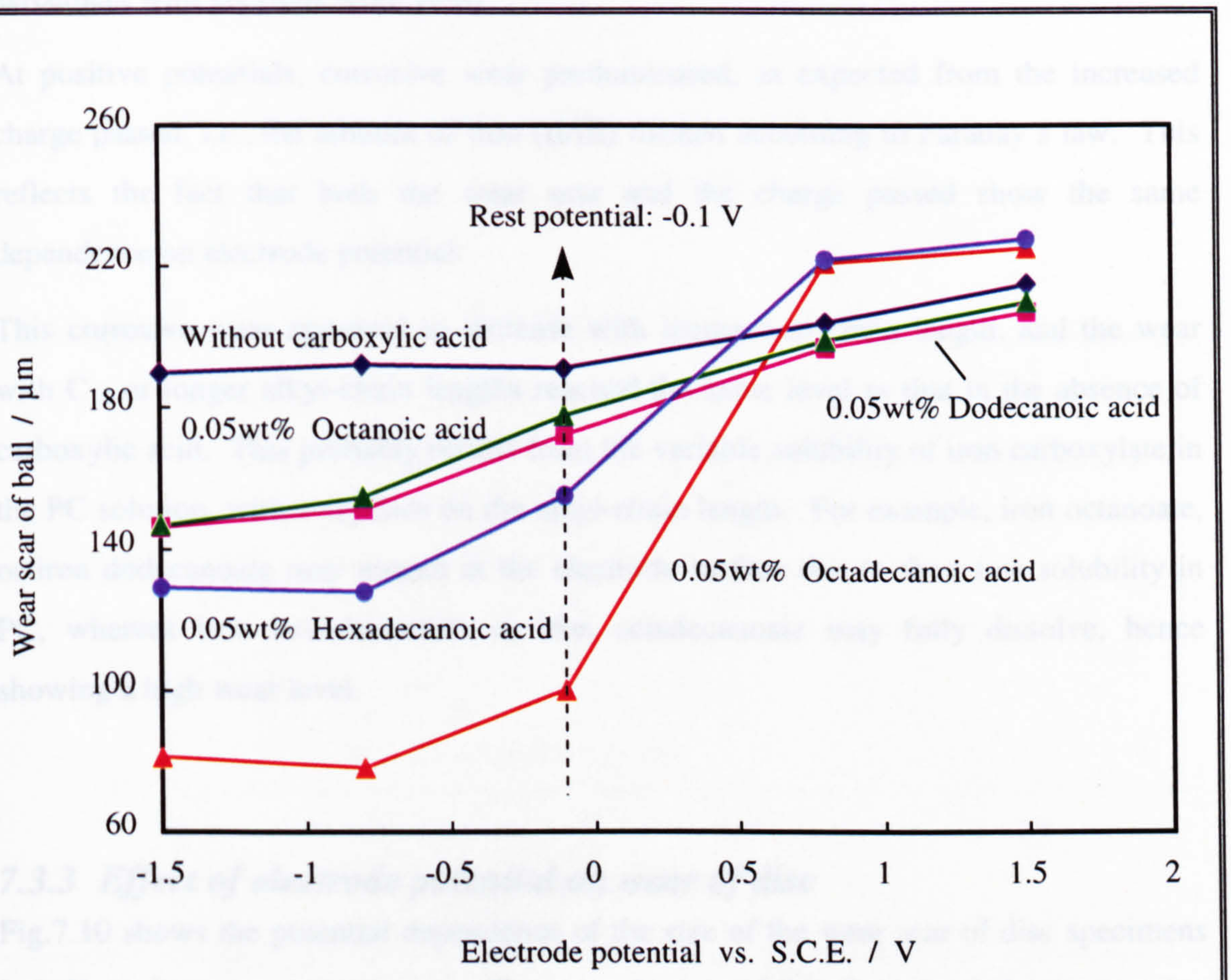


Fig.7.9 Effect of electrode potential on the wear scar of ball in 0.01 M (Et)4NBF$_4$ PC solutions with and without various types of 0.05 wt.% carboxylic acids as a function of alkyl-chain length.

7.3.2.2 Wear of ball with carboxylic acid

In the potential range of -1.5 V to -0.1 V, the size of wear scar decayed very significantly with increasing alkyl-chain length of the carboxylic acid additives. As was explained in the previous section, carboxylic acids and carboxylate anions produced from the reaction (7-5) adsorb on the iron electrode surface, to produce a decrease in the dynamic friction coefficient. As well as decreasing friction, this adsorption film also appears to protect the surface against adhesive wear, as indicated by the greater charge

passed in the Faradaic reaction to form adsorbed species during friction testing, as compared to that without carboxylic acid. This protective film was also more effective in decreasing the size of wear scar with longer chain carboxylic acids, which is in good agreement with previous work **[6-8]**.

At positive potentials, corrosive wear predominated, as expected from the increased charge passed, *i.e.*, the amount of iron (II/III) formed according to Faraday's law. This reflects the fact that both the wear scar and the charge passed show the same dependence on electrode potential.

This corrosive wear appeared to increase with increase in chain length, and the wear with C_{16} or longer alkyl-chain lengths reached the same level as that in the absence of carboxylic acid. This probably results from the variable solubility of iron carboxylate in the PC solution, which depends on the alkyl-chain length. For example, iron octanoate, or iron dodecanoate may remain at the electrode surface due to their low solubility in PC, whereas iron hexadecanoate or iron octadecanoate may fully dissolve, hence showing a high wear level.

7.3.3 Effect of electrode potential on wear of disc

Fig.7.10 shows the potential dependence of the size of the wear scar of disc specimens in ball-on-disc wear experiments. The rate of wear exhibited similar behaviour to that of the balls, though wear rates were higher than those of balls at negative electrode potentials.

7.3.3.1 Wear of disc at cathodic potential

Disc wear increased as the chain length of carboxylic acid decreased, as was also shown in Fig.7.9.

Compared to the ball wear results shown in Fig.7.9, wear scars at -1.5 V and -0.8 V were higher, especially in the presence of carboxylic acids. This is mainly because the hardness of the discs was much lower than that of the balls, so the wear of the former was greater than that of the latter under the same experimental conditions, even with the

formation of a protective film of adsorbed carboxylic acids and carboxylate anions on the electrode surface.

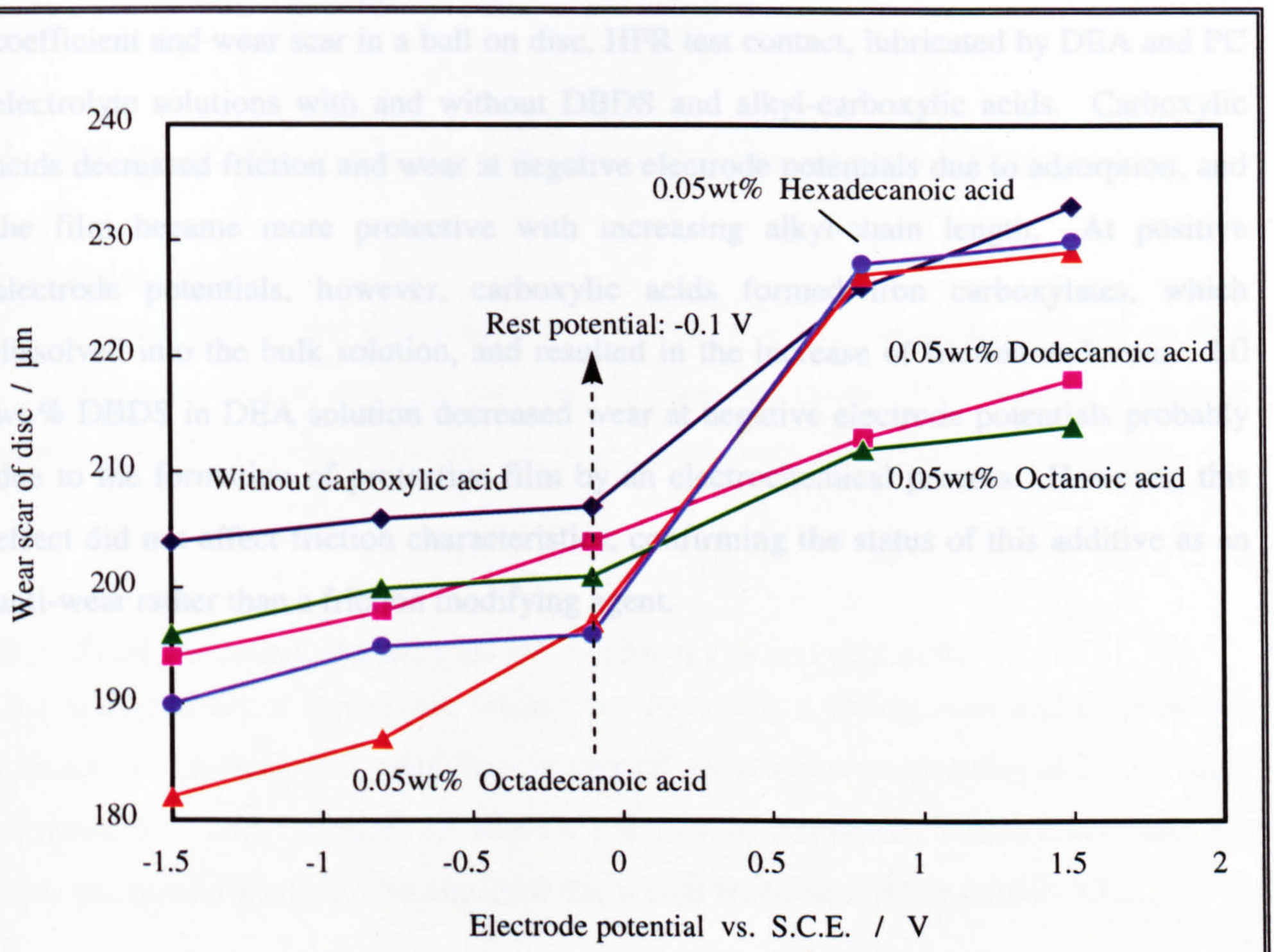


Fig.7.10 Effect of electrode potential on wear scar of disc in 0.01 M $(Et)_4NBF_4$ PC solutions with and without various types of 0.01 wt.% carboxylic acids.

7.3.3.2 Wear of disc at anodic potential

At the electrode potentials of 0.8 V and 1.5 V, the rate of wear of discs did not show a significant difference, compared to that of balls, presumably because the wear rate became controlled by the rate of corrosion rather than removal of protective film, so hardness became irrelevant.

Accordingly, both disc wear and the charge passed during friction testing show the same dependence on electrode potential, indicating that wear is controlled by an electrochemical process as well.

7.4 Conclusion

This chapter has investigated the effect of electrode potential on dynamic friction coefficient and wear scar in a ball on disc, HFR test contact, lubricated by DEA and PC electrolyte solutions with and without DBDS and alkyl-carboxylic acids. Carboxylic acids decreased friction and wear at negative electrode potentials due to adsorption, and the film became more protective with increasing alkyl-chain length. At positive electrode potentials, however, carboxylic acids formed iron carboxylates, which dissolved into the bulk solution, and resulted in the increase of friction and wear. 2.0 wt.% DBDS in DEA solution decreased wear at negative electrode potentials probably due to the formation of protective film by an electrochemical process. However, this effect did not affect friction characteristics, confirming the status of this additive as an anti-wear rather than a friction modifying agent.

CHAPTER 8

8. Effect of electrode potential on lubricant film thickness

8.1 Introduction

This chapter reports and discusses results of the effects of electrode potential on film thickness properties in a rolling steel ball on glass flat contact lubricated by propylene carbonate (PC) electrolyte solutions, with and without dissolved hexadecanoic acid.

8.2 Film forming abilities in PC without carboxylic acid

The measurement of liquid film thicknesses formed in a rolling steel ball on glass flat contact by PC electrolyte solutions was carried out at room temperature of 25 °C, using ultrathin film interferometry to provide namometre resolution, whilst controlling the steel electrode potential. The experimental set-up was described in section 3.3.3.

8.2.1 Lubricating film thickness at rest potential

8.2.1.1 Result of film thickness against rolling speed

From elastohydrodynamic (EHD) theory for a ball on flat contact, central film thickness depends on the rolling speed and lubricant properties according to Eq.(8-1) [1]:

$$h \propto U^{0.67}\eta^{0.67}\alpha^{0.53} \qquad (8\text{-}1)$$

where U is the mean entrainment speed, η is the lubricant dynamic viscosity at low pressure and α is the lubricant pressure viscosity coefficient. Thus, a fluid of constant viscosity and pressure viscosity coefficient should give a straight line relationship between log(film thickness) and log(rolling speed) with a gradient of 0.67. In previous studies, conventional fluids tested [2-4] have generally been found to give good straight lines in the high film thickness range, with gradients between 0.62 and 0.77.

Fig.8.1 shows plots of measured central film thickness *vs*. rolling speed for a PC solution containing 0.01 M $(Et)_4NBF_4$. The ball surface under lubricating conditions was employed as the electrode, with its open-circuit potential being -0.1 V vs. S.C.E.

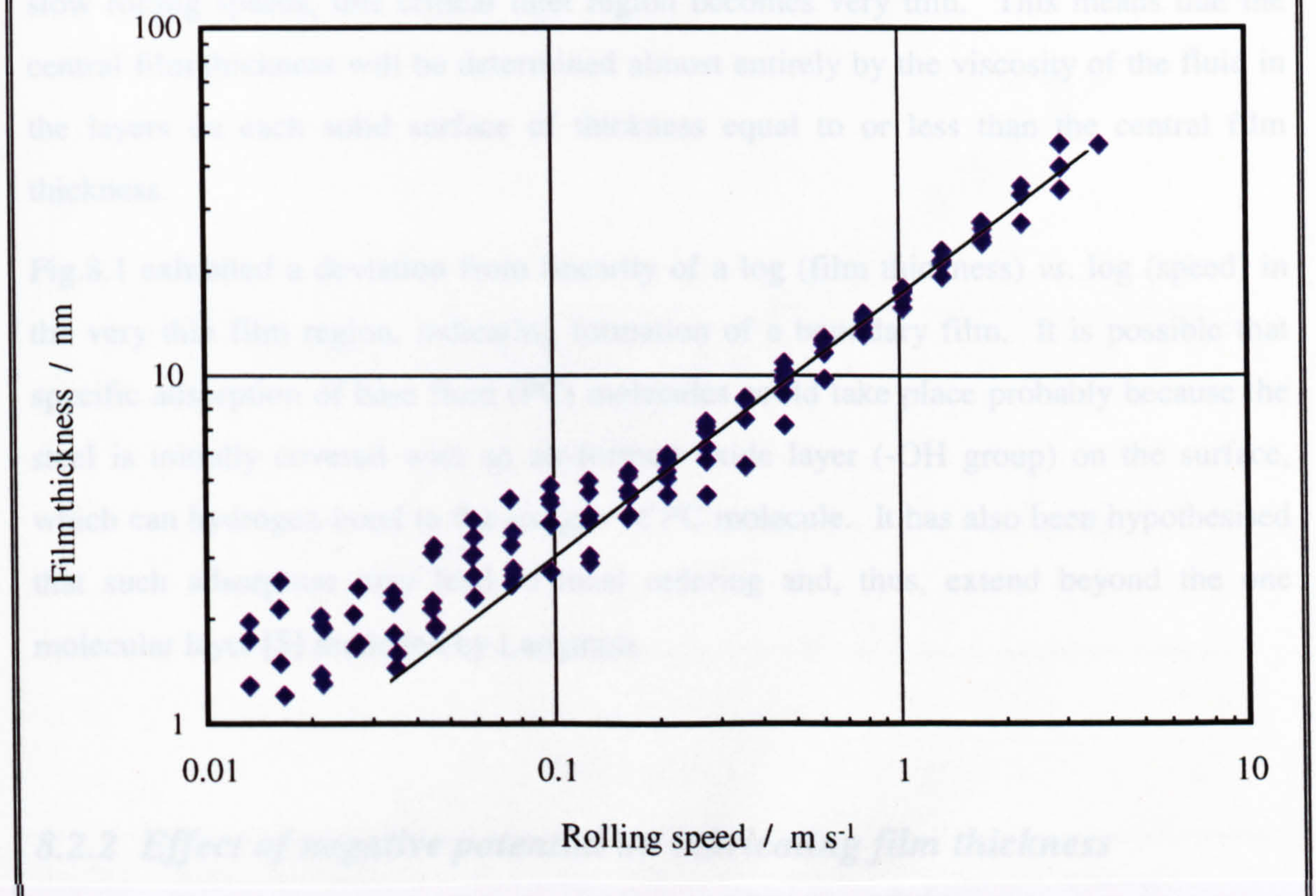


Fig.8.1 Effect of rolling speed on film thickness between a glass flat and a rolling steel ball at an electrode potential of -0.1 V vs. S.C.E. in 0.01 M $(Et)_4NBF_4$ PC solution.

The plot of log (film thickness) *vs*. log (rolling speed) has a gradient of 0.71 down to approximately 4 nm, suggesting that EHD theory **[1]** is obeyed down to this value, below which film thicknesses are greater than EHD theory. This higher film thickness indicates the presence of some type of boundary film. Previous results **[2]** showed similar plots for esters such as di-(2-ethylhexyl) sebacate and di-(ethylhexyl) phthalate, in which log(film thickness) decayed linearly with log(rolling speed) down to about 3 nm, but flattened out below this value.

8.2.1.2 Origins of non-linearity

To analyse the origins of boundary film effects, it is important to appreciate that the central film thickness in an EHD contact is determined mainly by the rheology of the fluid in the contact inlet, since this determines the quantity of fluid entrained. At very slow rolling speeds, this critical inlet region becomes very thin. This means that the central film thickness will be determined almost entirely by the viscosity of the fluid in the layers on each solid surface of thickness equal to or less than the central film thickness.

Fig.8.1 exhibited a deviation from linearity of a log (film thickness) *vs.* log (speed) in the very thin film region, indicating formation of a boundary film. It is possible that specific adsorption of base fluid (PC) molecules could take place probably because the steel is initially covered with an air-formed oxide layer (-OH group) on the surface, which can hydrogen-bond to the oxygen of PC molecule. It has also been hypothesised that such adsorption may lead to local ordering and, thus, extend beyond the one molecular layer **[5]** modelled by Langmuir.

8.2.2 Effect of negative potential on lubricating film thickness

8.2.2.1 Result of film thickness against rolling speed

Fig.8.2 compares plots of measured central film thickness *vs.* rolling speed for 0.01 M $(Et)_4NBF_4$ PC solution with the electrode potential controlled at -0.8 V vs. S.C.E., with a plot for the same fluid and the steel at rest potential. Repeated testing suggests that film thickness measurement using this technique is accurate to ± 10 % for film thickness greater than 10 nm, and ± 2 nm below 10 nm.

As was explained, classical EHD theory for Newtonian fluids predicts a straight line of gradient around 0.67. This is indeed observed at higher rolling speeds with the steel electrode potential controlled at -0.8 V vs. S.C.E. in 0.01 M $(Et)_4NBF_4$ PC solution, down to the minimum film thickness measured of 7 nm.

Below that, the film thickness departed from that obtained at open-circuit potential, and also became smaller than predicted from EHD theory.

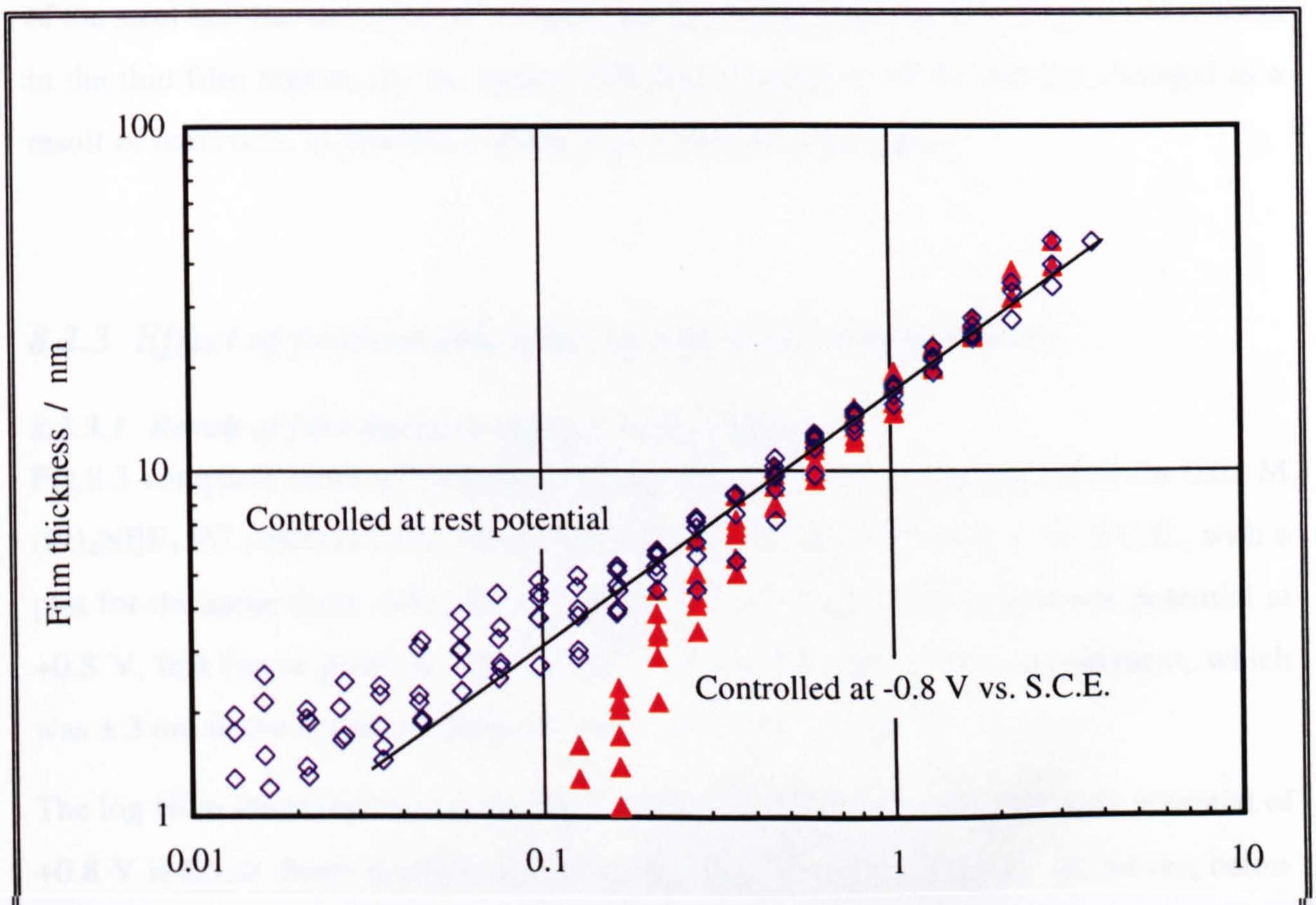


Fig.8.2 Effect of rolling speed on film thickness between a glass flat and rolling steel ball at an electrode potential of -0.8 V vs. S.C.E. in 0.01 M $(Et)_4NBF_4$ PC solution.

8.2.2.2 Deviation from EHD theory

In the case of PC electrolyte solution at -0.8 V vs. S.C.E., the film thickness became smaller than EHD theory at slow speeds. It is not fully understood yet, but one possible explanation is that the application of -0.8 V results in the concentration close to the surface of highly polar, very low viscosity impurities, formed either by reduction of PC or present as impurities all the time. Due to their high polarities, such impurities may have higher concentration close to the surface of ball and disc and thus form low viscosity surface layers. Hence these layers can give reduced film thickness in the thin

film region. A similar effect has been seen using PAO containing low viscosity ester, by the ultrathin film interferometry **[6,7]**.

It should be emphasised that there are at least two alternative explanations: (a) reduction of the steel ball has the effect of roughening the surface and thus reducing film thickness in the thin film region, (b) the optical reflection properties of the ball are changed as a result of reduction, to produce a phase shift in the reflected light.

8.2.3 Effect of positive potential on lubricant film thickness

8.2.3.1 Result of film thickness against rolling speed

Fig.8.3 compares plots of measured central film thickness *vs*. rolling speed for 0.01 M $(Et)_4NBF_4$ PC solution under electrode potential controlled at +0.8 V vs. S.C.E., with a plot for the same fluid under the rest potential. In the case of the electrode potential at +0.8 V, this figure gives an indication of the repeatability of the measurement, which was ± 3 nm in the measured range of film thickness.

The log (film thickness) *vs*. log (rolling speed) plot obtained at the electrode potential of +0.8 V is linear down to about 20 nm at the rolling speed of 1 m s^{-1}. However, below the film thickness of 20 nm, PC electrolyte solution at +0.8 V gives a thicker boundary film in the contact than the same PC solution with no externally applied potential.

8.2.3.2 Origin of boundary film

According to the explanation of Fig.6.14, decomposition of PC may occur at electrode potentials > 0.7 V. This oxidation process was assumed to involve the formation of CO_2 and other organic products of as yet unknown composition **[8]**. Such organic products are likely to adsorb or react with the iron electrode surface to form a layer of reduced mobility, either solid-like or higher viscosity. This will result in the thicker film thickness.

In addition to the adsorption, oxidative dissolution of iron(II/III) also occurs at 0.8 V, as previously discussed in Chapter 6. This process might also contribute to a thicker film

by forming semi-soluble iron salts such as iron carboxylate or hydroxide close to the surface of ball and disc.

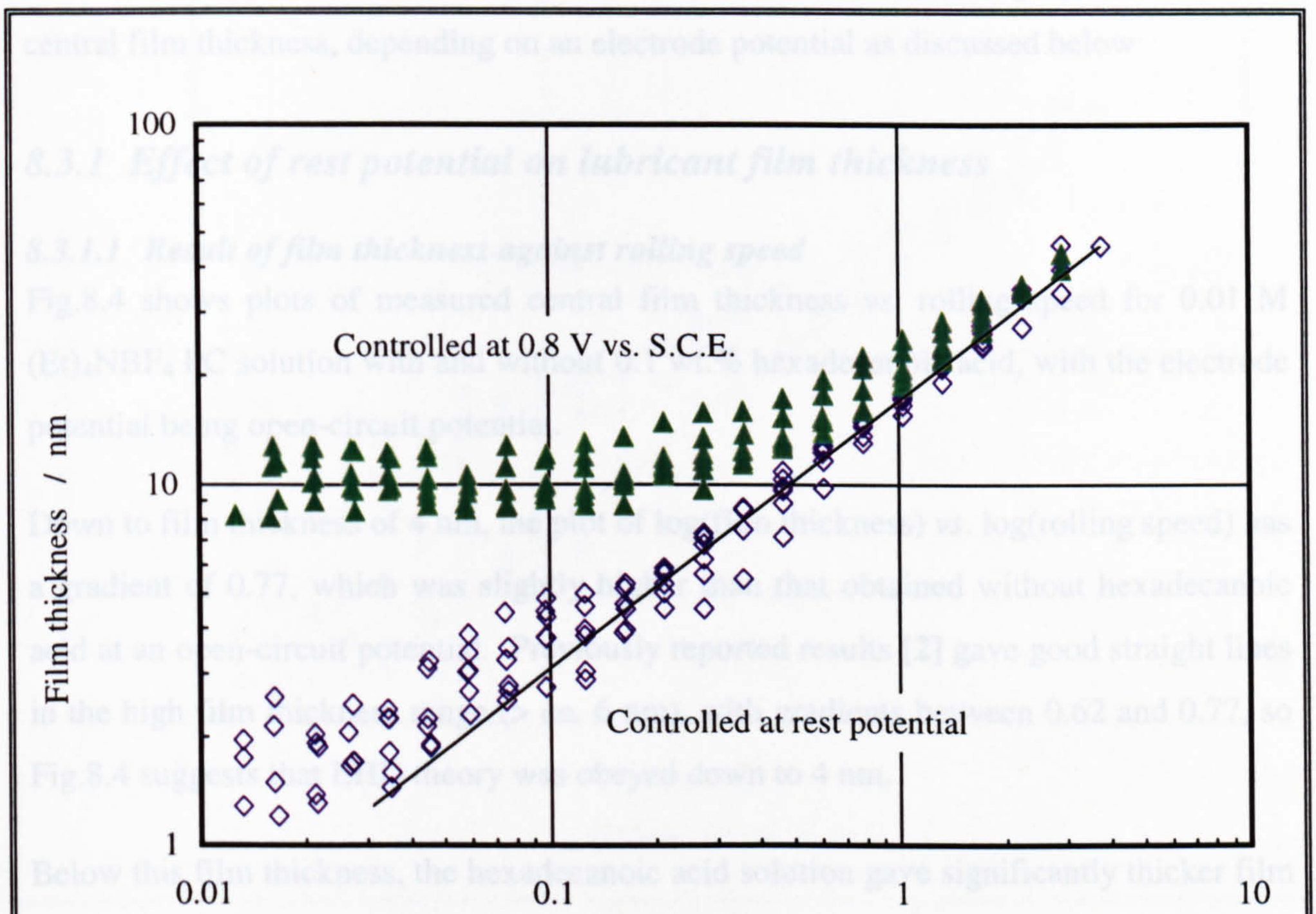


Fig.8.3 Effect of rolling speed on film thickness between a glass flat and a rolling steel ball at an electrode potential of +0.8 V vs. S.C.E. in 0.01 M $(Et)_4NBF_4$ PC solution.

8.3 Film forming abilities in PC with carboxylic acid

The friction modifier, hexadecanoic acid was found to have a significant effect on central film thickness, depending on an electrode potential as discussed below

8.3.1 Effect of rest potential on lubricant film thickness

8.3.1.1 Result of film thickness against rolling speed

Fig.8.4 shows plots of measured central film thickness *vs.* rolling speed for 0.01 M $(Et)_4NBF_4$ PC solution with and without 0.1 wt.% hexadecanoic acid, with the electrode potential being open-circuit potential.

Down to film thickness of 4 nm, the plot of log(film thickness) *vs.* log(rolling speed) has a gradient of 0.77, which was slightly higher than that obtained without hexadecanoic acid at an open-circuit potential. Previously reported results **[2]** gave good straight lines in the high film thickness range (> *ca.* 6 nm), with gradients between 0.62 and 0.77, so Fig.8.4 suggests that EHD theory was obeyed down to 4 nm.

Below this film thickness, the hexadecanoic acid solution gave significantly thicker film than the solution without dissolved acid.

8.3.1.2 Boundary film formed with hexadecanoic acid

The work carried out clearly shows that when hexadecanoic acid is added to 0.1 M $(Et)_4NBF_4$ PC electrolyte solution, it contributes to the formation of thick films in a rolling contact, even with a low concentration of 0.1 wt.%. The mechanism of action of hexadecanoic acid to form thicker film can be attributed to the competition of adsorption between hexadecanoic acid and PC molecules on the ball surface **[9]**. Carboxylic acid groups (-*COOH*) generally have a higher dipole moment than those of esters as present in PC, and thus have a stronger interaction with metal surfaces. Hence, the ball surface will selectively acquire a thicker layer of hexadecanoic acid, particularly under oxidising conditions when iron carboxylate phase will form.

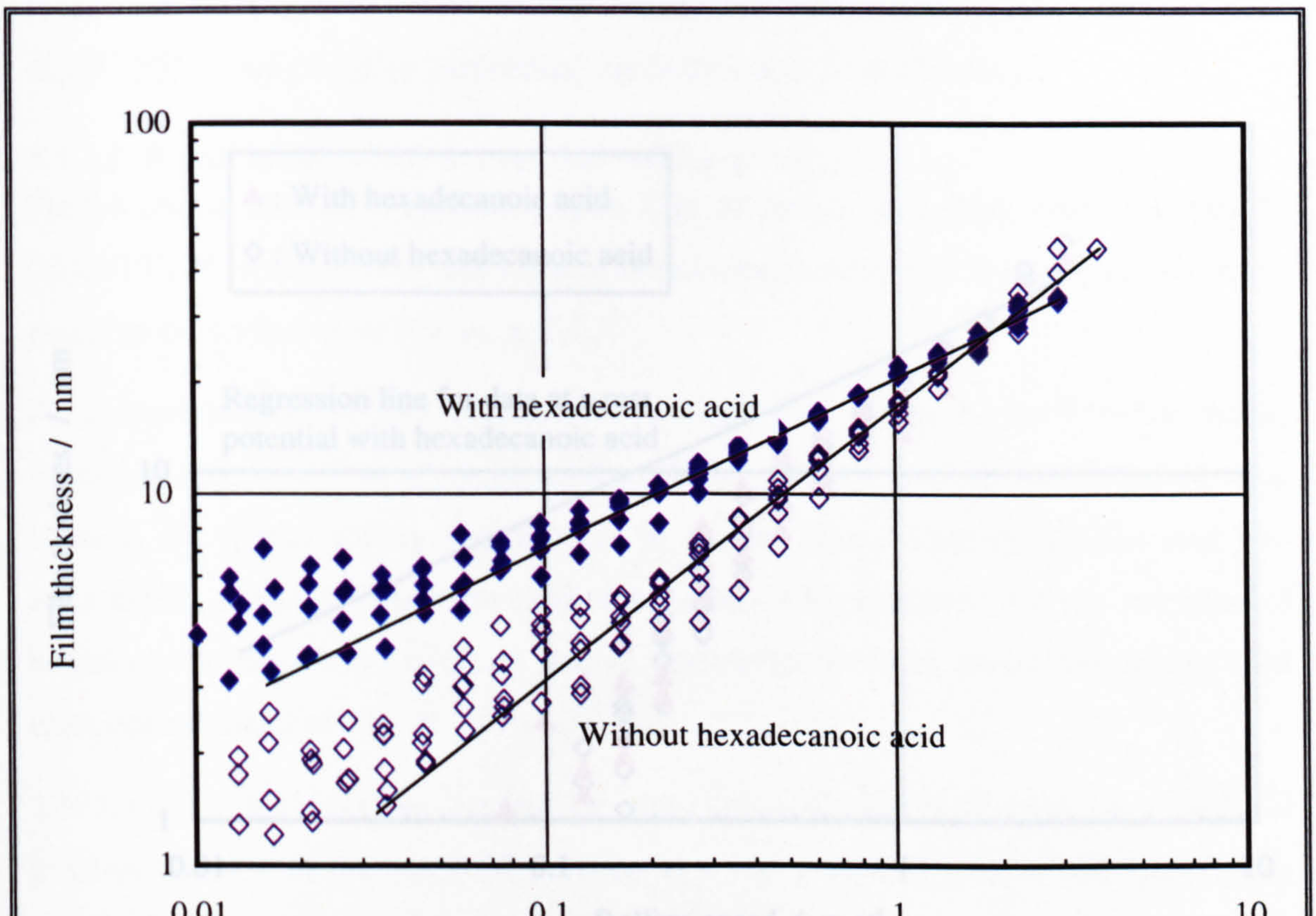


Fig.8.4 Effect of rolling speed on film thickness between a glass flat and a rolling steel ball at an open-circuit potential of -0.1 V vs. S.C.E., in 0.01 M $(Et)_4NBF_4$ PC solution with and without 0.1 wt.% hexadecanoic acid.

8.3.2 Effect of negative potential on lubricant film thickness

8.3.2.1 Result of film thickness against rolling speed

Fig.8.5 shows plots of measured central film thickness *vs.* rolling speed for 0.01 M $(Et)_4NBF_4$ PC solution containing 0.1 wt.% hexadecanoic acid with the steel electrode potential controlled at -0.8 V vs. S.C.E., together with a plot for 0.01 M $(Et)_4NBF_4$ PC without hexadecanoic acid at an open-circuit potential. The plot of log(film thickness) *vs.* log(rolling speed) with hexadecanoic acid shows almost the same behaviour, compared to the results without hexadecanoic acid.

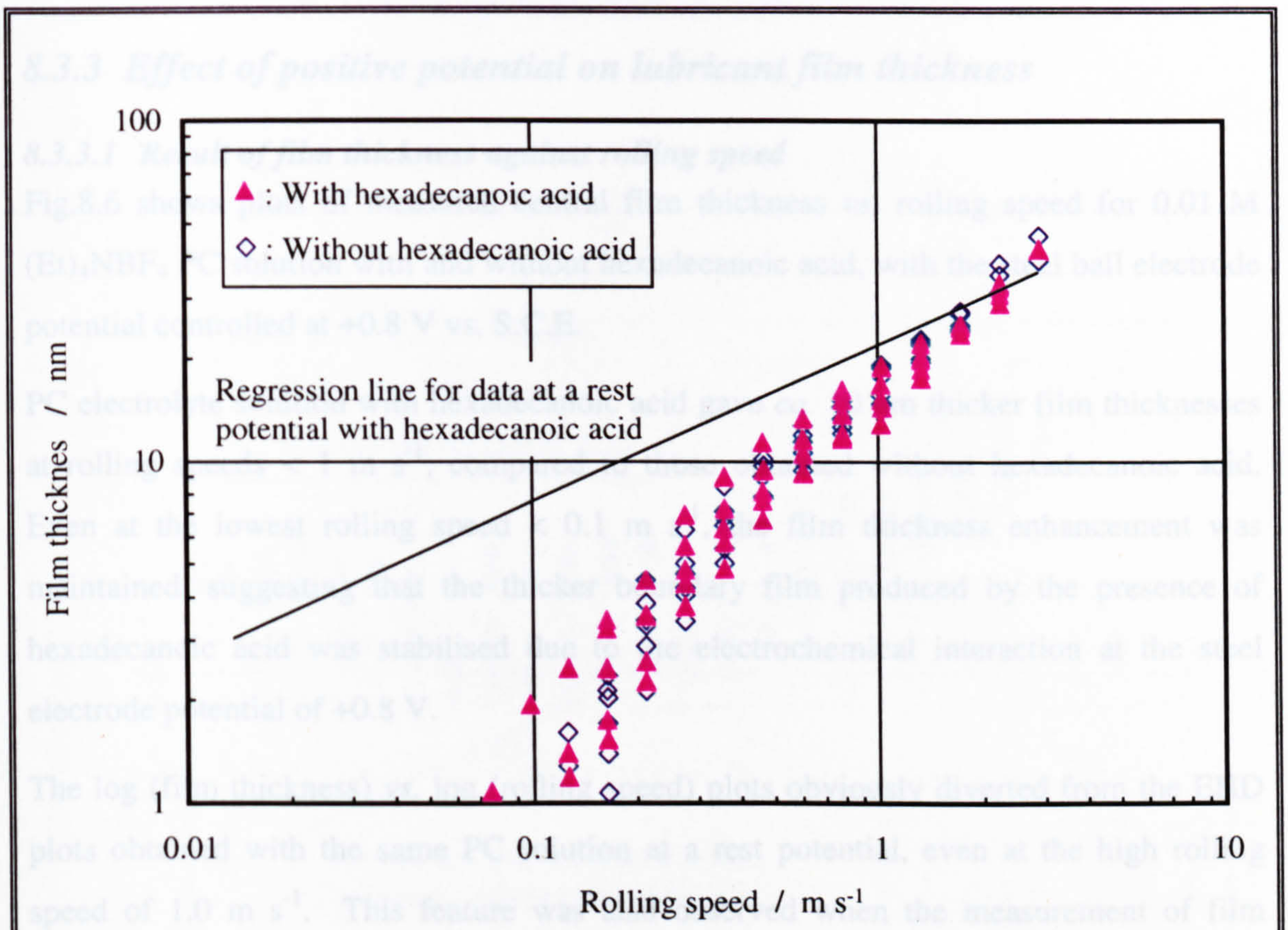


Fig.8.5 Effect of rolling speed on film thickness between a glass flat and a rolling steel ball at an electrode potential of -0.8 V vs. S.C.E. in 0.01 M $(Et)_4NBF_4$ PC solution with and without 0.1 wt.% hexadecanoic acid, together with a regression line for data at the rest potential of -0.1 V vs. S.C.E. in the presence of hexadecanoic acid.

8.3.2.2 Deviation from EHD theory

At an electrode potential of -0.8 V vs. S.C.E., film thicknesses with and without hexadecanoic acid became smaller than EHD theory at slow rolling speeds, for reasons not yet fully understood. However, as is explained in Fig.8.2., it was hypothesised that highly polar and very low viscosity impurities either produced from PC at -0.8 V or impurities present all the time, result in the higher concentration close to the metal surface. Such impurities can form low viscosity layers which give reduce film thickness in the thin film region. Further investigation is needed to understand the mechanism.

8.3.3 Effect of positive potential on lubricant film thickness

8.3.3.1 Result of film thickness against rolling speed

Fig.8.6 shows plots of measured central film thickness *vs.* rolling speed for 0.01 M $(Et)_4NBF_4$ PC solution with and without hexadecanoic acid, with the steel ball electrode potential controlled at +0.8 V vs. S.C.E.

PC electrolyte solution with hexadecanoic acid gave *ca.* 10 nm thicker film thicknesses at rolling speeds < 1 m s^{-1}, compared to those obtained without hexadecanoic acid. Even at the lowest rolling speed < 0.1 m s^{-1}, the film thickness enhancement was maintained, suggesting that the thicker boundary film produced by the presence of hexadecanoic acid was stabilised due to the electrochemical interaction at the steel electrode potential of +0.8 V.

The log (film thickness) *vs.* log (rolling speed) plots obviously diverted from the EHD plots obtained with the same PC solution at a rest potential, even at the high rolling speed of 1.0 m s^{-1}. This feature was also observed when the measurement of film thickness was conducted without hexadecanoic acid at the same steel electrode potential of +0.8 V.

8.3.3.2 Origin of boundary film

As mentioned in the explanation of Fig.8.3 given above, the oxidative decomposition of PC at electrode potentials > 0.7 V, shown in Fig.6.14, was assumed to involve the formation of CO_2 and other unknown organic products, which could adsorb or react with the iron electrode surface and thus lead to a surface film of enhanced viscosity. This might represent an inorganic or organic salt.

With hexadecanoic acid, it is likely that iron(II/III) carboxylate forms at such potentials, as evidenced by the current-time data obtained in the presence of hexadecanoic acid shown in Fig.6.17 and by the data of Z_{app} in Table 6.4. This supports the concept that the corrosion process of iron into iron(II/III) promoted by applied positive potential is accelerated by the presence of hexadecanoic acid and leads to the formation of iron

hexadecanoate. Hence, at the electrode potential of +0.8 V, the ball surface is likely to form a layer of iron hexadecanoate with reduced mobility, enhancing the local viscosity and resulting in a thicker film.

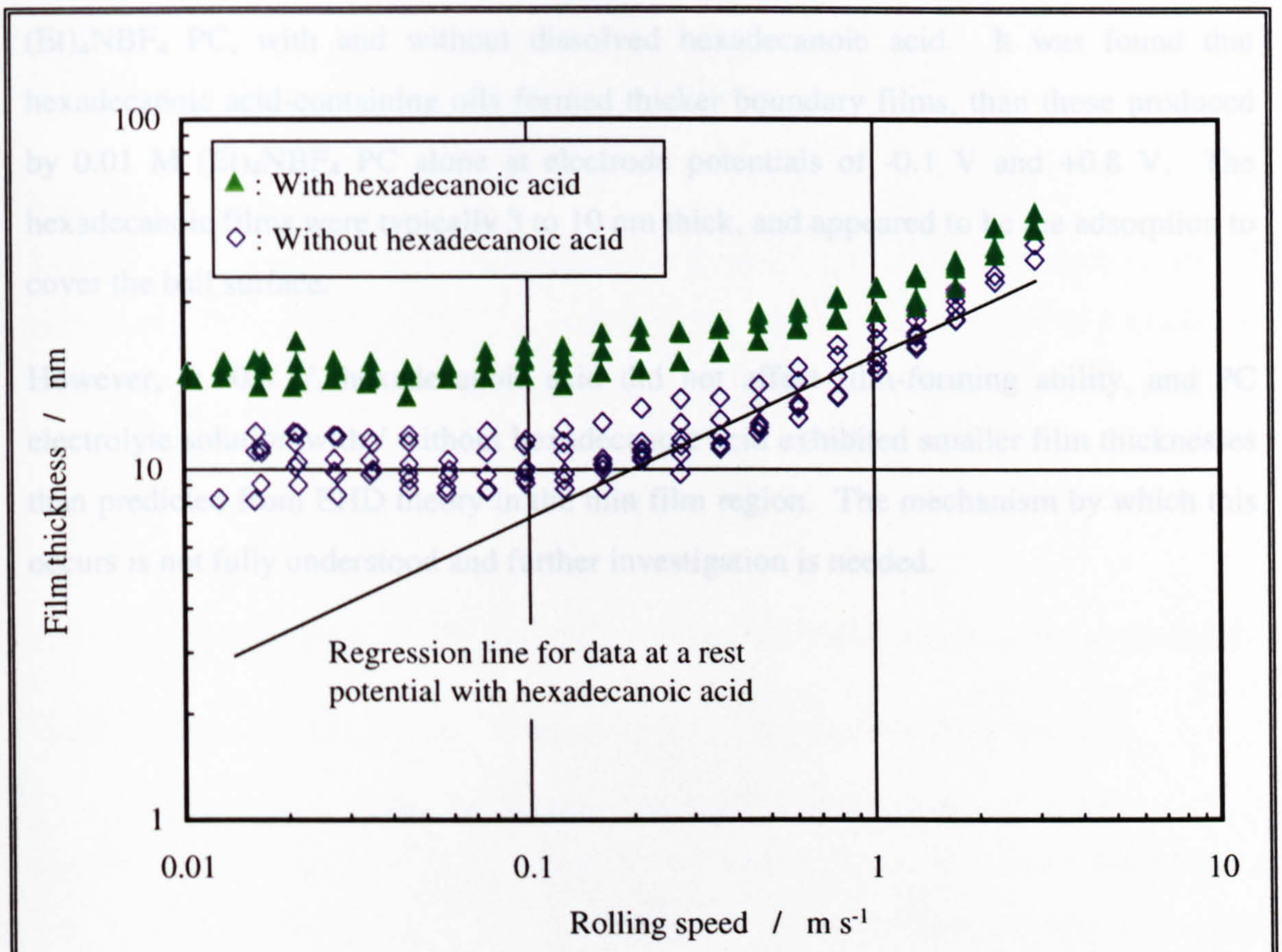


Fig.8.6 Effect of rolling speed on film thickness between a glass flat and a rolling steel ball at an electrode potential of +0.8 V vs. S.C.E. in 0.01 M $(Et)_4NBF_4$ PC solution with and without 0.1 wt.% hexadecanoic acid, together with a regression line for data at the open-circuit potential in the presence of hexadecanoic acid.

8.4 Conclusion

Ultra-thin film interferometry has been used to directly monitor film thicknesses between a glass flat and rolling steel ball under controlled electrode potential in 0.01 M $(Et)_4NBF_4$ PC, with and without dissolved hexadecanoic acid. It was found that hexadecanoic acid-containing oils formed thicker boundary films, than those produced by 0.01 M $(Et)_4NBF_4$ PC alone at electrode potentials of -0.1 V and +0.8 V. The hexadecanoic films were typically 3 to 10 nm thick, and appeared to be the adsorption to cover the ball surface.

However, at -0.8 V, hexadecanoic acid did not affect film-forming ability, and PC electrolyte solution with / without hexadecanoic acid exhibited smaller film thicknesses than predicted from EHD theory in the thin film region. The mechanism by which this occurs is not fully understood and further investigation is needed.

CHAPTER 9

9. Triboelectrochemistry in nano-metre scale

9.1 Introduction

This chapter reports and discusses the results of triboelectrochemical measurements of an iron electrode with an atomic force microscope (AFM), under controlled potential, to observe the consequences of oxide layers, or boundary films produced in PC solutions with and without carboxylic acids.

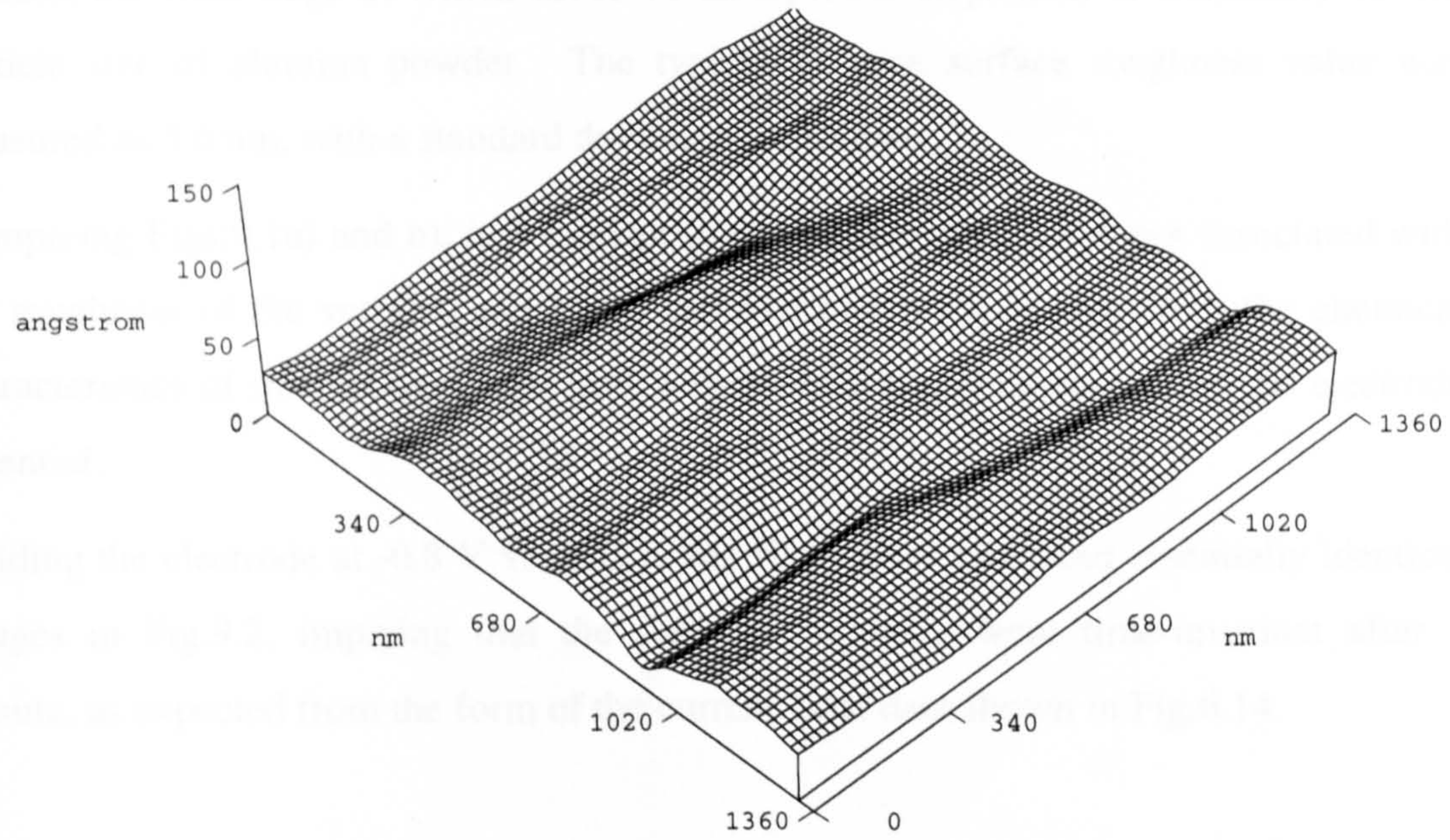
9.2 Nano-tribological behaviour in PC solution without carboxylic acid

9.2.1 Effect of electrode potential on friction and surface images

9.2.1.1 Measurements with constant electrode potential controlled at -0.8 V

Figs.9.1a) and b) show AFM topographical and friction images of an iron surface from a 1.4 × 1.4 μm region in 0.01 M $(Et)_4NBF_4$ PC solution, obtained with a constant electrode potential controlled at -0.8 V vs. S.C.E. for 1 minute. Under these reducing conditions, the electrode surface is predicted to be bare iron. The typical value of the friction coefficient was 0.06, but reached 0.07 in some of the grooves: the standard deviation was 0.007.

a) Topography



b) Friction force image

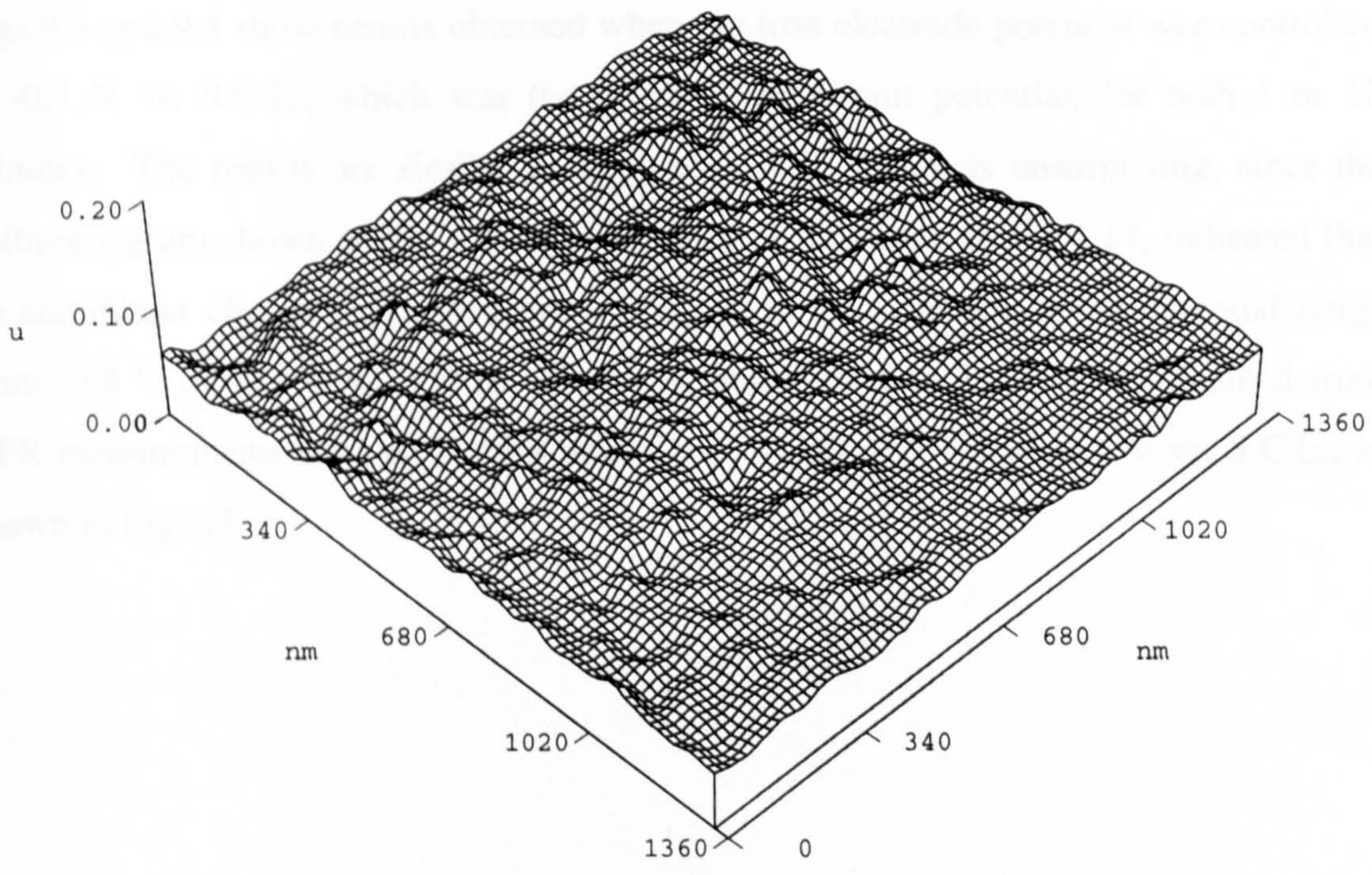


Fig.9.1 Images from iron surface measured with the constant electrode potential controlled at -0.8 V vs. S.C.E. for 1 minute in 0.01 M $(Et)_4NBF_4$ PC solution: a) AFM topography image; b) AFM friction force image.

As for the topography, the electrode surface was generally smooth within a few nano-metres, but it had a number of shallow grooves, probably produced during the polishing process, the final stage of which involved an aqueous dispersion of nominally 15 nm particle size of alumina powder. The typical average surface roughness value was measured as 3.6 nm, with a standard deviation of 0.9 nm.

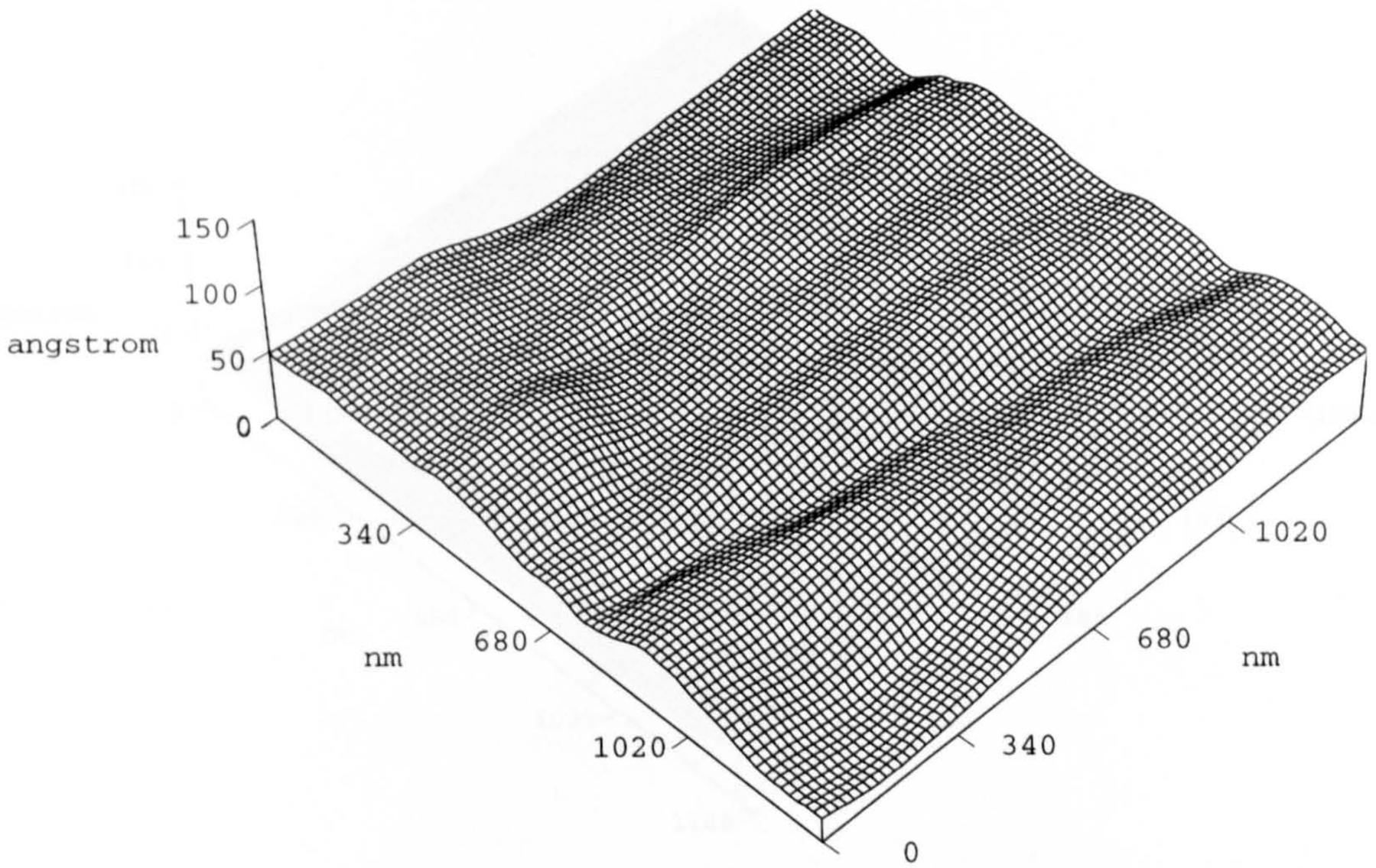
Comparing Figs.9.1a) and b), it is evident that the friction image is not associated with the roughness of the surface, and hence the friction results mainly from the chemical characteristics of iron surface, bare iron, which are strongly dependent on the electrode potential.

Holding the electrode at -0.8 V vs. S.C.E. for 10 minutes produced essentially identical images in Fig.9.2, implying that the surface properties were time-invariant after 1 minute, as expected from the form of the current-time data shown in Fig.6.14.

9.2.1.2 Measurements with constant electrode potential controlled at -0.1 V

Figs.9.3 and 9.4 show results obtained when the iron electrode potential was controlled at -0.1 V vs. S.C.E., which was the typical open-circuit potential, for both 1 or 10 minutes. The results are similar to those at -0.8 V, which is unsurprising, since the voltammogram shown in Fig.6.12 and the current-time data in Fig.6.14, indicated that no significant change in surface properties would be expected in the potential range from -0.8 V to -0.1 V vs. S.C.E. Similarly, macro-friction coefficients obtained from HFR measurements showed similar behaviour at both -0.8 V and -0.1 V vs. S.C.E., as shown in Fig.7.7.

a) Topographical image



b) Friction force image

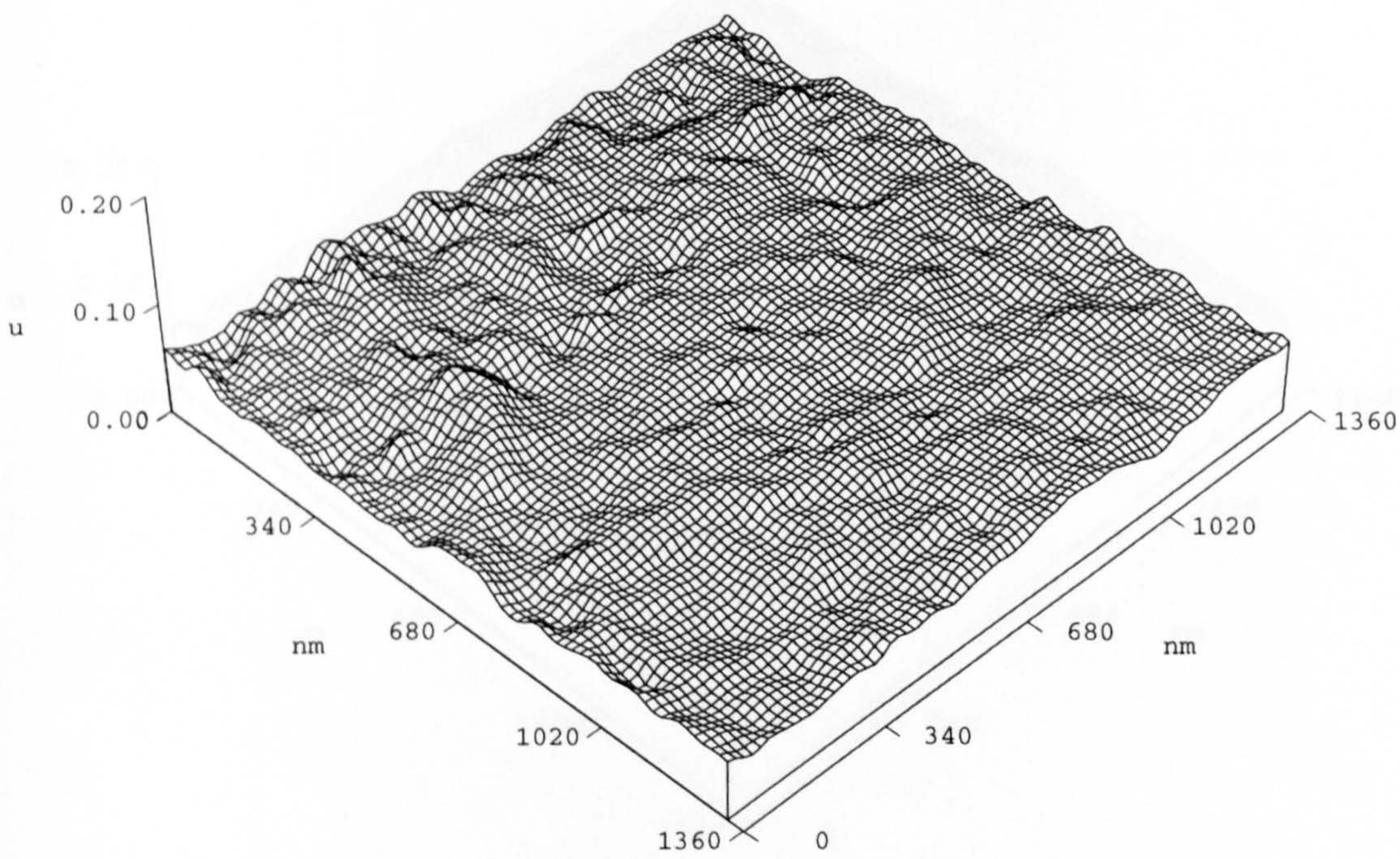
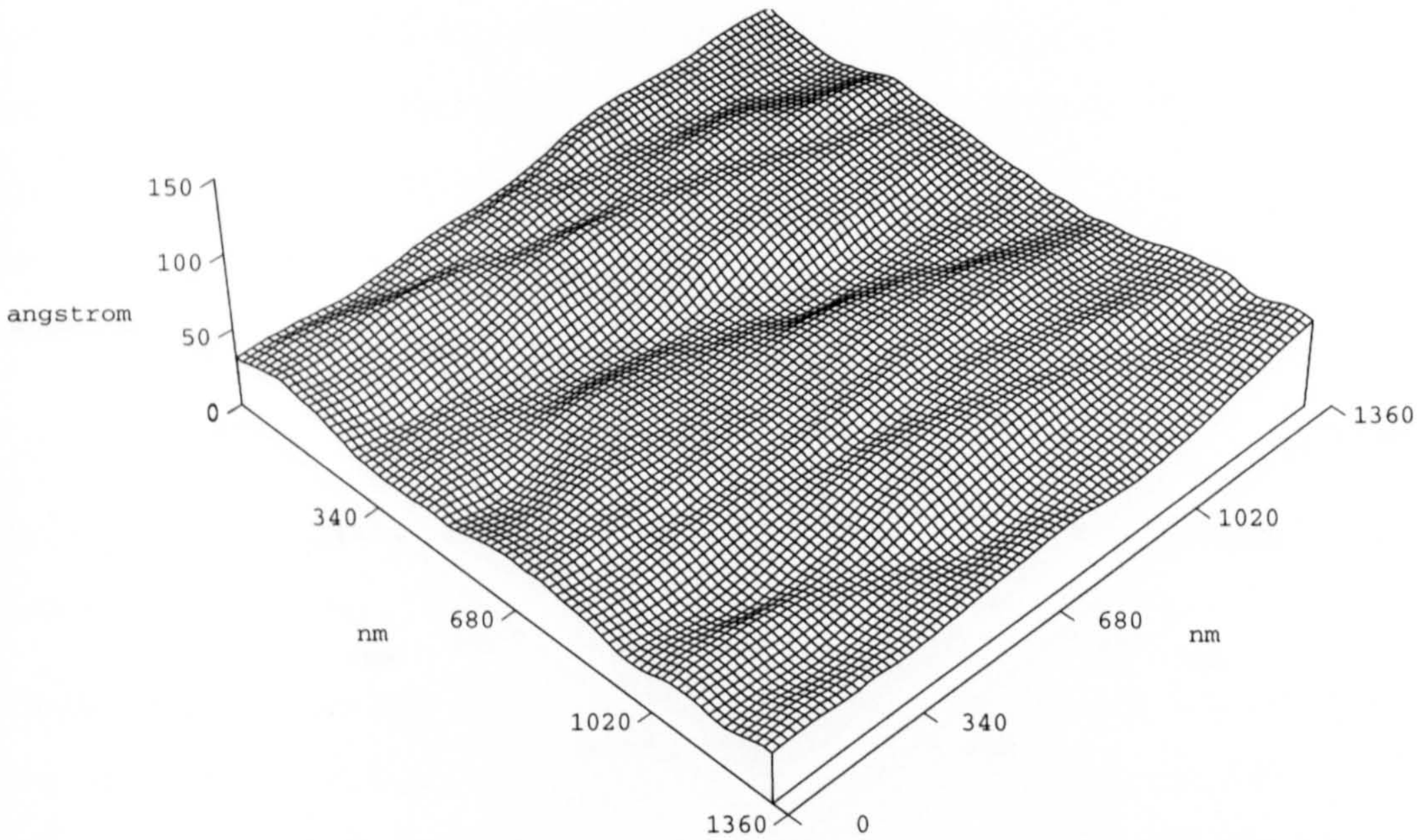


Fig.9.2 Images from iron surface measured with the constant electrode potential controlled at -0.8 V vs. S.C.E. for 10 minutes in 0.01 M $(Et)_4NBF_4$ PC solution: a) AFM topography image; b) AFM friction force image.

a) Topographical image



b) Friction force image

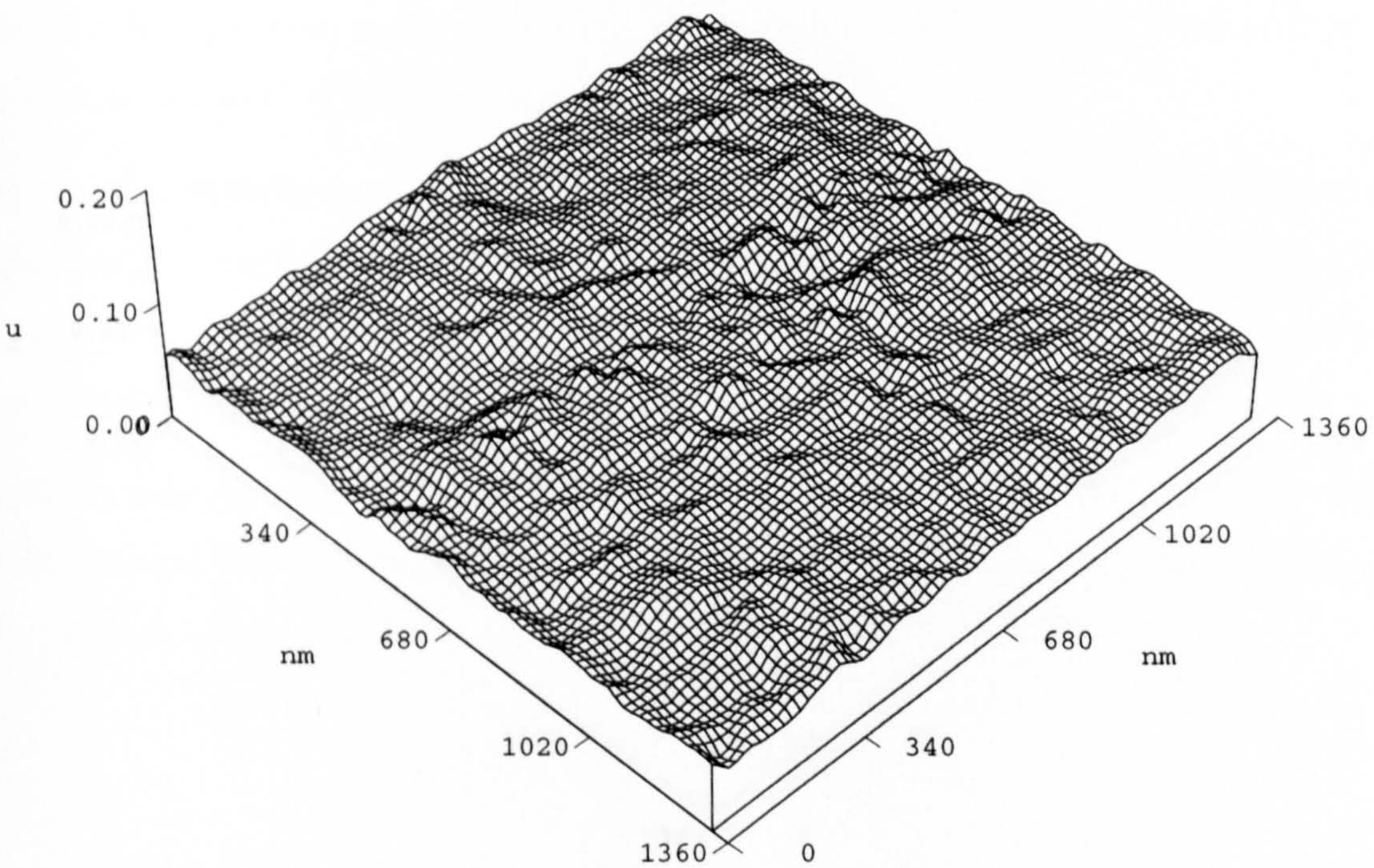
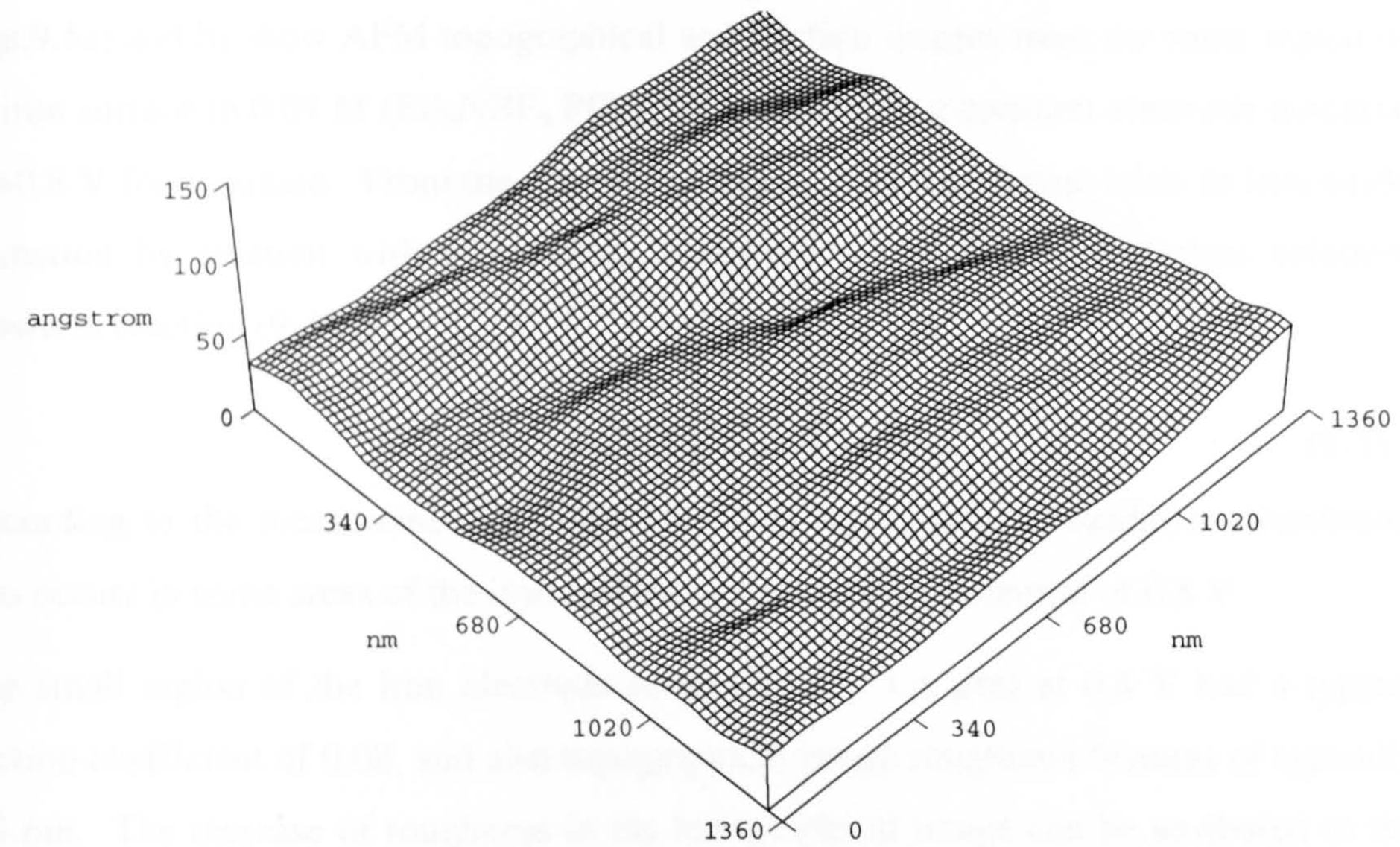


Fig.9.3 Images from iron surface measured with the constant electrode potential controlled at -0.1 V vs. S.C.E. for 1 minute in 0.01 M $(Et)_4NBF_4$ PC solution: a) AFM topography image; b) AFM friction force image.

a) Topography



b) Friction image

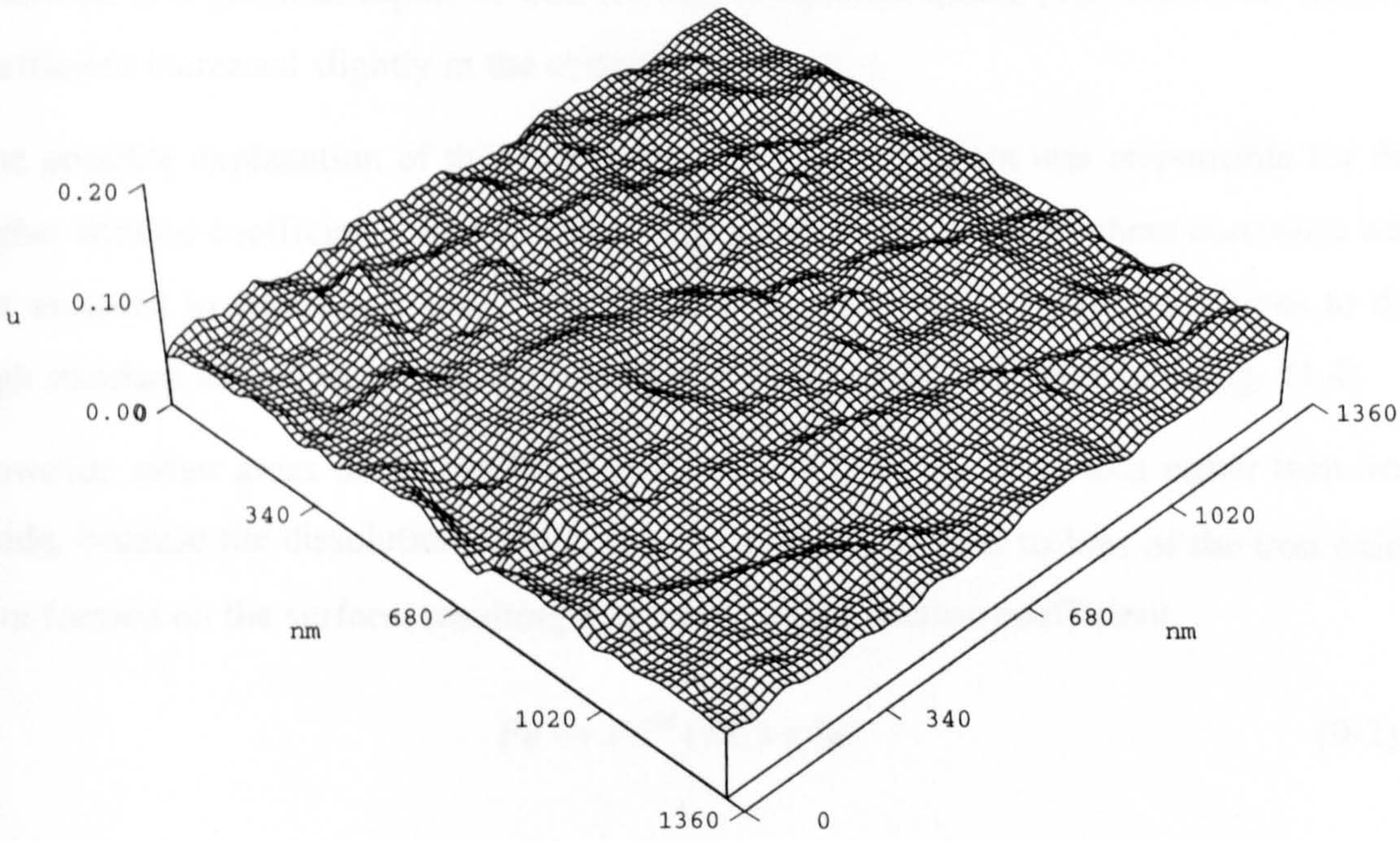


Fig.9.4 Images from iron surface measured after tip and surface have been subjected to constant electrode potential at -0.1 V vs. S.C.E. for 10 minutes in 0.01 M $(Et)_4NBF_4$ PC solution: a) AFM topography image; b) AFM friction force image.

9.2.1.3 Measurements with constant electrode potential controlled at 0.8 V for 1 min.

Figs.9.5a) and b) show AFM topographical and friction images from the same region of an iron surface in 0.01 M $(Et)_4NBF_4$ PC, after maintaining a constant electrode potential at +0.8 V for 1 minute. From the results in Chapter 6, this potential leads to iron oxide formation by reaction with adventitious dissolved water in the electrolyte solution, shown in reaction (9-1):

$$Fe + xH_2O \leftrightarrow FeO_x + 2xH^+ + 2xe^- \qquad (9\text{-}1)$$

According to the measurements of dissolved iron concentration, oxidative dissolution also occurs in some areas of the iron surface at an electrode potential of 0.8 V.

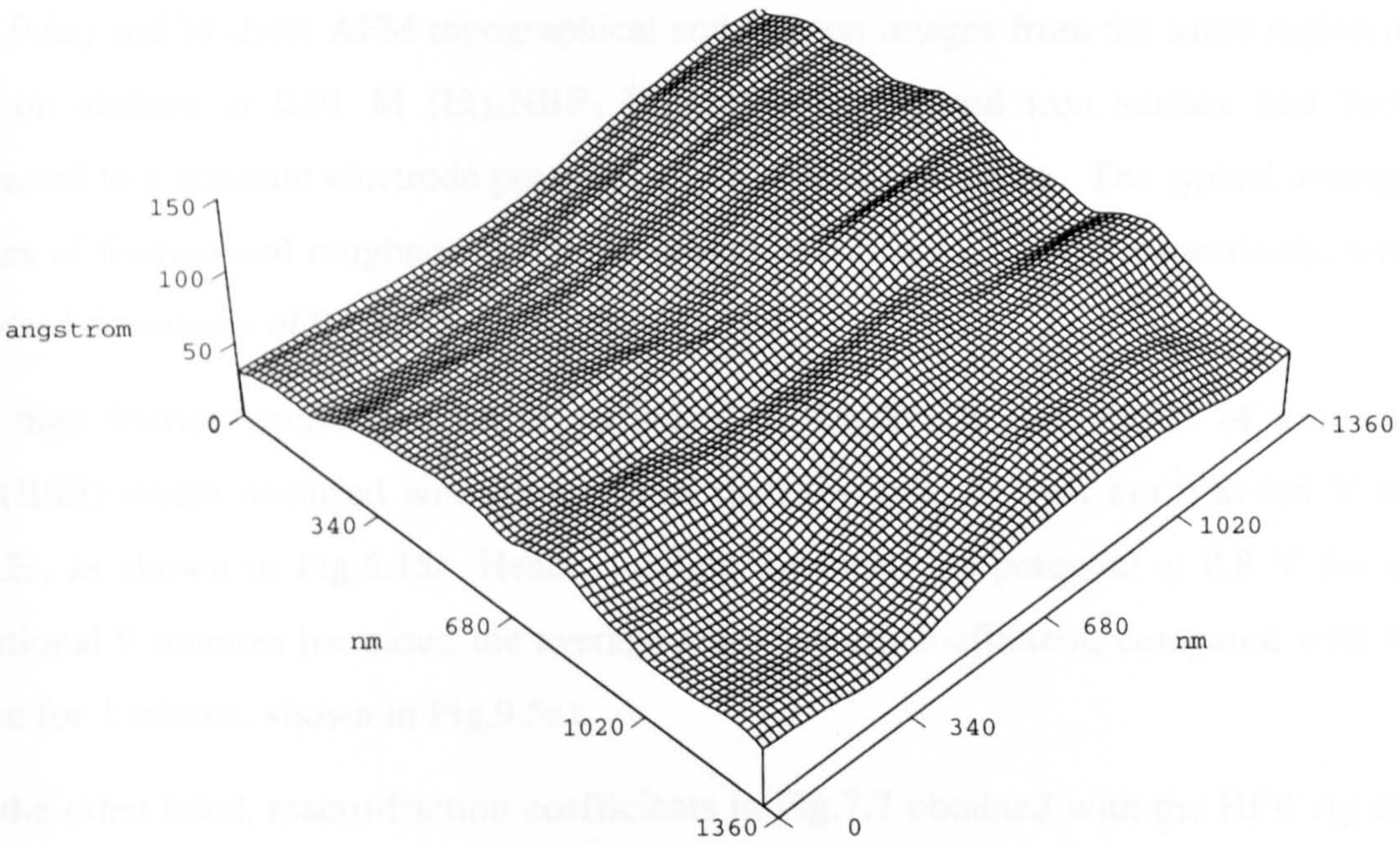
The small region of the iron electrode surface (1.4 × 1.4 μm) at 0.8 V had a typical friction coefficient of 0.08, and also topographical image roughness features of typically 5.5 nm. The increase of roughness in the topographical image can be attributed to the formation of iron oxide, which should significantly decrease friction coefficient described in a previous report of iron friction in aqueous media **[1]**. However, friction coefficient increased slightly in the currently study.

One possible explanation of this is that the dissolution process was responsible for the higher friction coefficient. Some of the small areas on the surface, where corrosion was not assumed to take place, had a low friction, typically 0.05, which contributes to the high standard deviations of friction coefficient (0.012) and topographical image (1.4).

However, other areas of the electrode surface were believed to be iron rather than iron oxide, because the dissolution reaction (9-2) was likely to lead to loss of the iron oxide film formed on the surface, resulting in a much higher friction coefficient.

$$Fe \rightarrow Fe^{III}(PC) + 3e^- \qquad (9\text{-}2)$$

a) Topographical image



b) Friction image

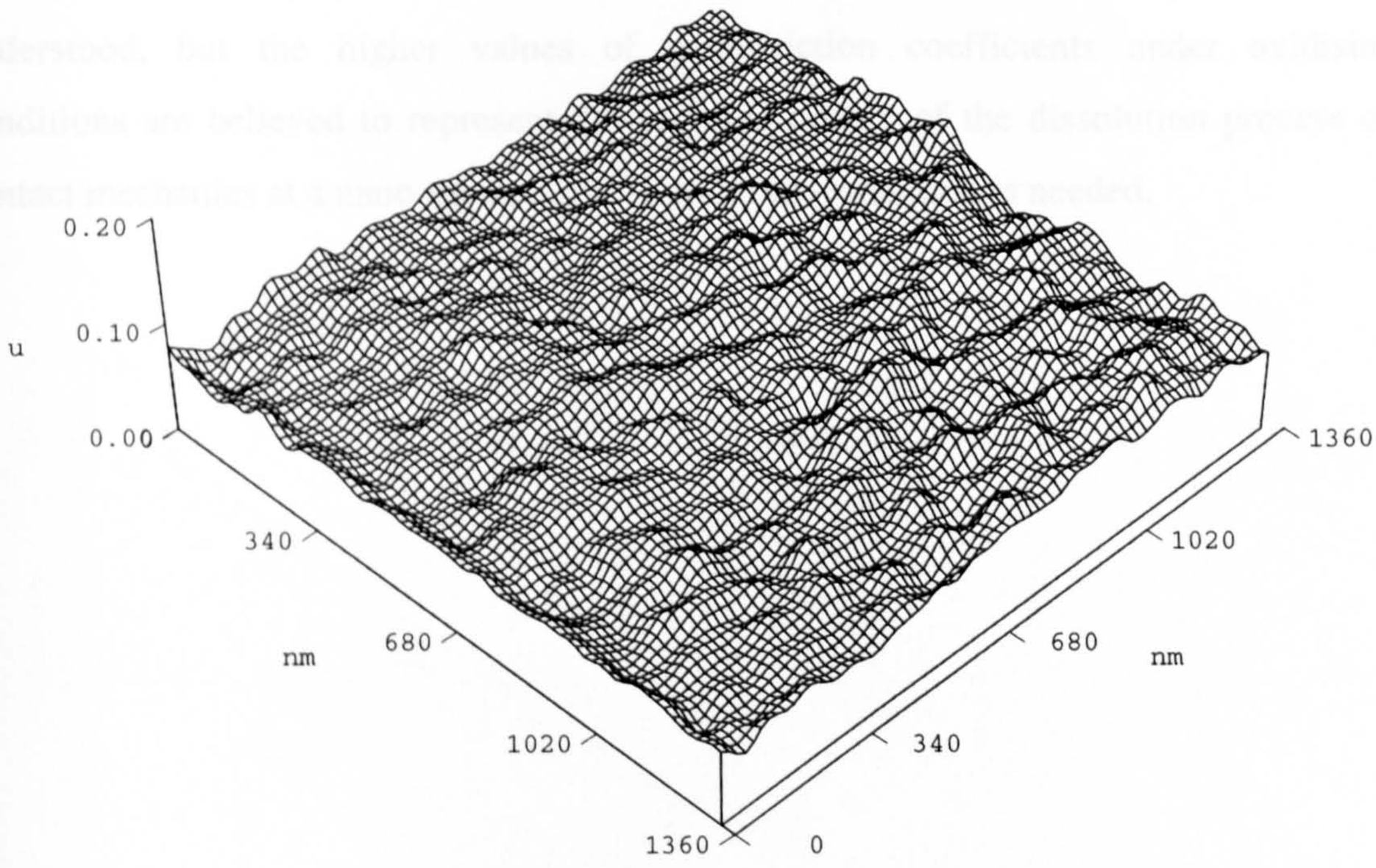


Fig.9.5. Images from iron surface measured with the constant electrode potential controlled at 0.8 V vs. S.C.E. for 1 minute in 0.01 M $(Et)_4NBF_4$ PC solution: a) AFM topography image; b) AFM friction force image.

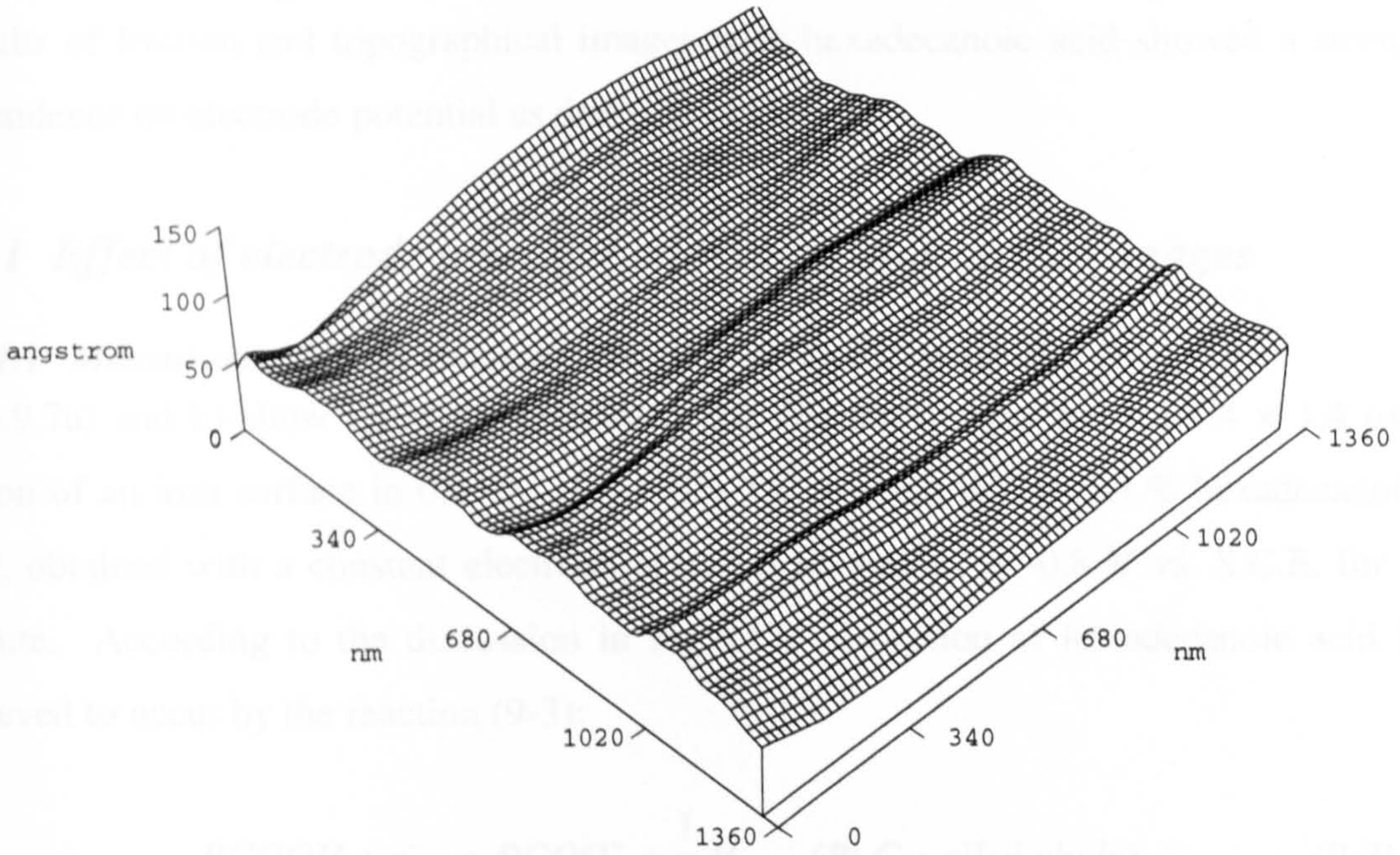
9.2.1.4 Measurements with electrode potential controlled at 0.8 V for 10 mins.

Figs.9.6a) and b) show AFM topographical and friction images from the same region of an iron surface in 0.01 M $(Et)_4NBF_4$ PC, after the tip and iron surface had been subjected to a constant electrode potential of 0.8 V for 10 minutes. The typical average values of friction and roughness scales increased to 0.12 and 7.2 nm, respectively, with standard deviations of 0.02 and 1.4 nm, respectively.

The high friction coefficient can be attributed to the dissolution process of iron into iron(II/III) which occurred with high current densities (*ca.* 1.0 mA cm^{-2}) at 0.8 V vs. S.C.E., as shown in Fig.6.15. Hence, holding the electrode potential at 0.8 V for an additional 9 minutes increased the average nano-friction coefficient, compared with its value for 1 minute, shown in Fig.9.5a).

On the other hand, macro-friction coefficients in Fig.7.7 obtained with the HFR rig did not show any substantial difference between -0.8 V and 0.8 V. This disparity of the effect of electrode potential on macro- and nano-friction coefficients is not yet fully understood, but the higher values of nano-friction coefficients under oxidising conditions are believed to represent the negative impact of the dissolution process on contact mechanics at a nano-metre scale. Further investigation is needed.

a) Topography



b) Friction image

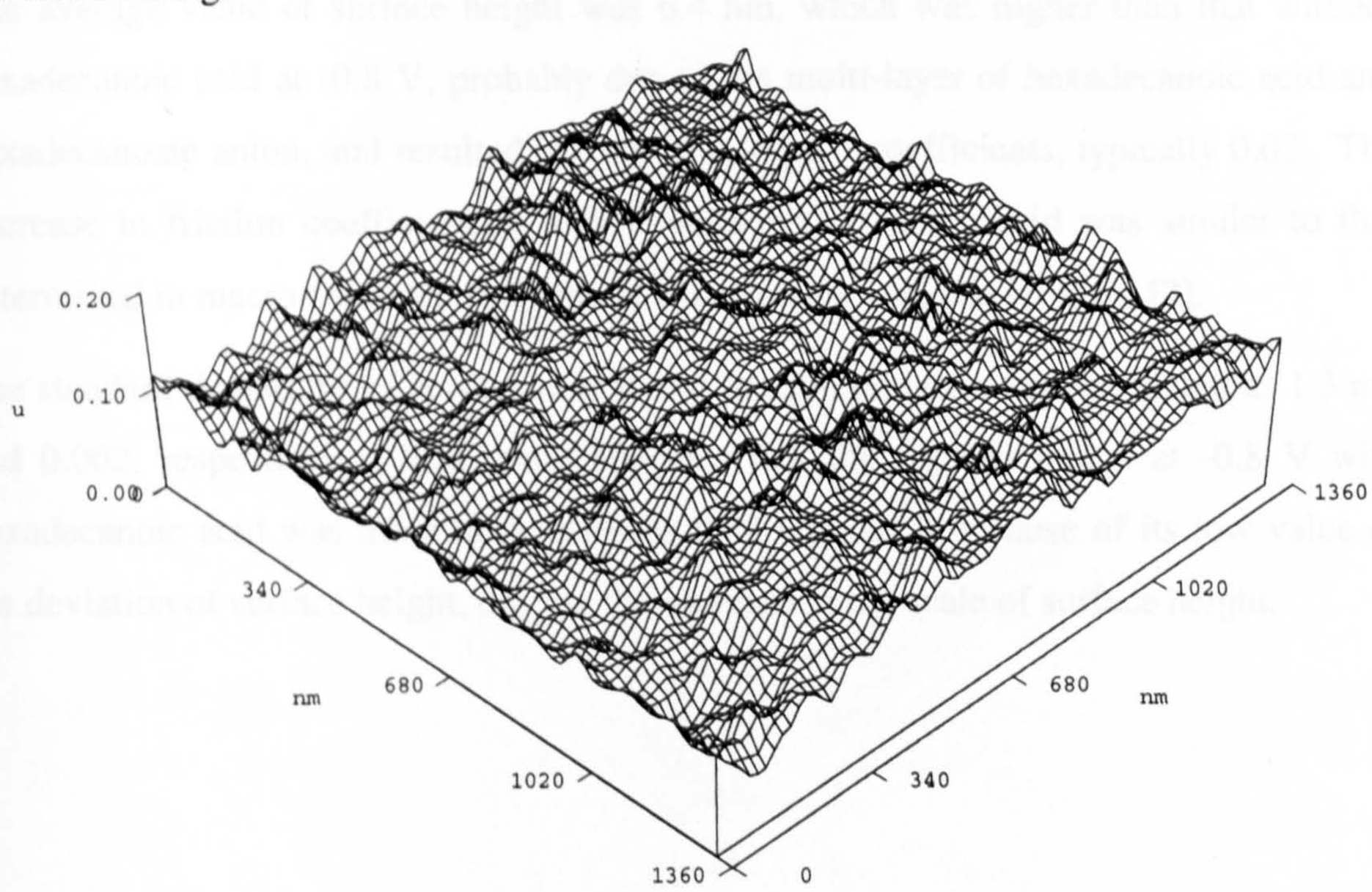


Fig.9.6. Images from iron surface measured after tip and surface have been subjected to constant electrode potential at 0.8 V vs. S.C.E. for 10 minutes in 0.01 M $(Et)_4NBF_4$ PC solution: a) AFM topography image; b) AFM friction force image.

9.3 Nano-tribological behaviour in PC solution with carboxylic acid

Results of friction and topographical images with hexadecanoic acid showed a strong dependence on electrode potential as described below.

9.3.1 Effect of electrode potential on friction and surface images

9.3.1.1 Measurements with constant electrode potential controlled at -0.8 V

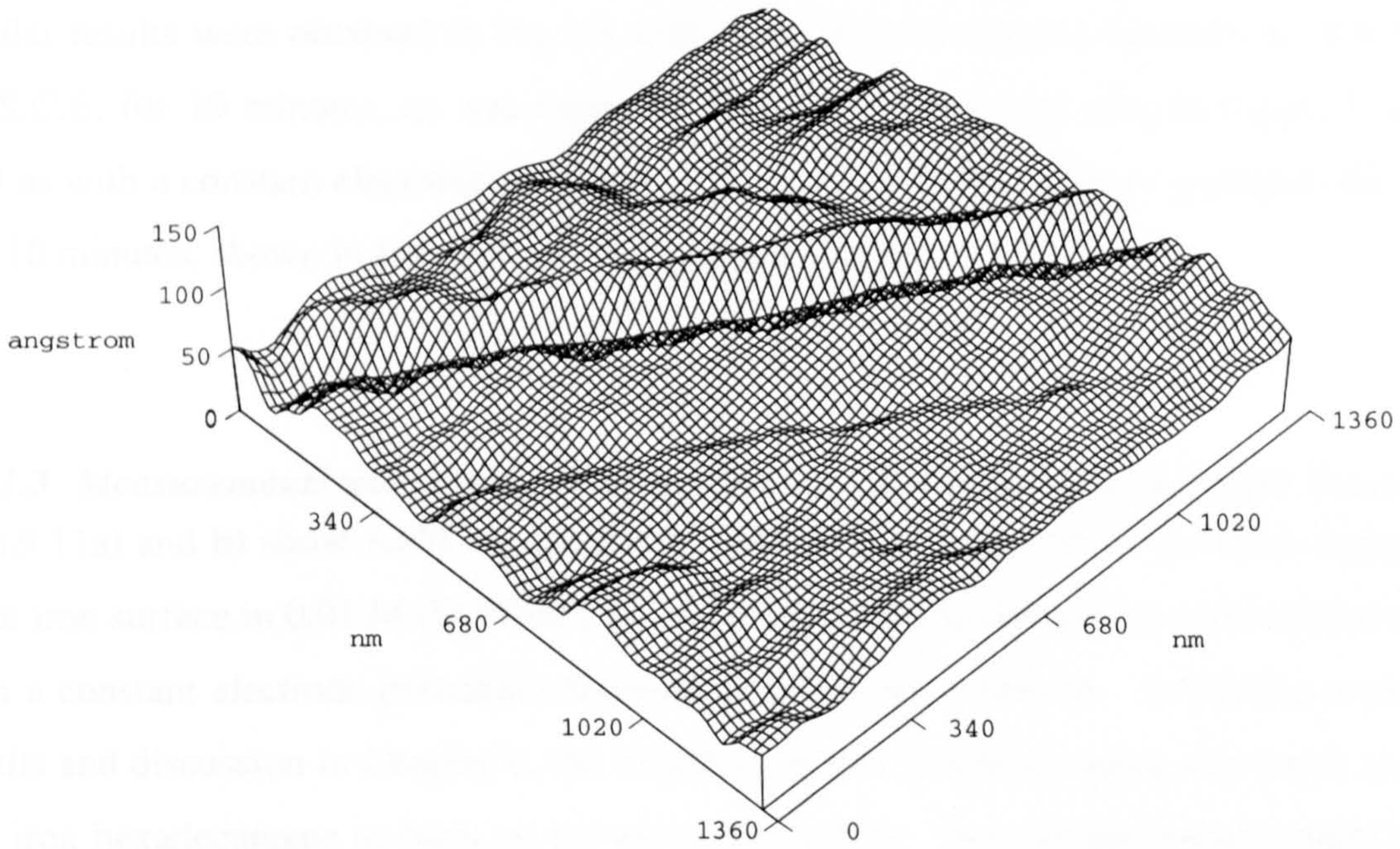
Figs.9.7a) and b) show AFM topographical and friction images from a 1.4 × 1.4 μm region of an iron surface in 0.01 M $(Et)_4NBF_4$ PC containing 0.01 wt.% hexadecanoic acid, obtained with a constant electrode potential controlled at -0.8 V vs. S.C.E. for 1 minute. According to the discussion in Fig.6.17, adsorption of hexadecanoic acid is believed to occur by the reaction (9-3):

$$RCOOH + e^- \rightarrow RCOO^- + \frac{1}{2}H_2 \quad (R: C_{15}\ alkyl\ chain) \qquad (9\text{-}3)$$

The average value of surface height was 6.4 nm, which was higher than that without hexadecanoic acid at -0.8 V, probably due to the multi-layer of hexadecanoic acid and hexadecanoate anion, and resulted in very low friction coefficients, typically 0.02. The decrease in friction coefficient at -0.8 V with hexadecanoic acid was similar to that determined in macro-triboelectrochemical experiments with the HFR rig [2].

The standard deviations of surface height and friction images were calculated as 1.3 nm and 0.002, respectively. The result suggests that the friction image at -0.8 V with hexadecanoic acid was more homogeneous than without it because of its low value of the deviation of surface height, despite the increase in the scale of surface height.

a) Topographical image



b) Friction image

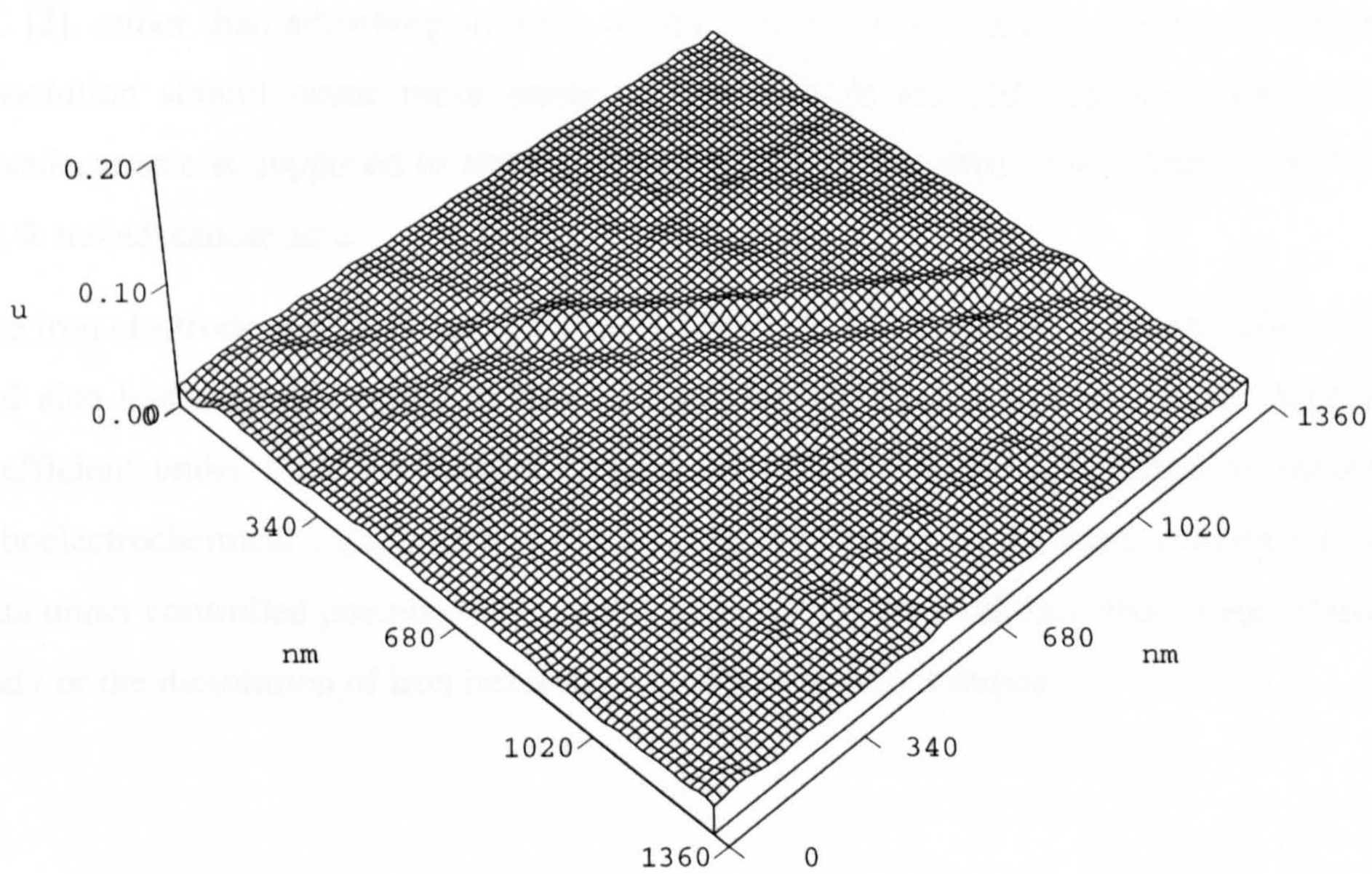


Fig.9.7 Images from iron surface measured with the constant electrode potential controlled at -0.8 V vs. S.C.E. for 1 minute in 0.01 M $(Et)_4NBF_4$ PC containing 0.01 wt.% hexadecanoic acid: a) AFM topography image; b) AFM friction force image.

9.3.1.2 Measurements with constant electrode potential controlled at -0.1 V

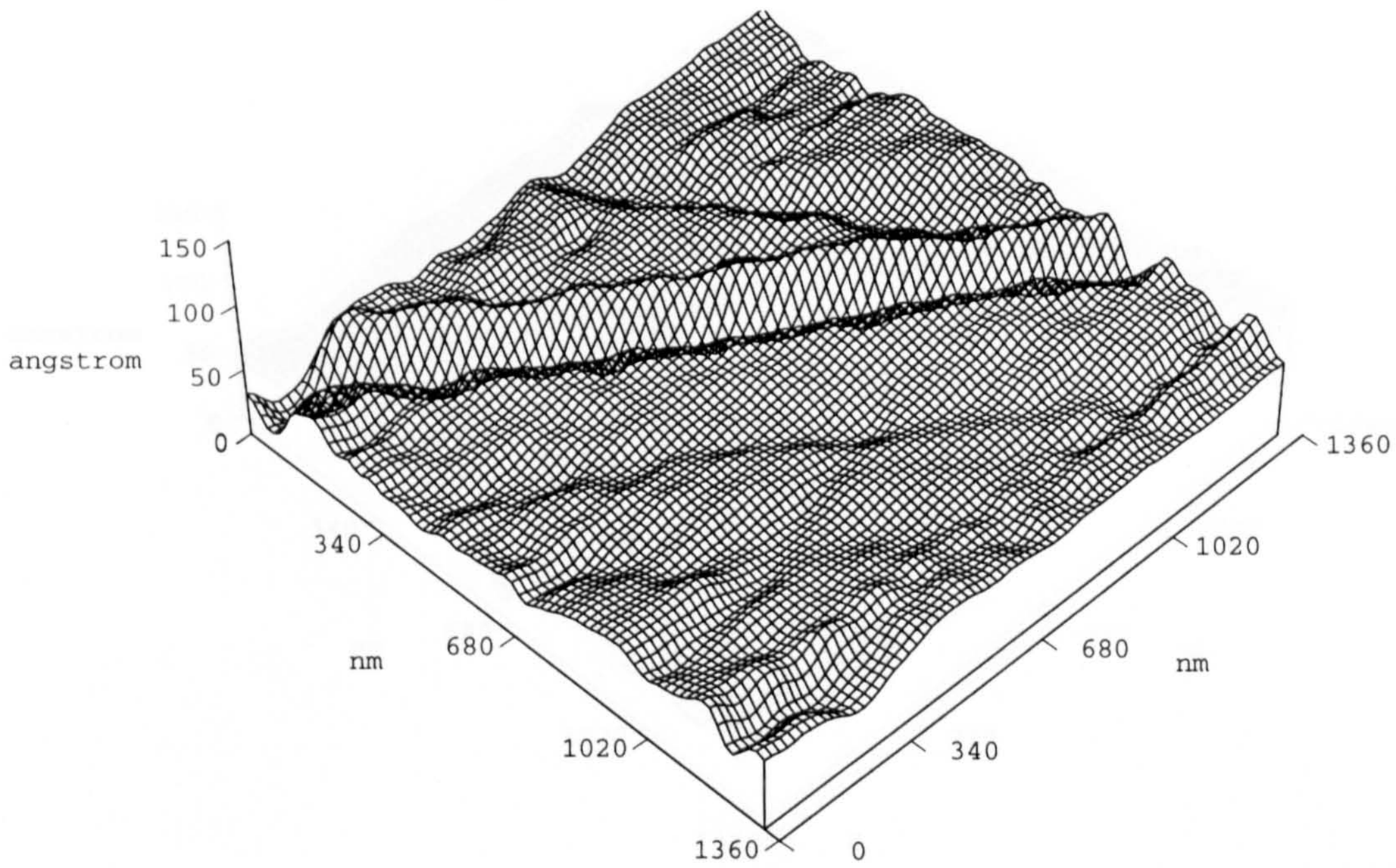
Similar results were obtained in Fig.9.8 with the constant electrode potential at -0.8 V vs. S.C.E. for 10 minutes, as was expected from the current-time data in Fig.6.17, as well as with a constant electrode potential at -0.1 V, typical open-circuit potential, for 1 and 10 minutes, shown in Figs.9.9 and 9.10, respectively.

9.3.1.3 Measurements with constant electrode potential controlled at 0.8 V for 1 min.

Figs.9.11a) and b) show AFM topographical and friction images from the same region of an iron surface in 0.01 M $(Et)_4NBF_4$ PC with 0.01 wt.% hexadecanoic acid, measured with a constant electrode potential controlled at 0.8 V for 1 minute. According to the results and discussion in Chapter 6, the oxidation at this potential causes iron oxide and / or iron hexadecanoate to form on the electrode surface. Iron hexadecanoate ought to dissolve easily in the bulk electrolyte solution due to its similar solubility parameter to PC [3], rather than adsorbing strongly on the iron electrode surface. Hence, oxidation dissolution should occur more easily on the area of electrode surface where iron hexadecanoate is supposed to form, compared to the same area in the absence of 0.01 wt.% hexadecanoic acid.

The iron electrode surface at 0.8 V had a high friction coefficient of value typically 0.12, and also had a high standard deviation, typically 0.009. The increase in the friction coefficient under such oxidising condition was similar to that determined in macro-triboelectrochemical experiments in Fig.7.7, and is believed, on the basis of current-time data under controlled potential in Fig.6.17, to be due to the oxidation dissolution of iron and / or the dissolution of iron hexadecanoate into the bulk solution.

a) Topography image



b) Friction image

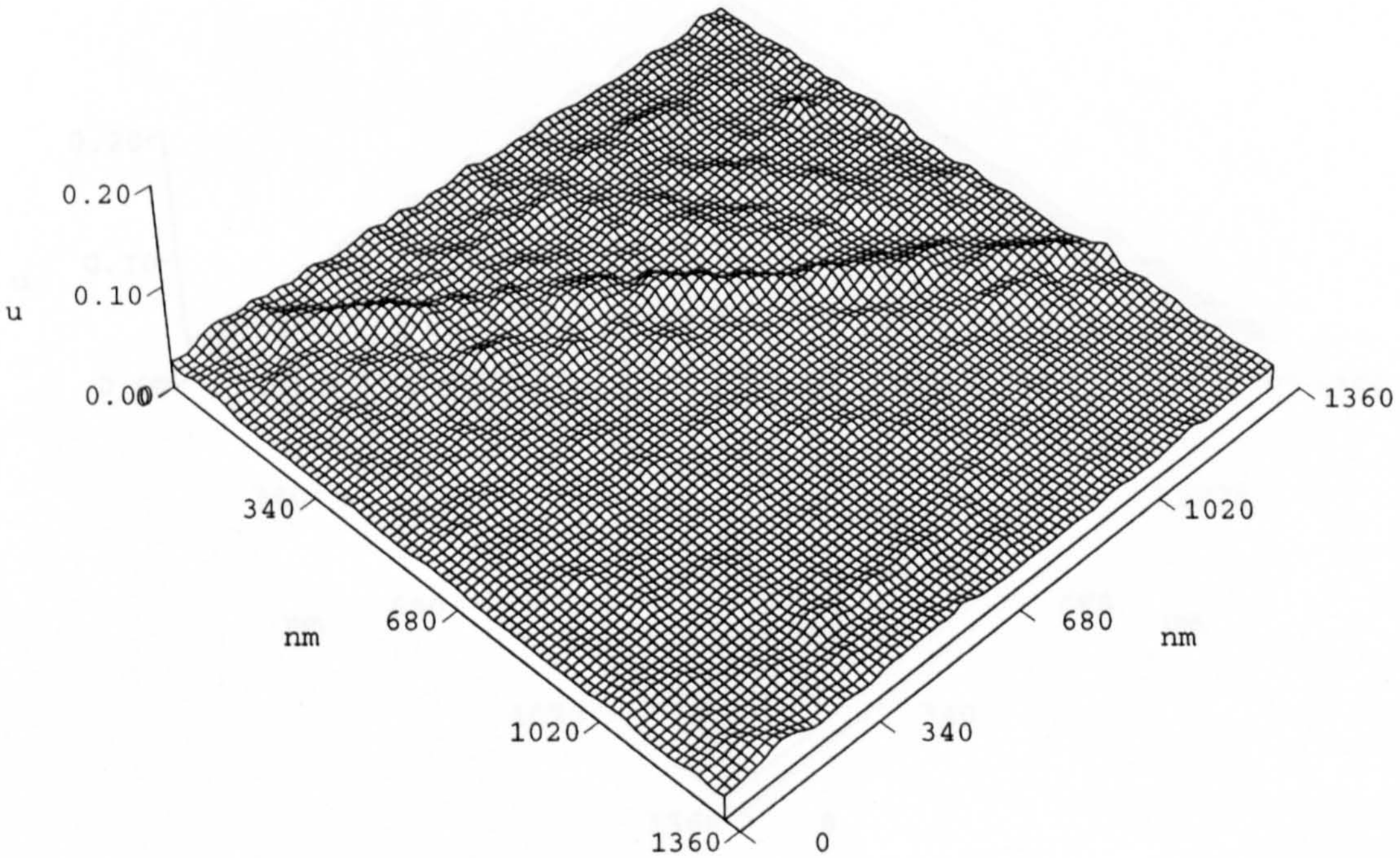
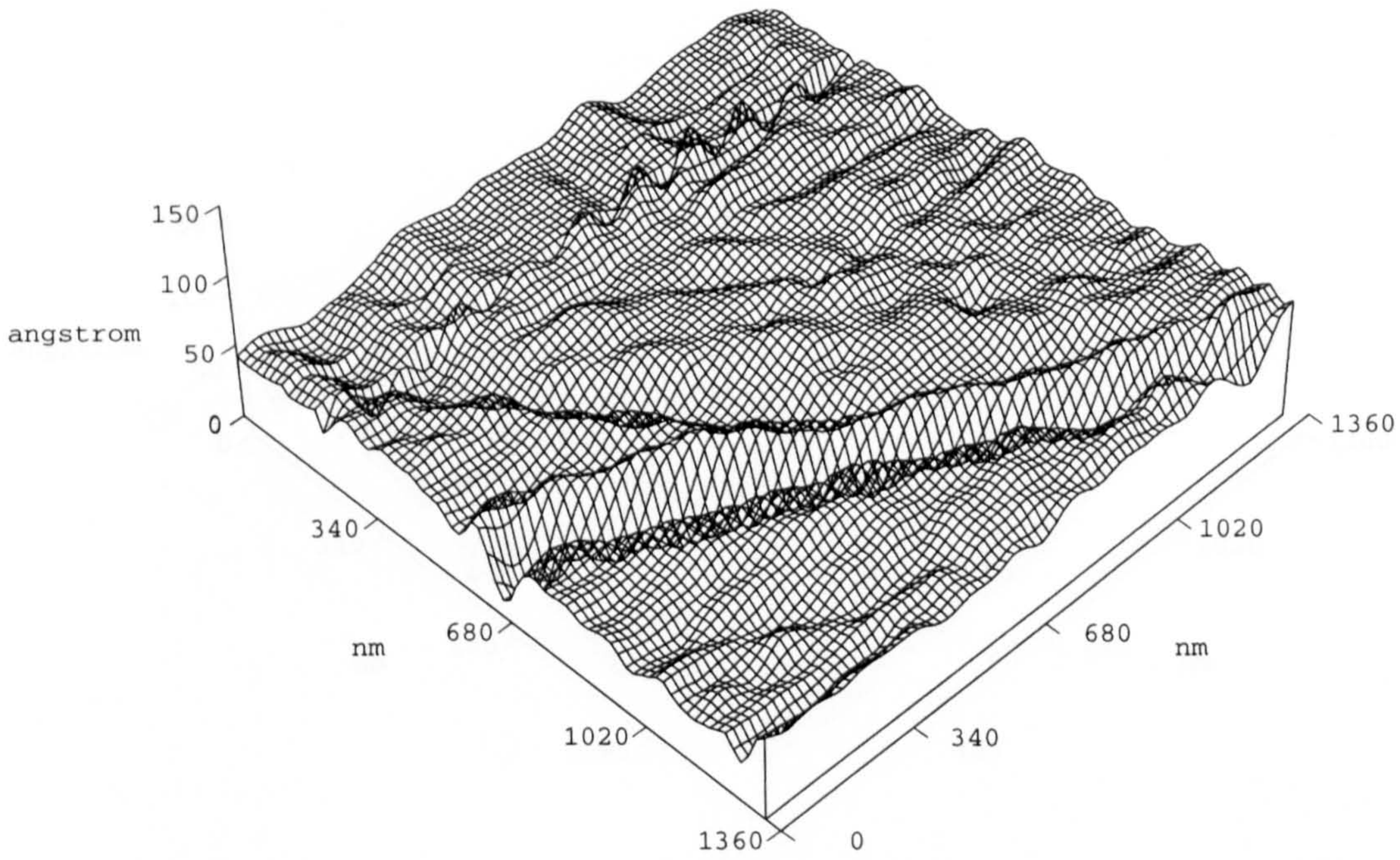


Fig.9.8 Images from iron surface measured after tip and surface have been subjected to constant electrode potential at -0.8 V vs. S.C.E. for 10 minutes in 0.01 M $(Et)_4NBF_4$ PC containing 0.01 wt.% hexadecanoic acid. a) AFM topography; b) AFM friction image.

a) Topographical image



b) Friction force image

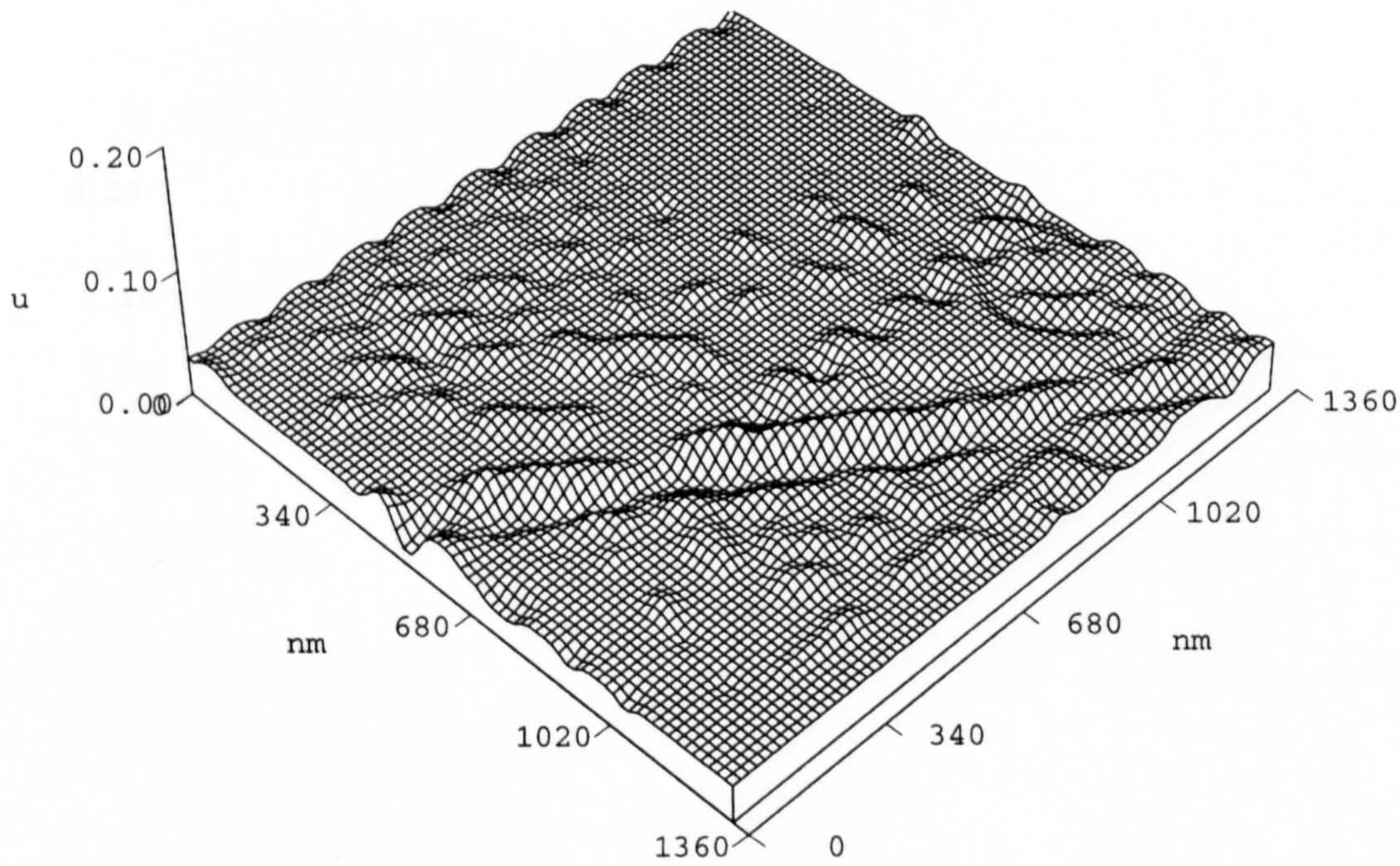
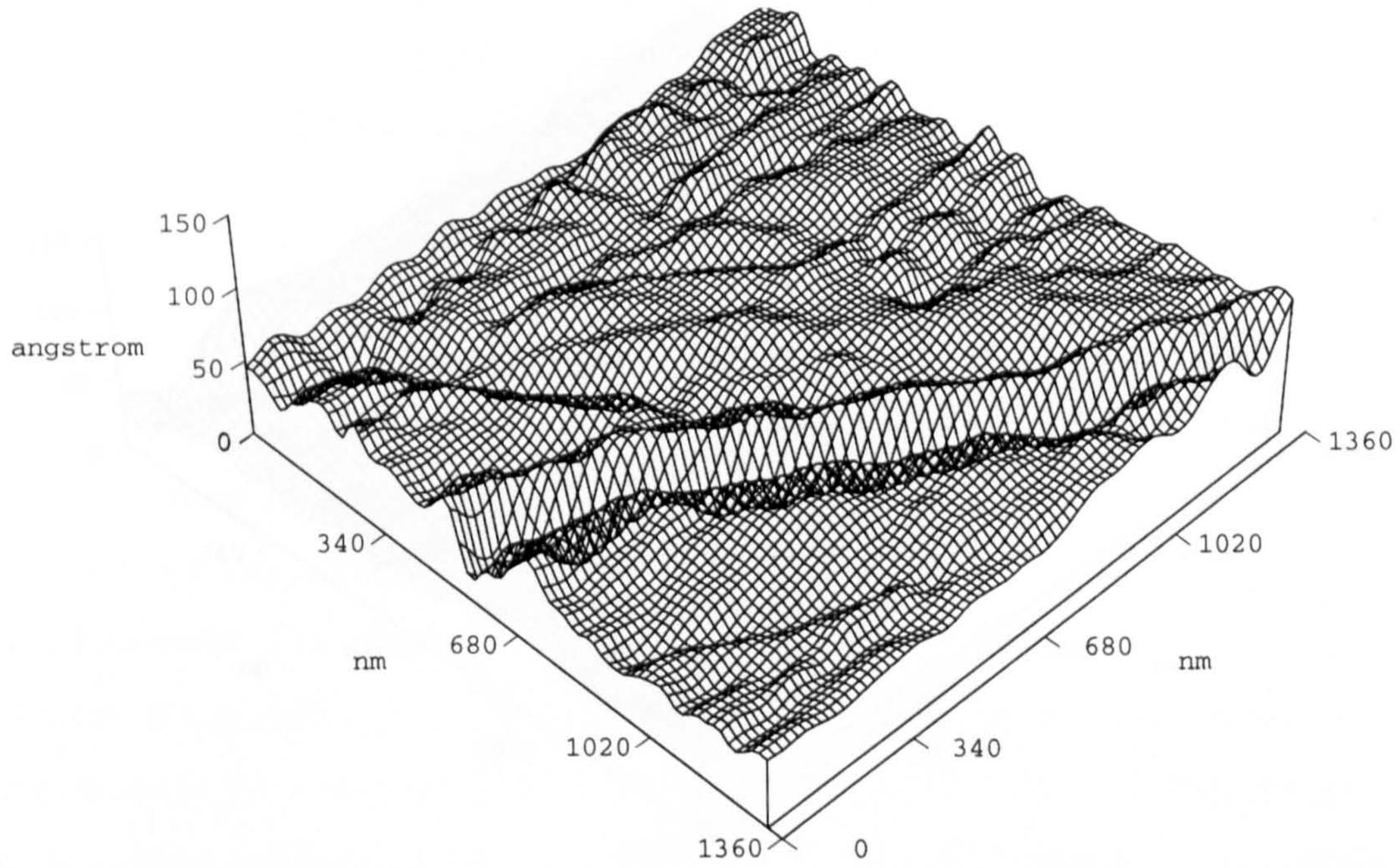


Fig.9.9 Images from iron surface measured with the constant electrode potential controlled at -0.1 V vs. S.C.E. for 1 minute in 0.01 M $(Et)_4NBF_4$ PC containing 0.01 wt.% hexadecanoic acid. a) AFM topography image; b) AFM friction force image.

a) Topographical image



b) Friction image

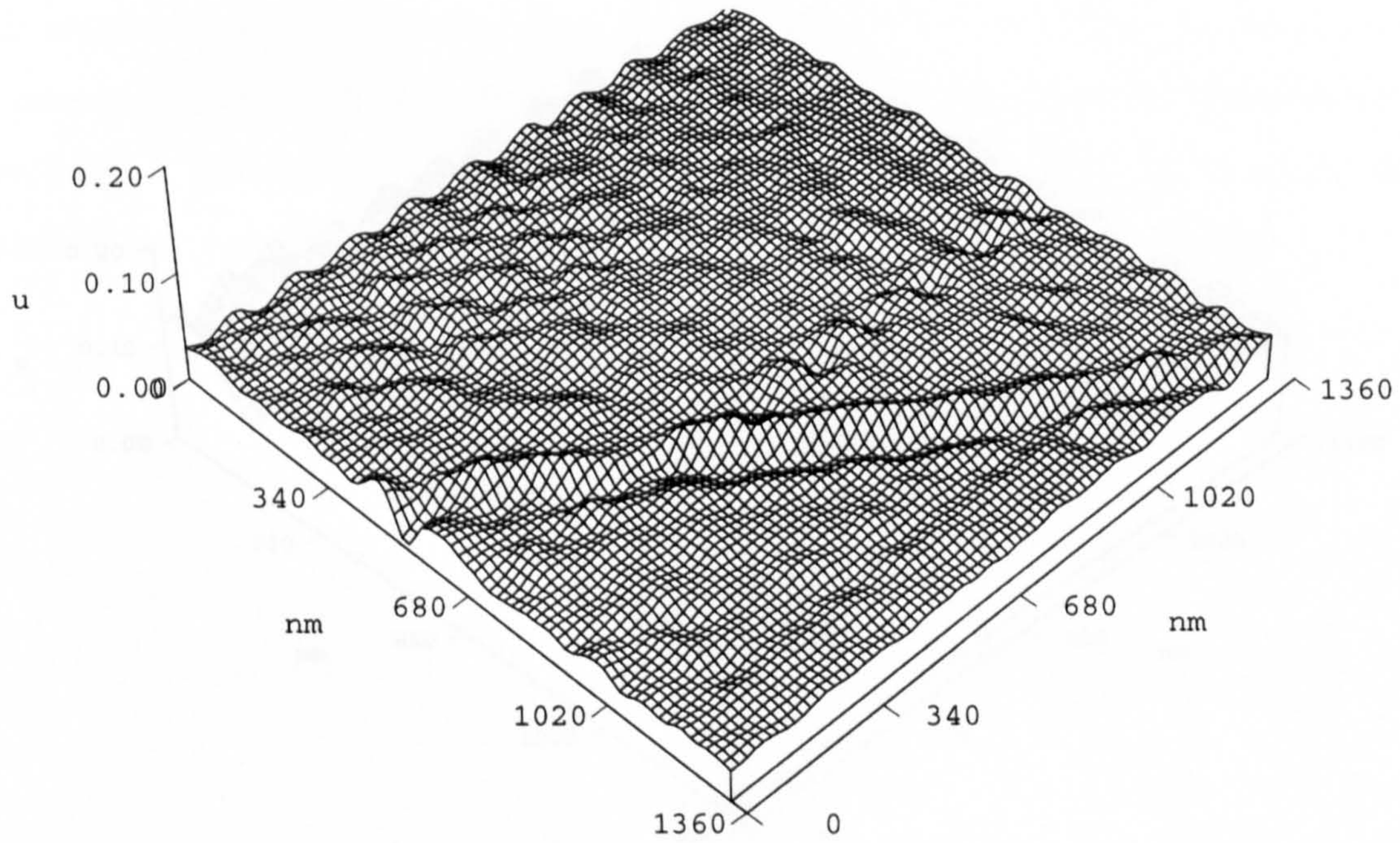
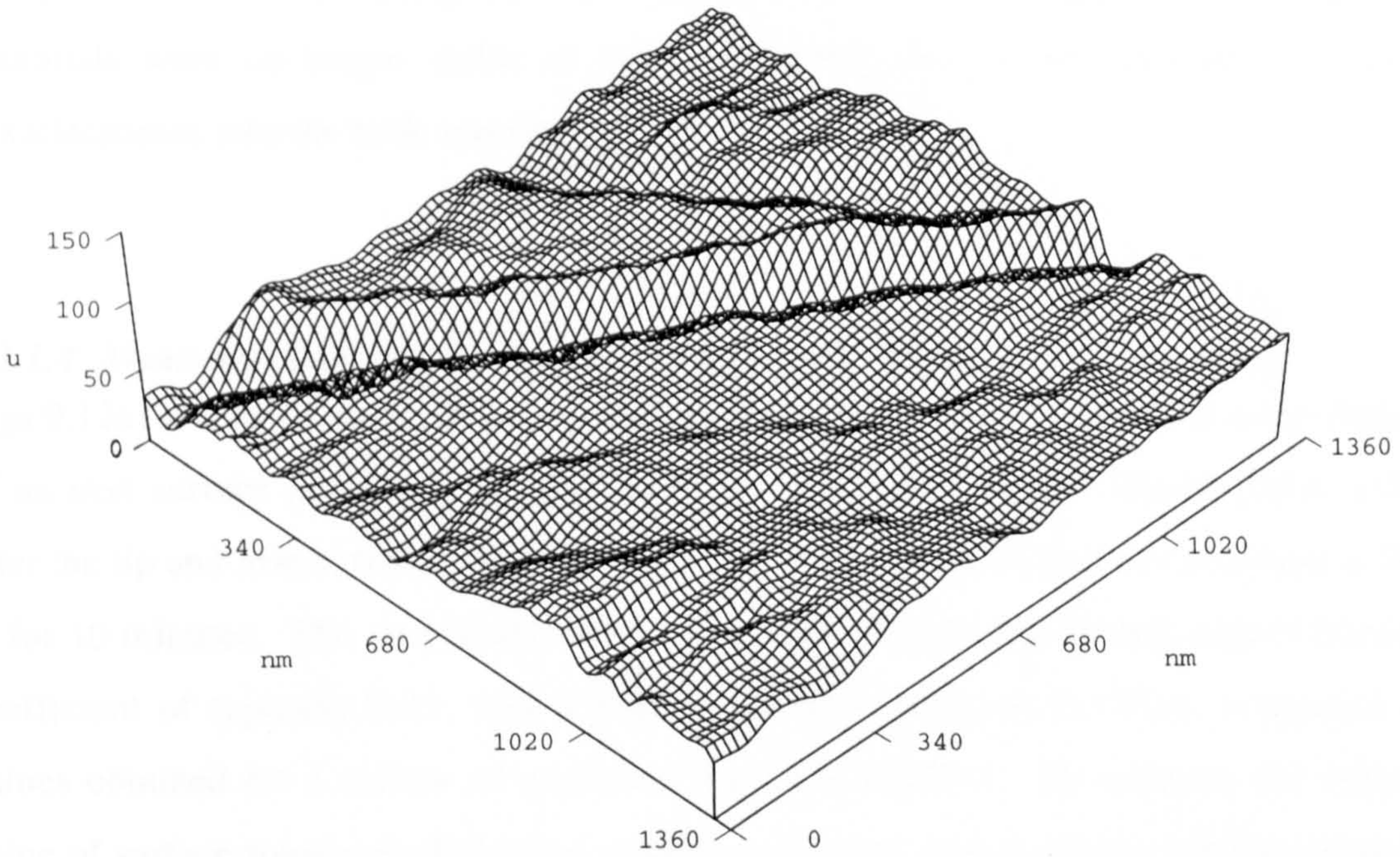


Fig.9.10 Images from iron surface measured after tip and surface have been subjected to constant electrode potential at -0.1 V vs. S.C.E. for 10 minutes in 0.01 M $(Et)_4NBF_4$ PC with 0.01 wt.% hexadecanoic acid. a) AFM topography; b) AFM friction image.

a) Topographical image



b) Friction image

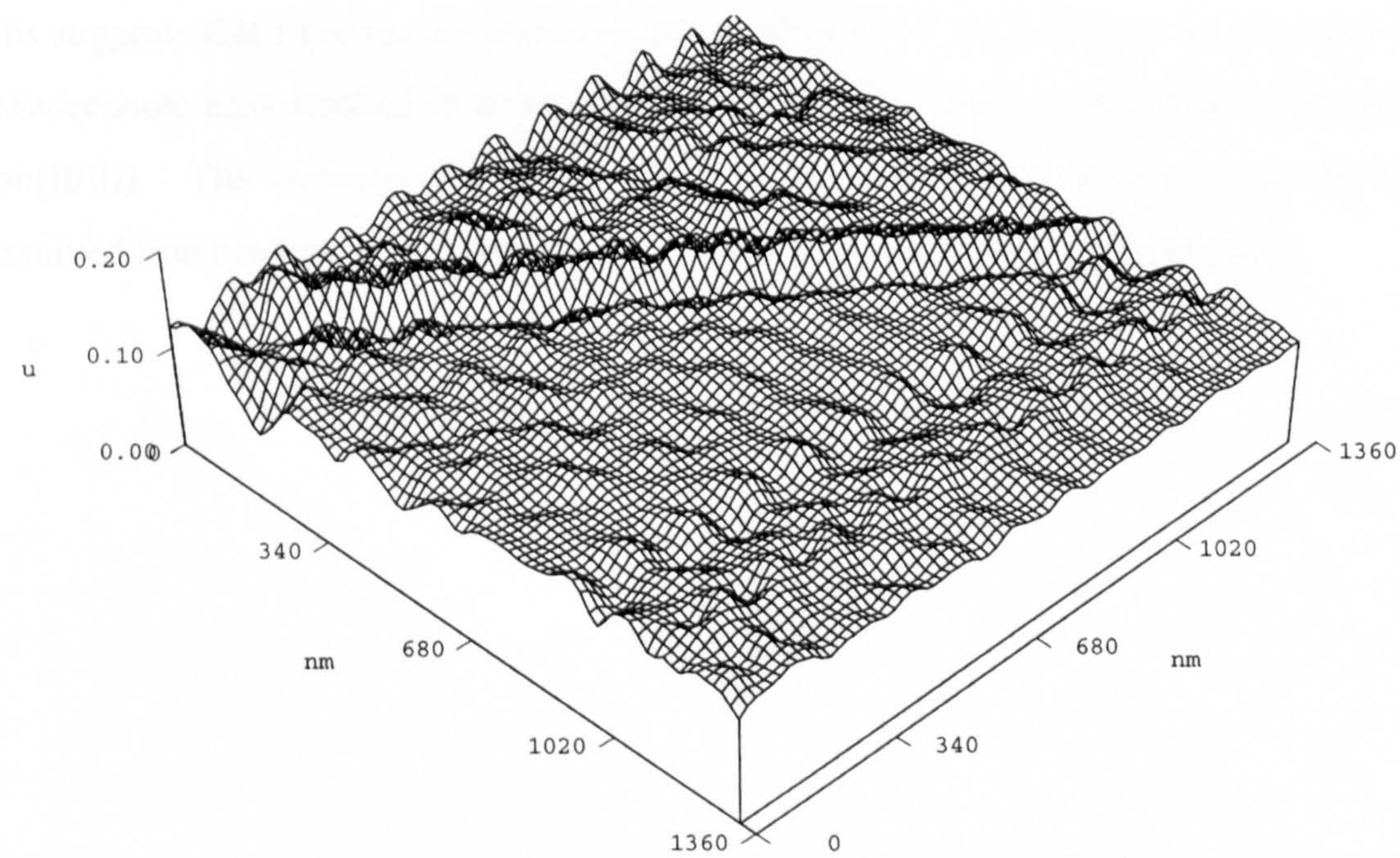


Fig.9.11 Images from iron surface measured with the constant electrode potential controlled at 0.8 V vs. S.C.E. for 1 minute in 0.01 M $(Et)_4NBF_4$ PC containing 0.01 wt.% hexadecanoic acid. a) AFM topography image; b) AFM friction force image.

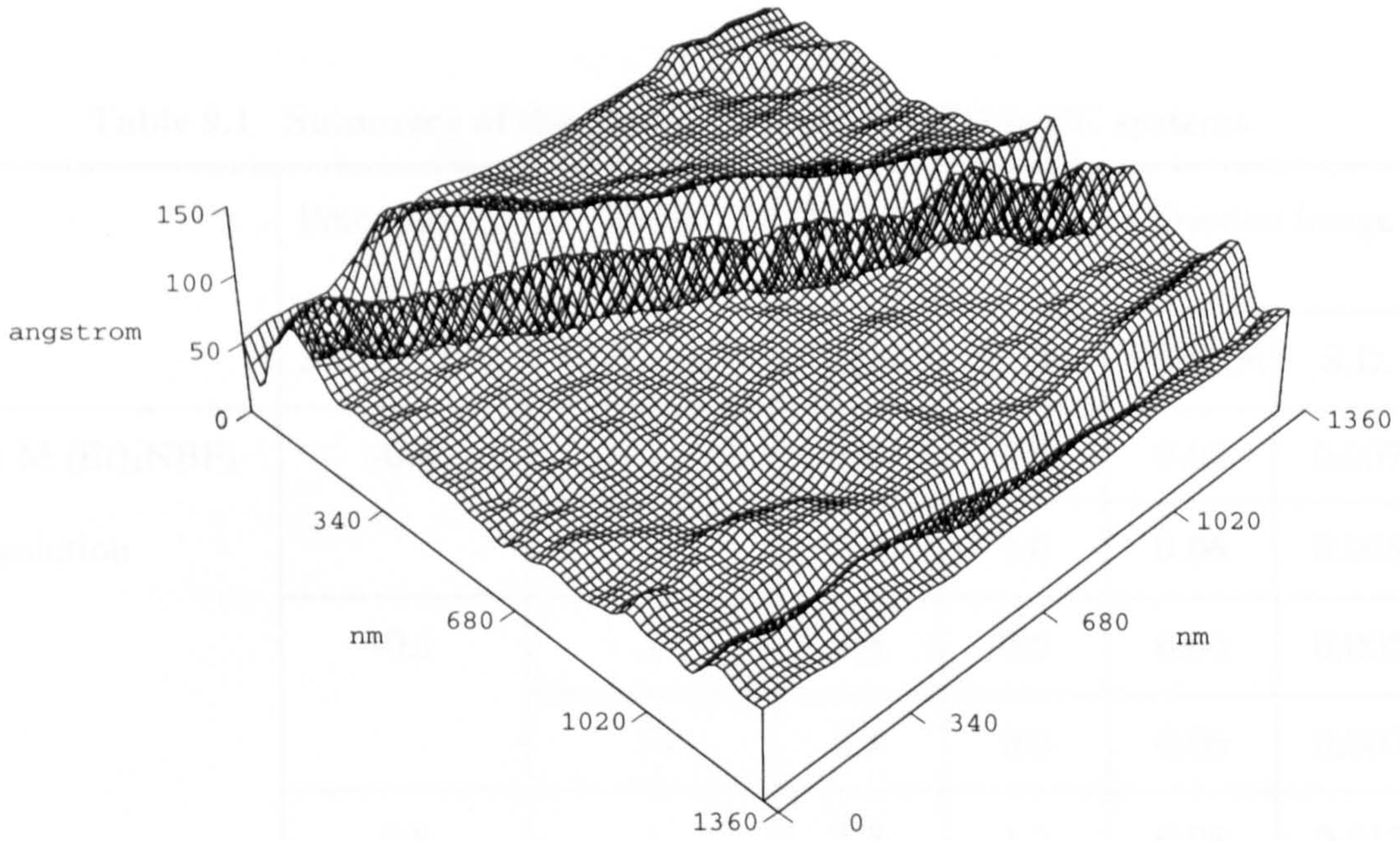
The electrode also had a surface roughness of typically 6.1 nm in height, which was slightly smaller compared to the values at negative and rest potentials. This indicates that protective films resulting from the adsorption of hexadecanoate anions at negative potentials were no longer stable at 0.8 V, probably due to the dissolution of iron hexadecanoate into the bulk solution.

9.3.1.4 Measurements with electrode potential controlled at 0.8 V for 10 mins.

Figs.9.12a) and b) show AFM topographical and friction images from the same region of an iron surface in 0.01 M $(Et)_4NBF_4$ PC containing 0.01 wt.% hexadecanoic acid, after the tip and iron surface had been subjected to the constant electrode potential at 0.8 V for 10 minutes. The area of the electrode surface imaged had slightly higher friction coefficient of typically 0.13, with a higher standard deviation of 0.014, compared to values obtained for 1 minute of oxidation shown in Fig.9.11. By contrast, the typical value of surface roughness decreased slightly to 5.7 nm, with a slightly greater standard deviation of 1.5 nm.

This suggests that the constant electrode potential of 0.8 V vs. S.C.E. in the presence of hexadecanoic acid resulted in an increase in friction, due to the oxidative dissolution of iron(II/III). The current-time data in Fig.6.17 support this interpretation as do the dissolved iron concentrations determined by ICP analysis, reported in Table 6.4.

a) Topographical image



b) Friction image

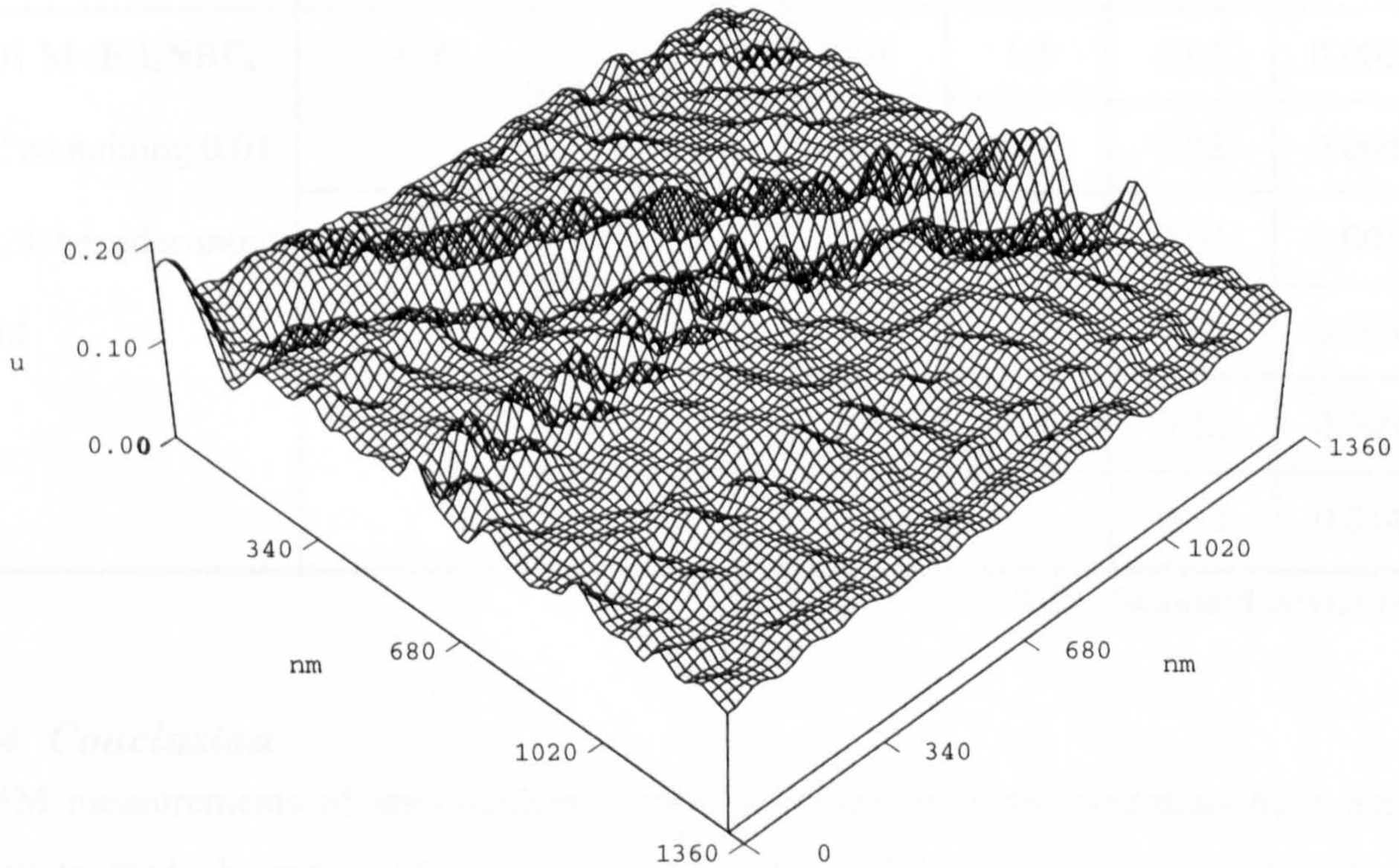


Fig.9.12 Images from iron surface measured after tip and surface have been subjected to constant electrode potential at 0.8 V vs. S.C.E. for 10 minutes in 0.01 M $(Et)_4NBF_4$ PC containing 0.01 wt.% hexadecanoic acid. a) AFM topography; b) AFM friction

Finally, a summary of the data obtained by AFM with PC electrolyte solutions as a function of electrode potential is given in Table 9.1.

Table 9.1 Summary of the data obtained by AFM in PC systems.

	Potential vs. S.C.E. / V	Time passed / mins.	Topography / nm		Friction image	
			Height	S.D.	Friction	S.D.
0.01 M $(Et)_4NBF_4$ PC solution	-0.8	1	3.6	0.9	0.06	0.007
		10	3.7	1.0	0.06	0.008
	-0.1	1	3.8	0.9	0.06	0.005
		10	3.8	0.9	0.06	0.007
	0.8	1	5.5	1.3	0.08	0.012
		10	5.6	0.9	0.12	0.02
0.01 M $(Et)_4NBF_4$ PC containing 0.01 wt.% hexadecanoic acid	-0.8	1	6.4	1.3	0.02	0.002
		10	6.4	1.3	0.02	0.004
	-0.1	1	6.6	1.3	0.03	0.005
		10	6.6	1.3	0.03	0.004
	0.8	1	6.1	1.4	0.12	0.009
		10	5.7	1.5	0.13	0.014

S.D.: Standard deviation

9.4 Conclusion

AFM measurements of steel surfaces under controlled electrode potentials have been used to study boundary lubrication in non-aqueous PC solutions, with and without hexadecanoic acid. An applied potential permits control of the nature of the surface film, while AFM enables the topography and friction characteristics of the film to be quantified.

It has been shown that a reducing potential produces spatially uneven friction, due to the formation of stable bare iron surfaces in 0.01 M $(Et)_4NBF_4$ PC. By contrast, an applied positive potential of 0.8 V vs. S.C.E. lead to the formation of an iron oxide layer as well as the oxidative dissolution of iron, which results in high friction.

Similar studies were carried out in PC solutions containing hexadecanoic acid. In this case, the application of reducing potential of -0.8 V vs. S.C.E. led to lower friction due to the adsorption of hexadecanoic acid as a free acid and hexadecanoate anions which was reduced from hexadecanoic acid on the surface of electrode, whereas oxidising potentials resulted in increased friction values due to the hexadecanoic acid exacerbating the iron dissolution, probably by the formation of soluble iron(III) carboxylate species.

CHAPTER 10

10. Conclusions and suggestions for future work

10.1 Conclusions

Electrochemical techniques have been used to investigate interactions between metal electrode and lubricant additives in non-aqueous systems. Applied potentials were able to control chemical reactions at the electrode surface and thereby influence both friction and wear characteristics.

The main results or the investigations described in this thesis will be summarised individually.

10.1.1 Selection of non-aqueous lubricated system

By investigating the electrochemical behaviour of a metal redox couple, ferrocene, in a range of organic solvents, two non-aqueous electrolyte systems were selected as suitable lubricants for electrochemical studies. One was 0.8 M $LiClO_4$-di-ethyl adipate (DEA) solution, in which DEA has chemical structure reasonably representative of some ester synthetic lubricant base oils. The other one was 0.01 M $(Et)_4NBF_4$-propylene carbonate (PC) solution, which showed almost ideal electrochemical behaviour even at low electrolyte concentrations, and also minimised the influence of electrolytes on friction and wear performance.

10.1.2 Electrochemical study of metal-additive interactions

The electrochemical kinetics of DEA and PC electrolyte solutions with and without DBDS or alkyl-carboxylic acids have been examined on iron and platinum, mainly by determination of voltammograms, to infer their interactions with electrode surfaces. For

the iron electrode, adsorption densities and dissolution processes on the iron electrode, resulting from the formation of iron carboxylates with alkyl-carboxylic acids, were determined as a function of electrode potential. The interactions between DBDS and iron in DEA electrolyte solution are still not fully understood, probably due to the simultaneous reduction of iron oxide which may mask the reduction of DBDS on the iron electrode surface.

10.1.3 Effect of electrode potential on friction and wear by HFRR

The effect of electrode potential on dynamic friction coefficient and wear scar in a ball on disc has been investigated using an HFR test rig, lubricated by DEA and PC electrolyte solutions with and without DBDS or alkyl-carboxylic acid additives. Carboxylic acids decreased friction and wear at negative electrode potentials due to the formation of adsorption film on the reduced electrode surfaces. The film became more protective with increasing alkyl-chain length. At positive electrode potentials, however, carboxylic acids formed iron carboxylates, which dissolved into the bulk solution, and resulted in the increase of friction and wear. 2.0 wt.% DBDS in DEA solution decreased wear at negative electrode potentials, probably due to the formation of protective film by an electrochemical process. However, this effect did not affect friction characteristics

10.1.4 Effect of electrode potential on lubricant film thickness

Ultra-thin film interferometry has been used to directly monitor film thicknesses between a glass flat and rolling steel ball under controlled electrode potential in 0.01 M $(Et)_4NBF_4$ PC, with and without dissolved hexadecanoic acid. It was found that hexadecanoic acid-containing oils formed thicker boundary films than those produced by 0.01 M $(Et)_4NBF_4$ PC alone at electrode potentials of -0.1 V and 0.8 V. The films from hexadecanoic acid were typically 3 to 10 nm thick, and appeared to cover the ball surface.

However, at -0.8 V, hexadecanoic acid did not enhance film-forming abilities, and PC electrolyte solution both with and without hexadecanoic acid exhibited smaller film

thicknesses than predicted from EHD theory in the thin film region. The mechanism by which this occurs is not fully understood and further investigation is needed.

10.1.5 Nano-tribological behaviour by AFM technique

AFM measurements of steel surfaces under controlled electrode potentials have been used to study boundary lubrication in non-aqueous PC electrolyte solutions, with and without hexadecanoic acid. An applied potential permits control of the nature of the surface film, while AFM enables the topography and friction characteristics of the film to be quantified.

An applied reducing potential produced spatially uneven friction, due to the formation of stable bare iron surfaces in 0.01 M $(Et)_4NBF_4$ PC. By contrast, an applied positive potential of 0.8 V vs. S.C.E. led to the formation of an iron oxide layer as well as the oxidative dissolution of iron, which resulted in high friction.

Similar studies were carried out in PC solutions containing hexadecanoic acid. In this case, the application of reducing potential of -0.8 V vs. S.C.E. led to lower friction due to the adsorption of hexadecanoic acid as a free acid and hexadecanoate anion produced at -0.8 V, from hexadecanoic acid, whereas oxidising potential of 0.8 V vs. S.C.E. resulted in increased friction values due to the hexadecanoic acid exacerbating iron dissolution, probably by the formation of soluble iron(II/III) carboxylate species. This is consistent with the HFRR work.

10.1.6 General conclusion

From the results obtained from the work described in this thesis, the following general conclusions about the metal-additive interactions for friction and wear control by using electrochemical techniques can be drawn:

1. In dynamic friction, wear and film thickness measurements, control of both ball and disc potential with respect to the lubricant, enables the reaction of additives in non-aqueous systems to be studied systematically by electrochemical techniques.

2. Selection of 0.8 M $LiClO_4$ DEA and 0.01 M $(Et)_4NBF_4$ PC as a non-aqueous electrolyte solution has made it possible to detect the electrochemical reactions of friction and wear-reducing additives such as DBDS and various types of alkyl-carboxylic acids under controlled electrode potential provided by a potentiostat.

3. The friction obtained with alkyl-carboxylic acid in 0.8 M $LiClO_4$ DEA and 0.01 M $(Et)_4NBF_4$ PC, decreased at negative electrode potentials, due to the adsorption of carboxylic acids on the iron surface. Carboxylic acids with longer alkyl-chain length were more effective to reduce friction and wear in PC electrolytes, possibly because of their higher density of adsorption produced by the greater lateral interaction between the vertically oriented alkyl-chains.

4. At positive electrode potentials, carboxylic acids formed iron carboxylates, which dissolved into the bulk solutions of DEA and PC, and resulted in the increase of friction and wear.

5. In rolling ball on flat contact, at the electrode potentials of -0.1 V and 0.8 V, the presence of hexadecanoic acid in 0.01 M $(Et)_4NBF_4$ PC electrolyte resulted in the formation of thicker boundary films than in its absence. However, at -0.8 V, PC electrolyte solution with and without hexadecanoic acid gave smaller film thicknesses than predicted from EHD theory in the thin film region, which is not fully understood.

This suggests quite difference in response of hexadecanoic acid in sliding versus rolling conditions. In HFR tests, a thin, "solid-like" adsorbed film of acid formed under reducing conditions was beneficial to friction, whilst oxidising conditions produced excessive corrosion and high friction. In rolling conditions, the iron hexadecanoate formed in oxidising conditions was able to assist in film formation, presumably due to entrainment.

6. Spatial distribution of topography and friction images in non-aqueous PC electrolyte solutions was measured by AFM. The topographical images made it possible to give a clear explanation for electrochemical reactions occurred under controlled electrode potentials in terms of the aspects of the surface physical properties. Friction exhibited similar features to the behaviour obtained in the HFR rig.

10.2 Suggestions for future work

Future work directly arising from the results presented in this thesis can be divided into two main areas. These are, (a) further investigations of film thickness in PC electrolyte solution with and without hexadecanoic acid at negative electrode potential, and (b) investigations into the electrochemical behaviour of DBDS on iron electrode.

In addition to alkyl carboxylic acids and DBDS, electrochemical studies of other friction and wear reducing additives on tribological performance will also be of considerable interest, using the electrochemical techniques developed in this study.

Finally, the development of supporting electrolytes which makes possible similar work in less polar solvents such as mineral oils is of great importance.

The suggestions for future work may thus be summarised as follows:

10.2.1 Film thickness in PC solutions at negative electrode potential

One important area of future work is concerned with the mechanism of the formation of thin film thickness in PC electrolyte solutions with and without hexadecanoic acid at negative electrode potential. As was explained in Chapter 8, the thin film thickness deviated from EHD theory may result from highly polar, very low viscosity impurities, formed either by reduction of PC or present as impurities all the time. Due to their higher polarities, such impurities may have higher concentration close to the surface of ball and disc and thus form low viscosity surface layers, and hence give reduced film thickness in the thin film region. A similar effect has been previously seen, using PAO containing low viscosity ester **[1,2]**.

There are, however, other alternative possible mechanisms for the phenomena. One is that, the reduction of the steel ball surface may be roughening the surface, which might cause an apparent film thickness decrease. Such an effect has been observed in previous work **[3]**., although it should be noted that roughening under reducing potentials was not observed in the AFM work in the current study.

Alternatively, the reduction of steel ball may be changing the reflectivity of the surface compared to the initial, zero measurement, thereby disturbing the ultrathin film technique slightly.

These three possibilities need to be tested.

10.2.2 Electrochemical behaviour of DBDS on iron electrode

In this study, the electrochemical behaviour of DBDS on iron electrode was not clearly detected by voltammetric technique, possibly because the reduction of iron oxide into iron masked the reaction of DBDS at the electrode potential < -0.9 V.

However, surface-enhanced Raman scattering spectroscopy (SERS) has been reported to be effective for investigating the adsorption behaviour of sulphur compounds, such as DBDS **[4]** and benzenthiol **[5]** in hydrochloric acid aqueous solution. In these previous studies, the SERS spectra of DBDS showed cleavage of S-S bond and adsorption of phenyl methanethiolate on the iron electrode surface. Application of the technique into DEA non-aqueous systems under controlled electrode potential would be worthwhile, to investigate the electrochemical behaviour of DBDS, since this *in-situ* technique enables direct observation of the behaviour of DBDS on iron surfaces.

10.2.3 Triboelectrochemistry with other additives

Electrochemical studies of other friction and wear reducing additives, such as halogen, phosphorus, molybdenum-containing additives and organometallic compounds such as zinc di-thiophosphate on tribological performance under controlled electrode potential would be of great interest. Although such compounds have proved difficult to analyse electrochemically in the past **[6]**, non-aqueous systems developed through this study should help understand the mechanism of action of lubricant additives.

10.2.4 Improved supporting electrolyte

Finally, one of the key problems encountered in this study has been the lack of suitable supporting electrolytes able to dissolve in non-aqueous solvents. This meant that the work has been limited to the quite polar base fluids, DEA and PC. Recent published work has indicated the possibility of using supporting electrolytes with soluble cation and anion species **[7]**. These have two potential advantages; (a) they are more soluble in low polarity solvents and have been used successfully in cyclohexane, (b) they may help keep in solution the products formed by the oxidation / reduction of additives, enabling kinetic work to be carried out more effectively. In future work, such electrolytes should be synthesised and tested for solubility and use in fluids such as mineral oils.

References

1. *Chapter 1 General introduction*

[1] **Lockwood, F. E., Benchaita, M. T. and Friberg, S. E.,** "Study of Lyotropic Liquid Crystal in Viscous Flow and Elastohydrodynamic Contact," *ASLE Trans.*, **33**, 539, (1987).

[2] **Block, I. T. and Kelly, J. P.,** Brit. Patent No. **2 170 510A**, (1986).

[3] **Waterhouse, R. B.,** "Tribology and Electrochemistry," *Trib.*, **3**, 158, (1970).

[4] **Postnikov, S. N.,** *Electrophysical and Electrochemical Phenomena in Friction , Cutting and Lubrication*, Van Norstrand Reinhold, New York, (1978).

[5] **Guruswamy, V. and Bockris, J. O'M.,** "Triboelectrochemistry," *in Comprehensive Treatise of Electrochemistry*, edited by Bockris, J. O'M., Conway, B. E., Yeager, E. and White, R. E., Vol. 4, Plenum Press, New York, p.463, (1981).

2. *Chapter 2 Literature review*

[1] **Edison, T.,** "Improvement in Telegraph Apparatus," US Patent No. **158787**, (1875).

[2] **Koch, K. R.,** "Change of the Surface of Platinum and Palladium through the Oxygen Polarization," *Weidemann's Ann.*, **7**, 92, (1879)

[3] **Krouchkoll, M. M.,** "Study of Electrical Double Layers," *Annal. de Chimie et de Phys.*, **17**, 129, (1889).

[4] **Waterhouse, R. B.,** "Tribology and Electrochemistry," *Trib.*, **3**, 158, (1970).

[5] **Endo, Y., Fukuda, Y., and Takamiya, O.,** "Effect of the Application of Electric Voltage on Wear Characteristics of Metals and Dissimilar Metal Pairs," *Transactions of Jpn. Soc. Mech. Eng., (Kikai Gakkai Ronbun Shu),* **37**, 670, (1971).

[6] **Waterhouse, R. B. and Pearson, B. R.,** "The Fretting Wear of Steel Ropes in Seawater : The Effect of Cathodic Protection," *Proc. Int. Conf. on Wear of Materials by ASME*, p.79, April, (1985).

[7] **Zaki, M. and Dowson, D.,** "The Influence of Applied Potential upon the Friction of Polyethylene and Articular Cartilage under Lubricated Conditions," *Proc. Leeds / Lyon Symp. on Trib.*, p.230, September, (1985).

[8] **Postnikov, S. N.,** *Electrophysical and Electrochemical Phenomena in Friction , Cutting and Lubrication*, Van Norstrand Reinhold, New York, (1978).

[9] **Guruswamy, V. and Bockris, J. O'M.,** "Triboelectrochemistry," *in Comprehensive Treatise of Electrochemistry*, edited by Bockris, J. O'M., Conway, B. E., Yeager, E. and White, R. E., Vol. 4, Plenum Press, New York, p.463, (1981).

[10] **Rehbinder, P. A. and Venstrem, E. K.,** "Electrocapillary Effects in the Reduction of the Rigidity and Hardness of Metals," *Acta Physicochim.* USSR, **19**, 36, (1944).

[11] **Bockris, J. O'M. and Parry-Jones, R.,** "Determination of the Relative Electrode Potential of an Uncharged Metal in Solution," *Nature*, **171**, 930, (1953).

[12] **Bowden, F. P. and Young, L.,** "Friction of Clean Metals and the Influence of Adsorbate Films," *Proc. Roy. Soc. London, Series A*, **208**, 311, (1951).

[13] **Bockris, J. O'M. and Argade, S. D.,** "Dependence of Friction at Wet Contacts upon Interfacial Potential," *J. Chem. Phys.*, **40**, 1662, (1969).

[14] **Bockris, J. O'M. and Sen, R. K.,** "Variation of the Coefficient of Friction with Potential for Solid-Solution Contact: A Revised Calculation," *Surf. Sci.*, **30**, 237, (1972).

[15] **Clark, R. E. D.,** "The Influence of Electric Potentials upon Friction. Part I. - In Aqueous Solutions of Salts -," *Trans. Farad. Soc.*, **40**, 449, (1945).

[16] **Roberts, A. D.,** "Role of Electrical Repulsive Forces in Synovical Fluid," *Nature*, **231**, 434, (1971).

[17] **Katafuchi, T. and Takano, N.,** "Electrical Characteristics between Lubricated Frictional Surface (I) Measurement of Voltage - Current Characteristics between Frictional Surfaces -," *J. Jpn. Soc. Lub. Eng., (Junkatsu)*, **25**, 395, (1980).

[18] **Yamamoto,Y. and Hirano, F.,** "Scuffing Resistance of Phosphate Esters (II): Effect of Applied Voltage," *Wear*, **66**, 77, (1981).

[19] **Tung, S. C. and Wang, S. S.,** "In-Situ Electro-charging for Friction Reduction and Wear Resistant Film Formation," *Trib. Trans.*, **34**, 479, (1991).

[20] **Kramer, J.,** *The Metallic Condition*, Vandenhoek and Ruprecht, Göttingen, (1950).: **Kramer, J., and Demmer, L. J.,** "Effect of Environment on Mechanical Properties of Metals," *Progress in Materials Sci.*, **9**, 131, (1961).

[21] **Grunberg, L.,** "A Survey of Exoelectron Emission Phenomena," *Brit. J. App. Phys.*, **9**, 85, (1958).

[22] **Veerman, C.,** "Registration and Mapping of Plastically Deformed Metal Surfaces by Means of Photoelectrons," *Materials Sci. Eng.*, **4**, 329, (1969).

[23] **Moore, J. and Tsang, S.,** "The Early Detection of Fatigue Damage by Exoelectron Emission and Acoustic Emission," *STP 515, ASTM*, 113, (1972).

[24] **Baxter, W.,** "A Study of Plastic Deformation by Exoelectron Emission," *Vacuum*, **22**, 571, (1974).

[25] **March, P. A. and Rabinowicz, E.,** "Exoelectron Emisson for the Study of Surface Fatigue Wear," *ASLE Trans.*, **20**, 315, (1977).

[26] **Ferrante, J.,** "Exoelectron Emission from a Clean Annealed Magnesium Single Crystal during Oxygen Adsorption," *ibid.*, **20**, 328, (1977).

[27] **Chaikin, S. W.,** "On Frictional Polymer," *Wear*, **10**, 49, (1967).

[28] **Vladikina, T. N., Derjaguin, B. V., Kluev, V. A., Toporov, Yu. P. and Krustalev, Yu. A.,** "Emission of High Energy Electrons during Friction and Wear of Dielectrics," *J. Lubr. Tech.*, **102**, 552, (1980).

[29] **Kobozev, N. I.,** *Exoelectronic Emission*, published in Russian by the Foreign Literature, Moscow, (1962).

[30] **Staicopolus, D. N.,** "Electrocapillary Studies on Solid Metals," *J. Electrochem. Soc.*, **108**, 900, (1961).

[31] **Bockris, J. O'M., Argade, S. D. and Gileadi, E.,** "The Determination of the Potential of Zero Charge on Solid Metals," *Electrochim. Acta*, **14**, 1259, (1969).

[32] **Dubois, J. E., Lacaze, P. C., Courtel, R., Herrmann, C. C. and Maugis, D.,** "Polaromicrotribometry: A Friction Method for the Study of Polarized Metal Solution Interfaces," *ibid.*, **122**, 1454, (1975).

[33] **Bowden, F. P. and Tabor, D.,** *Friction and Lubrication*, Methuen & Co Ltd., London, (1967).

[34] **Kreuz, K. L., Fein, R. S. and Rand, S. J.,** "Solubilization Effects in Boundary Lubrication", Symposium on Deposit, Wear and Emission Control by Lubricant and Fuel Additives, *Am. Chem. Soc.*, September, (1969).

[35] **Goldblatt, I. L.,** "Model for Lubrication Behavior of Polynuclear Aromatics," *Ind. and Eng. Chem., Prod. Res. and Dev.*, **10**, 270, (1971).

[36] **Kajdas, C.,** "On a Negative-Ion Concept of the Antiwear and Antiseizure Action of Hydrocarbons during Friction, *Wear*, **101**, 1, (1985).

[37] **Kajdas, C.,** "On a Negative-Iron Concept of EP Action of Organo-Sulfur Compounds," *ASLE Trans.*, **28**, 21, (1985).

[38] **Kajdas, C.,** "About an Anionic -Radical Concept of the Lubrication Mechanism of Alcohols," *Wear*, **116**, 167, (1987).

[39] **Ardenne, M. Von, Steinfelder, K. and Tuemmler, R.,** *Electron Mass-Spectrographic Analysis of Organic Substances*, Springer, Berlin, (1971).

[40] **Nakayama, K.,** "In-situ Metal Transfer Monitoring Using Photostimulated Exoelectron Emission," *Wear*, **140**, 175, (1990).

[41] **Nakayama, K., Fujiwara, T. and Hashimoto, H.,** "Exoelectron Measurement Apparatus Incorporated in a Scanning Electron Microscope," *J. Phys. E.*, **17**, 1199, (1984).

[42] **Hunter, R. J.,** *Foundations of Colloid Science*, Oxford University Press, Oxford, Vol. 1, p.409, (1989).

[43] **Johnston, K. L.,** *Contact Mechanics*, Cambridge University Press, Cambridge, p.125, (1989).

[44] **Hogg, R., Healy, T. W. and Fuerstenau, D. W.,** "Mutual Coagulation of Colloidal Dispersions," *Trans. Faraday Soc.*, **66**, 1638, (1966).

[45] **Kelsall, G. H., Zhu, Y-Y. and Spikes, H. A.,** "Electrochemical Effects on Friction between Metal Oxide Surface in Aqueous Solutions," *J. Chem. Soc. Faraday Tran.*, **89**, 267, (1993).

[46] **Moore, D. F.,** *Principles and Applications of Tribology*, Pergamon, Oxford, p.125, (1975).

[47] **Brandon, N. P., Bonanos, N., Fogarty, P. O., Mahmood, M. N., Moore, A. J. and Wood, R. J. K.,** "Influence Potential on the Friction and Wear of Mild Steel in a Model Aqueous Lubricant," *J. App. Electrochem.*, **23**, 456, (1993).

[48] **Mortier, R. M. and Orszulic, S. T.,** *Chemistry and Technology of Lubricants*, Blackie Academic and Professional, New York, p.42, (1992).

[49] **Van der Waal, G.,** "The Relationship between Chemical Structure of Ester Base Fluids and Their Influence on Elastomer Seals and Wear Characteristics," *J. Syn. Lub.*, **1**, 281, (1985).

[50] **Lund, H. and Baizer, M. M.,** *Organic Electrochemistry - An Introduction and Guide- Third Edition, Revised and Expanded*, Marcel Dekker, Inc., New York, p.487, (1991).

[51] **Hirayama, M.,** "Electron Spin Resonance of Anion Radicals of Aromatic Esters. I. The Anion Radicals of Methyl, Ethyl and Isopropyl Benzoates, and of Methyl and Ethyl Isonicotinates," *Bull. Chem. Soc. Jpn.*, **40**, 1822, (1967).

[52] **Mairanovskii, V. G., Loginova, N. F. and Mel'nik, S. Ya.,** "Polarographic Reduction of Esters of Aliphatic Carboxylic Acids," *Elektrokhimiya*, **9**, 1174, (1973).

[53] **Seeber, R., Magno, F. and Bontempelli, G.,** "An Investigation on the Cathodic Behaviour of Phenylbenzoate in Dimethylformamide Solution," *J. Electroanal. Chem.*, **72**, 219, (1976).

[54] **Wagenknecht, J. H., Goodin, R. D., Kinlen, P. J. and Woodard, F. E.,** "Decomposition of Benzoate Ester Radical Anions," *J. Electrochem. Soc.*, **131**, 1559, (1984).

[55] **Hu, K., Niyazymbetov, M. E. and Evans, D. H.,** "Electrochemical Reactions of Some Dimethyl Dialkylaminomaleates," *J. Electroanal. Chem.*, **396**, 457, (1995).

[56] **Webster, R. D., Bond, A. M. and Schmidt, T.,** "Electrochemical Reduction of Some 2,6-Disubstituted Pyridine-based Esters and S-esters in Acetonitrile," *J. Chem. Soc. Perkin Trans. II*, 1365, (1995).

[57] **Zuman, P.,** *Substituent Effects in Polarography*, Plenum, New York, (1967).

[58] **Cogley, D. R., Synnot, J. C., Butler, J. N. and Grunwald, E.,** "Preferential Solvation of Ions by Water in Propylene Carbonate," *Electrochem. Soc. Met., Washington, D.C., Extended Abstract* **122**, May, (1971)

[59] **Katritzky, A. R. and Rees, C. W.,** *Comprehensive Heterocyclic Chemistry - The Structure, Reactions, Synthesis and Use of Heterocyclic Compounds*, Vol. 6, p.780, (1984).

[60] **Nelson, R. F. and Adams, R. N.,** "Propylene Carbonate : A Versatile Solvent for Electrochemistry and EPR," *J. Electroanal. Chem.*, **13**, 184, (1967).

[61] **Eggert, G. and Heitbaum, J.,** "Electrochemical Reactions of Propylene Carbonate and Electrolytes Solved Therein - A Dems Study," *Electrochim. Acta,* **31**, 1443, (1986).

[62] **Dey, A. N. and Sullivan, B. P.,** "The Electrochemical Deposition of Propylene Carbonate on Graphite,"*J. Electrochem. Soc.*, **117**, 222, (1970).

[63] **Eichinger, G.,** "Cathodic Decomposition Reactions of Propylene Carbonate," *J. Electroanal. Chem.*, **74**, 183, (1976).

[64] **Sakurai, T.,** *Additives for Petroleum Products - New Edition - (Sekiyu Seihin Tenkazai)*, Saiwai Shobo Inc., Tokyo, p.220, (1986).

[65] **Allum, K. G. and Forbes, E. S,** "The Load-Carrying Properties of Organic Sulfur Compounds. Part II. The Influence of Chemical Structure on the Anti-wear Properties of Organic Disulfides," *J. Inst. Petrol.*, **53**, 174, (1967).

[66] **Kajdas, C.,** "Influence of Hydrocarbon Oil Components on Wear of Tribological Pairs," *Jugoma, '82 Lubr. Conf.*, Zadar, (1982).

[67] **Forbes, E. S.,** "The Load Carrying Action of Organic Sulfur Compounds. A Review," *Wear*, **15**, 87, (1970).

[68] **Von Ardenne, M., Steinfelder, K. and Tuemmler, R.,** "Systems of Electron Attached Mass Spectrography for Organic Substances," Springer-Verlag, Berlin-Heidelberg-New York, (1971).

[69] **Fry, A. J.,** *Synthetic Organic Electrochemistry - Second Edition* -, John Wiley & Sons Inc., New York, p.165, (1989).

[70] **Degrand, C. and Lund, H.,** "Electrochemical Synthesis of Sulfide Acids," *Acta Chem. Scand.*, **B33**, 512, (1974).

[71] **Bonifacic, M. and Asmus, K. D.,** "One-Electron Redox Potentials of $RSSR^{+}$-RSSR Couples from Dimethyl Disulfide and Lipoic Acid," *J. Chem. Soc., Perkin Trans. II*, 1805, (1986).

[72] **Bock, H., Stein, V. and Semkov, A.,** "Photoelectron Spectra and Molecular Properties: 1,2-Dithiolane - Bonding Model for α Lipoic Acid," *Chem. Ber.*, **113**, 3208, (1980).

[73] **Simonet, J. and Martinet, P.,** "Anodic Oxidation of Thiophanates Mercury(II) on a Platinum Electrode," *J. Electroanal. Chem.*, **88**, 425, (1978).

[74] **Bontempelli, G., Magno, F. and Mazzocchin, G. A.,** "Electrochemical Oxidation of Phenyldisulfide in Acetonitrile Medium," *ibid.*, **42**, 57, (1973).

[75] **Bewick, A., Coe, D. E., Libert, M. and Mellor, J. M.,** "Mechanism of Anodic Acetamidosulphenylation and Acetamidoselenation of Alkenes," *ibid.*, **144**, 235, (1983).

[76] **Giordan, J. and Bock, H.,** "Oxidative Rearrangement of Diphenyl Disulfides to Thianthrenes," *Chem. Ber.*, **115**, 2548, (1982).

[77] **Zweig, A. and Hoffmann, A. K.,** "Naphthalene 1,8-Disulfide," *J. Org. Chem.*, **30**, 3997, (1965).

[78] **Nogami, T., Tanaka, H., Ohnishi, S., Tasaka, Y. and Mikawa, H.,** "Electrical Conductivities of the Complexes of Naphthaceno[5,6-cd:11,12-c'd']-bis[1,2]dithiole and Its Analogs Obtained by Electrochemical Crystallization and Diffusion Method," *Bull. Chem. Soc. Jpn.*, **57**, 22, (1984).

[79] **Levine, O. and Zisman, W. A.,** "Physical Properties of Monolayers Adsorbed at the Solid-Air Interface. I Friction and Wetttability of Aliphatic Polar Compounds and Effect of Halogenation," *J. Phys. Chem.*, **61**, 1068, (1957).

[80] **Hardy, W. B. and Doubleday,** "Boundary Lubrication. - The Paraffin Series," *Proc. R. Soc. London, Series A,* **100**, 550, (1921).

[81] **Okabe, H., Masuko, M. and Sakurai, K.,** "Dynamic Behavior of Surface-Adsorbed Molecules under Boundary Lubrication," *ASLE Trans.*, **24**, 467, (1981).

[82] **Bear, W. G. and Bowden, F. P.,** "Physical Properties of Surfaces. I Kinetic Friction," *Philos. Trans. R. Soc. London, Series A*, **234**, 330, (1935).

[83] **Bowden, F. P. and Leben, L.,** "The Friction of Lubricated Metals," *ibid.*, **239**, 1, (1940).

[84] **Murry, S. F. and Burwell, J. T.,** *Symp. on Fundamentals of Lubrication, in Ann. N.Y. Acad. Sci.*, **53**, 906, (1951).

[85] **Pomey, J.,** *Friction and Wear, NACA Tech. Memo.* TM1318, (National Advisory Committee for Aeronautics), (1952).

[86] **Jahanmir, S.,** "Chain Length Effects in Boundary Lubrication," *Wear,* **102**, 331, (1985).

[87] **Henniker, J. C.,** "The Depth of the Surface Zone of a Liquid," *Review of Modern Physics*, **21**, 322, (1949).

[88] **Bowden, F. P. and Tabor, D.,** *Friction and Lubrication of Solids, Part I,* Oxford University Press, Oxford, (1950).

[89] **Beeck, O., Givens, J. W. and Smith, A. E.,** "On the Mechanism of Boundary Lubrication. I The Action of Long-chain Polar Compounds," *Proc. R. Soc. London, Series A*, **177**, 90, (1940).

[90] **Smith, A. J. and Cameron, A.,** "Rigid Surface Films," *ibid.*, **328**, 541, (1972).

[91] **Bair, S. and Winer, W. O.,** "Some Observations in high Pressure Rheology of Lubricants," *J. Lubr. Technol.*, **104**, 357, (1982).

[92] **Cameron, A.,** "Thin Liquid Films and Boundary Layers," *Spec. Discuss. Faraday Soc.*, **1**, 263, (1970).

[93] **Briscoe, B. J. and Evans, D. C.,** "The Shear Properties of Langmuir-Blodgett Layers," *Proc. R. Soc. London, Series A*, **380**, 389, (1982).

[94] **Adamson, A. W.,** *Physical Chemistry of Surfaces*, Wiley-Interscience, New York, p.88, (1960)

[95] **Weinberg, N. L.,** "Electrochemical Oxidation of Organic Compounds," in *Technique of Electroorganic Synthesis - Part 2* edited by Weinberg, N.L., John Wiley & Sons Inc., New York, p.96, (1974).

[96] *Chem. Abstr.*, **44**, 2873, (1950).: **Elving, P. J. and Teitelbaum, C.,** "Polarographic Behaviour of Organic Compounds. I. The Maleate and Fumarate Species," *Physical Chemistry of Surfaces*, **71**, 3916, (1949).

[97] **Coetzee, J. F. and Kolthoff, I. M.,** "Polarography in Acetonitrile. III. Bronsted Acids and Amperometric Titration of Amines with Perchloric Acid," *ibid.*, **79**, 6110, (1957).: **Kolthoff, I. M. and Reddy, T. B.,** "Polarography and Voltammetry in Dimethy-Sulfoxide," *J. Electrochem. Soc.*, **108**, 980, (1961).

[98] **Kolbé, H.,** "Investigations of the Electrolysis of Organic Bonds," *Ann. Chem. Pharm.*, **69**, 257, (1849).

[99] **Finkelstein, M. and Petersen, R. C.,** "The Kolbé Electrolysis in Dimethy-Formamide," *J. Org. Chem.*, **51**, 772, (1973).

[100] **Rand, L. and Mohar, A. F.,** "The Electrolytic Formation and Cleavage of N-Methyl N-(triphenylacetoxymethyl)formamide," *ibid.*, **30**, 3156, (1965).

[101] **Muck, D. L. and Wilson, E. R.,** "Preparation of N-Alkylacetamides by the Anodic Oxidation of Carboxylic Acid Salts," *J. Electrochem. Soc.*, **117**, 1358, (1970).

[102] **Torii, S., Okamoto, T. and Tanaka, H.,** "Electrolytic Decarboxylation Reactions. I. Electrosynthesis of γ-Substituted Butyrolactones and γ-Substituted α,β-Butenolides from γ-Substituted Paraconic Acids," *J. Org. Chem.*, **39**, 2486, (1974).

[103] **Sato, N., Sekine, T. and Sugino, K.,** "Anodic Process of Acetate Iron in Methanol and in Glacial Acetic Acid at Various Anode Materials," *J. Electrochem. Soc.*, **115**, 242, (1968).

[104] **Utley, J. H. P.,** *Techniques of Electroorganic Synthesis* - Edited by Weinberg, N.L. Part 1, Wiley, New York, p.72, (1974).

[105] **Coleman, J. P., Utley, J. H. P. and Weedon, B. C. L,** "Electro-Organic Reactions. Part II. Mechanism of the Kolbé Electrolysis of Substituted Phenylacetate Ions," *J. Chem. Soc. Perkin Trans. II*, 1064, (1974).

[106] **Mehrotra, R. C. and Bohra, R.,** *Metal Carboxyrates*, Academic Press, London, p.2, (1983)

[107] **Mehrotra, K. N. and Bhargave, S. C.,** "The Effect of Organic Additives on the Properties of the System: Water-Lithium Laurate and Butanol-1," *Z. Phys. Chem.*, **233**, 97, (1966).

[108] **Mehrotra, K. N. and Bhargave, S. C.,** "The Physical Properties of Lithium Soaps in Water Miscible Alcohols," *ibid.*, **237**, 327, (1968).

[109] **Mehrotra, K. N. and Varma, R. P.,** "Studies on Conductivity of the System: Barium Soap-Water and Propanol-1," *J. Amer. Oil Chem. Soc.*, **45**, 673, (1968).

[110] **Attar, A. A. A. Al. and Beck, W. H.,** "Alkaline Earth and Lanthanum Ion Electrodes of the Third Kind Based on the Hydrogen Ion-Responsive Glass Electrode: Thermodynamic Solubility Products of Long Lanthanum Salts in Water," *J. Electroanal. Chem.*, **27**, 59, (1970).

[111] **Kelsall, G. H., Zhu, Y-Y. and Spikes, H. A.,** "Information Survey on Carboxylic Acids and Metal Carboxylates," *Internal Report at Imperial College*, (1994).

[112] **Rietz, C. D. and Techn, D.,** *Carboxylic Acids and Esters*, edited by Patai, S., Interscience Publisher Inc., p.65, (1969).

[113] **Kelsall, G. H. and Wiliams, R. A.,** "Electrochemical Behavior of Ferrosilicides (Fe_xSi) in Neutral and Alkaline Aqueous Electrolytes - I. Thermodynamics of Fe-Si-H_2O systems at 298K -," *J. Electrochem. Soc.*, **138**, 931, (1991).

[114] **Kelsall, G. H. and Wiliams, R. A.,** "Electrochemical Behavior of Ferrosilicides (Fe_xSi) in Neutral and Alkaline Aqueous Electrolytes - II. Fe_xSi Electrochemical Kinetics and Corrosion Behavior -," *ibid.*, **138**, 941, (1991).

[115] **Kelsall, G. H. and Wiliams, R. A.,** "Electrochemical Behavior of Ferrosilicides (Fe_xSi) in Neutral and Alkaline Aqueous Electrolytes - III. The Nature of Passive Films on Fe_xSi Electrode -," *ibid.*, **138**, 951, (1991).

[116] **Kumar, N., Tuck, D. G. and Watson, K. D.,** "The Direct Electrochemical Synthesis of Some Transition -Metal Carboxylates," *Can. J. Chem.*, **65**, 740, (1987).

[117] **Palit, S. R. and McBain, J. W.,** "The Solubility of Heavy Metal Soaps in Co-Solvent Mixtures of Chloroform and Propylene Grycol," *J. Amer. Oil Chem. Soc.*, **24**, 190, (1947).

[118] **Martin, E. P. and Pink, R. C.,** "The Solubility of Zinc Soaps in Organic Solvents," *J. Chem. Soc.*, 1750, (1948).

[119] **Koenig, A. E.,** "On the Stearates and Palmitates of the Heavy Metals with Remarks Concerning Instantaneous Precipitations in Insulating Solutions," *J. Amer. Chem. Soc.*, **36**, 951, (1914).

[120] **Varma, R. P. and Shukla, SMT. S.,** "Solubility of Iron(III) Carboxylate in Mixed Organic Solvents," *Revue Roumaine de Chimie*, **26**, 1401, (1981).

[121] **Naerheim, Y. and Kendig, M. W.,** "The Influence of Electrochemical Potential on Wear," *Wear*, **104**, 139, (1985).

[122] **Pearson, B. R., Brook, P. A. and Waterhouse, R. B.,** "Influence of Electrochemical Potential on the Wear of Metals, particularly Nickel," *Tribology Int.*, **21**, 191, (1988).

[123] **El-Raghy, S. M., Abd-El-Kader, H. and Abou-El-Hassam, M. E.,** "Electrochemistry of Abrasion Corrosion of Low Alloy Steel in 1% NaCl Solution," *Corrosion* (NACE), **40**, 60, (1984).

[124] **Abd-El-Kader, H. and El-Raghy, S. M.,** "Wear Corrosion Mechanism of Stainless Steel in Chloride Media," *Corr. Sci.*, **26**, 647, (1986).

[125] **Brigham, R. J.,** "Crevice Corrosion Initiation and the Potential of Zero Charge," *ibid.*, **29**, 995, (1989).

[126] **Stott, F. H., Breakwell, J. E. and Newman, R. C.,** "The Corrosive Wear of Cast Iron under Potentiostatically-Controlled Conditions in Sulphuric Acid Solutions," *ibid.*, **30**, 813, (1990).

[127] **Iwabuchi, A., Tsukamoto, T., Tatsuyanagi, Y., Norifumi, N. and Nonaka, T.,** "Electrochemical Approach to Corrosive Wear of SKD61 Die Steel in Na_2SO_4 Solution," *Wear*, **156**, 301, (1992).

[128] **Brandon, N. P., Bonanos, N., Fogarty, P. O. and Mahmood, M. N.,** "The Effect of Interfacial Potential on Friction in a Model Aqueous Lubricant," *J. Electrochem. Soc.*, **139**, 3489, (1992).

[129] **Brandon, N. P. and Wood, R. J. K.,** "The Influence of Interfacial Potential on Friction and Wear in an Aqueous Drilling Mud," *Wear*, **170**, 33, (1993).

[130] **Zhu, Y-Y., Kelsall, G. H. and Spikes, H. A.,** "The Influence of Electrochemical Potentials on the Friction and Wear of Iron and Iron Oxides in Aqueous Systems," *Trib. Trans.*, **37**, 811, (1994).

[131] **Marti, A., Hahner, G. and Spencer, N. D.,** "The Sensitivity of Frictional Forces to pH - A Potential Route to Surface Nanochemical Imaging," *Langmuir*, **11**, 4632, (1995).

[132] **Israelachvili, J. N., Chen, Y-L. and Yoshizawa, H.,** "Relationship between Adhesion and Friction Forces," *J. Adhesion Sci.*, **8**, 1231, (1994).

[133] **Tung, S. C. and Wang, S. S.,** "Using Electrochemical and Spectroscopic Techniques as Probes for Investigating Metal-Lubricant Interactions," *Trib. Trans.*, **33**, 563, (1990).

[134] **Yamamoto, Y., Ono, B. and Ura, A.,** "Effect of Applied Voltage on Friction and Wear Characteristics in Mixed Lubrication," *Proc. Eurotrib.*, **5**, 82, August, (1993).

[135] **Bard, A. J. and Faulkner L. R.,** *Electrochemical Methods, Fundamentals and Applications*, Wiley, New York, p.22, (1980).

[136] **Fisher, A. C.,** *Electrode Dynamics - A Series of Oxford Chemistry Primers -*, Oxford University Press, Oxford, p.26, (1996).

[137] **Sakurai, T.,** *Physical Chemistry for Lubrication - New Edition - (Junkatsu no Butsuri Kagaku)*, Saiwai Shobo Inc., Tokyo, p.22, (1983).

[138] **Hutchings, I. M.,** *Tribology - Friction and Wear of Engineering Materials -*, Arnold Inc, London, p.70, (1992).

[139] **Takeuchi, A., Sato, M. and Aoki, H.,** "Effect of Applied Voltage on Friction Characteristics under Mixed Lubrication Conditions," *J. Jpn. Soc. Lub. Eng., (Junkatsu)*, **32**, 673, (1987).

[140] **Takeuchi, A., Sato, M. and Aoki, H.,** "Effect of Electric Current of Advance of Running-in," *J. Jpn. Tribologist*, **35**, 878, (1990).

[141] **Yamamoto, Y., Yagi, J. and Higaki, H.,** "Effect of Electric Field Externally Applied on Friction and Wear Characteristics," *Trans. of Jpn. Soc. Mech. Eng., (Kikai Gakkai Ronbun Shu) Series C,* **57**, 2734, (1991).

[142] **Wang, S. S., Maheswari, S. P. and Tung, S. C.,** "The Nature of Electrochemical Reaction between Several Zinc Organodithiophosphate Antiwear Additives and Cast Iron," *Trib. Trans.*, **32**, 91, (1989).

[143] **Morizur, M. F. and Briant, J.,** "Modification of Electron Properties of Friction Surfaces in Boundary Lubrication," *Proc. Inst. Mech. Eng. Int. Conf. Tribology - Friction, Lubrication & Wear Fifty years On*, p.447, (1987).

[144] **Tung, S. C. and Wang, S. S.,** "Friction Reduction From Electrochemically Deposited Films," *Trib. Trans.*, **34**, 23, (1991).

[145] **Kawamura, M.,** "Electrical Method to observe Lubricant Films under Dynamic Conditions," *J. Jpn. Soc. Lub. Eng., (Junkatsu),* **24**, 331, (1979).

[146] **Takeuchi, A., Sato, M. and Aoki, H.,** "Effect of Applied Voltage on Wear Characteristics under Mixed Lubrication Conditions," *Proc. of Jpn. Tribology Conf.*, p.427, May (1991).

[147] **Katafuchi, T.,** "Effect of Electric Current on Wear under Lubricated Conditions (I) - Electric Current ~ Wear Characteristics -," *J. Jpn. Soc. Lub. Eng., (Junkatsu)*, **30**, 883, (1986).

[148] **Goldblatt, I. L.,** "The Importance of Electron Transfer Process to the Wear Process: Microscope Aspects of Adhesion and Lubrication," *Proc. 34th Int'nl. Meeting of the Societe de Chimie Physique Paris,* edited by Georges, J. M., Elesiver, 512, (1982).

[149] **Anderson, T. N., Anderson, J. L. and Eyring, H.,** "The Nature of Fresh Metal Surfaces in Aqueous Solutions," *J. Phys. Chem.*, **73**, 3652, (1969).

[150] **Adams, A. A. and Foley, R. T.,** "Scrape Potential Measurements on Aluminum Alloys," *Corrosion*, **31**, 84, (1975).

[151] **Beck, T. R., Mahaffey, D. W. and Olsen, J. H.,** "Wear of Small Orifices by Streaming Current Driven Corrosion," *Trans. ASME, J. Basic Eng.*, **92**, 782, (1970).

[152] **Beck, T. R.,** "Wear by Generation of Electrokinetic Streaming Currents," *ASLE Trans.*, **26**, 144, (1983).

[153] **Monvernay, A. D., Dubois, J. E. and Lacaze, P. C.,** "Polaromicrotribometric (PMT) Study of the Electrochemical Formation of Polymer Films on Metallic Surfaces: Polyacrolein," *J. Electroanal. Chem.*, **89**, 149, (1978).

[154] **Volkov, A., Tourillon, G., Lacaze, P. C. and Dubois, J. E.,** "Electrochemical Polymerization on Aromatic Amines: - IR, XPS and PMT Study of Thin Film Formation on a Pt -," *ibid.*, **115**, 279, (1980).

[155] **Dubois, J. E., Monvernary, A. D. and Lacaze, P. C.,** "Polaromicrotribometric (PMT) and IR, ESCA, EPR Spectroscopic Study of Colored Radical Films Formed by the Electrochemical Oxidation on Carbazoles," *ibid.*, **132**, 177, (1982).

3. *Chapter 3 Experimental techniques*

[1] **Bard, A. J. and Faulkner L. R.,** *Electrochemical Methods, Fundamentals and Applications*, Wiley, New York, p.22, (1980).

[2] **Fisher, A. C.,** *Electrode Dynamics - A Series of Oxford Chemistry Primers* -, Oxford University Press, Oxford, p.26, (1996).

[3] **Hills, G. J.,** *Reference Electrode - Theory and Practice* - edited by Ives, D. J. G. and Jang, G. J., Academic Press, London, p.439, (1961).

[4] **Kostuch, J. A. and Kuhn, A. T.,** "Infrared Spectroelectrochemistry," *in Modern Techniques in Electrochemistry, Corrosion and Metal Finishing*, edited by Kuhn, A. T., John Wiley & Sons Ltd., New York, p.214, (1987).

[5] **Tschinkel, W., Neugebaueuer. and Neckel, A.,** "*In-Situ* FT-IR Spectroscopy of Iron Electrodes in Alkaline Solution II. External Reflection Adsorption Spectroscopy," *J. Electrochem. Soc.*, **137**, 1475, (1990).

[6] **Zhu, Y-Y., Kelsall, G. H. and Spikes, H. A.,** "The Influence of Electrochemical Potentials on the Friction and Wear of Iron and Iron Oxides in Aqueous Systems," *Trib. Trans.*, **37**, 811, (1994).

[7] **Micka, K.,** *Introduction into the Theory of Impedance Measurements*, Institute of Chemical Technology, Prague, p.29, (1994).

[8] **Gabrielli, C.,** *Identification of Electrochemical Process by Frequency Response Analysis*, Technical Report No. 004/83.

[9] **Ogano, S.,** "Electrochemical Control of Friction and Wear," *Transfer Seminar at Imperial College*, December, (1996).

[10] **Dowson, D. and Higginson, G. R.,** *Elasto-hydrodynamic Lubrication*, Pergamon, Oxford, (1966).

[11] **Binning, G., Roher, H., Gerber, C. And Weibel, E,** "Surface Studies by Scanning Tunneling Microscopy," *Phys. Rev. Lett.*, **49**, 57, (1981).

[12] **Israelachvili, J. N.,** *Intermolecular and Surface Forces*, Academic Press, New York, p.104, (1985).

[13] **Sarid, D.,** *Scanning Force Microscopy - with Applications to Electric, Magnetic and Atomic Forces - (Revised Edition)*, Oxford University Press, Oxford, p.181, (1994).

[14] **Zhu, Y-Y., Kelsall, G. H. and Spikes, H. A.,** "Triboelectrochemistry on a Nanometre Scale," *Trib. Lett.*, **2**, 287, (1996).

[15] **Ruan, J. and Bhushan, B.,** "Nano-Indentation Studied of Sublimed Fullerene Films using Atomic Force Microscopy," *J. Materials Research*, **8**, 3019, (1993).

[16] **Johnston, G. J.,** "A Study of Lubricating Films Generated by Organo-Phosphorus Anti-Wear Additives", PhD Thesis, Imperial College, University of London, (1990).

[17] **Wedeven, L. D.,** "Optical Measurements in Elastohydrodynamic Rolling Contact Bearings", PhD Thesis, Imperial College, University of London, (1970).

[18] **Westlake, F. J.,** "An Interferometric Study of Thin Fluid Films", PhD Thesis, Imperial College, University of London, (1970).

[19] **Gunsel, S. and Spikes, H. A.,** "In-situ Measurements of ZDDP Films in Concentrated Contacts", *Trib. Trans.*, **36**, 276, (1993).

4. Chapter 4 Chemicals and materials used

[1] **Bailey, S. I., Leung, W-P. and Ritchie, I. M.,** "Reference Redox Systems in Tetrahydrofuran," *Electrochim. Acta*, **30**, 861, (1985).

[2] **Groat, K. A. and Creager, S.,** "Self-Assembled Monolayers in Organic Solvents: Electrochemically at Alkanethiolate-Coated Gold in Propylene Carbonate," *Langmuir*, **9**, 3668, (1993).

[3] **Cooper, J. B. and Bond, A. M.,** "Microelectrode Studies in the Absence of Deliberately Added Supporting Electrolyte: Solvent Dependence for Neutral and Singly Charged Species," *J. Electroanal. Chem.*, **315**, 143, (1991).

[4] **Silva, M. E., Pombeiro, A. J. L., Silva, J. R. F., Herrmann, R., Deus, N., Castilho, T. J. and Silva, M. F. C,** "Redox Potential and Substituent Effects at Ferrocene Derivatives. Estimates of Hammett σ_p and Taft Polar σ^* Substituent Constants," *J. Organometal. Chem.*, **421**, 75, (1991).

[5] **Silva, M. E., Pombeiro, A. J. L., Silva, J. R. F., Herrmann, R., Deus, N. and Bozak, R. E.,** "Redox Potential and Substituent Effects in Ferrocene Derivatives: II," *ibid.*, **480**, 81, (1994).

5. Chapter5 Selection of non-aqueous system for electrochemical work

[1] **Shinoda, K.,** *Solutions and Solubility (Youeki to Youkaido),* Maruzen Press, Tokyo, (1966)

[2] **Fedors, R. F.,** "A Method for Estimating Both the Solubility Parameters and Molar Volumes of Liquids," *Polym. Eng. Sci.*, **14**, 147, (1974).

[3] **Bailey, S. I., Leung, W-P. and Ritchie, I. M.,** "Reference Redox Systems in Tetrahydrofuran," *Electrochim. Acta*, **30**, 861, (1985).

[4] **Groat, K. A. and Creager, S.,** "Self-Assembled Monolayers in Organic Solvents: Electrochemically at Alkanethiolate-Coated Gold in Propylene Carbonate," *Langmuir*, **9**, 3668, (1993).

[5] **Cooper, J. B. and Bond, A. M.,** "Microelectrode Studies in the Absence of Deliberately Added Supporting Electrolyte: Solvent Dependence for Neutral and Singly Charged Species," *J. Electroanal. Chem.*, **315**, 143, (1991).

[6] **Funt, B. L., Richardson, D. and Bhadani, S. N.,** "Electrolytic Formation of Living Polymers from Styrene," *Can. J. Chem.*, **44**, 711, (1966).

[7] **Prejza, J., Lundstorm, I. and Skotheim, T.,** "Electropolymerization of Pyrrol in the Presence of Fluoborate," *J. Electrochem. Soc.*, **129**, 1685, (1982).

[8] **Fish, D. and Smid, J.,** "Solvation of Lithium ions in Mixtures of Tetraethylene Glycol Dimethyl Ether and Propylene Carbonate," *Electrochim. Acta*, **37**, 2043, (1992).

[9] **Fisher, A. C.,** *Electrode Dynamics - A Series of Oxford Chemistry Primers* -, Oxford University Press, Oxford, p.26, (1996).

[10] **Bard, A. J. and Faulkner L. R.,** *Electrochemical Methods, Fundamentals and Applications*, Wiley, New York, p.22, (1980).

[11] **Cooper, J. B. and Bond, A. M.,** "Microelectrode Studies in the Absence of Deliberately Added Supporting Electrolyte: Solvent Dependence for a Neutral and Singly Charged Species," *J. Electroanal. Chem.*, **315**, 143, (1991).

[12] **Sakurai, T.,** *Additives for Petroleum Products - New Edition - (Sekiyu Seihin Tenkazai)*, Saiwai Shobo Inc., Tokyo, p.228, (1986).

[13] **Oehme, F.,** *From Sensors: A Comprehensive Survey,* edited by Gopel, W., Hesse, J.and Zemel, J. N., Vol. 2, Part 7, VCH, New York, p.314, (1991).

[14] **Monk, C. B.,** *Electrolyte Dissociation*, Academic Press, London, p.130, (1961).

[15] **Jensen, M. L. and Yeager, H. L.,** "Conductance Measurements of Alkali Metal Trifluoroacetates in Propylene Carbonate," *J. Phys. Chem.*, **78**, 1380, (1974).

[16] **Mehrotra, K. N. and Varma, R. P.,** "Studies on Conductivity of the System: Barium Soap-Water and Propanol-1," *J. Amer. Oil Chem. Soc.*, **45**, 673, (1968).

[17] **Zhou, H. and Dong, S.,** "An Ultramicroelectrode Study of Ferrocene Diffusion and Heterogeneous Electron Transfer Rate in Polyelectrolyte," *Electrochim. Acta*, **42**, 1801, (1997).

6. Chapter 6 Electrochemical study of metal-additive interactions

[1] **Pourbaix, M.,** *Atras of Electrochemical Equilibria*, Pergamon, Oxford, (1966).

[2] **Okubo, T. and Tsutsumi, S.,** "The Anodic Oxidation of Esters," *Bull. Chem. Soc. Jpn.*, **37**, 1794, (1964).: **Weinberg, N. L.,** "Electrochemical Oxidation of Organic Compounds," in *Technique of Electroorganic Synthesis - Part 1* edited by Weinberg, N. L., John Wiley & Sons Inc., New York, p.442, (1974).

[3] **Zhu, Y-Y., Kelsall, G. H. and Spikes, H. A.,** "Triboelectrochemistry on a Nanometre Scale," *Trib. Lett.*, **2**, 287, (1996).

[4] **Kelsall, G. H., Zhu, Y-Y. and Spikes, H. A.,** "Information Survey on Carboxylic Acids and Metal Carboxylates," *Internal Report at Imperial College*, (1994).

[5] **Pearson, B. R., Brook, P. A. and Waterhouse, R. B.,** "Influence of Electrochemical Potential on the Wear of Metals, particularly Nickel," *Tribology Int.*, **21**, 191, (1988).

[6] **Iversen, P. E. and Lund, H.,** "Electrolytic Generation of Nucleophiles. IV. Reductive Alkylation and Acylation of Disulfides," *Acta Chem. Scand.*, **B28**, 827, (1974).

[7] **Ohno, N., Uehara, J. and Aramaki, K.,** "A SERS Study on Adsorption of Dibenzyl Disulfide, Sulfide, and Sulfoxide on an Iron-Deposited Silver Electrode in a Hydrochloric Acid Solution," *J. Electrochem. Soc.*, **140**, 2512, (1993).

[8] **Degrand, C. and Lund, H.,** "Electrochemical Synthesis of Sulfide Acids," *Acta Chem. Scand.*, **B33**, 512, (1974).

[9] **Lund, H. and Baizer, M. M.,** *Organic Electrochemistry - An Introduction and Guide- Third Edition, Revised and Expanded*, Marcel Dekker, Inc., New York, p.487, (1991).

[10] **Banwell, C. N. and McCash, E. M.,** *Fundamentals of Molecular Spectroscopy - Fourth Edition* -, McGraw-Hill Ltd., London, p.86, (1994).

[11] **Zelenay, P., Winnicka-Maurin, M. and Sobkowski, J.,** "Radiotracer and Voltammetric Study of Water at the Platinum / Propylene Carbonate Interface," *J. Electroanal. Chem.*, **278**, 361, (1990).

[12] **Zelenay, P., Szklarczyk, M., Winnicka-Maurin, M. and Sobkowski, J.,** "Voltammetric and Radiotracer Study of the Interaction of Water with Platinum in the TBAP + Propylene Carbonate Solution," *ibid.*, **308**, 269, (1991).

[13] **Atanasoski, R. T., Law, H. H., McIntosh, R. C. and Tobias, C. W.,** Electrochemical Analysis of Trace Amounts of Water in Propylene Carbonate Electrolytes," *Electrochim. Acta*, **32**, 877, (1987).

[14] **Eichinger, G.,** "Cathodic Decomposition Reactions of Propylene Carbonate," *J. Electroanal. Chem.*, **74**, 183, (1976).

[15] **Rasch, B., Cattaneo, E., Novak, P. and Vielstich, W.,** "The Influence of Water on the Oxidation of Propylene Carbonate on Platinum - An Electrochemical, In Situ FT-IR and On-Line MS Study," *Electrochim. Acta*, **36**, 1397, (1991).

[16] **Eggert, G. and Heitbaum, J.,** "Electrochemical Reactions of Propylene Carbonate and Electrolytes Solved Therein - A Dems Study," *ibid.*, **31**, 1443, (1986).

[17] **Burrows, B. and Kirkland, S.,** "Electrochemical Behavior of H_2O in Nonaqueous Media," *J. Electrochem., Soc.*, **115**, 1164, (1968).

[18] **Kaesche, H.,** *Metallic Corrosion*, National Association of Corrosion Engineers, Houston, Texas, p.252, (1985)

[19] **Kelly, R. G., Moran, P. J. and Kruger, J.,** "Passivity of Fe in Anhydrous Propylene Carbonate," *J. Electrochem. Soc.*, **136**, 3262, (1989).

[20] **Sakurai, T.,** *Physical Chemistry for Lubrication - New Edition - (Junkatsu no Butsuri Kagaku)*, Saiwai Shobo Inc., Tokyo, p.65, (1983).

[21] **Jüttner, K., Lorentz, W. J., Kendig, M. W. and Mansfeld, F.,** "Electrochemical Impedance Spectroscopy on 3-D Inhomogeneous Surfaces - Corrosion in Neutral Aerated Solutions," *J. Electrochem. Soc.*, **135**, 332, (1988).

[22] **Mansfeld, F.,** "Concerning the Display of Impedance Data," *Corrosion*, **44**, 856, (NACE), (1988).

[23] **Kendig, M. W., Allen, E. T. and Mansfeld, F.,** "Optimized Collection of AC Impedance Data," *J. Electrochem. Soc.*, **131**, 935, (1984).: **Mansfeld, F., Kendig, M. W. and Lorenz, W. J.,** "Corrosion Inhibition in Neutral Aerated Media," *ibid.*, **132**, 290, (1985).

[24] **Nyikos, L. and Pajkossy, T.,** "Fractal Dimension and Fractal Power Frequency-Dependent Impedance of Blocking Electrode," *Electrochim. Acta*, **30**, 1533, (1985).

[25] **Brandon, N. P., Bonanos, N., Fogarty, P. O. and Mahmood, M. N.,** "The Effect of Interfacial Potential on Friction in a Model Aqueous Lubricant," *J. Electrochem. Soc.*, **139**, 3489, (1992).

[26] **Kalman, E., Varhegyi, B., Bako, I., Felhosi, I., KarmanF. H. and Shaban, A.,** "Corrosion Inhibition by 1-hydroxy-ethane-1,1-diphosphonic Acid - An Electrohemical Impedance Spectroscopy Study -," *ibid.*, **141**, 3357, (1994).

7. Chapter 7 Effect of electrode potential on friction and wear

[1] **Zhu, Y-Y., Kelsall, G. H. and Spikes, H. A.,** "The Influence of Electrochemical Potentials on the Friction and Wear of Iron and Iron Oxides in Aqueous Systems," *Trib. Trans.*, **37**, 811, (1994).

[2] **Zhu, Y-Y., Kelsall, G. H. and Spikes, H. A.,** "Triboelectrochemistry on a Nanometre Scale," *Trib. Lett.*, **2**, 287, (1996).

[3] **Brandon, N. P., Bonanos, N., Fogarty, P. O., Mahmood, M. N., Moore, A. J. and Wood, R. J. K.,** "Influence Potential on the Friction and Wear of Mild Steel in a Model Aqueous Lubricant," *J. App. Electrochem.*, **23**, 456, (1993).

[4] **Kyriacou, D.,** *Modern Electroorganic Chemistry*, Springer-Verlag Press, Berlin, p.146, (1994).

[5] **Varma, R. P. and Shukla, SMT. S.,** "Solubility of Iron(III) Carboxylate in Mixed Organic Solvents," *Revue Roumaine de Chimie*, **26**, 1401, (1981).

[6] **Jahanmir, S.,** "Chain Length Effects in Boundary Lubrication," *Wear*, **102**, 331, (1985).

[7] **Okabe, H., Masuko, M. and Sakurai, K.,** "Dynamic Behavior of Surface-Adsorbed Molecules under Boundary Lubrication," *ASLE Trans.*, **24**, 467, (1981).

[8] **Pomey, J.,** *Friction and Wear, NACA Tech. Memo.* TM1318, (National Advisory Committee for Aeronautics), (1952).

8. Chapter 8 Effect of electrode potential on lubricant film thickness

[1] **Hamrock, B. T. and Dowson, D.,** *Ball Bearing Lubrication: The Elastohydro-dynamics of Elliptical Contact*, John Wiley, New York, (1981).

[2] **Guangteng, G. and Spikes, H. A.,** "Boundary film thickness by Lubricant Base Fluids," *Trib. Trans.*, **39**, 448, (1996).

[3] **Cann, P. M. and Spikes, H. A.,** "The Behavior of Polymer Solutions in Concentrated Contacts: Immobile Surface Layer Formation," *ibid.*, **37**, 580, (1994).

[4] **Smeeth, M., Spikes, H. A. and Gunsel, S.,** "Boundary Film Formation by Viscosity Index Improvers," *ibid.*, **39**, 726, (1996).

[5] **Allen, C. M. and Drauglis, A.,** "Boundary layer Lubrication: Monolayer or Multilayer," *Wear*, **14**, 363, (1968).

[6] **Guangteng, G. and Spikes, H. A.,** "Boundary film thickness by Lubricant Base Fluids," *Trib. Trans.*, **39**, 448, (1996).

[7] **Guangteng, G. and Spikes, H. A.,** "Fractionation of Liquid Lubricants at Solid Surfaces," *Wear*, **200**, 336, (1996).

[8] **Eggert, G. and Heitbaum, J.,** "Electrochemical Reactions of Propylene Carbonate and Electrolytes Solved Therein - A Dems Study," *Electrochim. Acta.*, **31**, 1443, (1986).

[9] **Sakurai, T.,** *Additives for Petroleum Products - New Edition - (Sekiyu Seihin Tenkazai)*, Saiwai Shobo Inc., Tokyo, p.241, (1986).

9. Chapter 9 Triboelectrochemistry in nano-metre scale

[1] **Zhu, Y-Y., Kelsall, G. H. and Spikes, H. A.,** "Triboelectrochemistry on a Nanometre Scale," *Trib. Lett.*, **2**, 287, (1996).

[2] **Ruan, J-A. and Bhushan, B.,** "Atomic-scale Friction Measurement Using Friction Force Microscopy: Part I - General Principles and New Measurement Techniques", *ASME Trans., J. of Tribology*, **116**, 378, (1994).

[2] **Kelsall, G. H. and Spikes, H. A.,** "Triboelectrochemistry - Investigation and Control of Friction and Wear by Electrochemical Techniques," *Final Report for EPSRC GR/H77354*, p.4, (1996).

[3] **Zhu, Y-Y., Kelsall, G. H. and Spikes, H. A.,** "The Influence of Electrochemical Potentials on the Friction and Wear of Iron and Iron Oxides in Aqueous Systems," *Trib. Trans.*, **37**, 811, (1994).

10. Chapter 10 Conclusions and future work

[1] **Guangteng, G. and Spikes, H. A.,** "Boundary film thickness by Lubricant Base Fluids," *Trib. Trans.*, **39**, 448, (1996).

[2] **Guangteng, G. and Spikes, H. A.,** "Fractionation of Liquid Lubricants at Solid Surfaces," *Wear*, **200**, 336, (1996).

[3] **Guangteng, G. and Spikes, H. A.,** "An Experimental Study of Film Thickness in the Mixed Lubrication Regime," *Proc. Leeds-Lyon Symposium, Elastohydrodynamics '96, Leeds, Sepember, edited by D. Dowson et al.,* Elsevier, Amsterdam, p.159, (1997).

[4] **Ohno, N., Uehara, J. and Aramaki, K.,** "A SERS Study on Adsorption of Dibenzyl Disulfide, Sulfide, and Sulfoxide on an Iron-Deposited Silver Electrode in a Hydrochloric Acid Solution," *J. Electrochem. Soc.*, **140**, 2512, (1993).

[5] **Uehara, J. and Aramaki, K.,** "A SERS Study on Adsorption of Some Sulfur-Containing Corrosion-Inhibitors on Iron in Hydrochloric Acid Solutions," *ibid.*, **138**, 3245, (1991).

[6] **Tung, S. C. and Wang, S. S.,** "In-Situ Electro-charging for Friction Reduction and Wear Resistant Film Formation," *Trib. Trans.*, **34**, 479, (1991).

[7] **Abbott, A. P. and Harper, J. C.,** "Electrochemical Investigations in Supercritical Carbon Dioxide," *J. Chem. Soc. Frarad. Trans.*, **92**, 3895, (1996).

BIBL. LONDON UNIV.